QUARTERLY PROGRESS REPORT

January 1 to March 31, 2017

Florida International University's Continued Research Support for the Department of Energy's Office of Environmental Management

Principal Investigator:

Leonel E. Lagos, Ph.D., PMP®

Prepared for:

U.S. Department of Energy
Office of Environmental Management
Under Cooperative Agreement No. DE-EM0000598

Applied Research Center
FLORIDA INTERNATIONAL UNIVERSITY

Introduction

The Applied Research Center (ARC) at Florida International University (FIU) executed work on four major projects that represent FIU-ARC's continued support to the Department of Energy's Office of Environmental Management (DOE-EM). The projects are important to EM's mission of accelerated risk reduction and cleanup of the environmental legacy of the nation's nuclear weapons program.

The period of performance for FIU Performance Year 7 under the DOE Cooperative Agreement (Contract # DE-EM0000598) is August 29, 2016 to August 28, 2017. The information in this document provides a summary of the FIU-ARC's activities under the Cooperative Agreement for the period of January 1 to March 31, 2017. Executive highlights during this reporting period include:

Project 1: High level waste (HLW)/waste processing

FIU is assisting DOE EM to meet the challenges of an aging HLW infrastructure through the development of robotic inspection tools and the evaluation of sensors that can assist in assessing the integrity of the DSTs and the waste transfer components. To aid in this process, FIU is evaluating aged polymers that have been exposed to multiple stressors. Materials composed in hose-in-hose transfer lines, gaskets and O-rings are being investigated. This information can provide valuable insight into understanding the life expectancy of non-metallic components. FIU is also assisting DOE EM in evaluating the double-shell tank structural integrity and to ensure that the stringent operating conditions of the DSTs are being met through technology evaluations and the use of sensors. A significant task under this category is to estimate the temperatures within the tanks which are a key to reducing the risk of corrosion. There is a critical need for measurement and calculations of actual temperatures inside the tanks to ensure that corrosion is minimized. To support this need, FIU is investigating the use of an infrared (IR) sensor to measure the outside wall temperature from within the annulus and correlate those measurements with waste temperatures within the tank.

1. FIU hosted three engineers from WRPS in February to discuss progress on each of the tasks related to Project 1. In particular, they observed burst pressure tests of HIHTL coupons that have been aged for 6 months with a 25% NAOH solution at three different temperatures. Results indicated that there were minimal changes from the burst pressures when compared to baseline specimens. Tests were also conducted on aged EPDM and Garlock coupons to understand how the material properties change under multiple stressors. The results indicate that a significant change in tensile strength occurred for all test conditions.
2. A mini infrared temperature sensor from Raytek (MI3) has been validated and verified as a viable option to accurately measure the temperature of the inner walls in DSTs. Bench-scale and engineering-scale tests have been conducted successfully to evaluate the sensor for deployment at the Hanford site. Testing included development of test matrices, implementation and emissivity configuration of the IR sensor. Currently, FIU is investigating the integration of the mini IR sensor with inspection devices for use in additional applications for temperature measurements.

Project 2: Environmental remediation (ER)

FIU is assisting DOE EM to meet the challenges of managing the environmental restoration of subsurface contamination in soil and groundwater. In support of this effort, FIU is working in collaboration with SRNL to investigate the effect of sodium silicate additions on the restoration of groundwater pH to control uranium mobility as well as to develop a surface water model of the Tims Branch watershed at the Savannah River Site.

1. A manuscript entitled, *Sodium silicate treatment for the attenuation of U(VI) in iron-bearing acidic sediments*, written by Vasileios Anagnostopoulos, Yelena Katsenovich and Miles Denham, was accepted for the publication in the Journal of Chemical Technology & Biotechnology. The study explores the use of sodium silicate for the restoration of neutral pH of the impacted zone and consequently, uranium immobilization under circumneutral conditions.
2. FIU completed the calibration processes for the MIKE SHE and MIKE 11 models. The MIKE SHE model calibration was completed and modifications were made to improve the model performance based on the model results and the sensitivity analyses that were carried out. Numerical errors encountered during calibration of the MIKE 11 model are still being investigated to find and correct the source of these errors.

Project 3: Deactivation and decommissioning (D&D)

FIU is assisting DOE EM to meet high priority D&D needs and technical challenges across the DOE complex through technology development, demonstration and evaluation. FIU is investigating the use of intumescent coatings to mitigate the release of radioisotopes during fire and/or extreme heat conditions that can potentially occur at a DOE contaminated facility/building. Standardizing and implementing proven processes to refine and better synchronize DOE-EM technology needs, requirements, testing, evaluation, and acquisition by development of uniformly accepted testing protocols and performance metrics is an essential component of these efforts.

1. The final test plan, titled, *Adapting Intumescent Coatings as Fire Resilient Fixatives in Support of SRS 235-F D&D Activities Phase II: Construction of SRS 235-F Hot Cell Test Bed and Application Demonstration,* received concurrence and was signed by all stakeholders at FIU and SRNL on February 6, 2017.
2. Two draft standard specifications related to permanent and removable / strippable coatings and fixatives were balloted for a formal ASTM International E10.03 Subcommittee vote. Both the “Standard Specification for Permanent Coatings Used to Mitigate Spread of Radioactive Contamination” and the “Standard Specification for Strippable & Removable Coatings to Mitigate Spread of Radioactive Contamination” were unanimously approved by the Subcommittee members, with only minor editorial comments. The standards are now ready for a full E10 Committee vote, which is the final step in the approval process.

Project 4: STEM workforce development

FIU created the DOE Fellows Program in 2007 to assist DOE EM to address the problem of an aging federal workforce. The program provides training, mentorship, and professional development opportunities to FIU STEM students. The DOE Fellows provide critical support to the DOE EM research being conducted on high impact/high priority research being conducted at FIU.

1. DOE Fellows have been busy this spring sharing the research that they have performed in support of DOE-EM at FIU-ARC and during their summer internships at DOE sites, DOE Headquarters, and national research laboratories. These presentations have been in the research areas of high level waste/waste processing, soil and groundwater modeling and remediation, deactivation and decommissioning, and technology development. In addition to the seventeen (17) DOE Fellows who presented technical posters during the student poster session at the Waste Management 2017 Symposium on March 6, 2017, as well as the two (2) DOE Fellows who gave professional oral presentations at the same conference, twelve (12) additional presentations have been given by the DOE Fellows in the last few months to a wide range of audiences.

Project deliverables and milestones during this reporting period include:

***Project 1*: High level waste (HLW)/waste processing**

- Milestone 2016-P1-M17.1.1 was completed and a summary document was provided to DOE-HQ and WRPS engineers on February 17, 2017. This milestone was associated with completing the literature review of baseline experimental cases that could be used to improve the modeling capability for retrieval processes.
- Milestone 2016-P1-M19.2.1 was completed and a summary document was provided to DOE-HQ and WRPS engineers on March 31, 2017. This milestone was associated with completing the experimental testing of the non-metallic components that were aged for 6 months.
- Milestone 2016-P1-M18.3.1 was completed on March 31, 2017 and a summary document will be sent on April 14, 2017, summarizing the results from the bench-scale tests using an IR sensor.
- Due to funding issues, milestones 2016-P1-M18.2.1 and 2016-P1-M17.1.2 will be reforecast. The expected delay has been communicated to the site points-of-contact as well as the DOE HQ Project Lead, Gary Peterson, during regular project teleconferences. A reforecast date of completion will be set once future funding amounts and dates are known.

***Project 2:* Environmental remediation (ER)**

- The technical report deliverable associated with subtask 1.3 on the results of columns monitoring using geochemical and SIP analyses, was submitted on January 30, 2017.
- The first part of milestone 2016-P2-M5 (subtask 1.4), to complete training on the LSC analytical technique, was completed with a 4-hour training webinar conducted on November 7, 2016. The second part of the milestone, to complete trial-and-error experiments for separations and determination of Tc(IV) and Tc(VII), will be completed on April 4, 2017.

- A technical progress report on "Investigation of the Properties of Acid-Contaminated Sediment and its Effect on Contaminant Mobility" was submitted to DOE-HQ and site contacts on February 13, 2017 for subtask 2.1.
- Milestone 2016-P2-M8 which involved completion of the calibration processes of the MIKE SHE and MIKE 11 models was completed on March 1, 2017.
- Milestone 2016-P2-M9, to complete batch experiments on the biodissolution of Na-autunite (subtask 1.2) has been reforecast due to an experimental delay from the first set of samples developing contamination. FIU has repeated the experiment with fresh preparations and estimates the milestone will be completed by May 15, 2017.
- The deliverable for a technical report on the synergy between colloidal Si and HA on the removal of U(VI) (subtask 2.2) has been reforecast due to the KPA instrument having very low sensitivity. This task is heavily dependent on this instrument for uranium analysis. Once repairs to the KPA instrument are complete, FIU will reforecast the date for this deliverable, proceed with analyzing the samples collected to date under this subtask, and complete the technical report.
- FIU also reforecast milestone 2016-P2-M6 for subtask 2.3 due to the same issues with the requisite KPA instrument. This milestone will complete the batch experiments for uranium removal by Huma-K on SRS sediments. FIU is reforecasting the completion of the milestone by August 18, 2017. FIU has received the replacement nitrogen laser for the KPA instrument and repairs are in progress. All project delays have been communicated to the project task points-of-contact during regular project teleconferences and agreement has been reached on the planned path forward.

Project 3: Deactivation and decommissioning (D&D)

- The deliverable associated with subtask 2.2.2, draft test plan for the technology demo/test & evaluation at FIU was completed. The draft test plan, titled *"Adapting Intumescent Coatings as Fire Resilient Fixatives ISO SRS 235-F D&D Activities Phase II: Construction of SRS 235-F Hot Cell Test Bed and Application Demonstration"* was submitted on January 6, 2017 to SRNL for review/comments, and the final document received concurrence and was signed by all stakeholders at FIU and SRNL on February 6, 2017.
- Milestone 2016-P3-M2.1 was completed with the participation in the January ASTM E10 Committee Meeting to coordinate the development of standardized testing protocols and performance metrics for D&D technologies (subtask 2.2.1).
- The preliminary metrics progress report on outreach and training activities for D&D KM-IT was completed in March and sent to DOE on April 4 and the latest infographic on Knowledge Management was revised and sent to DOE on February 1.
- A D&D KM-IT workshop was provided to the D&D community via demonstrations at the FIU conference booth at Waste Management 2017 from March 5-9, which completed a project deliverable.

- The four Wikipedia integration edits/articles, for milestone 2016-M3-M3.2 is in progress and has been reforecast for completion by June 30, 2017.
- Milestone 2016-P3-M2.2 is being reforecast to June 16. The test plan associated with this milestone includes constructing a to-scale SRS 235-F Hot Cell Test Bed on site at ARC that mirrors the operating environment encountered in an adjoining corner and middle hot cell configuration at the SRS 235-F facility. The second main objective involves an evaluation on the mechanics and processes associated with applying the selected intumescent coatings in the hot cell. The first part of this test plan is currently being executed as allowed by the incremental funding received and construction of the hot cell test bed is expected to be completed by May 12. The second part of the text plan is expected to be executed in late May to early June. FIU has communicated closely with the project contacts at Savannah River on the progress and scheduling of this task. They are in agreement with the new dates and will be visiting FIU to review the completed construction of the hot cell test bed and preparations for the execution of the testing and evaluation, tentatively planned for May 18.

Project 4: **STEM workforce development**

- Milestone 2016-P4-M4, submission of student poster abstracts to Waste Management Symposium 2017, was completed with the submission of 17 student abstracts.

The program-wide milestones and deliverables that apply to all projects (Projects 1 through 4) for FIU Performance Year 7 are shown on the following table.

Task	Milestone/ Deliverable	Description	Due Date	Status	OSTI
Program-wide (All Projects)	Deliverable	Draft Project Technical Plan	9/30/16	Complete	
	Deliverable	Monthly Progress Reports	Monthly	On Target	
	Deliverable	Quarterly Progress Reports	Quarterly	On Target	
	Deliverable	Draft Year End Report	10/13/17	On Target	OSTI
	Deliverable	Presentation overview to DOE HQ/Site POCs of the project progress and accomplishments (Mid-Year Review)	4/7/17* Reforecast TBD	Reforecast	
	Deliverable	Presentation overview to DOE HQ/Site POCs of the project progress and accomplishments (Year End Review)	9/29/17*	On Target	

**Completion of this deliverable depends on availability of DOE-HQ official(s).*

Project 1
Chemical Process Alternatives for Radioactive Waste

Project Manager: Dr. Dwayne McDaniel

Project Description

Florida International University has been conducting research on several promising alternative processes and technologies that can be applied to address several technology gaps in the current high-level waste processing retrieval and conditioning strategy. The implementation of advanced technologies to address challenges faced with baseline methods is of great interest to the Hanford Site and can be applied to other sites with similar challenges, such as the Savannah River Site. Specifically, FIU has been involved in: modeling and analysis of multiphase flows pertaining to waste feed mixing processes, evaluation of alternative HLW instrumentation for in-tank applications and the development of technologies to assist in the inspection of tank bottoms at Hanford. The use of field or *in situ* technologies, as well as advanced computational methods, can improve several facets of the retrieval and transport processes of HLW. FIU has worked with site personnel to identify technology and process improvement needs that can benefit from FIU's core expertise in HLW. The following tasks are included in FIU Performance Year 7:

Task No	Task
Task 17: Advanced Topics for Mixing Processes	
Subtask 17.1	Computational Fluid Dynamics Modeling of HLW Processes in Waste Tanks
Task 18: Technology Development and Instrumentation Evaluation	
Subtask 18.2	Development of Inspection Tools for DST Primary Tanks
Subtask 18.3	Investigation Using an Infrared Temperature Sensor to Determine the Inside Wall Temperature of DSTs
Task 19: Pipeline Integrity and Analysis	
Subtask 19.1	Pipeline Corrosion and Erosion Evaluation
Subtask 19.2	Evaluation of Nonmetallic Components in the Waste Transfer System

Task 17: Advanced Topics for HLW Mixing and Processing

Task 17 Overview

This task will use the knowledge acquired at FIU on multiphase flow modeling to build a CFD computer program in order to obtain simulations at the engineering-scale with appropriate physics captured for the analysis and optimization of various mixing processes. Focus will be given to turbulent fluid flow in nuclear waste tanks that exhibit both Newtonian and non-Newtonian fluid characteristics.

The objective of this task is to provide the sites with mathematical modeling, validation, and testing of computer programs to support critical issues related to HLW retrieval and processing. FIU engineers will work directly with site engineers to plan, execute, and analyze the results of the research and development.

Task 17 Quarterly Progress

Subtask 17.1.1: CFD Modeling of HLW Processes in Waste Tanks

Additional data collection from various tests carried out in 2011 and 2013 were performed. In addition, data from a test with a single-component solid simulant in 2010 was collected. FIU created a summary presentation for the WRPS POC regarding various performance metrics, system dimensions, and operating conditions from different retrieval tests to be presented to DOE.

Test 2010 (ZrO_2 , 6 wt% in Water)

This test was conducted using a single component solid simulant (ZrO_2) in water according to Wells et al. (2011) and private communications with DOE. In this simple test (simplicity for working with single solid and single liquid), ZrO_2 had a 6 wt% of the tank material and specific gravity of 5.7. This test was also used as a baseline for a CFD simulation study conducted by Wells and his colleagues where simulations and test data about normalized cloud height (HC/HL) and undissolved solid (UDS) concentration were compared (Table 1-1). However, more information regarding operating conditions (rotation rate and capture velocity) and properties of the supernatant (Report RPP-48358) are needed for a simulation study of this case.

Table 1-1. Cloud Height Data for Test 2010, 6 %wt ZrO_2 (Wells et al., 2011)

metric ⬇	**43.2" tank Nozzle vel. (ft/s)**			**120" tank Nozzle vel. (ft/s)**		
	13	**19**	**22**	**22**	**25**	**28**
HC/HL	0.61	0.87	1.02	0.71	0.90	1.02
UDS	0.46	0.46	0.49	0.77	0.60	0.53

Test 2011-1 (Four-Part Simulant in Water)

This test was performed using a multi-component simulant composed of gibbsite, zirconium oxide, silicon carbide, and bismuth oxide in water and inside 43.2" and 120" tanks. Thien et al., (2011) and Wells et al. (2013) reported density variation along a riser near the tank center, referred to as riser 30, for different nozzle flow rates inside the 43" and 120" tanks, respectively (Table 1-2 and Table 1-3).

Table 1-2. Density Data (Specific Gravity) at Different Elevations (Thien and Greer, 2011)

Elevation ⬇	**Flow rate (gpm)**							
	7	**7.5**	**8**	**8.5**	**9**	**9.5**	**10**	**10.5**
@ 0.5 in	1.043	1.078	1.069	1.068	1.077	1.075	1.074	1.076
@ 1.5 in	1.042	1.076	1.067	1.068	1.074	1.073	1.073	1.075
@ 3.5 in	1.040	1.074	1.066	1.066	1.072	1.072	1.072	1.074
@ 5.5 in	1.038	1.071	1.064	1.065	1.071	1.070	1.070	1.073
@ 7.5 in	1.037	1.071	1.063	1.065	1.070	1.069	1.070	1.074
@ 9.5 in	1.035	1.065	1.062	1.063	1.069	1.068	1.069	1.073
@ 11.5 in	1.033	1.061	1.058	1.062	1.069	1.067	1.068	1.073
@ 13.5 in	1.029	1.049	1.053	1.059	1.065	1.064	1.067	1.072
@ 15.5 in	1.008	1.003	1.016	1.039	1.047	1.050	1.060	1.068

Table 1-3. Density Data at Different Elevations (Wells et al., 2013- 120” Tank)

Flow rate* (gpm)	**80**	**85**	**90**	**95**	**100**	**105**	**110**	**115**
@ 2 in	1.094	1.094	1.084	1.071	1.069	1.071	1.082	1.082
@ 4.5 in	1.092	1.091	1.083	1.071	1.067	1.071	1.079	1.080
@ 10 in	1.089	1.089	1.078	1.068	1.066	1.070	1.078	1.079
@ 15 in	1.086	1.085	1.076	1.067	1.065	1.069	1.076	1.076
@ 21 in	1.081	1.081	1.074	1.065	1.063	1.068	1.076	1.076
@ 26.5 in	1.074	1.074	1.070	1.063	1.062	1.066	1.073	1.073
@ 32 in	1.038	1.062	1.063	1.060	1.059	1.064	1.071	1.072
@ 37 in	1.003	1.002	1.031	1.054	1.055	1.060	1.069	1.069
@ 42.5 in	0.982	0.994	0.971	1.003	1.040	1.043	1.053	1.059
Flow rate* (gpm)	**120**	**125**	**130**					
@ 2 in	1.084	1.084	1.084					
@ 4.5 in	1.083	1.083	1.083					
@ 10 in	1.081	1.081	1.081					
@ 15 in	1.080	1.081	1.081					
@ 21 in	1.078	1.080	1.080					

Test 2011 (Complex five-part simulant)

Additional information about this test, as compared to previously reported data, is normalized cloud height data, as shown in Table 1-4. HC refers to normalized cloud height (maximum height which particles reach in the tank) and HL is the liquid height that depends directly on nozzle jet velocity. These parameters can be found as output of a simulation study.

Table 1-4. Metrics Measured for 5-Part Simulant, (Wells et al., 2013)

metric ⬇	**43.2” tank Nozzle vel. (ft/s)**				**120” tank Nozzle vel. (ft/s)**			
	16.9	**22.1**	**24.8**	**27.6**	**22.3**	**28.7**	**31.9**	**35.4**
HC/HL	0.76	0.92	1.01-0	1.005	0.67	0.83	0.89	0.97

Test 2013 (Four-Part/Base Simulant in Suspension)

As mentioned before, this test had a very populated matrix and was done for three capture velocities, CV=3.8, 7.3, and 11.3 ft/s, and five jet rotation rates. However, available information was limited to two tests: Test 2013-1 with capture velocity CV=7. 3 ft/s, typical solid (density=2721 kg/m^3), modified high supernatant (density=1.32 g/mL, viscosity=8 cP), and CV=7.3 ft/s; and Test 2013-2 with capture velocity CV=11. 3 ft/s, typical solid (density=3584.2 kg/m^3), high supernatant (density=1.37 g/mL, viscosity=15 cP), and CV=11.3 ft/s. One thing in common between these tests is that only 13% of the initial weight of slurry was solid, according to Lee and Thien (2013). Additional information is related to extracted data from Test 2013-1 and ECR data for Test 2013-2, as shown in Table 1-5 to Table 1-7.

Table 1-5. Batch and (Pre-transfer) UDS Concentrations in 2013 Test, CV = 7.3 ft/s (Wells et al., 2013)

Tank Diameter	43.2”		120”	
Nozzle vel.* (Flow rate) † ➡	18.3 (7)	34.8 (13)	28.9 (90)	38.16 (120)
Element ⬇	UDS concentration (lb/gal) ⬇			
$Al(OH)_3$	0.99 (0.74)	1.11 (1.0)	0.87 (0.85)	1.14 (0.88)
Sand	0.28 (0.10)	0.20 (0.16)	0.20 (0.2)	0.21 (0.18)
ZrO_2	0.11 (0.10)	0.15 (0.16)	0.14 (0.15)	0.11 (0.1)
SS	0.00081 (0.0018)	0.051 (0.050)	0.0128 (0.028)	0.147 (0.056)
Total batch trns¤	0.59	0.74	0.66	0.80

* values in ft/s † values in gpm

¤ Percentage of total batch transferred compared to the initial solid content

Table 1-6. ECR Data Based on Length and Depth of Cleaning, Test 2013, CV = 7.3 ft/s (Rector 2013)

Vessel	Nozzle vel. (ft/s)	Flow (gpm)	Length (in)	Depth (in)	Raduis (in)
120	38.16	120	35	8	38.2
120	28.9	90	64	19	53.9
43.2	34.8	13	11	1 1/2	23.7
43.2	18.3	7	28	8	18.9

Table 1-7. ECR Data for 2013 Test, CV = 11.3 ft/s (Wells et al., 2013)

Tank ID	43.2” tank				120” tank			
Nozzle vel. (ft/s)	**18.2**	**22.1**	**26.1**	**33.9**	**28.7**	**31.1**	**33.5**	**38.3**
ECR (in)	14.72	16.05	16.84	19.11	46.01	48.27	50.41	53.82

Baseline simulation data

Existing simulations of waste retrieval in literature used single and multiple-particle solid simulants. In single-particle studies, ZrO_2 with 6 wt% in water was used in both scaled (43.2” and 120”-diameter) and full-size tanks, as reported by Wells et al. (2011&2013) and Rector et al. (2010). Data regarding HCL and UDS concentrations are available in Wells et al. (2013), as shown in Table 1-8.

Table 1-8. Cloud Height Data for Test 2010, 6 %wt ZrO_2 (Wells et al., 2011)

metric ⬇	**43.2” tank Nozzle vel. (ft/s)**			**120” tank Nozzle vel. (ft/s)**			**Full scale Nozzle vel. (ft/s)**	
	13	**19**	**22**	**22**	**25**	**28**	**48**	**59**
HC/HL	-	0.99	-	-	0.87	0.98	0.82	0.94
UDS	-	0.51	-	-	0.61	0.55	0.64	0.56

A simulation study using a four-particle simulant (Test 2013-1) was conducted by Rector et al. (2013), and information about UDS concentration, ECR, and cleaning radius was provided to FIU through private communications with DOE. These simulation data were carefully reviewed to complete the information about problem setup which was not found in the literature and also to distinguish potentials for accuracy and performance improvements.

Table 1-9. Batch and (Pre-transfer) UDS Concentrations in 2013 Test, CV = 7.3 ft/s (Wells et al., 2013)

Tank Diameter	**43.2”**		**120”**		**Full-Scale DST (AY-102)**
Nozzle vel.,* (Flow rate) † ➡	18.3 (7)	34.8 (13)	28.9 (90)	38.16 (120)	58.8 (5182)
Element ⬇	**UDS concentration (lb/gal)** ⬇				
$Al(OH)_3$	0.9	1.02	0.96	1.06	1.09
Sand	0.18	0.29	0.26	0.31	0.271
ZrO_2	0.13	0.18	0.17	0.19	0.115
SS	0.0037	0.081	0.038	0.12	0.172
Total batch trns¤	0.59	0.74	0.66	0.80	
* values in ft/s † values in gpm ¤ Percentage of total batch transferred compared to the initial solid content					

Table 1-10. ECR Data, Test 2013, CV = 7.3 ft/s, (Rector 2013)

Vessel	**Flow (gpm)**	**Length (in)**	**Depth (in)**	**ECR/D**
120”	120	32	10	-
120”	90	56	16	-
43.2”	13	9	2 1/2	-
43.2”	7	24	7	-
Full (900”)	5182	-	-	0.55

Geometrical Dimensions and Operational Conditions

FIU reviewed key setup parameters related to previously-mentioned tests in order to obtain consistent and accurate information about operational conditions and geometrical dimensions of system elements such as tank, nozzle, and transfer line intake for both scaled tanks. FIU’s review concludes that the same scaled tanks were used for various tests. Relevant data were extracted from Lee and Thien (2013) and Jensen et al. (2012), as shown in Table 1-11.

Table 1-11. Geometrical Dimensions for Tank and Accessories (Lee and Thien, 2013)

Property	**43.2” tank**	**120” tank**	**Full scale**$^{€}$
Tank internal diameter (m)	1.1	3.05	22.9
MJP’s Nozzle Diameter (m)	0.0071	0.0203	0.152
MJP’s Nozzle Elevation (m)	0.0218	0.0610	0.457
MJP’s Suction Diameter (m)	0.0135	0.0373	0.279
MJP’s Suction Elevation (m)	0.0061	0.0170	0.127
MJP’s Axial Offset in 0° & 180° angles (m)	0.323	0.8840	6.71
Transfer Pump Suction Inlet Diameter (m)	0.0064* 0.0071†	0.0081* 0.0081†	0.057-0.061* 0.057†
Transfer Line Diameter (m)	0.0095* 0.0079†	0.0095* 0.0095†	0.078* 0.078†
Transfer Pump Suction Velocity (m/s)	1.16 – 3.44*	1.16 – 3.44*	2.21 – 3.44†
Transfer Line Velocity (m/s)	0.53-1.56$^{¤*}$ 0.94-2.78$^{¤\dagger}$	0.84-2.50$^{¤*}$ 0.84-2.50$^{¤\dagger}$	1.19-1.86$^{¤*}$ 1.19-1.86$^{¤\dagger}$
Transfer Line flow rate (gpm)	1.15-2.17	1.5-2.8	90-140
Transfer Pump Suction Elevation (m)	0.0071	0.0203	0.152
Transfer Pump Axial Offset in 90° angles (m)	0.0884	0.244	1.83

€ Tank AY-102

* Lee and co-authors (2012, 2013). $^{¤*}$ Calculated based on data from Lee and co-authors (2012, 2013)

† Jensen et al. (2012) for SSMD $^{¤\dagger}$ Calculated based on data from Jensen et al. (2012)

FIU then presented the work performed over the last six months regarding data collection from various experimental and simulation studies to WRPS. As a critical step, it was necessary to reconfirm some technical specifications, acquire inaccessible data related to various tests, and receive critical advice regarding preferences and priorities that might exist. A poster was also created which focuses on non-Newtonian flow modeling and will be presented at the 2017 Waste Management Conference in Phoenix, AZ. In addition, investigations on suspension rheology modeling in STAR-CCM+ was performed using a simple jet-induced erosion modeling.

Suspension Rheology Model in STAR-CCM+

In fluid-particle mixtures, the presence of particles can cause non-linear viscoplasticity behavior. Viscosity in these systems can be significantly affected by solid volume fraction. It is possible to simulate the effect of the solid volume fraction using a suspension rheology model in two-fluid (Eulerian-Eulerian) multiphase flow modeling. In this modeling approach, both solids and liquids are continuous phases, where one phase (liquid) is the carrying phase and the particle is dispersed (being carried). In STAR-CCM+, the Eulerian-segregated model provides this ability. According to STAR-CCM+, the quantity relative viscosity can be introduced, which is defined by Eq. 1. Among several models that exist in the application, the shear thinning model option (Eq. 2 to Eq. 4) is a volume fraction-dependent Herschel-Buckley model, which represents a viscoplastic fluid.

$$\eta_r = \eta / \eta_c. \qquad \text{Eq. 1}$$

$$\eta_r(\dot{\gamma},\Phi)=\frac{\tau_y}{\dot{\gamma}}-\eta_{r\infty}(\Phi)-\left[\eta_{r0}(\Phi)-\eta_{r\infty}(\Phi)\right].\left(1-(\lambda.\dot{\gamma})^2\right)^{\frac{n-1}{2}} \qquad \text{Eq. 2}$$

$$\eta_{r0}(\Phi)=1-2.5\Phi\left(1-\frac{\Phi}{\Phi_{m0}}\right)^{-1}-K_{s0}\left(\frac{\Phi}{\Phi_{m0}}\right)^{2}\cdot\left(1-\frac{\Phi}{\Phi_{m0}}\right)^{-2} \qquad \text{Eq. 3}$$

$$\eta_{r\infty}(\Phi)=1-2.5\Phi\left(1-\frac{\Phi}{\Phi_{m\infty}}\right)^{-1}-K_{s\infty}\left(\frac{\Phi}{\Phi_{m\infty}}\right)^{2}\cdot\left(1-\frac{\Phi}{\Phi_{m\infty}}\right)^{-2} \qquad \text{Eq. 4}$$

Here, η_r, $\dot{\gamma}$, Φ, τ_y, λ, and k_s are relative viscosity, shear rate, solid volume fraction yield stress, relaxation time, and contact contribution, respectively. Indices 0 and ∞ refer to zero shear and infinity shear states. According to Willenbacher and Georgieva (2013), the particle arrangement can be different in high and zero shear and this affects the maximum packing density of the particles. This equation is an extension to the classical model of Einstein (1906) and Quemada (1977) for suspension rheology. This model is not limited to any specific regime of flow. An explanation of the different terms is available in Morris and Boulay (1999).

Yield stress (τ_y) in suspension, present in Eq. 2, may also depend on solid content. According to Willenbacher and Georgieva (1995) and Darbouret et al. (2005), dependency is on the solid content raised to the 3rd power and an inverse of particle size squared. Leong et al. (1995) studied yield stress values for a zirconium oxide-water suspension under the influence of pH levels (by addition of HNO_3 and KOH). FIU extracted yield stress values in different solid loading conditions but at constant pH levels (pH = 5.5, 6.0, 7.0, 8.0, and 8.5) and it was observed that a 3rd order polynomial could perfectly fit the data for all pH levels, which confirmed the observations of the literature references (Leong et al., 1995; Darbouret et al., 2005). However, large discrepancies were observed between the yield stress values reported by Wells et al. (2013).

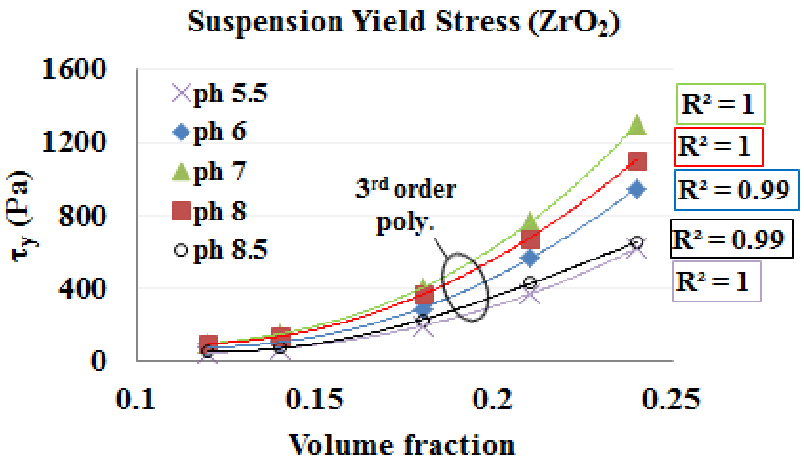

Figure 1-1. Dependency of yield stress of ZrO_2-water suspension.

In STAR-CCM+, shear thinning uses a formula based on the square of the solid volume fraction. Particle size is not present explicitly, as shown by Eq. 5.

$$\tau_y = \tau_{y0}\left(\frac{\Phi}{\Phi - \Phi_{my}}\right)^2 \qquad \text{Eq. 5}$$

Here, τ_{y0} and Φ_{my} are a pre-factor of order unity and maximum packing ratio in yield condition, respectively.

Use of Suspension Rheology Model

Implementation of the suspension rheology in modeling of a jet-induced erosion problem was possible with small time step sizes ($\Delta t = 5\times10^{-6}$ sec). Application of this model is still in progress, as it was observed that a larger time step size led to divergence. Simulation modeling without use of suspension rheology is possible with $\Delta t = 1\times10^{-3}$ sec, which is significantly faster. More investigation is needed to observe the prominent differences between these simulation cases.

Next, FIU created a three dimensional model of 43"-diameter tank with all air lift circulators (ALCs), mixer jet pumps (MJPs), a transfer line, and a sediment layer. In addition, a two-dimensional model was created to check all boundary conditions and assumptions and also to track the convergence of simulation runs. Some investigations with single phase flow in the two-dimensional model was performed as well. FIU presented improved RANS simulation results using a modification model in quasi-direct numerical simulation (Q-DNS) at the Waste Management 2017 Symposium in early March.

Three-dimensional model for 43"-diameter tank

A three-dimensional model of the 43"-diameter tank was created in Star-CCM+. This model, as shown in Figure 1-2, shows the initial condition where a supernatant fluid sits on a layer of solid and mixing/retrieval has not started. The interface between the upper (supernatant fluid) and the lower domain (sediment layer) along with ALCs, a transfer line, and a nozzle of a mixer jet pump is also shown.

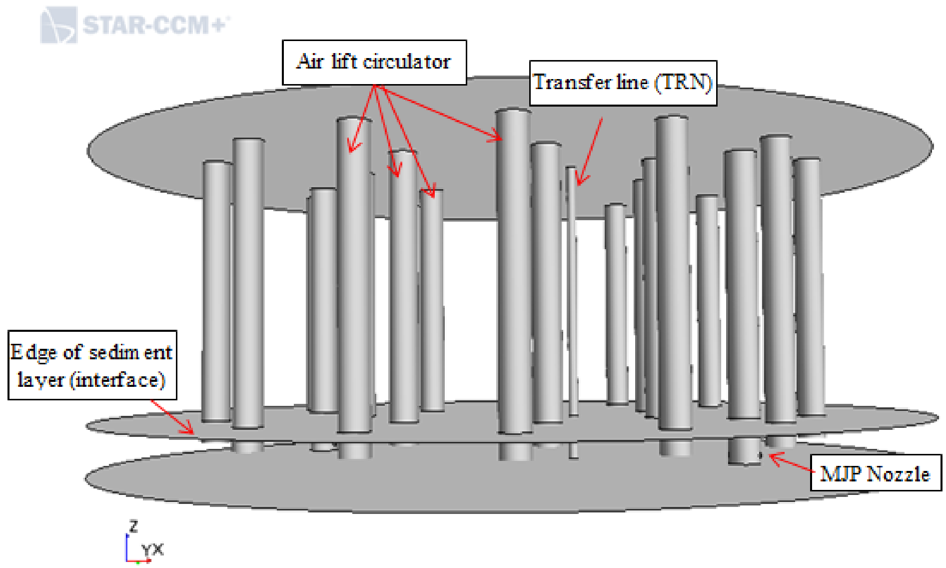

Figure 1-2. Scaled tank constructed in STAR-CCM+.

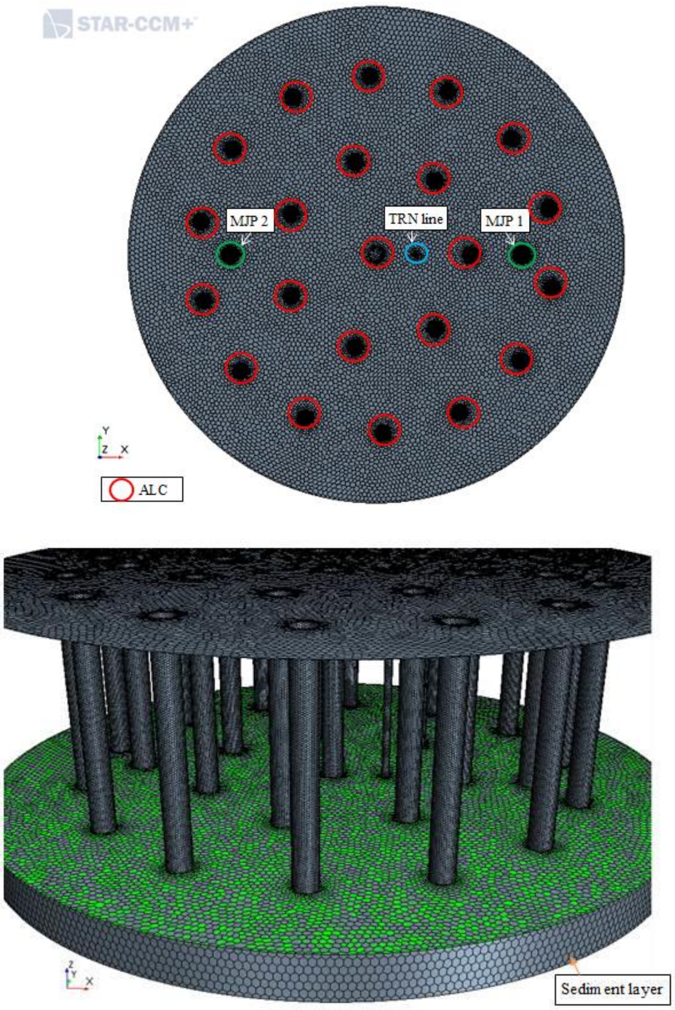

Figure 1-3. Mesh created using 2.7 million cells for the 43” tank in STAR-CCM+.

Two-dimensional model for 43”-diameter tank

A two-dimensional model was created for quick assessments of boundary conditions and the effect that the MJP suction port would have on convergence of simulation results. The two-dimensional model was created based on a plane passing through the 43”-diameter tank at a 0° angle. The model was created with fixed nozzles for simplicity and meshed with polyhedral elements as shown in Figure 1-4. This figure shows different boundaries which include the interface, MJP nozzle, MJP suction, and transfer line suction. A velocity value at the nozzle was set to 13 ft/sec (3.96 m/s) according to Wells et al. (2011). Pressure values at suction ports of both the transfer and MJP pumps were not explicitly mentioned in the reports reviewed thus far. For the MJP, the pressure values at the suction port must be consistent with the nozzle flow rate, which is 6.5 gpm according to Rector et al. (2010). For the transfer pump, this value must be consistent with capture velocity of 7.3 ft/s (2.2 m/s). One possible approach was to use a stagnant inlet type boundary condition where static pressure was set equal to the negative of the dynamic pressure. This condition might not be accurate because of conditions in the vicinity of these suction ports. Another possible approach was to use pressure outlet boundary conditions with the target mass flow rate. Therefore, mass flows were calculated based on the average tank density of 1.057 kg/m^3. A small change in density (between 1.01 and 1.08 according to Wells et al., 2013) justifies the use of this representative density value. The mass flow rate values were obtained as 0. 31 kg/s and 0.43 kg/s at suction ports of the transfer line and MJP, respectively.

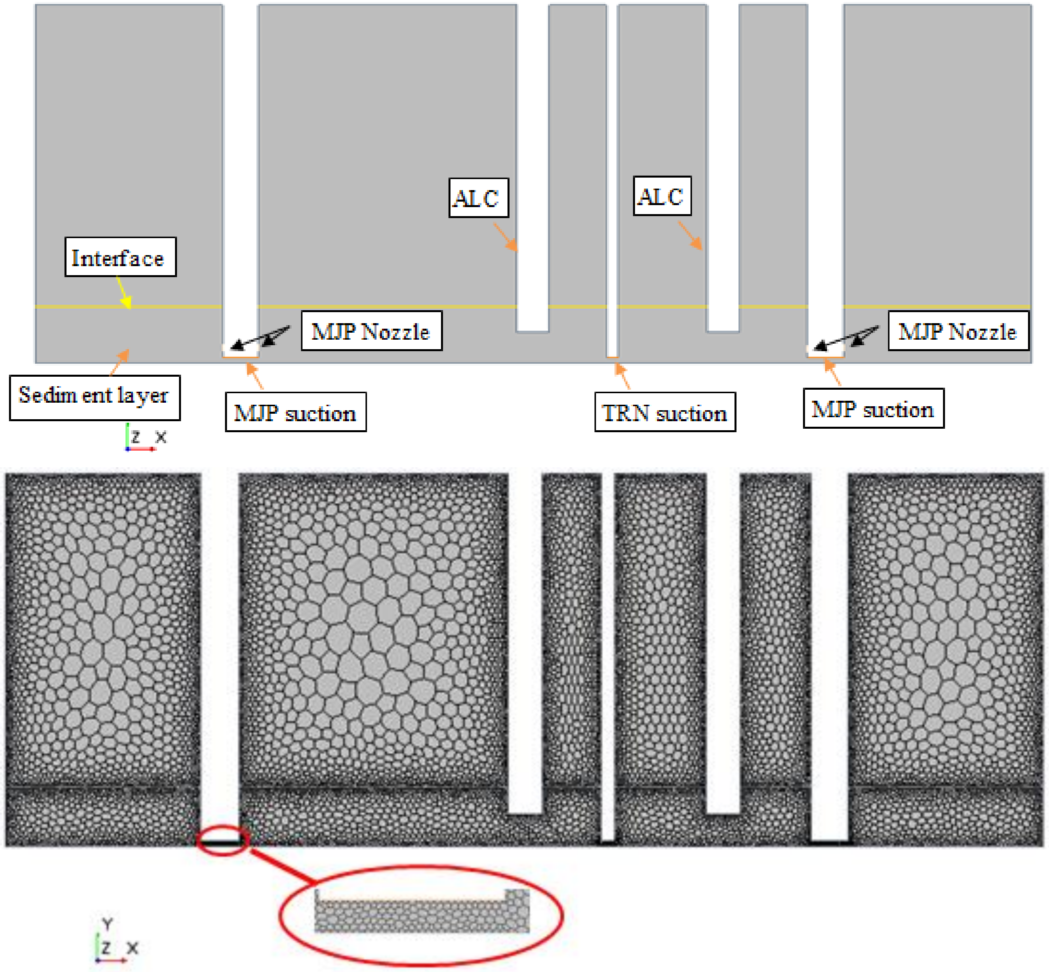

Figure 1-4. Two-dimensional domain and the mesh created for the 43" tank in STAR-CCM+.

Two-dimensional simulations with fixed jets

A two-dimensional simulation in steady and single-phase modes with fixed jets and the standard k-ε model was the first steps in this work. In this step, the nozzle and suction ports of the MJPs were not connected using a field function for mass flow rate. Instead, FIU assigned a constant value for the target mass flow rate that represents a steady situation for this step of the work. In reality, these ports are connected by a slurry pump. Automatic connection using a field function guarantees that the same solid and liquid concentration exists at both ports and the simulation can capture the gradual removal of particles and liquid from the tank.

This simulation encountered difficulties in convergence and fluctuation of results were observed. The contour of velocity magnitude, shown in Figure 1-5, indicated the presence of large vortices in the entire domain as a result of jet penetration effects. The reported values for mass flow rate were 0.163 and 0.49 kg/s in the suction ports of the transfer line and MJP, respectively, which were slightly different from the target values. However, the results don't show long straight penetrations of jets as expected and the jets are immediately attached to the tank bottom in a very short distance, according to the vectors of velocity shown in Figure 1-5. In addition, the results show a strong radial velocity just under the MJPs (shows as red vectors) where strong upward motion was expected to occur due to suction effects. By looking at any of the MJPs, it was observed that this large velocity was created as a result of backward flow of one of the jets and realignment with another jet, which were supposed to be moving oppositely in radial directions. The reason for this backward flow behavior is unclear. FIU also plotted three velocity profiles at these suction ports for qualitative and quantitative assessments.

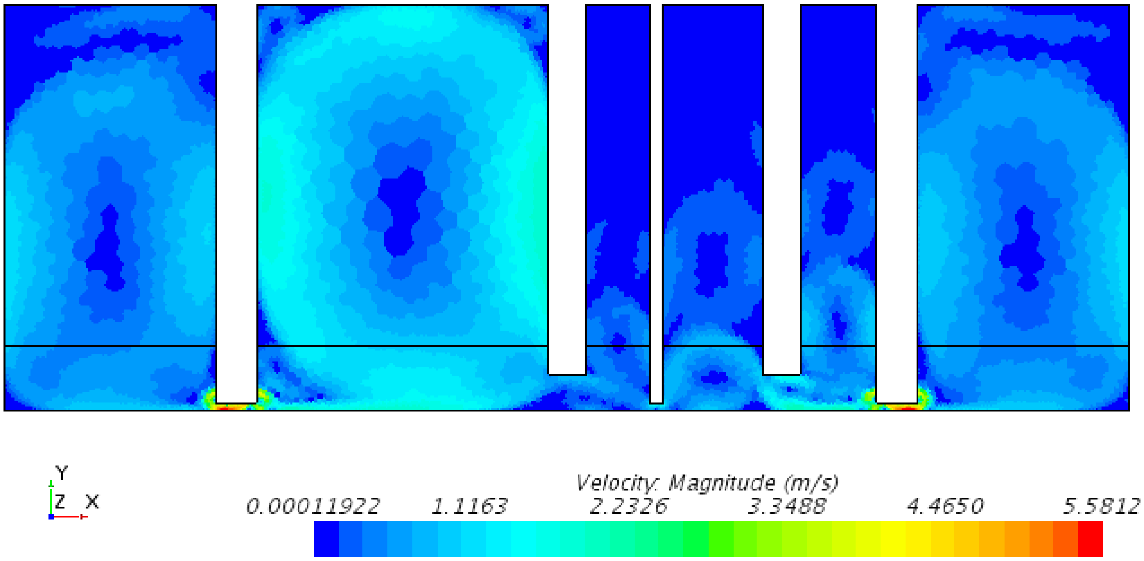

Figure 1-5. Velocity contour in 2-d simulation of 43” tank with MJP suction ports.

As Figure 1-7 shows, symmetric profiles were not observed at any of the ports. The calculated average velocity value at the transfer line was 1.78 m/s which was slightly different from the target value of 2.2 m/s. This discrepancy could be caused by the rectangular configuration of the ports, pipes, and the tanks two-dimensional domain as opposed to circular configurations.

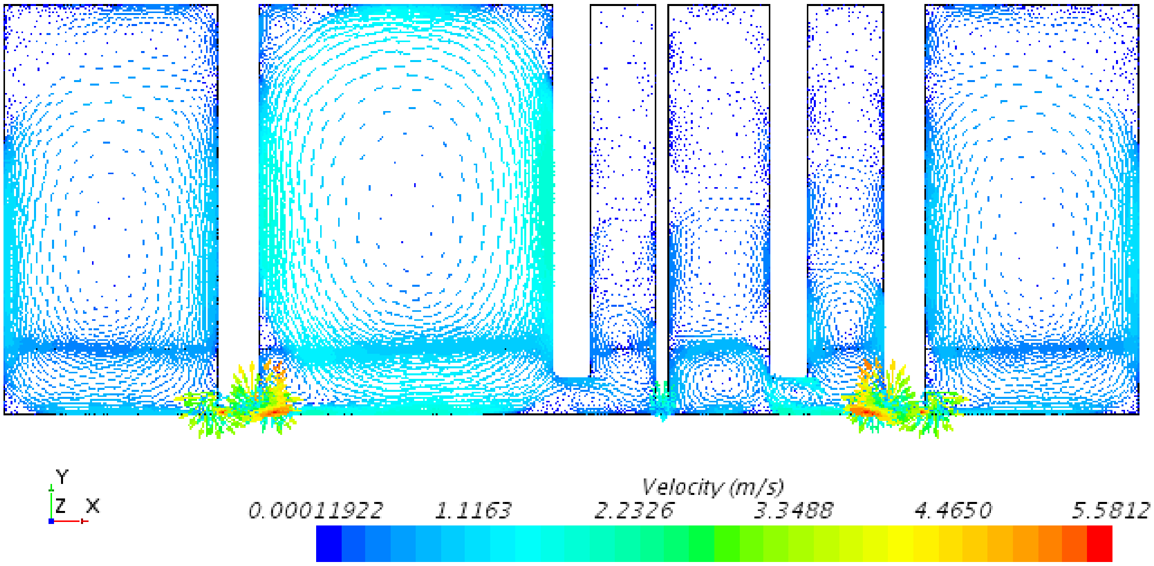

Figure 1-6. Velocity vectors in 2-d simulation of 43” tank with MJP suction ports.

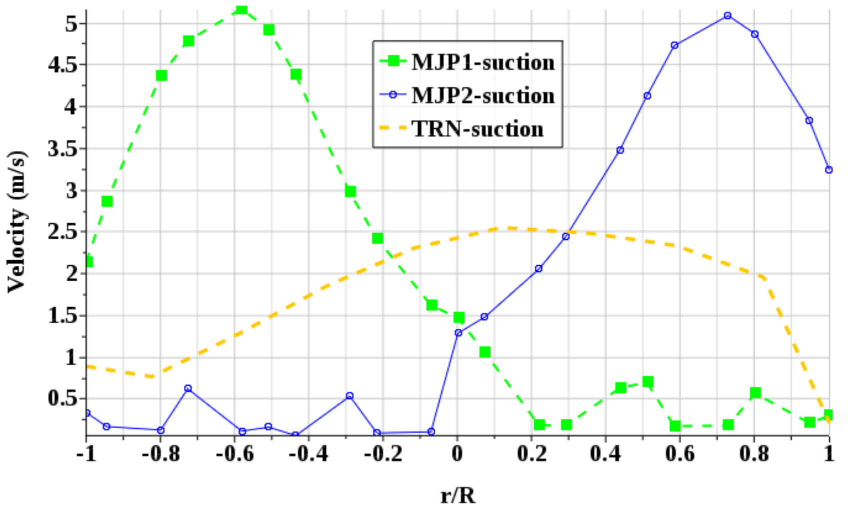

Figure 1-7. Velocity profile at MJP and TRN suction ports in 2-d simulation of 43” tank with MJP suction ports.

The effect of treating the suction ports of MJPs as closed (wall boundary condition) was also studied. The purpose was to see if a strong asymmetry was caused by the presence of the MJP’s suction ports. This simulation with MJP suction ports set to wall boundary conditions converged to results that did not fluctuate. As shown in Figure 1-8, only a dominant large vortices existed in the domain which was located between the left MJP and the central ALC. A display of velocity vectors in Figure 1-9 showed penetration of two opposing jets in the domain; however, an immediate backflow of one of the two jets was observed for either of the MJPs. Investigations are ongoing to discover the cause of this flow behavior. Another observation is that a high-velocity region under the suction ports of the MJPs and transfer lines were not observed which was not the case in the previous simulation. Also, the velocity profiles at the suction port of the transfer line was symmetrical, according to Figure 1-10.

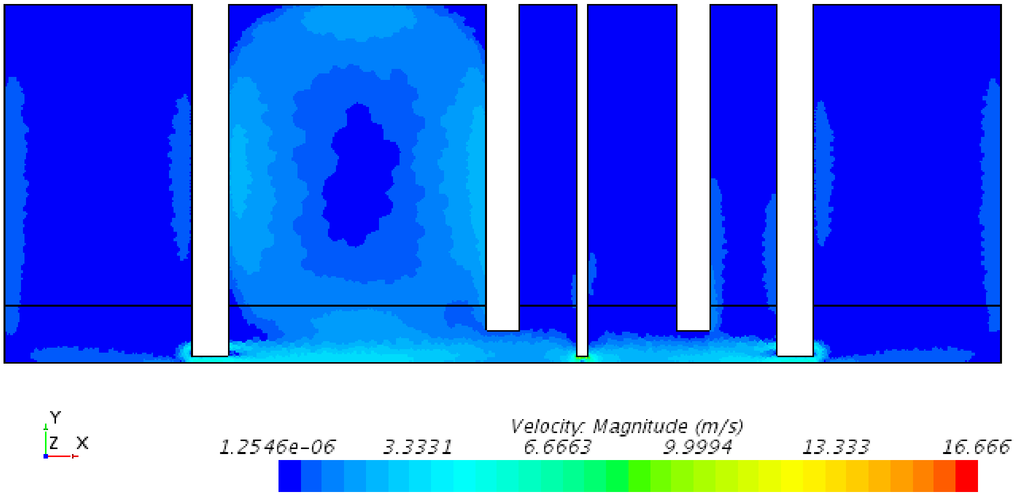

Figure 8. Velocity contour in 2-d simulation of 43” tank without MJP suction ports.

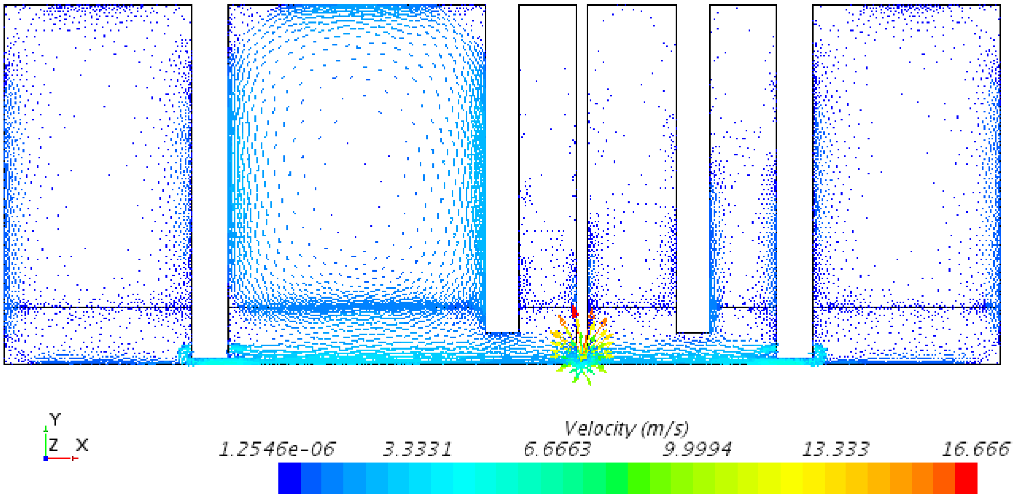

Figure 9. Velocity vectors in 2-d simulation of 43" tank without MJP suction ports.

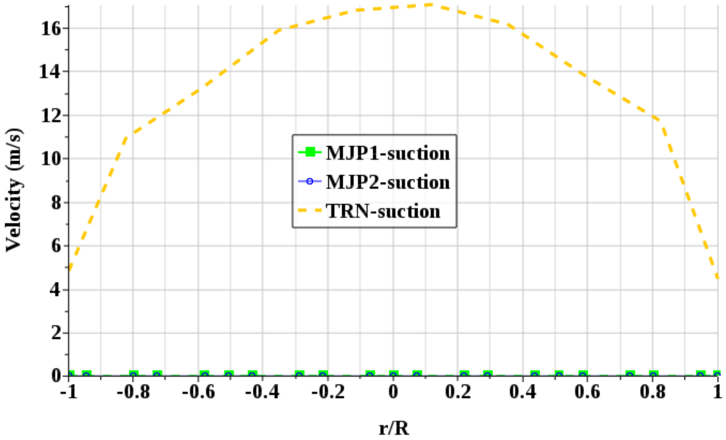

Figure 10. Velocity profile at MJP and TRN suction ports in 2-d simulation of 43" tank without MJP suction ports.

This findings clearly show that the presence of the MJP suction port was responsible for the confronted convergence asymmetry issues. This could be due to improper settings or numerical limitations caused by extreme closeness of the ports to the tank bottom and MJP nozzles. In the next steps, the effects of mesh and other parameters such as solution schemes on the confronted issues will be investigated. The aim will be to obtain converged solutions with the presence of MJP suction ports that are connected to MJP nozzles via a field function for mass flow rate. After this step, a rotating jet created via sliding mesh will be added to the model and the same investigations will be performed.

References

B.E. Wells, J.A. Fort, P.A. Gauglitz, D.R. Rector, P.P. Schonewill, 2013, Preliminary Scaling Estimate for Select Small Scale Mixing Demonstration Tests.

B.E. Wells, P.A. Gauglitz, D.R. Rector, 2011, Comparison of Waste Feed Delivery Small Scale Mixing Demonstration Simulant to Hand Waste, PNNL-20637).

F. Mercier, S. Bonelli, P. Pinettes, , F. Golay, F. Anselmet, and P. Philippe, Comparison of Computational Fluid Dynamics Simulation with Experimental Jet Erosion Results, J. Hydraul. Eng., 2014, 140(5): 04014006.

M.G. Thien, D.A. Greer., P. Townson. 2011, Estimating High Level Waste Mixing Performance in Hanford Double Shell Tanks – 11193, WM2011 Conference, February 27 - March 3, 2011, Phoenix, AZ.

M.R. Powell, G.R. Golcar, C.R. Hymas, R.L. McKay. 1995. Fiscal Year 1993 1/25th-Scale Sludge Mobilization Testing. PNL-10464, Pacific Northwest Laboratory, Richland, Washington.

D. J. Adamson, P. A. Gauglitz, 2011, Demonstration of Mixing and Transferring Settling Cohesive Slurry Simulants in the AY-102 Tank, SRNL-STI-2011-00278, Rev. 0.

J. Jensen, P. Townson, M. Vanatta, 2012, Small Scale Mixing Demonstration Batch Transfer and Sampling Performance of Simulated HLW – 12307.

J. Jensen, P. Townson, M. Vanatta, 2012, Small Scale Mixing Demonstration Batch Transfer and Sampling Performance of Simulated HLW – 12307, WM2012 Conference, 2012, Phoenix, Arizona, USA.

K. P. Lee, M. G. Thien, 2013, Evaluating Feed Delivery Performance In Scaled Double-Shell Tanks – 14070, WRPS-55760 –FP, Revision 0.

K.P. Lee, 2012, One System Waste Feed Delivery Mixing and Sampling Program System Performance Test Plan, RPP-PLAN-52623, Rev. 0.

N. Willenbacher and K. Georgieva, 2013, Rheology of Disperse Systems, DOI: 10.1002/9783527654741.ch1.

A. Einstein, “Eine neue Bestimmung der Moleküldimensionen”, 1906, Ann. Phys 19, 289M.

D. Quemada, “Rheology of concentrated disperse systems and minimum energy dissipation principle I. Viscosity-concentration relationship”, Rheol. Acta., 16 (1977) 82

J.F. Morris, F. Boulay, 1999. "Curvilinear flows of noncolloidal suspensions: The role of normal stresses", Journal of Rheology, 43, p. 1213

Y.K. Leong, P.J. Scales, T.W. Healy, D.V. Boger, 1995, Effect of Particle Size on Colloidal Zirconia Rheology at the lsoelectric Point, Journal of American Ceramic, SOC., 78 181 2209-12 (1995).

M. Darbouret, J. Cournil, M. Herri, 2005. "Rheological study of an hydrate slurry for air conditioning application", Fifth International Conference on Gas Hydrates (ICGH 5), Tromdheim, Norway, page 2005.

D.R. Rector, M.L. Stewart and J. Bao, 2010, Modeling of HLW Tank Solids Resuspension and Mixing Processes-12337, WM2012 Conference, Feb. 26 - March 1, 2010, Phoenix, AZ.

Subtask 17.1.2: Computational Fluid Dynamics Modeling of a Non-Newtonian Fluid Undergoing Sparging for Estimating PJM Mixing Times

During this reporting period, it was decided that a simulation of the bubble column developed by McClure et al would be replicated as detailed in their work “Development of a CFD Model of

Bubble Column Bioreactors: Part Two – Comparison of Experimental Data and CFD Predictions" published in 2013. This simulation is already validated by experimental data and would provide a foundation on which this research can progress. The simulation was run using ANSYS CFX so efforts were made to get acquainted with the workflow and user interface. The virtual domain and physics models were implemented as detailed in the paper. The physical domain as well as the current model replicating the simulations are shown in Figure 1-11 below:

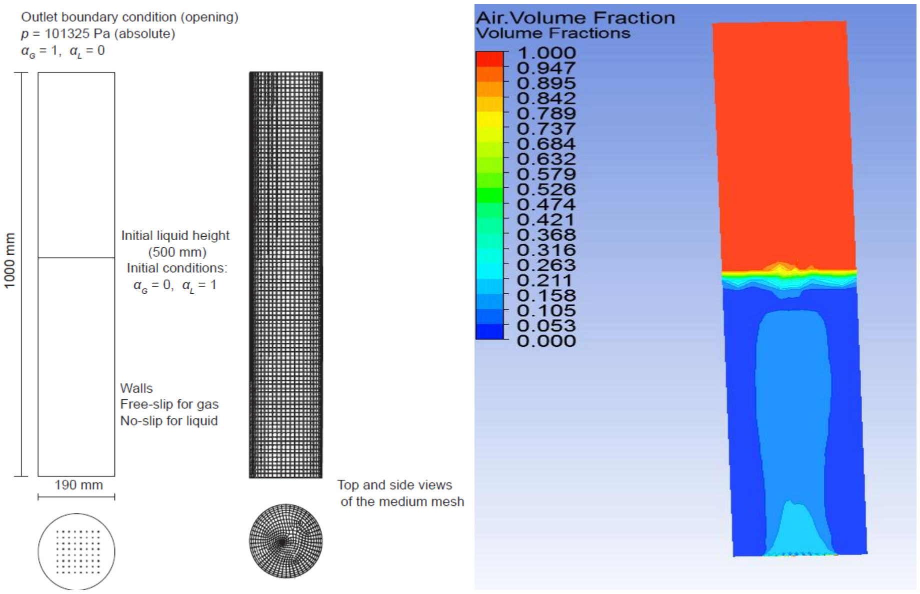

Figure 1-11. (a) Mesh, domain, boundary and initial conditions detailed by McClure et al. (left) and current simulation volume fraction profile at 5s (right).

The mesh count, physical domain, and initial conditions were replicated exactly. The inlet boundary condition in the paper was modeled by 117 point mass sources while the current simulation physically models 117 circular inlets. The simulation was run for 10 seconds as detailed in the paper. The metrics by which to compare the current simulation and that of the paper are water velocity and air volume fraction profiles at particular locations of the cylindrical domain. The comparison between the developed simulation and the one detailed in the paper is shown in Figure 1-12 below:

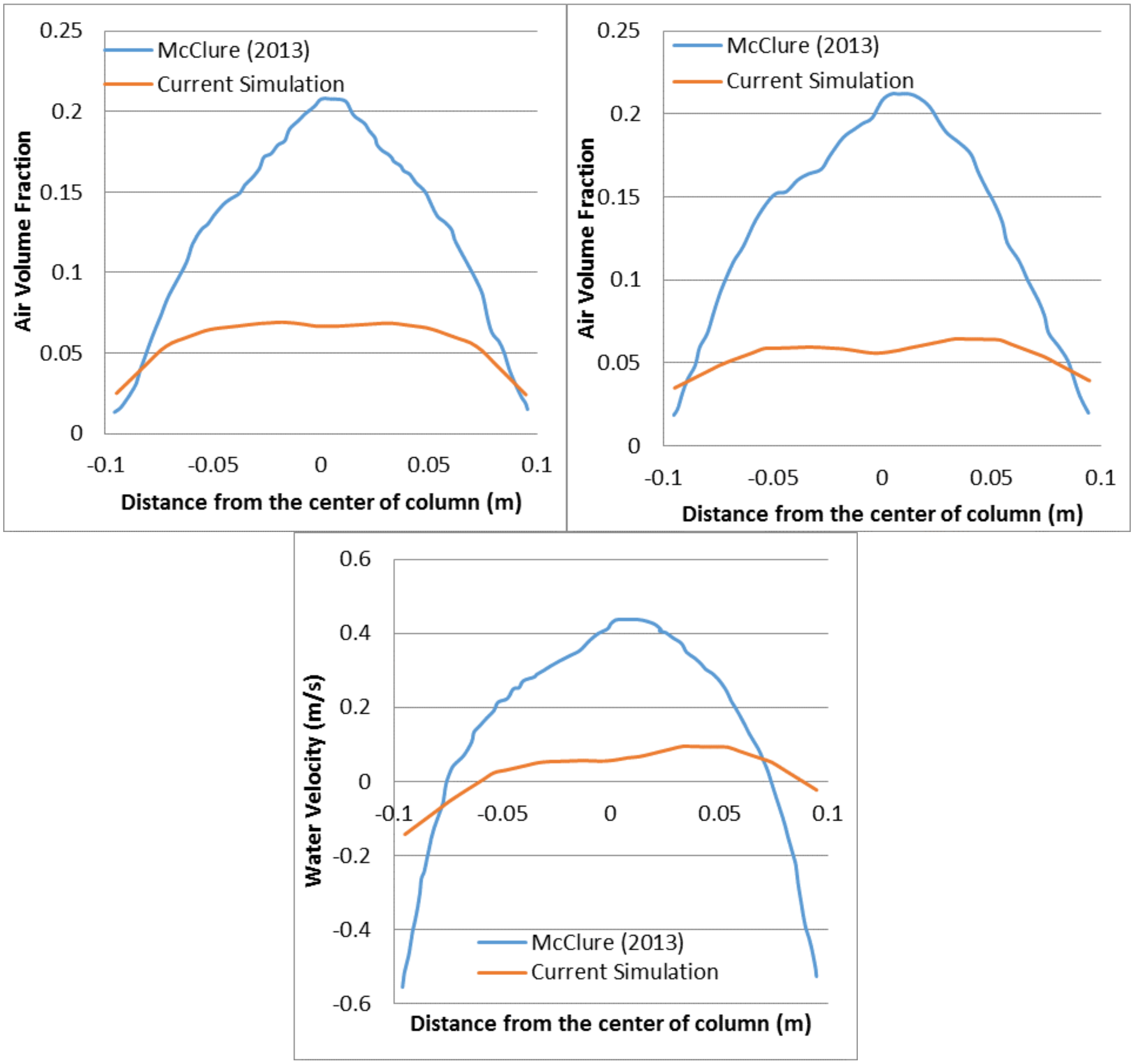

Figure 1-12. Simulation comparison between current simulation and simulation being replicated. Gas volume fraction comparison at 450 mm above spargers (top left), gas volume fraction comparison at 270 mm above spargers (top right), and water velocity profile comparison at 450 mm above spargers (bottom).

It can be observed that the volume fraction and water velocity profile are under predicted by the model. This indicates that there is not enough mass flow rate of air at the inlets.

Additional attempts at modeling the bubble column developed by McClure et al. (2013) were next made by adjusting the mass flow rate. Below are the results:

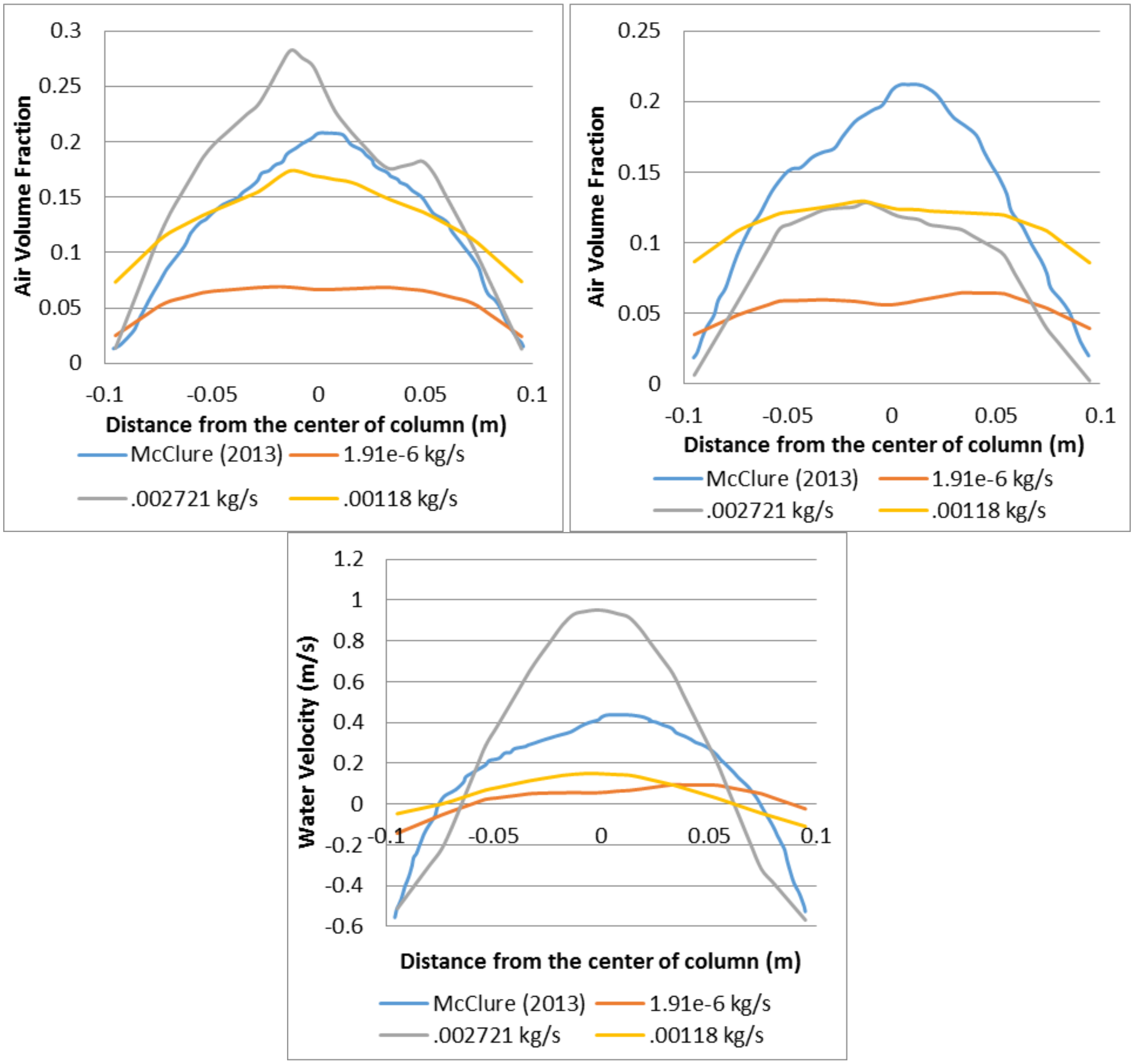

Figure 1-13.-Simulation comparison between current simulation and simulation being replicated: Gas volume fraction comparison at 270 mm above spargers (top left), gas volume fraction comparison at 450 mm above spargers (top right), and water velocity profile comparison at 450 mm above spargers (bottom).

Each mass flowrate corresponds to a different assumed inlet area. This descrepancy is born out of the language used in the paper. McClure et al. (2013) claim to use a superficial gas velocity of .08 m/s in their simulation. Superficial gas velocity refers to an equivalent velocity that would occur if the mass flow rate were evenly distributed through a total area. First, the superficial gas velocity area was assumed to be of the total sparger nozzle area (1.91-6 kg/s). Second, the entire inlet area (diameter of bubble column) was assumed to be the area of interest (.002721 kg/s). Lastly, the inlet area was assumed to be the square area which the 117 sparger configuration covers. Since the superficial velocity is held constant at .08 m/s, the larger the assumed area the larger the mass flow rate that is introduced at the inlet. This can be observed in the volume fraction profiles (Figure 1-13) at the two different heights. It was observed that using the diameter of the bubble column as inlet produced too high of a volume fraction profile. When the area was decreased to the square configuration of the spargers, the volume fraction observed was comparable to experimental data at the 270 mm location. The 450 mm location was heavily under-predicted. Finally, the velocity profile for any mass flow rate attempted did not concur with the experimental data.

Due to the prolonged times that these 3D simulations take, a 2D approach was taken in order to speed up the investigation process. The 2D simulations conducted in CFX have convergence issues. Therefore, the same simulations were conducted in 2D. Below is a volume fraction profile on Fluent in 2D:

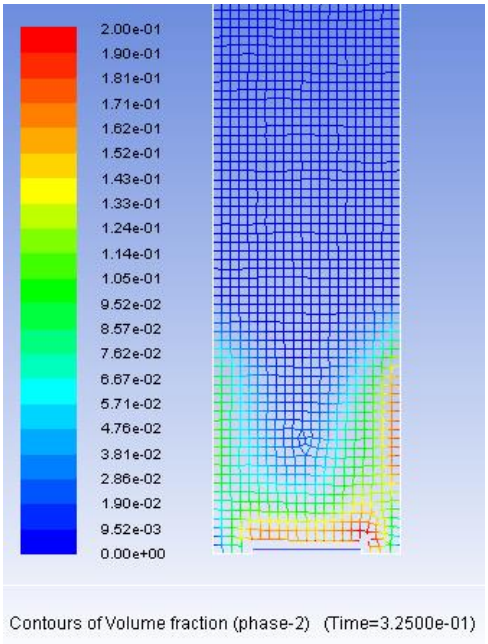

Figure 1-14. Air volume fraction in 2D fluent simulation replication of McClure (2013).

Numerous attempts have been made in order to obtain a regular parabolic profile including changes in mesh density and discretization schemes. Ways to regain the parabolic profile are being investigated. FIU evaluated the master’s thesis written by Robert Picardi (2015) which presented work in which he matched experimental data of a bubble column using 2D simulations in Fluent. Efforts at FIU have been made to replicate this simulation. The results are shown in the figures below.

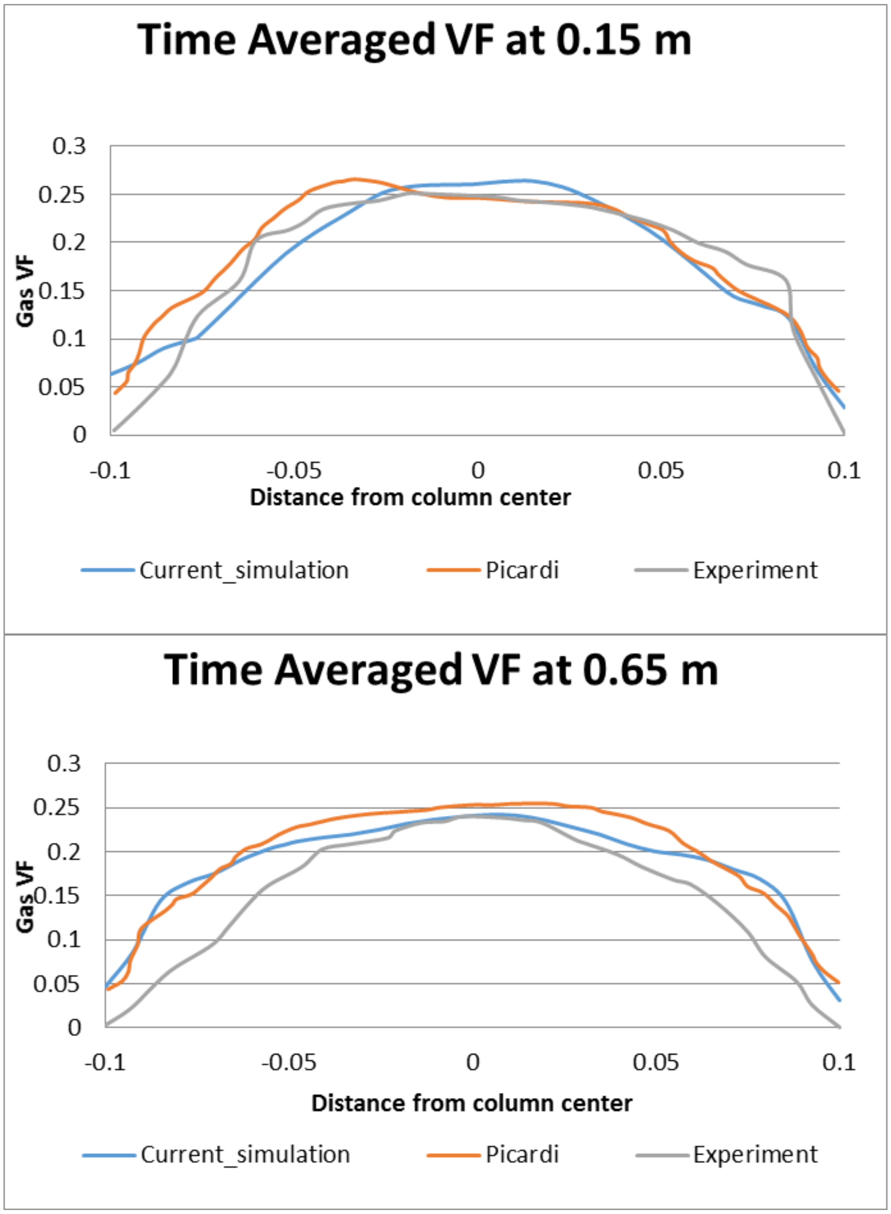

Figure 1-15. Time averaged volume fraction profile comparison at .15 (m) and .65 (m) above the spargers.

The results show that Picardi's simulation was matched well. It can also be seen that good agreement is observed in the time averaged volume fraction profiles. The experimental volume fraction profile at the height of .65 meters above the sparger has higher gradients near the wall. The experimental time averaged volume fraction profiles were obtained by averaging 80 seconds of simulation time. In addition to the volume fraction profile, the velocity profiles were compared to experimental data. This is shown below.

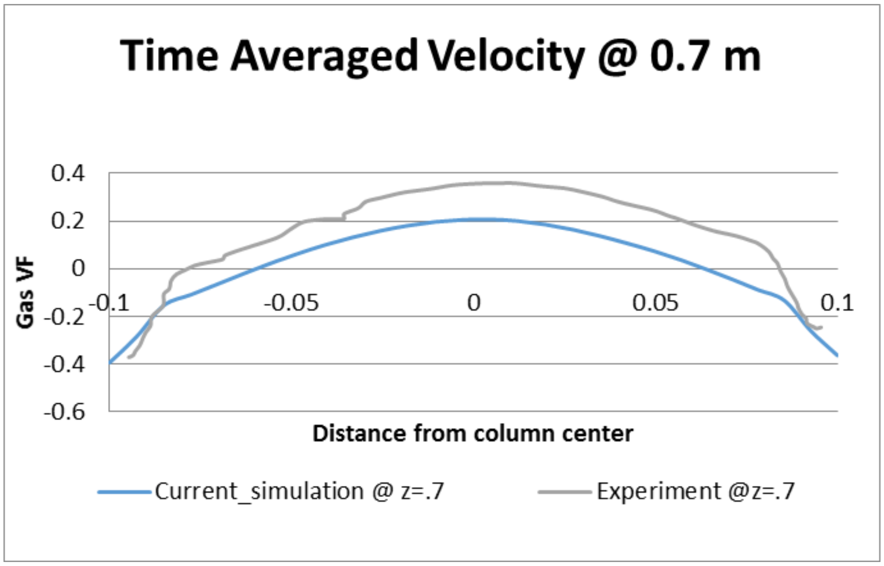

Figure 1-16. Velocity profile comparison at .7 (m) above sparger.

Looking at the velocity profile comparison at 0.7 meters above the spargers, it is observed that the maximum velocity is under predicted. The experimental results measured a mean value of 0.4 m/s while the simulation predicts about half that. The negative velocities near the wall are slightly over predicted, but are in decent agreement with experimental data. The path forward will be to address the discrepancies observed in the current 2D simulation in-order to get a better matching velocity profile. Once this is achieved, the same simulation can be used to observe what effects a Bingham plastic would add to the volume fraction and velocity profile.

Task 18: Technology Development and Instrumentation Evaluation

Task 18 Overview

The objective of this task is to assist site engineers in developing tools and evaluating existing technologies that can solve challenges associated with the high level waste tanks and transfer systems. Specifically, the Hanford Site has identified a need for developing inspection tools that provide feedback on the integrity of the primary tank bottom in DSTs. Under this task, FIU is developing inspection tools that can provide visual feedback of DST bottoms from within the insulation refractory pads and other pipelines leading to the tank floor.

As part of the Hanford DST integrity program, engineers at Hanford are also interested in understanding the temperatures inside the primary tanks and to safeguard against exceeding specified limits. These limits are set to ensure that the tanks are not exposed to conditions that could lead to corrosion of the tank walls. Previously, analysis was conducted to determine the viability of using an infrared (IR) temperature sensor within the annulus space to estimate the temperature of the inside wall of the tank. The analysis suggested that variations due to heat loss would be minimal and reasonable estimates using the sensor within the annulus is viable. Under this task, FIU is also evaluating the ability of IR sensors to detect inner tank wall temperatures via bench scale testing.

Task 18 Quarterly Progress

Subtask 18.2: Development of Inspection Tools for DST Primary Tanks

Miniature Rover Inspection Tool

FIU performed multiple redesigns of the miniature rover inspection tool. The latest version made significant changes to the internal wiring along with the adapter used to connect to the power/control box. FIU completed the design for a fully custom-made printed circuit board (PCB) to replace the internal wiring (Figure 1-17). The absence of wiring not only reduces the electrical noise that the unit experienced during operation, but also makes it more organized. It also helps to maximize the amount of space available within the unit for potential sensor integration in the future.

The previous male adapter was exchanged for a female RJ45 adapter, which allows it to be connected directly to the cable management system, instead of connecting through an Ethernet adapter that could potentially pose issues of loose connections and a bulky adapter. Furthermore, this also removes tension on the wires within the unit and diverts it to the PCB, which is firmly attached to the body of the inspection tool.

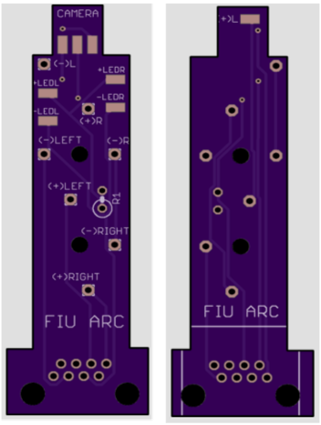

Front Back

Figure 1-17. PCB board (front and back) for the inspection tool.

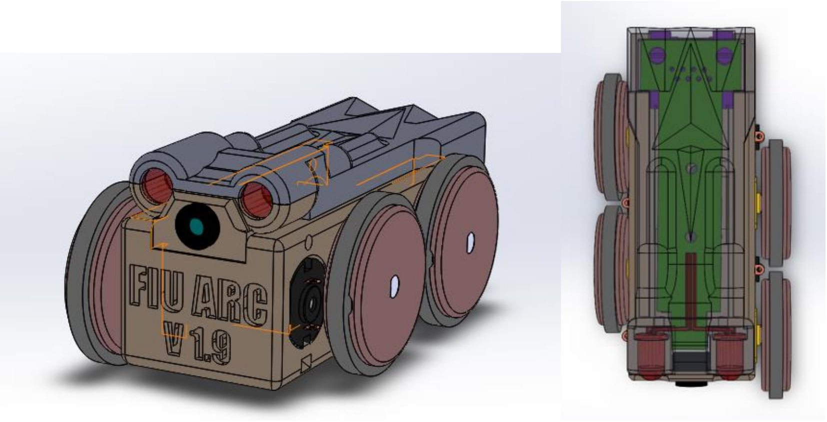

Figure 1-18. Latest version of the inspection tool. Picture on the right shows the new PCB meant to eliminate complicated wiring.

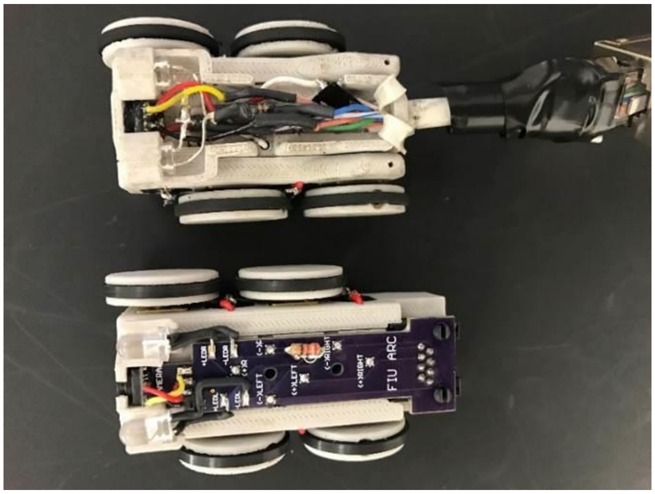

Figure 1-19. Old inspection tool with wire cluttering issue (top). New inspection tool with custom-made PCB design (bottom).

A waterproof enclosure has been designed and fabricated to house all the electronic components that interface with the inspection tool and the operator. The component includes a single board computer (SBC), analog video capture card, voltage converter and a motor controller. Once completed, the enclosure would act as the control box for the inspection tool. With all the components packed in a single enclosure, it would allow plug-and-go capability so that field-testing can be conducted more efficiently and reduces the turn-around time. The component placement layout would also provide crucial information for future versions where miniaturization may be desired, so that it could be attached on top of the delivery platform. Figure 1-20 shows the schematic drawing as well as the assembled box in its testing stage.

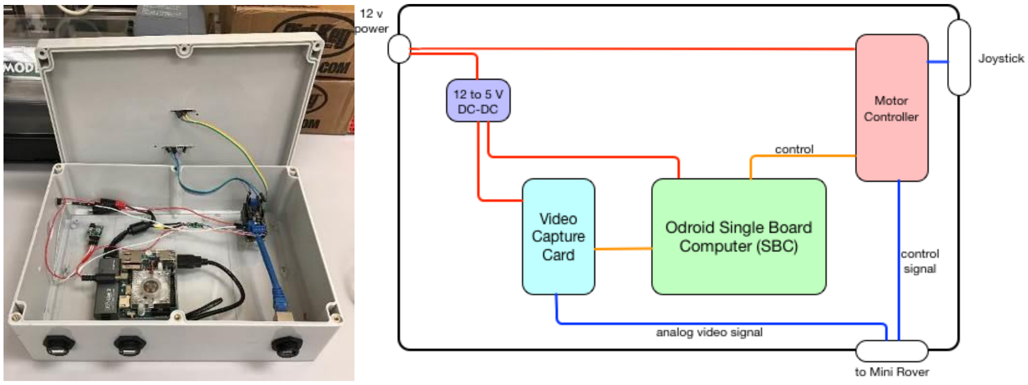

Figure 1-20. Waterproof enclosure housing all the electronic components that interface with the inspection tool and operator (left) and schematic drawing showing the layout of the control box (right).

In addition, FIU worked on designing a deployment system suitable for the miniature magnetic rover. Figure 1-21 shows a full-scale illustration of the proposed inspection of the ventilation channel at the bottom of the double shell tanks. During inspection, the miniature tool will drive from a large deployment platform responsible for providing power, control and communication. The parent platform will manage the tool's tether and retrieve the unit in case of a failure. The omnidirectional platform is being designed to be potentially autonomously driven.

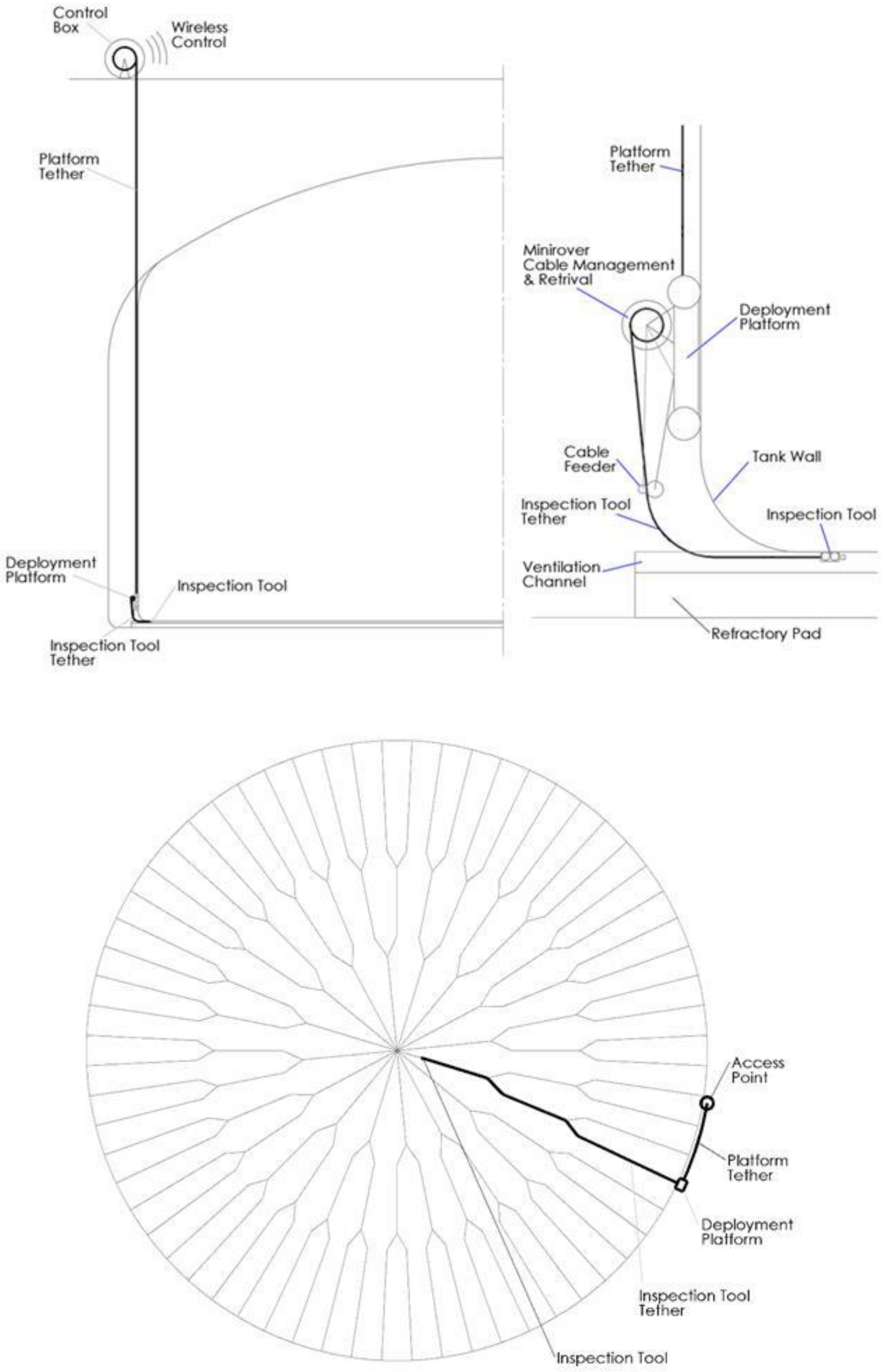

Figure 1-21. Ventilation channel proposed inspection.

Figure 1-22 shows the most updated design of the automated cable management system.

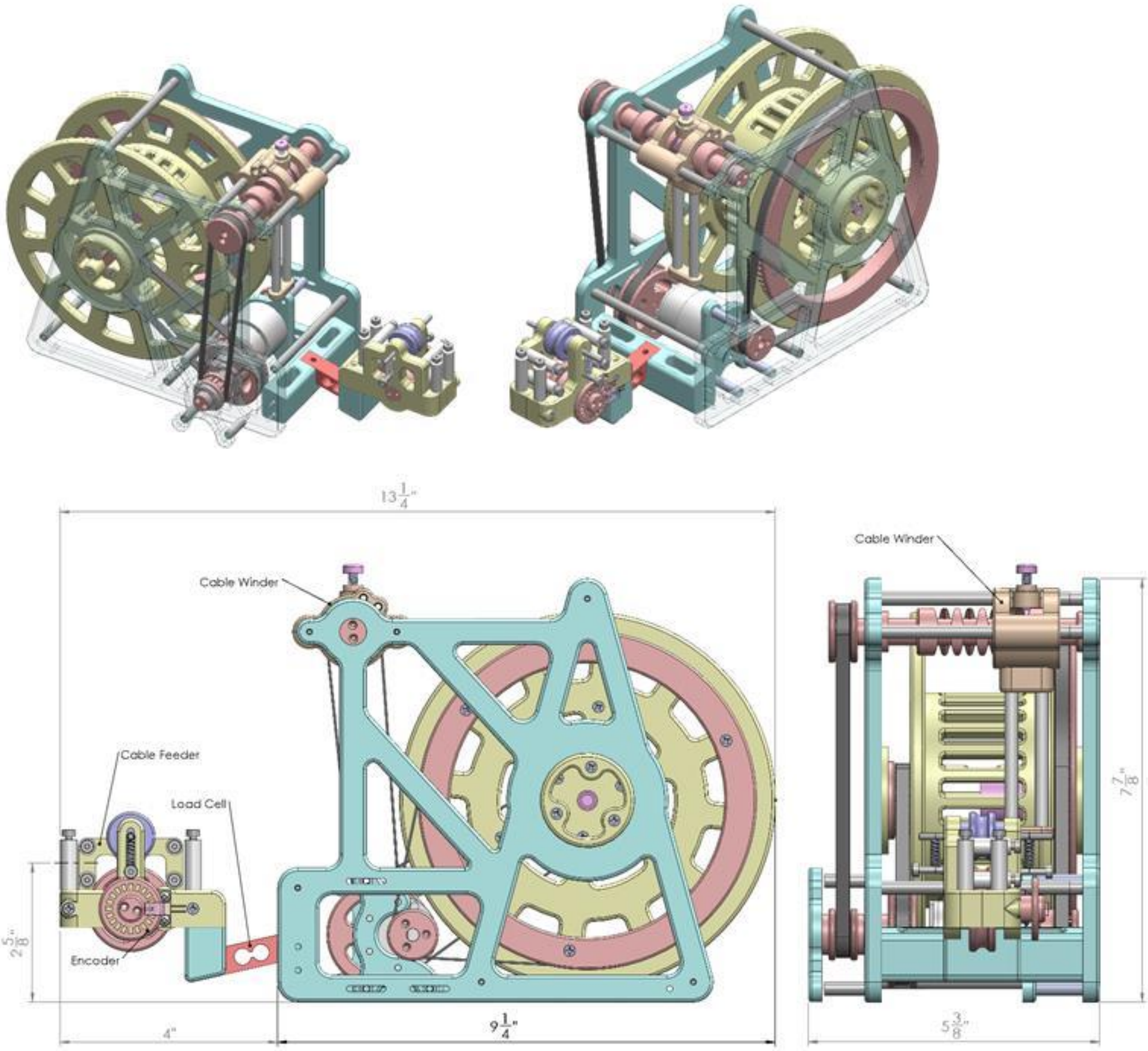

Figure 1-22. Automated cable management system.

As described in the previous report, the cable management system consists of a self-layering spool guide to keep the cable reel neat, tidy, and protected from damage. A load cell senses the movement of the inspection tool and a mechanism that slides back and forth in sync with the spool wind so that the reel is always properly wound. Figure 1-23 shows two prototypes being tested, where improvements in the design are also being incorporated as needed.

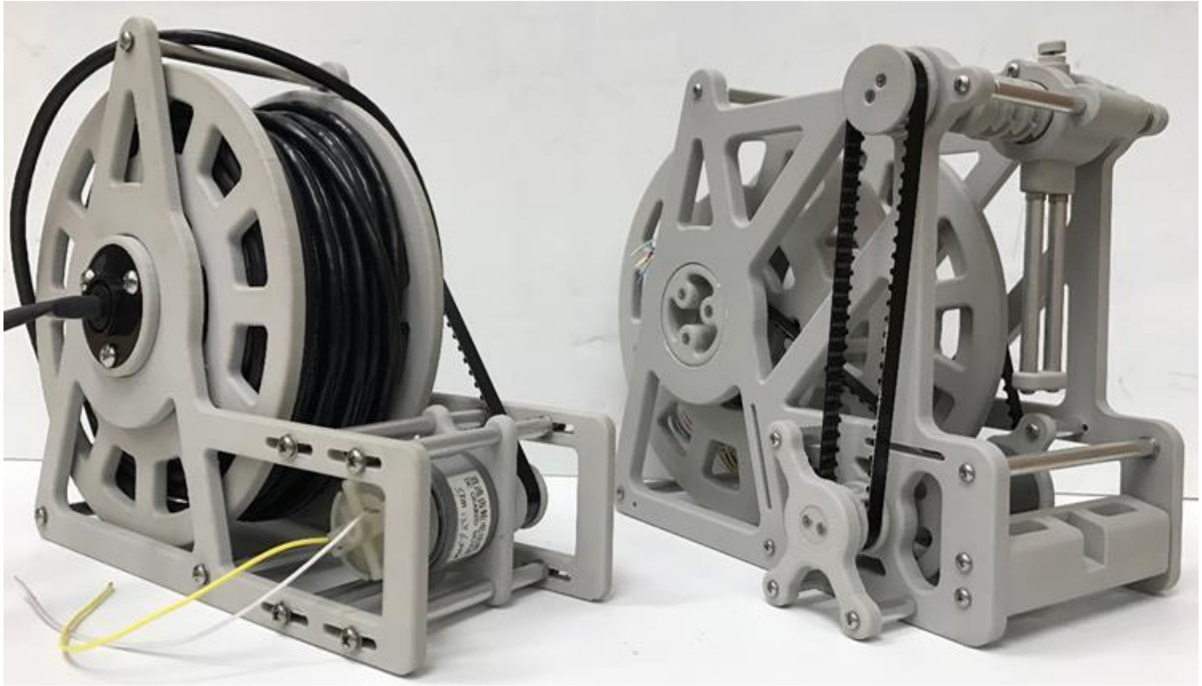

Figure 1-23. Original cable management (left) and redesign prototype with winder (right).

The cable management system is portable and designed to be easily integrated with a small wall crawler, such as the robotic platform currently being developed at FIU. Shown in Figure 1-24, the multi-purpose all-terrain platform could be re-engineered to deploy the miniature inspection tool.

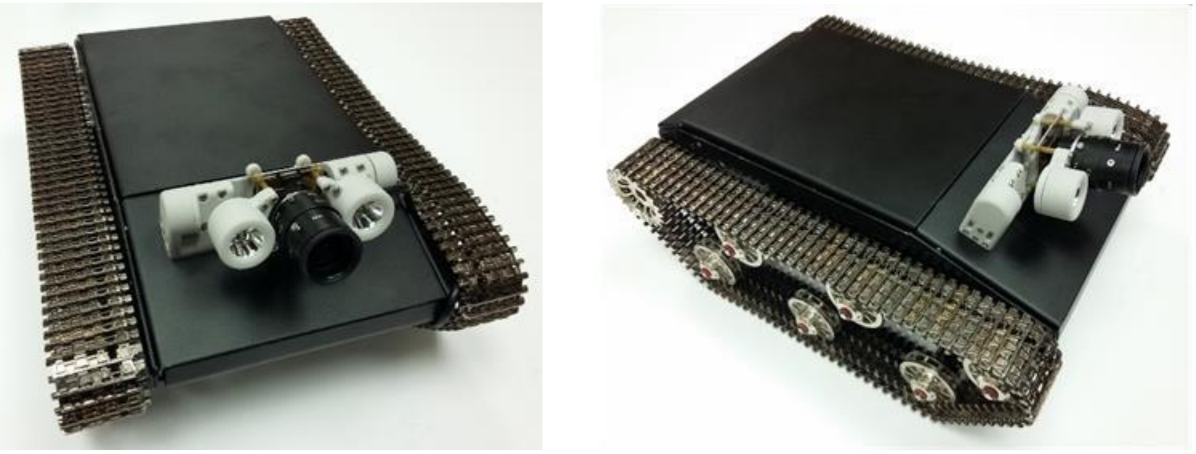

Figure 1-24. FIU's robotic platform.

Manual control of the inspection tool using joystick or keypads is challenging for the operators due to the tight channels underneath the tank. Having a semi-autonomous navigational capability would alleviate the complexity of the inspection tasks and allow the operator to focus on the channel inspection. The goal is to implement lane-keeping capability, akin to that of a driverless car, for the inspection tool, so that it will maintain its relative position with respect to the walls of the channel. This is illustrated in Figure 1-25 where an image stream from the inspection tool's onboard camera is processed to identify the channel boundaries (red lines), which in turn, is used for the estimation of the central line (dotted green line) for the inspection tool to track.

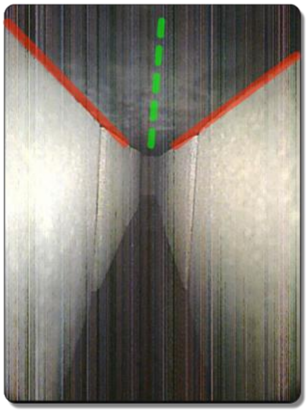

Figure 1-25. Image stream obtained from the onboard camera during a test in the mock up channel. Red lines show the wall boundaries while the dotted-green line is the estimated central line, with respect to the wall boundaries.

An image processing pipeline has been implemented using both the ROS and OpenCV for the wall boundaries detection (Figure 1-26). The image stream from the inspection tool's onboard camera is first converted to a grayscale image and passed through a thresholding algorithm (Figure 1-26 (b)) to remove the image noise. The edge and line detection algorithm (Figure 1-26 (c-d) is then applied to the resultant image to extract line structures in the image and remove outliers. The channel boundaries are then estimated from the detected lines and drawn on the image (Figure 1-26 (e)). Although the preliminary image processing pipeline is currently functional, its performance is highly dependent on the lighting conditions and image noise.

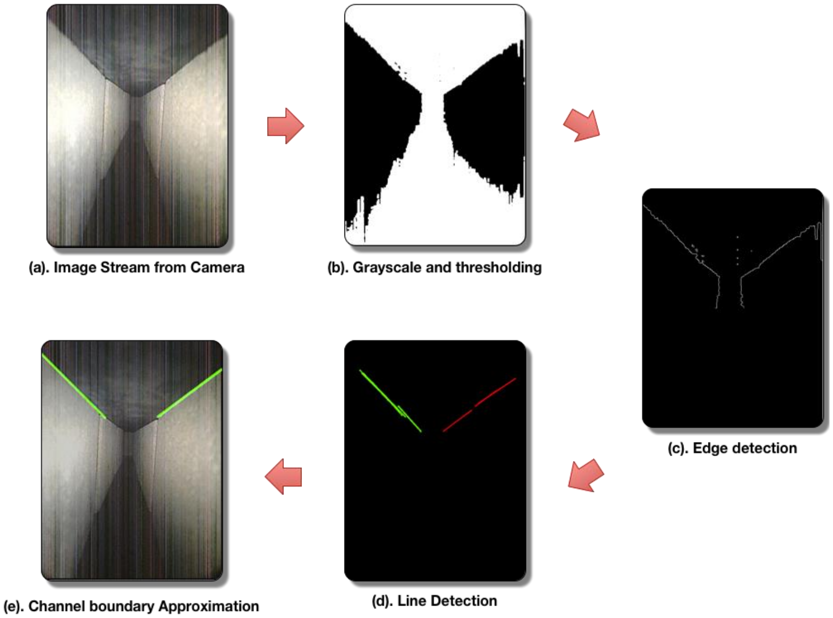

Figure 1-26. Image processing pipeline

Image quality improved with the latest version of the inspection tool (Figure 1-27). This can be attributed to the PCB, as with the reduction of wiring comes the reduction of noise. Image quality is important, as the inspection tool's primary purpose is visual inspection. It is also important for the image-processing component for the purpose of semi-autonomous control. Nevertheless, lighting still poses a determining factor on the image quality produced by the camera. The next step will be to improve the LED brightness, while making sure that images captured by the camera are within the camera's exposure limits. Concurrent work is also being performed to improve the performance of semi-autonomous control of the inspection tool, as well as to implement the sensing and control of the cable management system.

Figure 1-27. Image capture of the old inspection tool (left). Image capture of the new inspection tool (right).

Pneumatic Crawler Inspection Tool

During this performance period, the primary activities for the pipe crawler were focused on:

- manufacturing a prototype of the automated cable management system,
- enhancing the design and manufacturing the full-scale sectional mockup of a double shell tank (DST), and
- initiating the design of an inspection tool suitable for inspection of the DST's leak detection lines and channels.

The evaluation of auxiliary technologies such as nondestructive techniques, sensors, LIDAR, SONAR, communication protocols and microcontrollers were continued with the objective of improving the current crawler design and capabilities.

In addition, FIU continued to review existing crawler technologies looking for potential designs capable of inspecting the leak detection channels and drain lines. FIU has also started evaluating suitable designs to inspect the corrosion of the secondary liner bottom. The inspection tool will likely be a combination of a larger tool to crawl through the drain lines in order to deploy a version of the miniature magnetic rover into the foundation drain channels.

As part of the continuous improvement of the crawler, FIU is considering the impact of using a pancake pneumatic cylinder, shown in Figure 1-28, combined with return springs in the design of the grippers. The actuator use has the potential to reduce the module size, improving the inspection tool maneuverability, and allowing more clearance for redesign of the suspension guides.

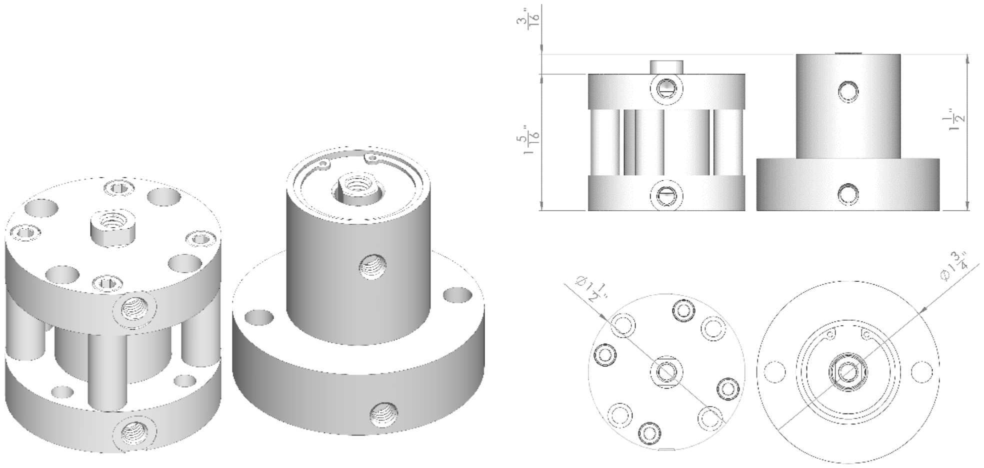

Figure 1-28. Current crawler (left) and pancake (right) cylinders.

FIU has also worked to redesign the grippers, which would reduce the module size as well as improve the inspection tool's maneuverability and retrieval.

Full-Scale Sectional Mockup

The design of the full-scale sectional mockup is being enhanced to address corrosion problems faced by the secondary liner bottom of the DSTs. The redesigned mockup not only will include the ventilation channels in the refractory pad of the primary tank, but it will also include the leak detection system in the foundation slab of the secondary tank liner, as illustrated in Figure 1-29.

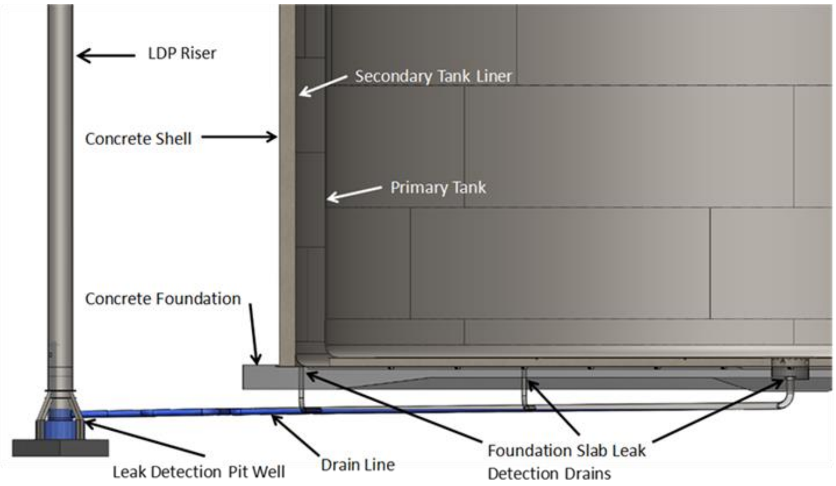

Figure 1-29. DST's Leak detection system.

Figure 1-30 shows the existing leak detection configurations used in the DSTs at Hanford. The FIU's mockup will be customizable and capable of being modified to emulate various designs.

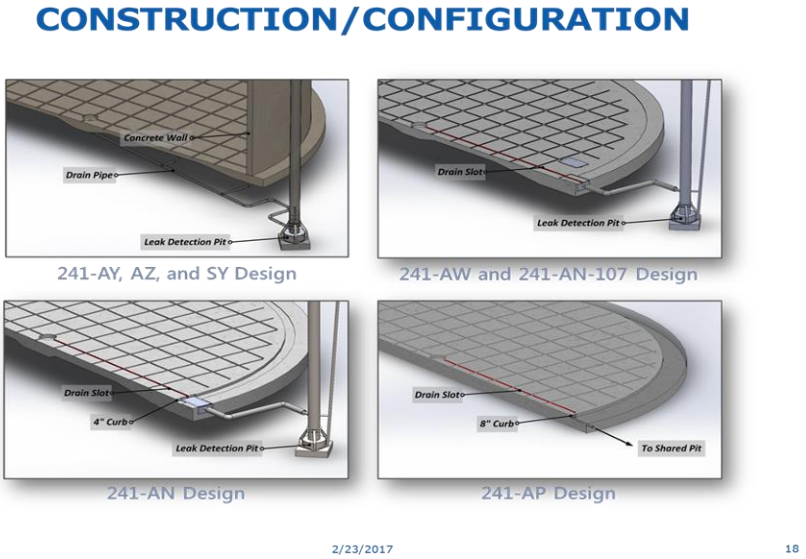

CONSTRUCTION/CONFIGURATION

2/23/2017 18

Figure 1-30. Existing configuration of the DST's leak detection system.

The mockup will be used for full-scale testing and evaluation of robotic and sensor technologies at FIU. Shown in Figure 1-31, the full-scale sectional mockup simulates the:

- concrete foundation with draw slots,
- 6" drain line,
- concrete shell,
- secondary tank liner,
- refractory pad with cooling channels,
- 4" ventilation line,
- primary tank, and
- tank center plenum.

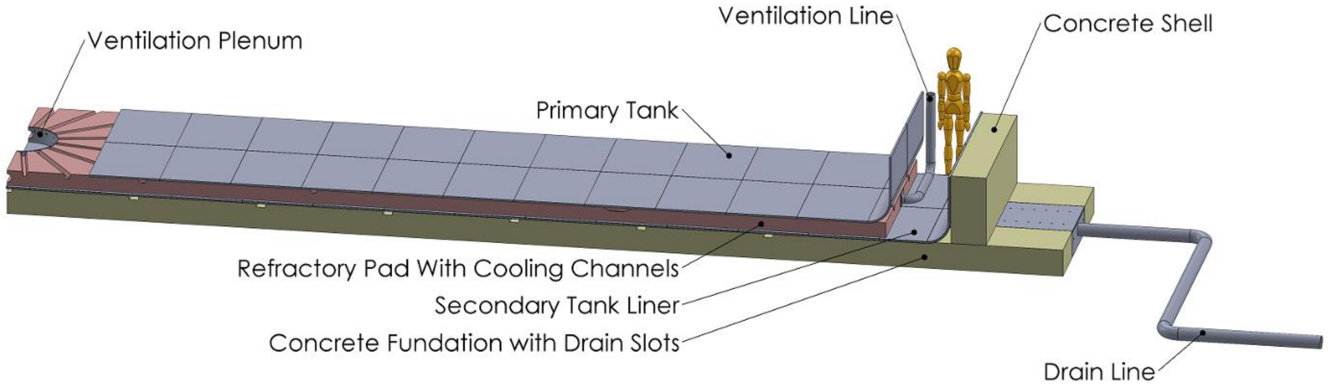

Figure 1-31. DST's full scale sectional mockup.

As illustrated in Figure 1-32, the mockup will cover approximately 7% of the DST's foundation.

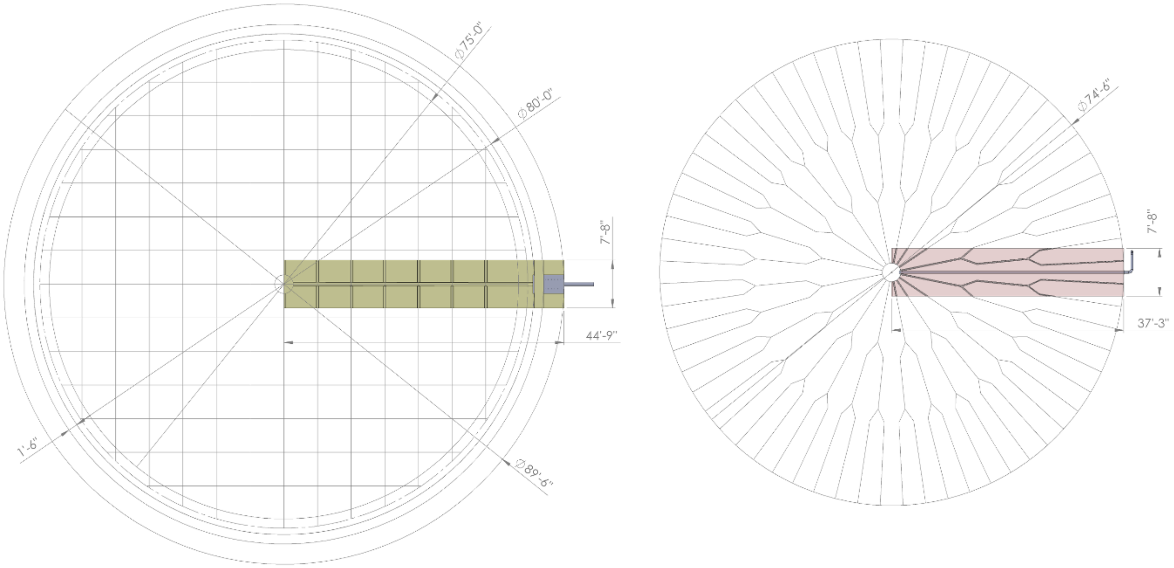

Figure 1-32. Foundation drains (left) and cooling (right) channels layout.

Figure 1-33 shows the layout of the concrete foundation in the mockup under the secondary tank liner. The foundation leak detection system has a maze of sloped drains. In the mockup, the drains are sloped and angled according to the DST's shop drawings, and they will be suitable to address corrosion issues in the inspection of the bottom of the secondary tank liner.

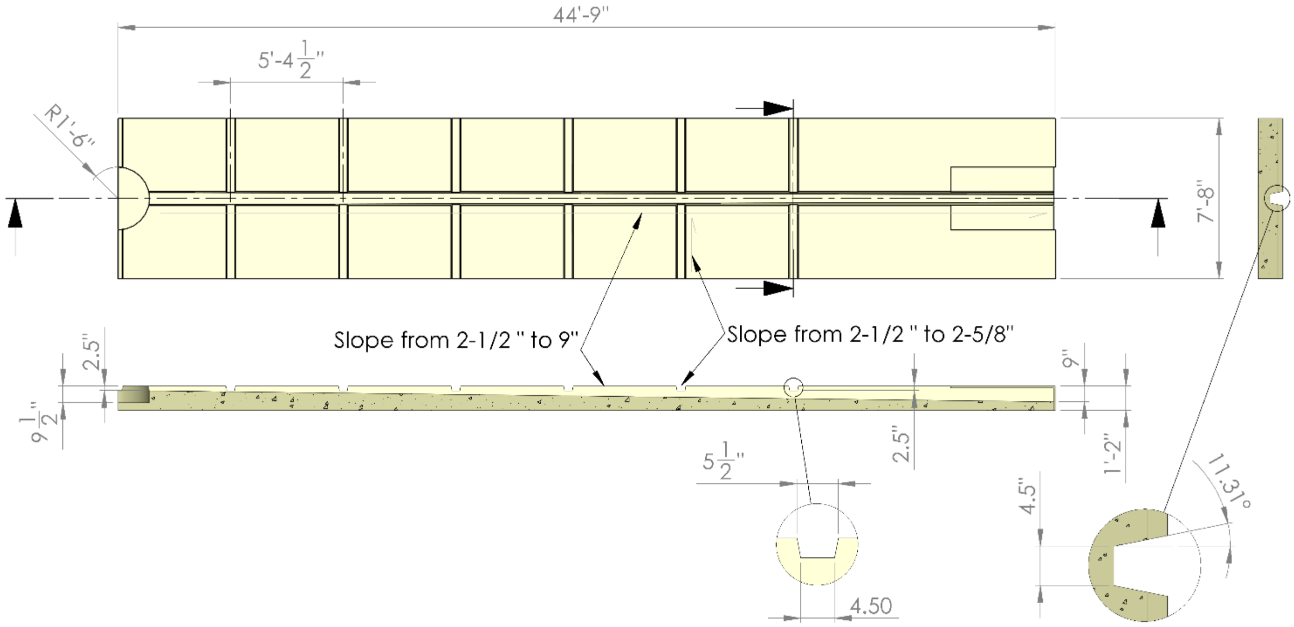

Figure 1-33. Concrete foundation with drain slots.

Figure 1-34 shows the layout of the refractory pad in the mockup under the primary thank. The mockup has two full length cooling channels reaching from the tank annulus to the center plenum. This configuration is suitable for testing emitter-receiver sensor technologies, such as long-range guided ultrasonic waves, which would require multiple sensors simultaneously located in both channels. The refractory mockup also includes one of the carbon steel 4” ventilation pipe lines, the only feasible way to provide access to the tank central plenum.

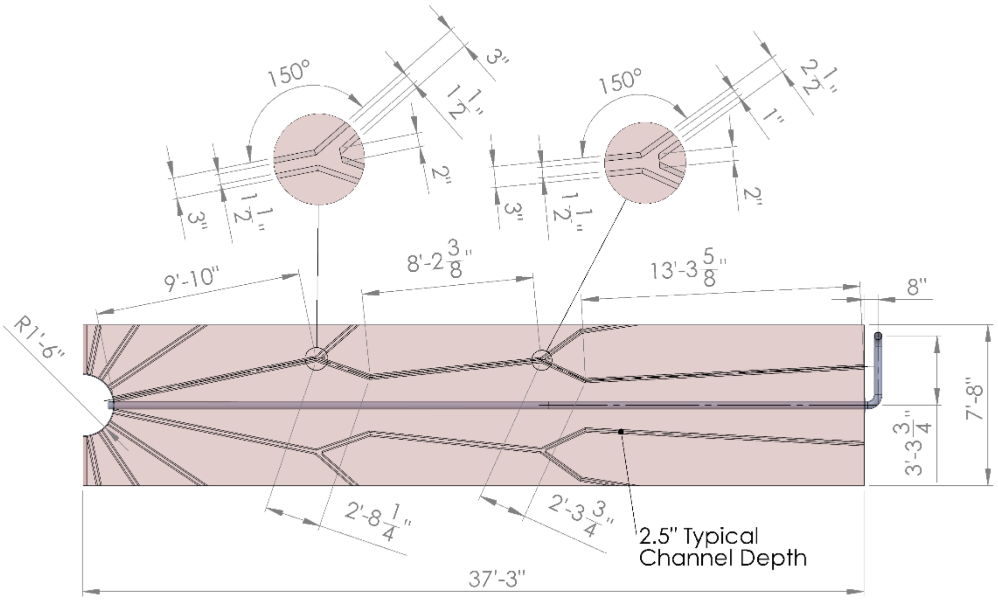

Figure 1-34. Refractory pad with cooling channels.

Figure 1-35 shows the mockup central plenums, which will be constructed according to the DST’s shop drawings.

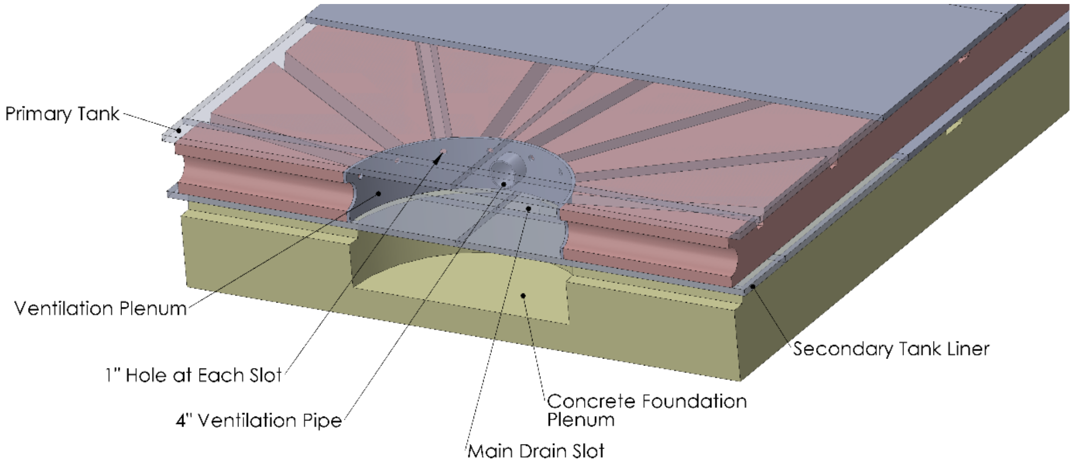

Figure 1-35. Tank central plenum.

The mockup foundation and refractory pad will be made of wood and coated with concrete held together by a metal mess. The concrete coating will have approximately ¼” thickness and will be held by a metal mesh attached to the wood frame. Shown in Figure 1-36, this combination provides a lighter structure combined with surface properties similar to the original ones.

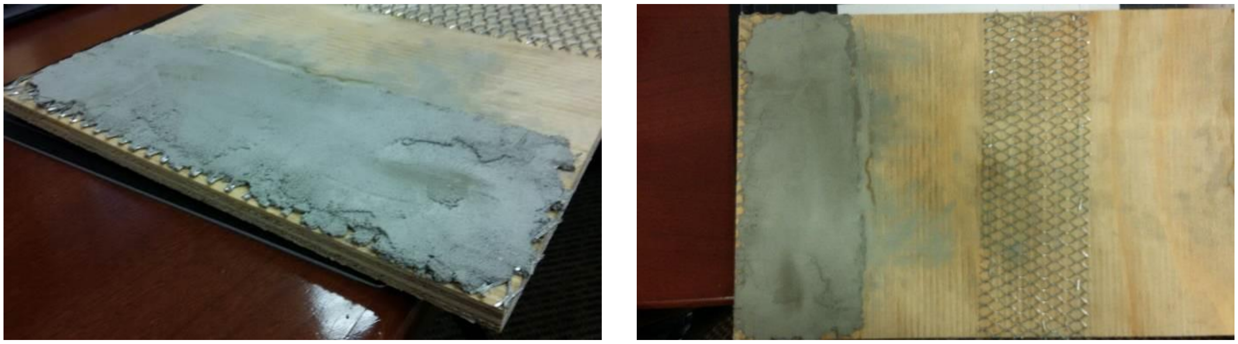

Figure 1-36. Mockup foundation and refractory pad concrete coating.

Figure 1-37 shows the layout of the primary tank wall. In the mockup, the concrete foundation and the refractory pad will lay on the floor covered by the metal plates. The tank walls are made of 3’-long by 4’-wide metal plates with 1/4” thickness.

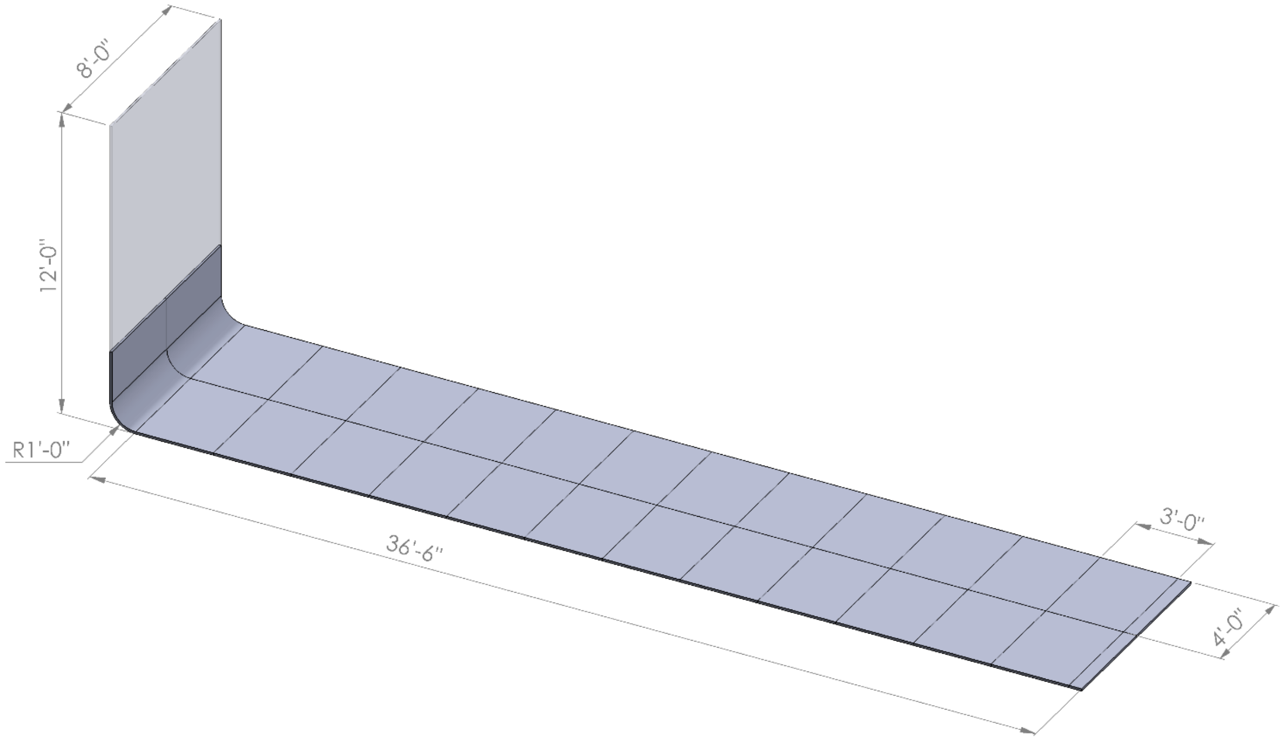

Figure 1-37. Primary tank layout.

Figure 1-38 shows a picture of the metal plates that will be used in the mockup. The mockup has a modular design, in which the plates can be replaced to simulate several inspection conditions, such as different thickness, defects, corrosion, damaged weld beds, and in-situ cracks.

Figure 1-38. Primary tank metal plates.

Subtask 18.3: Investigation Using an Infrared Temperature Sensor to Determine the Inside Wall Temperature of DSTs

FIU conducted experiments for emissivity calibration of the infrared (IR) sensors. Tests were performed to precisely determine the emissivity levels of two materials - carbon steel and stainless steel.

The first experiment was conducted using the carbon steel plate. Since the precise emissivity value of carbon steel was not available in the literature, an initial estimate of 0.75 was chosen and a range of values above and below the initial estimate was recorded. The experiment consisted of the ambient temperature measurement on a carbon steel plate (1/2 inch thick) using both a Raytek and a hermitically sealed thermocouple as shown in Figure 1-39 (left). The second experiment was conducted on the tank wall which was made of stainless steel. Emissivity values were changed from 0.3 to 0.6 and the experimental set up is as shown in Figure 1-39 (right).

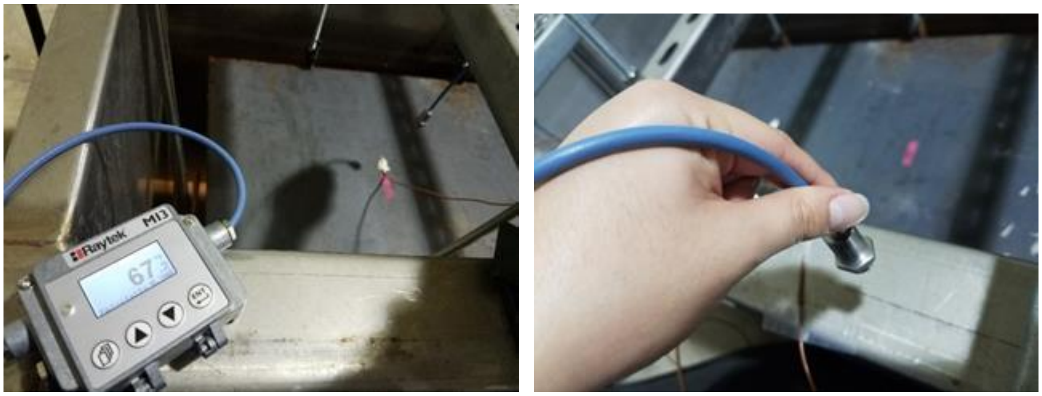

Figure 1-39. Emissivity experiment with Raytek sensor using a carbon steel plate (left) and a stainless steel tank wall (right).

Results obtained from both experiments are provided in Table 1-12 and Table 1-13. In Table 1-12, the temperature is recorded at three different points using both sensors. It is evident from the table that the temperature readings are close when the emissivity values range from 0.76 to 0.79 and is almost precise at 0.78. Also, it is to be noted that for the emissivity change from 0.7 to 0.8, the temperature values are precise within a maximum of 2-3ºF. Hence, the emissivity of carbon steel can be assumed as 0.78.

Table 1-12. Experimental Results with ½ in Carbon Steel Plate (Temperature Readings in ºF)

Emissivity (Raytek)	Raytek (point 1)	Raytek (point 2)	Raytek (point 3)	Thermocouple (point 1)	Thermocouple (point 2)	Thermocouple (point 3)
0.7	69.5	68.5	68.7	72.88	73.25	71.66
0.71	65.9	64.4	66.8	73.43	71.13	75.78
0.72	68.2	70.2	70.2	73.05	71.33	71.07
0.73	68.9	67.4	67.8	73.13	70.77	73.97
0.74	66.4	67.6	66.8	72.92	71.37	72.42
0.75	68.4	68.6	68.1	62.98	66.08	66.49
0.76	66.8	68.7	68.3	68.69	69.97	68.22
0.77	70.6	67.5	66.9	69.65	68.08	70.03
0.78	70.9	69.7	68.9	70.49	70.15	70.58
0.79	70.9	69.8	68.5	71.24	70.14	72.28
0.8	70.6	71.4	70.2	72.19	73.2	72.54

Table 1-13. Experimental Results with Stainless Steel Plate (Temperature Readings in ºF)

Emissivity (Raytek)	Raytek temperature	TC temperature
0.3	40.4	73.42
0.4	52.8	73.54
0.5	61.4	73.23
0.6	73.7	74.34

In the case of stainless steel, it is observed (Table 1-13) that the emissivity value of 0.4 to 0.5 provides an inaccurate temperature reading, but at an emissivity of 0.6, both Raytek and thermocouple readings are close with less than a 1ºF temperature difference. Hence, the emissivity of stainless steel can be assumed as 0.6.

To summarize, experiments were conducted to investigate the sensitivity of the Raytek IR sensor to different emissivity values and materials. A method has been established to accurately calibrate the sensor for different material types and emissivity values.

Integration of the IR sensor with the inspection devices developed in task 18.2 was also investigated. The miniature magnetic rover developed for carbon steel pipe inspections was chosen as a base model to integrate the mini IR sensor. The objective is to have the sensor attached for a “piggy back ride” on the rover and other similar instruments.

The IR sensor head was initially placed on an empty chassis of the mini rover to estimate the size and appearance of the unified system, as shown in Figure 1-40 (left). The sensor head was placed along the length of the rover and the cable can be directly attached to the tether of the mini rover.

Next, the sensor head was temporarily mounted to the actual mini rover and basic temperature readings were obtained. The sensor head attached to the mini rover inside the scaled DST mock-up channels is shown in Figures 1-40 (middle and right).

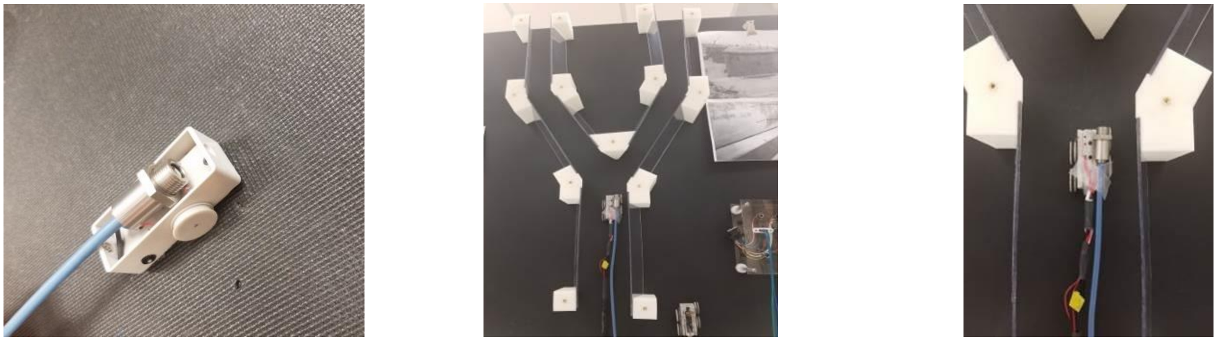

Figure 1-40. IR sensor head on the rover (left), empty chassis (middle), actual rover in the tank channels (right).

Alternative positions as shown in Figure 1-41 have also been considered, since frontal, rear and angular measurements are often needed inside the pipe.

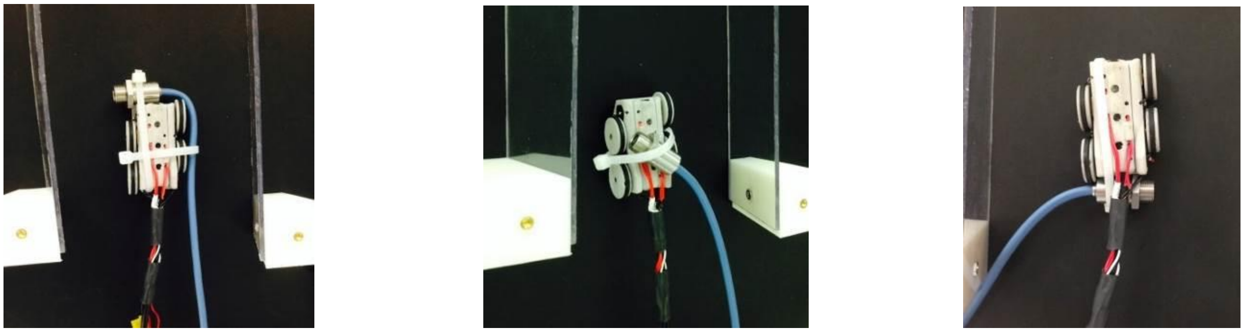

Figure 1-41. IR sensor head attached: front (left), top-angular (middle), rear (right).

Various mounting techniques such as “clip on and clip off,” glue or adhesive bonding, and screws are being considered for semi-permanent mounting of the sensor head to the mini rover and similar pipe inspection tools to investigate the feasibility of its use in pipes and tanks. In addition, efforts are being focused on the multi-physics model based heat transfer simulations for temperature estimations inside the tanks.

The integration of the IR sensor with the pneumatic pipe crawler developed for tank inspections, was also explored. The pneumatic crawler is modular and the sections connecting the modules provide a decent base for the IR sensor incorporation. The IR sensor was fixed temporarily next to the camera module of the crawler as shown in Figure 1-42 (left). This area is untouched by the springs and the pipe. The pneumatic crawler with the Raytek sensor was inserted into the clear pipe PVC loop as shown in Figure 1-42 (right).

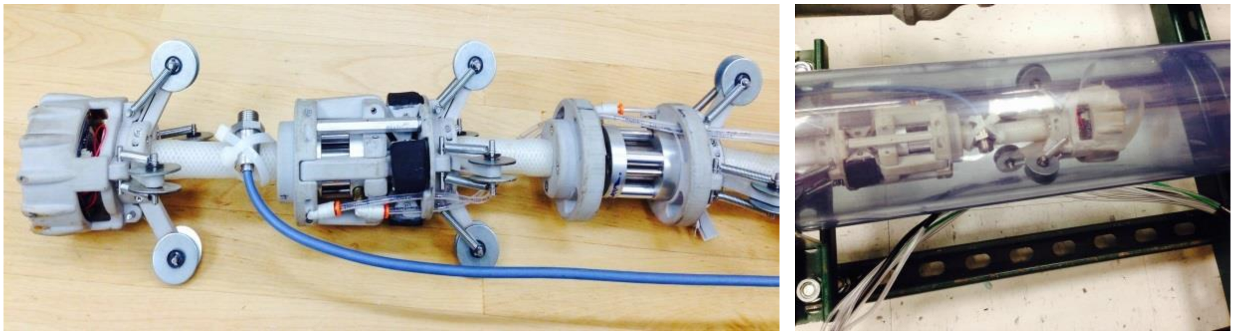

Figure 1-42. **IR sensor head on the pneumatic pipe crawler (left) and sensor head and crawler inside the clear pipe (right).**

Currently, FIU is researching options on permanent integration of the IR sensor with the pneumatic pipe crawler. Options include designing an additional sleeve to house the sensor and remodeling the crawler tether housing in the modules to accommodate the IR sensor's tether. In addition, sample tests will be run in carbon steel pipes using this assembly.

Task 19: Pipeline Integrity and Analysis

Task 19 Overview

The objective of this task is to support the DOE and site contractors at Hanford in their effort to evaluate the integrity of waste transfer system components. The objective of this task is to evaluate potential sensors for obtaining thickness measurements of HLW pipeline components. Specific applications include straight sections, elbows and other fittings used in jumper pits, evaporators, and valve boxes. FIU will assess the accuracy and use of down selected UT systems for pipe wall thickness measurements. FIU will also demonstrate the use of the sensors on the full-scale sectional mock-up test bed of the DSTs. An additional objective of this task is to provide the Hanford Site with data obtained from experimental testing of the hose-in-hose transfer lines, Teflon® gaskets, EPDM O-rings, and other nonmetallic components used in their tank farm waste transfer system under simultaneous stressor exposures.

Task 19 Quarterly Progress

Subtask 19.1: Pipeline Corrosion and Erosion Evaluation

FIU investigated the pump options for pumping abrasive fluids through the pipe loop and measuring erosion/corrosion wear rates using the Permasense UT sensors. Various pump options have been investigated and a few have been down selected. Three of the down selected pumps include the Grainger-Dayton chemical resistant centrifugal pump, the Laing Thermotech chemical resistant centrifugal pump, and the Little Giant chemical resistant centrifugal pump, as shown in Figure 1-43. Each of these pumps has varying length, height, weight, width, and maximum head and flow rate (gpm) ranges. Specifications and tolerance features of each of the pumps are given in Table 1-14.

Figure 1-43. Chemical resistant centrifugal pumps: a) Dayton, b) Laing Thermotech, c) Little Giant.

Table 1-14. Pump Specifications

Pump	**Size**	**Tolerance features**
Dayton chemical resistant centrifugal pump	Length range: 12-5/8" to 17-13/16" Height range: 7-1/2" to 8" Width range: 6-1/2" to 10-1/2" Max Head range: 48 ft. to 86 ft. Max GPM range: 21 gpm @5 ft. to 150 gpm @ 5 ft.	Help move mild acidic fluids, chemicals and other corrosive liquids through piping systems. Available housing materials include 304 and 316 stainless steel, Noryl, polypropylene, aluminum and nylon.
Laing Thermotech chemical resistant centrifugal pump	Height range: 2-1/2" to 4-7/8"" Length 6" Width range: 3" to 4-5/6" Max Head range: 13 ft. to 22.5 ft. Max GPM range: 4.2 gpm @1.75 ft. to 11.6 gpm @ 1 ft.	Help move mild acidic fluids, chemicals and other corrosive liquids through piping systems. Available housing materials include 304 and 316 stainless steel, Noryl, polypropylene, aluminum and nylon.
Little Giant chemical resistant centrifugal pump	Length range: 4-1/4" to 8-15/16" Height range: 4-3/8" to 5" Width range: 1/4" to 4" Max Head range: 12.3ft. Max GPM range: 8.5 gpm @1 ft. and 9.8 gpm @ 1 ft.	Help move mild acidic fluids, chemicals and other corrosive liquids through piping systems. Available housing materials include 304 and 316 stainless steel, Noryl, polypropylene, aluminum and nylon.

WRPS visited FIU during February 2017 and the task progress was presented to the team. In addition, a literature review was conducted to investigate the abrasive effects of specific chemicals on steel; these will be used to wear the pipes for continuous monitoring of the wear rate (thickness changes) with Permasense sensors. The effect of various salt solutions on the corrosion rate of stainless steel is given in Table 1-15.The chemical concentration in the solutions was chosen as 5 g/liter at room temperature. The steel specimens are immersed in the salt solutions for a period of 30 days. It is evident from the table that sodium chloride (NaCl) has the highest corrosion rate while lead nitrate ($Pb(NO_3)_2$) has the lowest corrosion rate. The corrosion rate in the table is specified as meters per year (mpy).

Table 1-15. Corrosive Effect of Various Brine Solutions on Stainless Steel [1]

Salt Solution	Corrosion rate (mpy)x10^{-2}
NaCl	1.85
KCl	1.77
Na_2SO_4	1.67
$CaCl_2$	1.55
$MgSO_4$	1.32
$MnSO_4$	1.24
$NaNO_3$	1.17
KBr	1.05
$CaCO_3$	0.93
KI	1.02
$NaHCO_3$	0.74
$Pb(NO_3)_2$	0.66

The corrosion response of carbon steel to different chemical solutions is as shown in Figure 1-44. The data is based on immersing carbon steel (API 5L X42) coupons in NaCl, Na_2SO_4 and Na_2CO_3 environments. A weight loss technique was used in which sample coupons with known weight were totally immersed in a non-flowing media of these chemicals for a total exposure time of 1008 hrs. (42 days). Weight loss was calculated using the following equation:

$$corrosion\ rate\ (mmpy) = \frac{87.6\ \times weight\ loss}{area\ \times time\ \times density}$$

In the equation, weight loss was measured in mg, surface area of the coupon in cm^2, time of exposure in hours, and metal density in g/cm^2. The experimental results showed that the corrosiveness of carbon steel in 1.0M of Na_2CO_3 was highest which was mainly a function of its higher concentration based on the fact that no film was formed on the coupon, followed by a 0.5M solution of NaCl while the least was recorded in a 1.0M solution of Na_2SO_4.

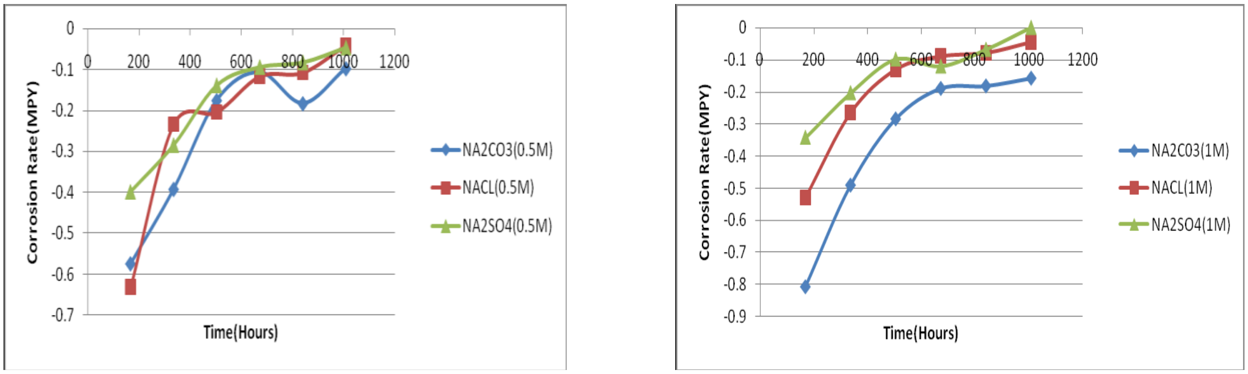

Figure 1-44. Corrosion rate in carbon steel a) 0.5M chemical concentration b) 1M chemical concentration [2]

It was concluded that carbon steel would degrade fastest in an environment with Na_2CO_3 solution at high concentrations.

FIU completed the initial validation testing of the Permasense UT sensors and a new test loop has been designed for aging the carbon steel pipes. Validation of the UT sensors was conducted for 3 months and thickness data was recorded every 6 hrs. There was no change observed in the thickness data obtained and, hence, it was concluded that the UT sensors are robust in acquiring real-time thickness data. The next phase of testing involves aging the test loop with abrasive fluids. For this, a preliminary design has been proposed as shown in Figure 1-45. The loop consists of 2- and 3-inch diameter pipe sections along with bends and a reducer. The idea is to pump fluids that can degrade the pipe [such as saline (NaCl) or Na_2SO_4 solution] for about 6 months and record the real-time thinning of the pipe using the UT sensors.

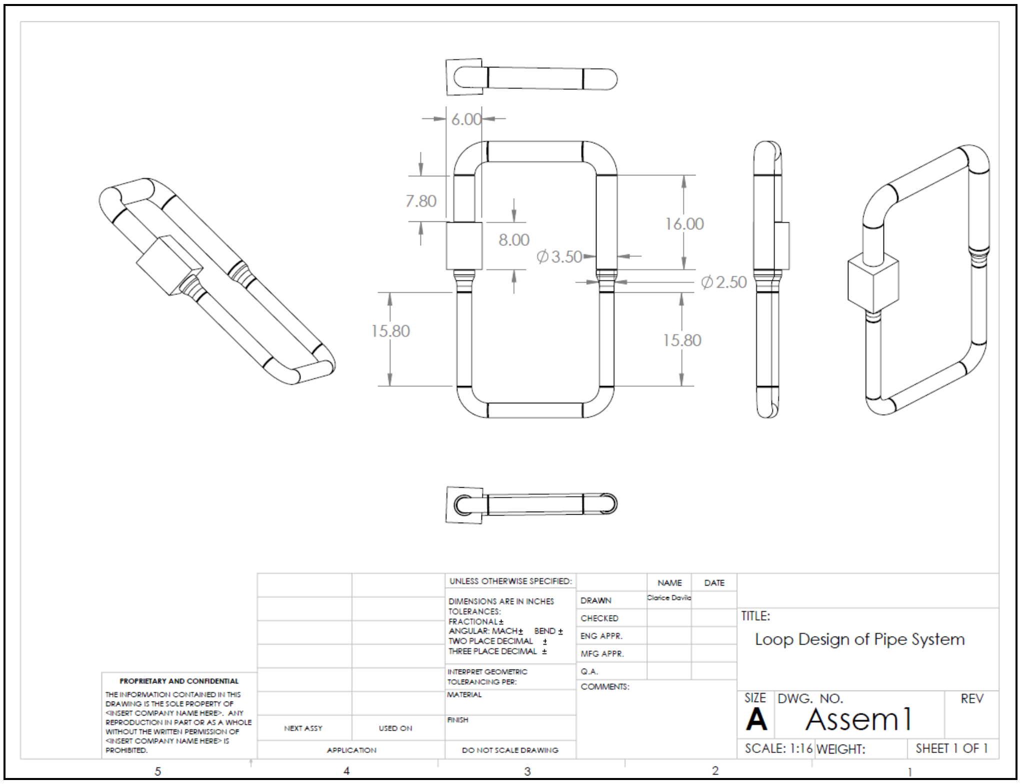

Figure 1-45. **Pipe loop design for aging.**

Currently, FIU is in the process of acquiring the pump, abrasive fluids and welding the pipe sections to form the loop. Upon completion, a test matrix will be generated to begin the aging process.

Subtask 19.2: Evaluation of Nonmetallic Components in the Waste Transfer System

The six-month aging period for the nonmetallic components being tested was reached on January 18, 2007. Half of the test specimens were removed in order to conduct material strength tests. This involved removing three of the six specimens out of each loop. Each specimen (Figure 1-46) included a hose-in-hose inner hose, an EPDM O-ring and a Garlock gasket. Three of the six specimens of EPDM and Garlock material were also removed from the aging vessels in each loop (Figure 1-47).

Figure 1-46. 6-month test specimens.

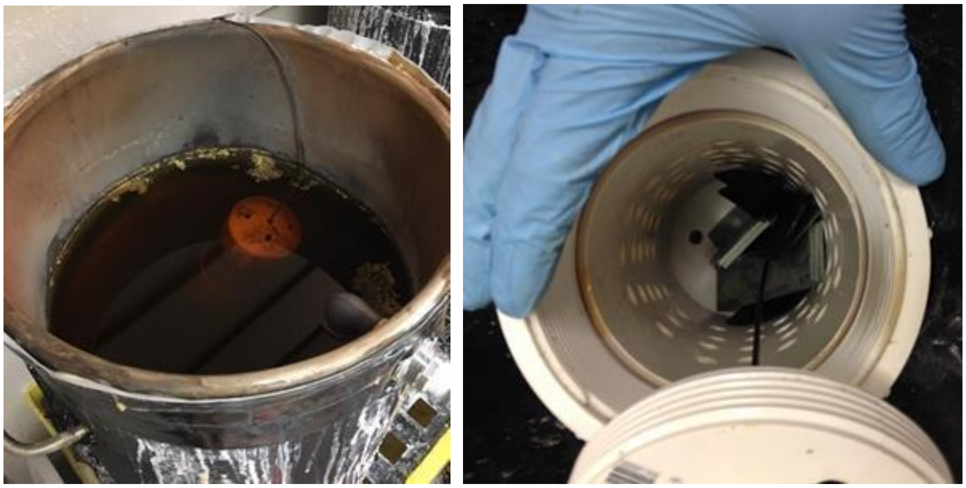

Figure 1-47. Coupon test vessel.

After the specimens were removed, the piping on each loop was reconfigured to only three test specimens each. In addition, as expected, the pump on loop #1 developed a leak from the motor barrier. The pump's barrier as well as the impeller were replaced with the redesigned parts acquired earlier. All three loops were restarted and the aging of the remaining specimens and coupons resumed.

The performance and material tests were subsequently conducted on the specimens that have been aged 6-months. Hose blowout tests were conducted on the aged hose specimens. Figure 1-48 shows a hose blowout test during the rupture of the hose as well as the failure location. The graph in Figure 1-49 shows the burst pressure data for each sample hose vs the baseline data.

Figure 1-48. Hose blowout test.

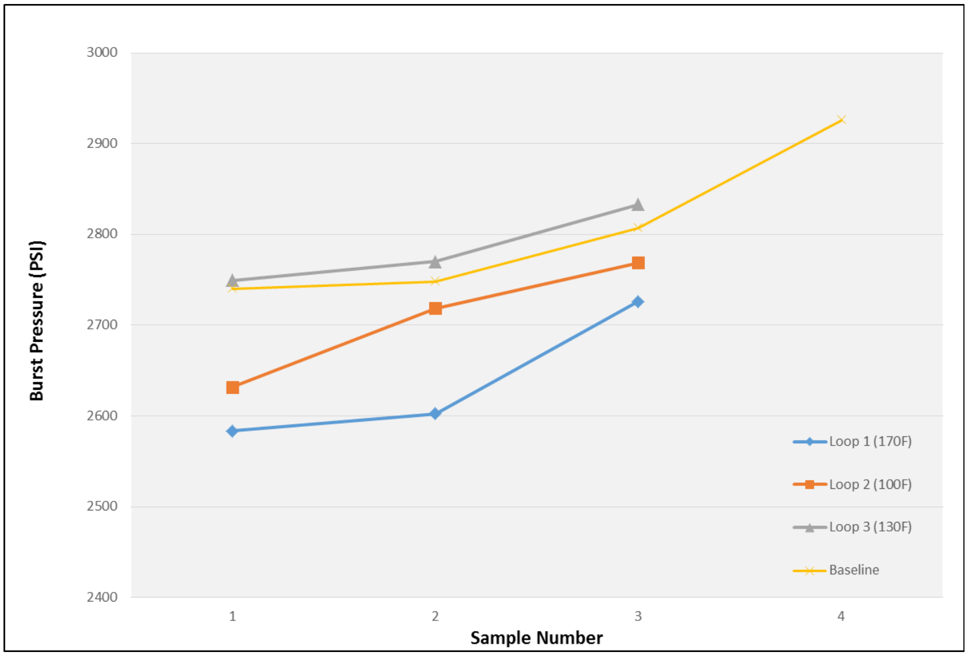

Figure 1-49. Hose burst pressure results vs baseline data.

Material properties tests were also conducted on the aged material coupons. These tests determined the tensile strength of aged EPDM as well as Garlock® sample coupons. Figure 1-50 shows an EPDM sample being tested.

Figure 1-50. EPDM sample tensile test.

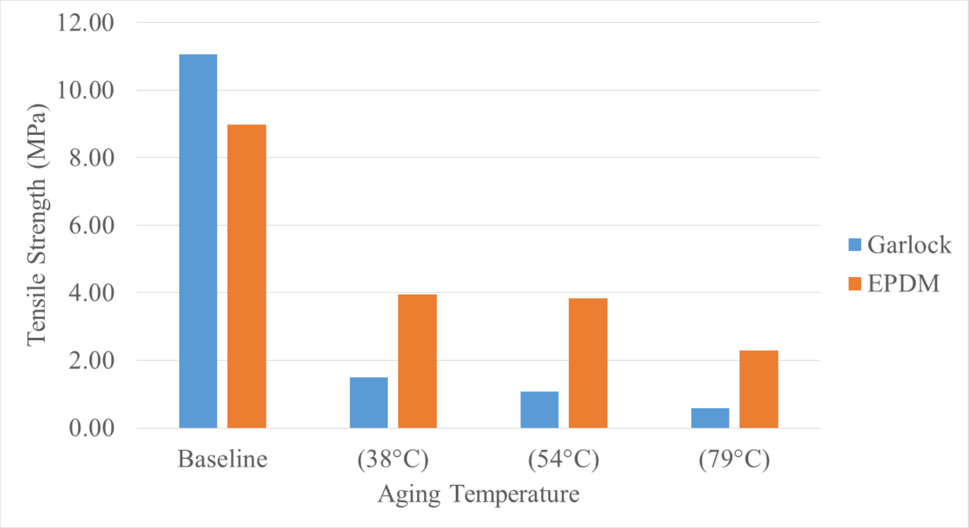

Figure 1-51. Material strength of aged materials vs baseline data.

The graph in Figure 1-51 shows the material strength of the aged materials vs baseline data. As can be seen from the graph, the material strength has been significantly reduced due to the aging process when compared to the baseline data.

Leak tests were conducted on the EPDM O-rings as well as Garlock® gaskets that were aged for a 6-month period. The aged O-ring pressure testing was conducted for nine EPDM O-ring specimens (three from each loop). Table 1-16 shows the results of the testing and Figure 1-52 shows the O-ring test apparatus. An average pressure of 1650 KPa was maintained for five minutes without any leaks.

Table 1-16. Six-Month O-Ring Pressure Test Results

Sample Number	O-01-4	O-01-5	O-01-6	O-02-4	O-02-5	O-02-6	O-03-1	O-03-2	O-03-3	Average
Water Temperature (°C)	23.00	23.00	22.00	22.00	22.00	22.00	22.00	22.00	22.00	22.22
Ambient Temperature (°C)	26.00	26.00	24.00	24.00	24.00	24.00	26.00	26.00	26.00	25.11
Humidity (%)	65.00	66.00	85.00	85.00	85.00	85.00	76.00	76.00	76.00	77.67
Holding Pressure (Pa)	1.63E+06	1.61E+06	1.61E+06	1.65E+06	1.61E+06	1.63E+06	1.68E+06	1.72E+06	1.75E+06	1.65E+06
Pressure Maintained?	Yes	Yes	Yes	Yes	Yes	Yes	Yes	Yes	Yes	N/A
Time Until Failure (s)	N/A	N/A	N/A	N/A	N/A	N/A	N/A	N/A	N/A	N/A

Figure 1-52. O-Ring test apparatus.

The aged Garlock® gaskets pressure testing was conducted for nine Garlock® gasket specimens (three from each loop). Table 1-17 shows the results the results of the testing and Figure 1-53 shows the test apparatus. Of the nine specimens, only four gaskets were able to maintain pressure. Of the four that maintained pressure, an average pressure of 487 KPa was maintained for five minutes without any leaks. The leaks are believed to be due to the gaskets being compressed when they were installed in the aging loop. Since the Garlock® material maintains a memory after it has been compressed, when it is reinstalled into the pressure test rig, it does not always create a good seal.

Table 1-17. Six-Month Garlock® Gasket Testing Results

Sample Number	G-01-4	G-01-5	G-01-6	G-02-4	G-02-5	G-02-6	G-03-1	G-03-2	G-03-3	Average
Water Temperature (°C)	22.44	22.44	22.44	22.44	22.44	22.44	22.44	22.44	22.44	22.44
Ambient Temperature (°C)	26.67	26.67	26.11	26.11	26.11	26.11	26.11	26.11	26.11	26.23
Humidity (%)	50.00	50.00	54.00	54.00	54.00	54.00	54.00	48.00	53.00	52.33
Holding Pressure (Pa)	1.09E+06	1.12E+06	1.12E+06	0.00E+00	1.05E+06	0.00E+00	0.00E+00	0.00E+00	0.00E+00	4.87E+05
Pressure Maintained?	Yes	Yes	Yes	No	Yes	No	No	No	No	N/A
Time Until Failure (s)	N/A	N/A	N/A	0.00	N/A	0.00	0.00	0.00	0.00	N/A

Figure 1-53. Gasket test apparatus.

Milestones and Deliverables

The milestones and deliverables for Project 1 for FIU Performance Year 7 are shown on the following table. Milestone 2016-P1-M17.1.1 was completed and a summary document was provided to DOE-HQ and WRPS engineers on February 17, 2017. This milestone was associated with completing the literature review of baseline experimental cases that could be used to improve the modeling capability for retrieval processes. Milestone 2016-P1-M19.2.1 was completed and a summary document was provided to DOE-HQ and WRPS engineers on March 31, 2017. This milestone was associated with completing the experimental testing of the non-metallic components that were aged for 6 months. Milestone 2016-P1-M18.3.1 was completed on March 31, 2017 and a summary document will be sent on April 14, 2017, summarizing the results from the bench-scale tests using an IR sensor. Due to funding issues, milestones 2016-P1-M18.2.1 and 2016-P1-M17.1.2 will be reforecast. The expected delay has been communicated to the site points-of-contact as well as the DOE HQ Project Lead, Gary Peterson, during regular project teleconferences. A reforecast date of completion will be set once future funding amounts and dates are known.

FIU Performance Year 7 Milestones and Deliverables for Project 1

Task	**Milestone/ Deliverable**	**Description**	**Due Date**	**Status**	**OSTI**
Task 17: Advanced Topics for Mixing Processes	2016-P1-M17.1.1	Complete literature review and selection of baseline experimental cases	2/3/17	Complete	
	Deliverable	Draft Summary Report for Subtask 17.1.1	2/17/17	Complete	OSTI
	2016-P1-M17.1.2	Complete CFD simulations of air sparging experiments	4/21/17	Reforecast Date TBD	
	Deliverable	Draft Summary Report for Subtask 17.1.2	5/5/16	Reforecast Date TBD	OSTI
Task 18: Technology Development and Instrumentation Evaluation	2016-P1-M18.2.1	Complete assembly of full-scale sectional mock-up test bed	12/16/16	Reforecast Date TBD	
	Deliverable	Draft Summary Report for Subtask 18.3.1	4/14/17	On Target	OSTI
	2016-P1-M18.2.2	Complete evaluation of sensor integration into inspection tools	5/26/17	On Target	

	Deliverable	Draft Summary Report for Subtask 18.2.3	6/30/17	On Target	OSTI
	2016-P1-M18.2.4	Complete conceptual design of miniature rover platform	8/25/17	On Target	
	2016-P1-M18.2.5	Complete conceptual design of 6 inch peristaltic crawler	8/25/17	On Target	
	2016-P1-M18.3.1	Complete bench-scale testing for temperature measurements using IR sensors	3/31/17	Complete	
Task 19: Pipeline Integrity and Analysis	2016-P1-M19.1.1	Assess the accuracy of the down selected UT system via bench-scale testing	5/12/17	On Target	
	2016-P1-M19.1.2	Develop test loop for evaluating UT sensors	8/25/17	On Target	
	2016-P1-M19.2.1	Complete experimental testing of 6 month aged materials	3/17/17	Complete	
	Deliverable	Draft Summary Report for Subtask 19.2.2	3/31/17	Complete	OSTI
	Deliverable	Draft Summary document on UT assessment for Subtask 19.1.1	5/26/17	On Target	OSTI

Work Plan for Next Quarter

Task 17: Advanced Topics for Mixing Processes

Recently FIU has had a number of visitors from the national laboratories and DOE HQ. After discussions with the visitors, it was suggested that FIU utilize the current 300 ft test loop to address technical gaps related to particle re-suspension and flushing. FIU currently has the capability to expand the loop to 2000 ft. During the next few months, FIU will continue to evaluate the relevant literature and discuss with key stakeholders, potential plans for next year's task.

Task 18: Technology Development and Instrumentation Evaluation

- For the pneumatic crawler and miniature rover tasks, FIU will complete conceptual designs that will allow for the integration of various sensors in both systems. This will include thermal and radiation sensors. In addition, FIU will continue to develop the sectional full scale mock-up of the DSTs that will allow for the demonstration of robotics/sensor systems from FIU as well as other collaborators.
- For the IR sensor task, FIU will continue to investigate the integration of the sensor into both the pneumatic crawler and miniature rover. After integration, both systems will be validated on the sectional full scale mock-up.

Task 19: Pipeline Integrity and Analysis

- For the ultrasonic sensor task, FIU will begin the process of assembling a loop that will contain abrasive particles that can erode the loop real time. This will allow for demonstrating the capabilities of the Permasense sensors.
- For the non-metallic materials task, FIU will continue to age the specimens. It is anticipated that the aging for one year will be completed at the end of August. FIU will

also complete the surface characterization of the 6-month specimens and investigate the feasibility of irradiating the coupon samples.

Project 2
Environmental Remediation Science and Technology

Project Description

This project will be conducted in close collaboration between FIU and national laboratory scientists and engineers at SRNL, SREL, PNNL and LANL in order to plan and execute research that supports the resolution of critical science and engineering needs, leading to a better understanding of the long-term behavior of contaminants in the subsurface. Research involves novel analytical methods and microscopy techniques for characterization of various mineral and microbial samples. Tasks include studies which predict the behavior and fate of radionuclides that can potentially contaminate the groundwater system in the Hanford Site 200 Area; laboratory batch and column experiments, which provide relevant data for modeling of the migration and distribution of natural organic matter injected into subsurface systems in the SRS F/H Area; laboratory experiments investigating the behavior of the actinide elements in high ionic strength systems relevant to the Waste Isolation Pilot Plant; surface water modeling of Tims Branch at SRS supported by the application of GIS technology for storage and geoprocessing of spatial and temporal data.

The following tasks are included in FIU Performance Year 7:

Task No	Task
Task 1: Remediation Research and Technical Support for the Hanford Site	
Subtask 1.1	Remediation Research with Ammonia Gas for Uranium
Subtask 1.2	Investigation on Microbial-Meta-Autunite Interactions - Effect of Bicarbonate and Calcium Ions
Subtask 1.3	Investigation of Electrical Geophysical Response to Microbial Activity in the Saturated and Unsaturated Environments
Subtask 1.4	Contaminant Fate and Transport Under Reducing Conditions
Task 2: Remediation Research and Technical Support for Savannah River Site	
Subtask 2.1	Investigation on the Properties of Acid-Contaminated Sediment and its Effect on Contaminant Mobility
Subtask 2.2	The Synergistic Effect of Humic Acid and Colloidal Silica on the Removal of Uranium (VI)
Subtask 2.3	Humic Acid Batch Sorption and Column Experiments with SRS Soil
Task 3: Surface Water Modeling of Tims Branch	
Subtask.3.1	Modeling of Surface Water and Sediment Transport in the Tims Branch Ecosystem
Subtask 3.2	Application of GIS Technologies for Hydrological Modeling Support
Subtask 3.3	Biota, Biofilm, Water and Sediment Sampling in Tims Branch Watershed
Task 5: Remediation Research and Technical Support for WIPP	

Task 1: Remediation Research and Technical Support for the Hanford Site

Task 1 Overview

The radioactive contamination at the Hanford Site created plumes that threaten groundwater quality due to potential downward migration through the unsaturated vadose zone. FIU is supporting basic research into the fate and remediation of radionuclides such as uranium in the vadose zone as a cost effective alternative to groundwater pump and treat technologies. One technology under consideration to control U(VI) mobility in the Hanford vadose zone is a manipulation of sediment pH via ammonia gas injection to create alkaline conditions in the uranium-contaminated sediment. This project also investigates the biodissolution of autunite solids created in sediments after injections of polyphosphate amendments and studies the potential detection of biofilms via the spectral induced polarization method (SIP). Another focus of this project is to investigate the properties of Tc and its compounds under Hanford Site conditions to better understand and predict Tc fate and transport in the subsurface and for designing remedial strategies for this contaminant.

Task 1 Quarterly Progress

Subtask 1.1. Remediation Research with Ammonia Gas for Uranium

During the month of March, DOE Fellow Silvina Di Pietro presented a student poster and a professional oral presentation at the 2017 Waste Management Symposia Conference in Phoenix, Arizona. Her poster was titled "Fate of U and Mineral Dissolution upon Treatment with NaOH or NH_4OH" while her oral presentation was titled "Ammonia Gas Treatment for Uranium Immobilization at the DOE Hanford Site." She received second place in the student poster competition.

At the same conference, Dr. Katsenovich gave two oral presentations based on the results obtained for this project, including: "Removal of U(VI) in the Alkaline Conditions Created by NH3 Gas" during session 011, Sustainable Remediation Processes - Global Insights or Applications; as well as "Iron Behavior in Microcosms Simulating Bioreduction in SRS Sediments" during session 124, Technical Innovations in Environmental Remediation and Site Closure.

Ammonia Gas Treated Batch Experiments with Pure Minerals

Sample preparation and protocol development

During the month of January, analysis of controls for ammonia gas injection for the batch experiments continued, and based on these results, batch experiments were designed for ammonia gas injection in the presence of minerals. FIU also continued experiments with NaOH and NH_4OH injection in the presence of NaCl for batch samples containing the following minerals: calcite, Hanford sediment, muscovite and illite. Further, ICP-OES analysis and kinetic modeling continued for samples from Silvina Di Pietro's summer internship.

All future ammonia gas-treated samples will be prepared via exposure to $95\%N_2/5\%NH_3$ within a glovebag placed inside a fume hood. The target pH should be attained within a few hours following exposure of the samples to the atmosphere inside the glovebag. This will allow for consistent, repeatable treatment of samples without the concerns of calcite precipitation as highlighted below and described in the December monthly report.

During the one day sampling of 15-mL tubes treated directly with NH_3 gas, the pH error was ±0.33 as compared to ±0.12 for gas injected directly into the one liter stock solution. Furthermore, the error on the U fraction in the aqueous phase was 11% and 1% respectively for samples with 500 ppb U initially with gas injection into individual vials, and the one liter stock solution. Figure 2-1 represents the aqueous fraction of U for samples with initial concentrations of 50 ppb and 500 ppb of U with injection of ammonia gas to the individual vials in triplicate. The error is much greater than that presented in the December monthly report for ammonia gas treatment of the stock solutions prior to U addition.

Figure 2-2 below depicts the results for ammonia gas injection into the stock solutions of NaCl with either immediate injection of U or injection following settling for more than one week. The results for synthetic groundwater (SGW) show that control recovery is nearly 100% for samples that were injected with the stock solution following settling, while significant losses occurred with those spiked with U immediately following ammonia gas injection into the stock solutions. This is likely because calcite is precipitating in those not allowed to settle (confirmed by Geochemist Workbench, Figure 2-3). Furthermore, U is co-precipitating with the calcite in these samples leading to a decreased recovery in the aqueous phase. However, in those samples prepared after settling, calcite has been allowed to precipitate from solution in the absence of U and is not included in the stock solution used in the experiments.

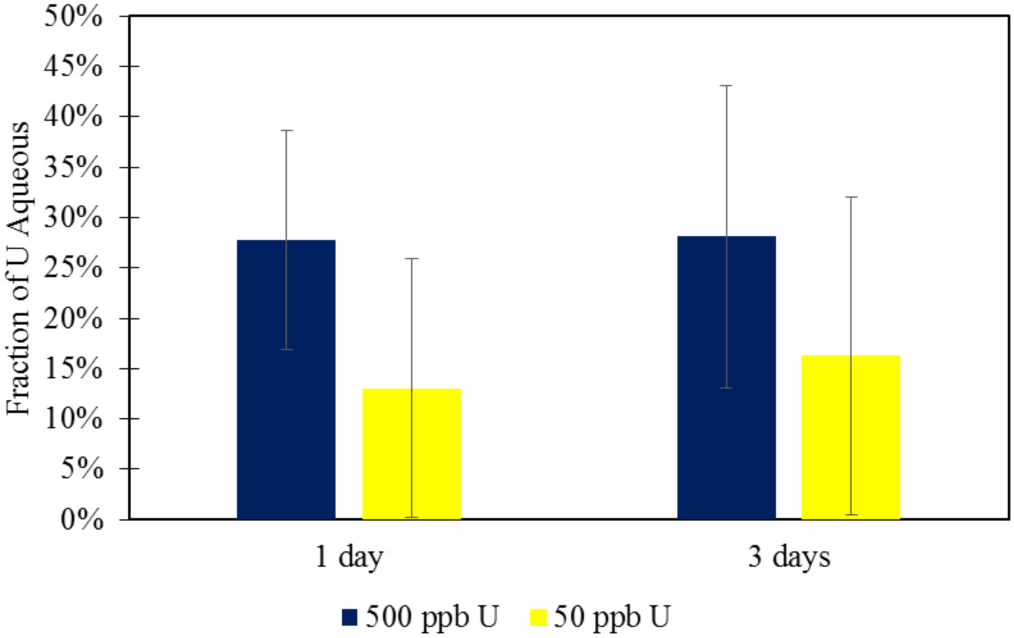

Figure 2-1. Fraction of aqueous U for SGW control samples prepared in triplicate with injection of NH_3 gas directly into 15-mL vials.

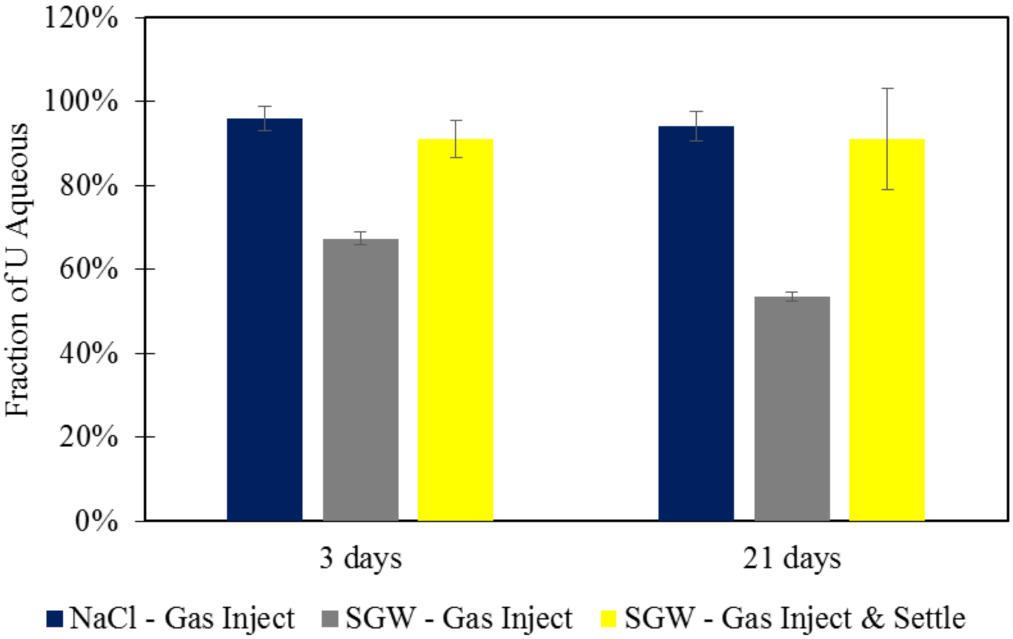

Figure 2-2. Fraction of aqueous U (500 ppb) for control samples prepared in synthetic groundwater (SGW) and 7.2 mM NaCl with immediate preparation after gas treatment of stock solutions (blue, gray) or following settling (yellow).

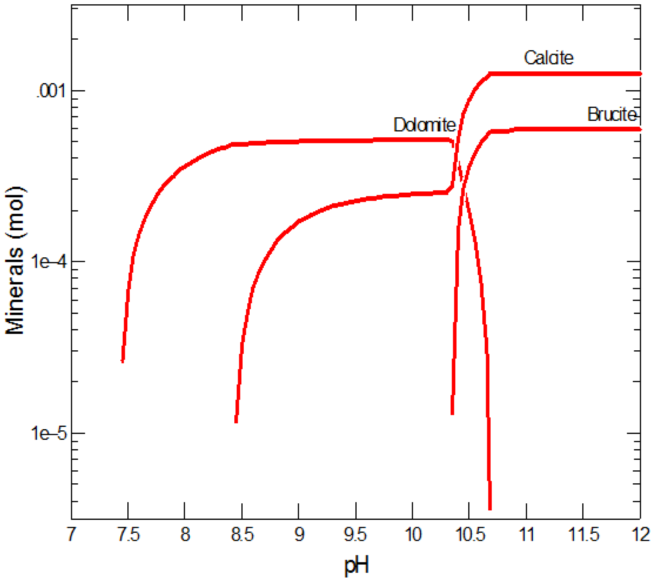

Figure 2-3. Geochemist Workbench Model predicting solid carbonate phases with respect to pH in synthetic groundwater (SGW).

Batch experimental results:

Experimental results are presented for three day sampling of NaOH and NH_4OH injection for batch samples in the presence of NaCl for the following minerals: calcite, Hanford sediment, muscovite and illite. Data analysis is ongoing for NaCl and SGW background electrolyte in the presence of Hanford sediment, illite and muscovite treated with NH_3 gas as described above.

Figure 2-4 summarizes the preliminary results for U partitioning at three days at pH 11.5 with base treatment by either NH_4OH or NaOH as described in previous monthly reports. It should be noted that the recovery of U in the control samples (without minerals) was 88 ± 11% throughout these experiments. These results show that there is very little removal of U in the presence of calcite, likely due to formation of aqueous U-carbonate complexes as the calcite equilibrates with the aqueous phase. However, significant sorption is observed for Hanford sediments, muscovite and illite. Current work is ongoing to explain the significant difference in U sorption for muscovite with the two base treatments.

Figure 2-5 compares the results for U partitioning for synthetic groundwater (SGW) and 7.2 mM NaCl. For calcite, there is approximately an order of magnitude greater removal of U in the presence of SGW for both treatments. However, removal is at least an order of magnitude greater for Hanford sediments in the presence of NaCl as opposed to SGW. Each of these phenomenon is likely due to carbonate complexation. For the calcite samples, there may be some co-precipitation of calcite from the components of the SGW at elevated pH, which may increase removal of U. However, in the presence of the Hanford sediments, removal is greater for NaCl because there is not sufficient carbonate present in the aqueous phase to form uranyl-carbonate species which are known to decrease sorption of U. Removal of U in the presence of muscovite is similar for both treatments and background electrolytes with the exception of NaCl-NH_4OH. However, the processes influencing this result are still under investigation. The greatest removal is observed in the presence of illite in SGW for both base treatments. This is likely a result of both sorption and co-precipitation (with calcite) processes.

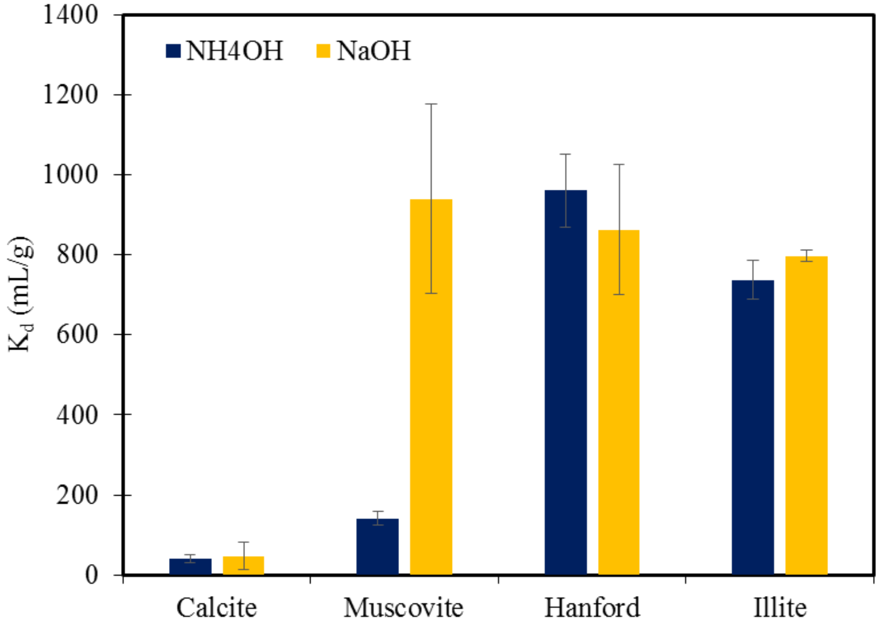

Figure 2-4. Results for partitioning of $[U]_{initial}$ = 500 ppb in 7.2 mM NaCl after three days of equilibration with 5 g/L calcite, 25 g/L muscovite, 25 g/L Hanford sediments or 5 g/L illite and treatment to pH near 11.5 with either NH_4OH (blue) or NaOH (yellow), error bars are based on measurement of triplicate samples.

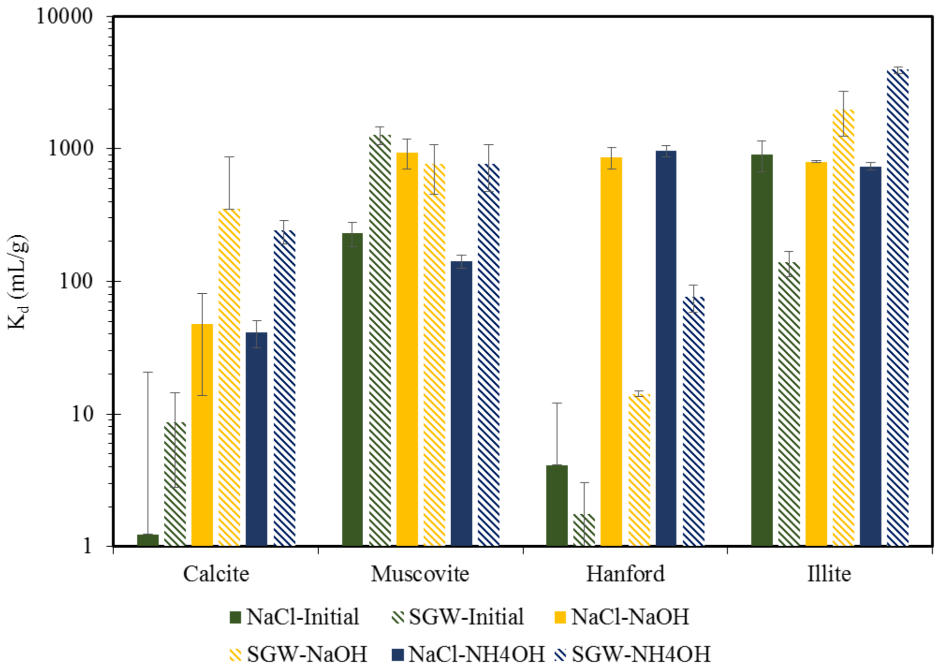

Figure 2-5. Comparison of results for partitioning of $[U]_{initial}$ = 500 ppb in 7.2 mM NaCl (solid) and SGW (stripes) after three days of equilibration with 5 g/L calcite, 25 g/L muscovite, 25 g/L Hanford sediments or 5 g/L illite. Data shown for initial conditions at pH 7.5 (green) and treatment to pH near 11.5 with either NH_4OH (blue) or NaOH (yellow), error bars are based on measurement of triplicate samples.

Batch mineral dissolution kinetics experiments (as PNNL internship 2016)

Silvina Di Pietro continued analysis of the mineral dissolution data from her summer internship experience at Pacific Northwest National Laboratory. These data will be presented in an oral presentation at the spring American Chemical Society meeting in April. Figure 2-6 and Figure 2-7 represent the aqueous Si leached per gram of mineral for six sampling events (1 hour, 1 day, 3 days, 10 days, 30 days, and ~ 60 days) under two different conditions: anaerobic (Figure 2-6) and aerobic (Figure 2-7). Figures 2-8 through 2-10 represent aqueous Si leached per gram of layered silicate minerals for three different conditions: anaerobic in DIW + 3.1 M NH_4OH, aerobic in DIW + 3.1 M NH_4OH and anaerobic in DIW + 0.031 M NaOH.

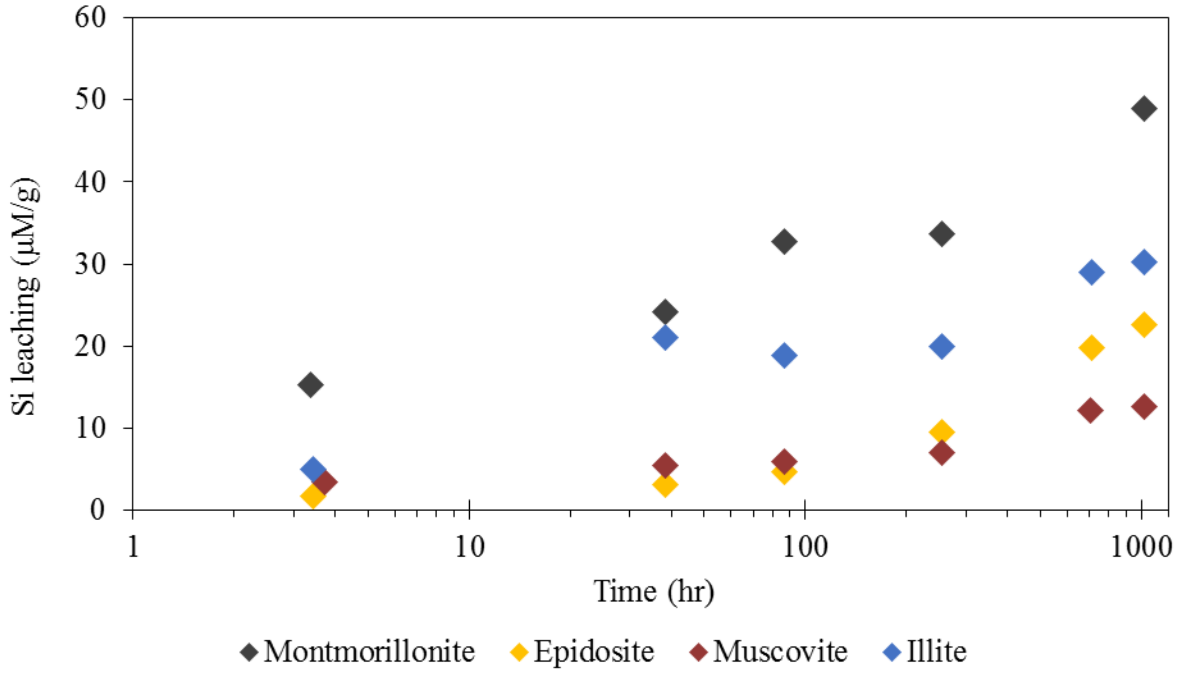

Figure 2-6. Silica leaching [µM/g] (montmorillonite, epidosite, muscovite and illite) for anaerobic+DIW with 3.1 M NH_4OH condition as a function of time.

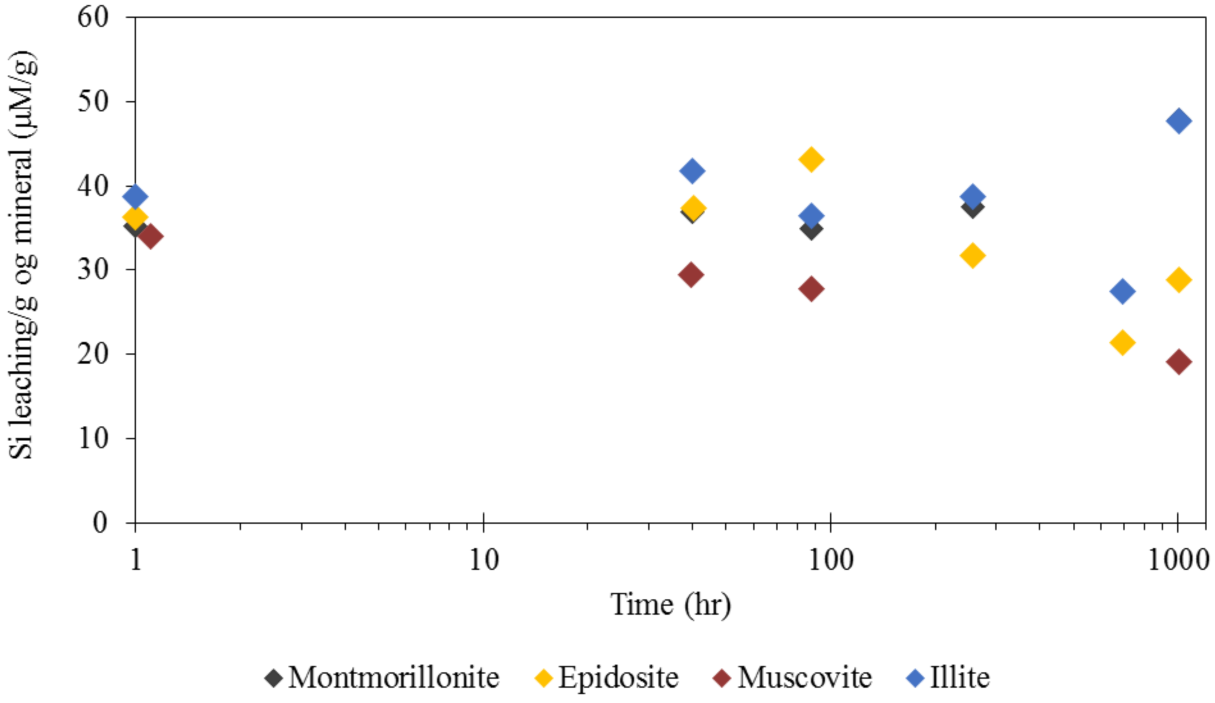

Figure 2-7. Silica leaching [µM/g] (montmorillonite, epidosite, muscovite and illite) for aerobic+DIW with 3.1 M NH_4OH condition as a function of time.

Muscovite, illite and montmorillonite are phyllosilicate sheet clays with muscovite and illite in the mica group and montmorillonite within the clay smectite group. Epidosite is a metasomatic rock with essential mineral components of quartz and epidote. These minerals underwent three different conditions to quantify silica leaching to the aqueous phase. Although further investigation is needed to understand the dominant mechanisms, results for dissolution under anaerobic conditions presented in Figure 2-8 show an increasing trend in silica leached to the aqueous solution as a function of time for all four different minerals (montmorillonite, epidote, muscovite and illite). Although not as distinct as Figure 2-8, Figure 2-9 shows a different trend with the silica leaching at a fairly constant rate but slightly decreasing as a function of time.

The anaerobic condition in DIW with 0.1 M NaOH shows an increase in Si leaching as a function of time (Figures 2-8 through 2-10). Also, as previously mentioned, the lowest aqueous Si was observed in aerobic conditions in DIW with 3.1 M NH_4OH samples. Previous studies by Szecsody et al. demonstrate that there is a slow release (i.e., 10 s to 100 s) of silica in alkaline solutions under aerobic conditions (Szecsody et al., 2013). Lastly, anaerobic conditions in DIW with 3.1 M NH_4OH are seen as a steady rate as the sampling days progressed.

Huang and Keller reported similar results with a “near-constant concentration” after 5 to 21 days of study in different solutions (organic acids, CO_2-charged water or DIW) (Huang & Keller, 1970). For this particular experiment, there is a distinct difference between the dissolution of alkaline earth metals and Si according to the solutions.

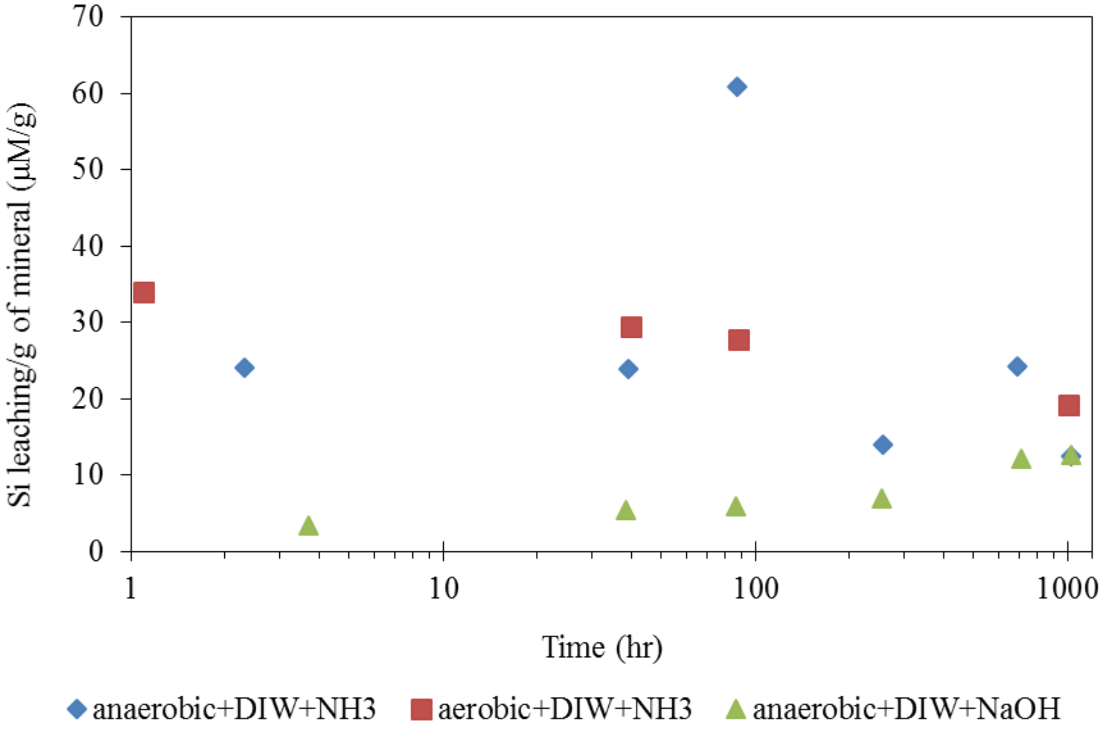

Figure 2-8. Silica leaching per gram of mineral muscovite for anaerobic+DIW with 3.1 M NH_4OH (blue), aerobic+DIW in NH_4OH (red) and anaerobic+DIW with 0.1 M NaOH (green) as a function of time.

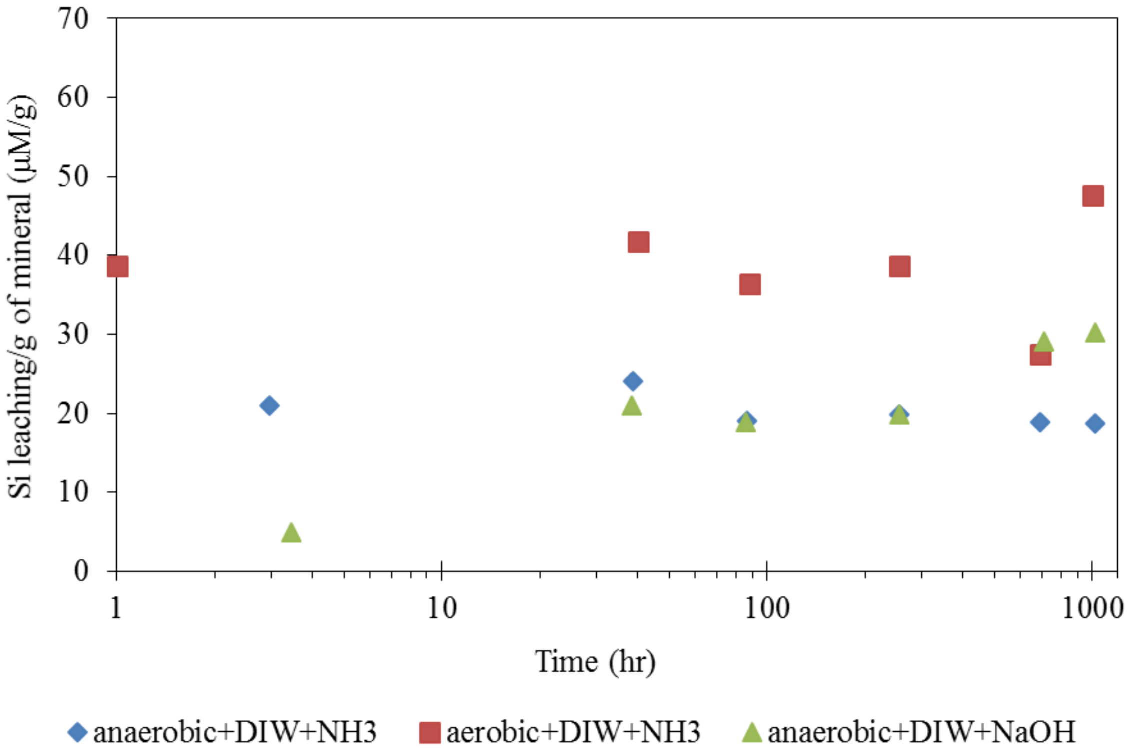

Figure 2-9. Silica leaching per gram of mineral illite for anaerobic+DIW with 3.1 M NH_4OH (blue), aerobic+DIW in NH_4OH (red) and anaerobic+DIW with 0.1 M NaOH (green) as a function of time.

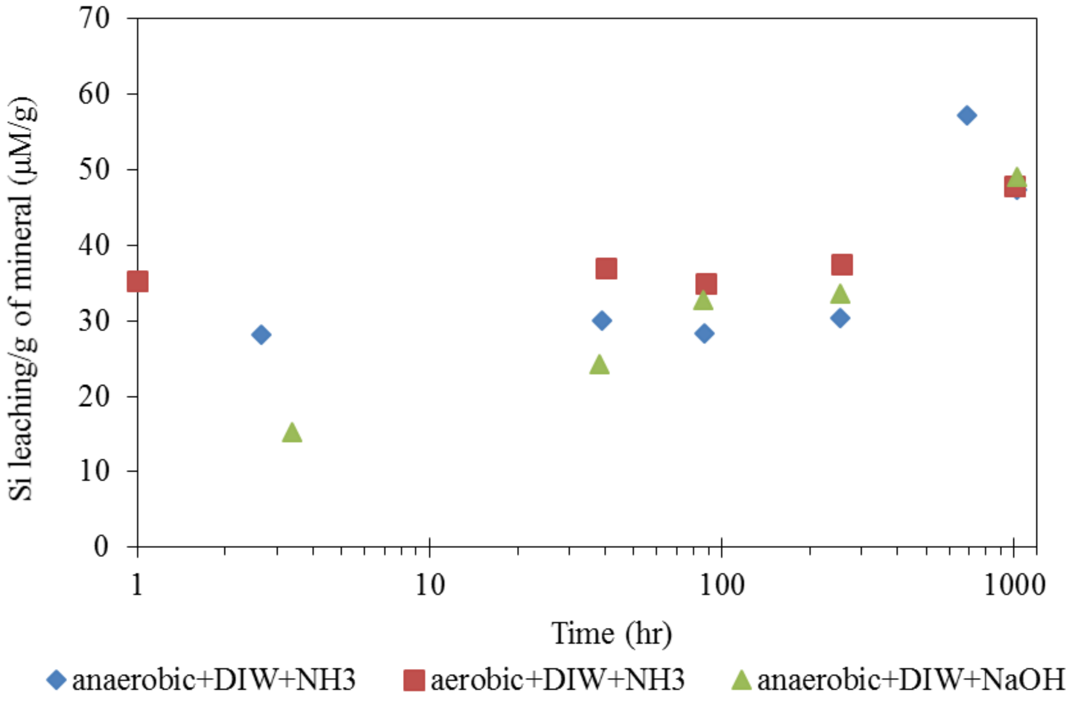

Figure 2-10. Silica leaching per gram of mineral montmorillonite for anaerobic+DIW with 3.1 M NH_4OH (blue), aerobic+DIW in NH_4OH (red) and anaerobic+DIW with 0.1 M NaOH (green) as a function of time.

In the future, thermodynamic literature and speciation modeling will be used as a reference to determine if the solutions are saturated with respect to the aqueous ions dissolved from the minerals. The saturation level is calculated based on the solubility of the minerals and the measured aqueous concentrations of ions. The quotient of the IAP and K_{so} is called the saturation index, given by Ω (Sposito, 1994). These estimates are based on Eq. 1 below, where the ion-activity product (IAP) represents the experimental ratio of the products to reactants. The solubility product, K_{so}, is the theoretical ratio of products to reactions at equilibrium (aka equilibrium constant) for the mineral dissolving in the aqueous solution.

$$\Omega = \frac{IAP}{K_{so}} \qquad \text{Eq. 1}$$

Preliminary modeling was conducted to predict precipitation of minerals within the range of aqueous concentrations of elements measured in the experiments conducted with montmorillonite. Figure 2-11 and Figure 2-12 summarize the results. Figure 2-11 and Figure 2-12 show a titration of Al into a solution at pH of 12.5 with either the lowest or highest Si and Ca measured in the dissolution experiments, respectively. Further, the Al concentration begins at the lowest measured concentration and is titrated up to the highest value.

At the lowest concentrations of aqueous cations, the magnesium silicate mineral antigorite is predicted to form at some level across the Al titration. However, at higher concentrations of Si and Ca, wollastonite ($CaSiO_3$) and diopsite ($CaMgSi_2O_6$) are predicted.

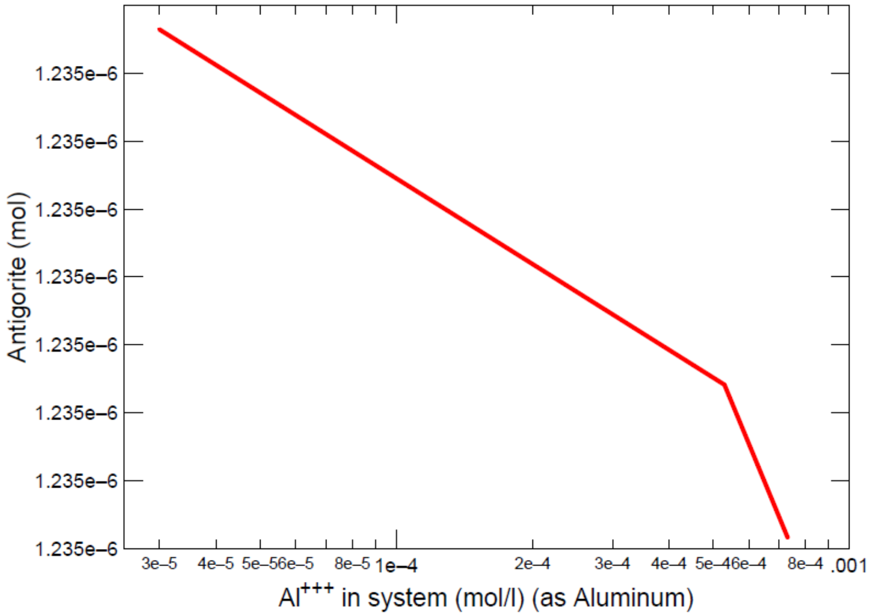

Figure 2-11. Titration of Al^{3+} into a solution containing the lowest concentrations of major elements measured in the dissolution experiments for montmorillonite (initial conditions: $[Al^{3+}] = 3x10^{-5}$ M, $[Ca^{2+}] = 2x10^{-5}$ M, $[Na^{+}] = 2x10^{-4}$ M, $[K^{+}] = 2x10^{-4}$ M, $[SiO_2(aqu)] = 1x10^{-4}$ M, pH = 12.5, and $[CO2(aqu)] = 1.33x10^{-5}$ M.

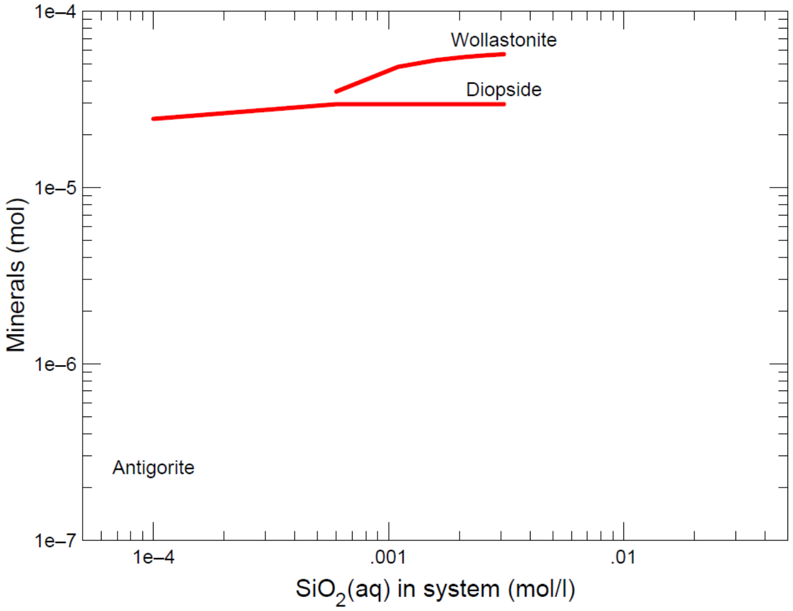

Figure 2-12. Titration of Al^{3+} into a solution containing lowest concentrations of major elements measured in dissolution experiments for montmorillonite (initial conditions: $[Al^{3+}] = 3x10^{-5}$ M, $[Ca^{2+}] = 1.2x10^{-4}$ M, $[Na^{+}] = 2x10^{-4}$ M, $[K^{+}] = 2x10^{-4}$ M, $[SiO_2(aqu)] = 2.7x10^{-3}$ M, pH = 12.5, and [CO2(aqu)] = $1.33x10^{-5}$ M.

References

Huang, W., & Keller, W. (1970). Dissolution of rock-forming silicate minerals in organic acids-simulated first-stage weathering of fresh mineral surfaces. *American Mineralogist, 55*(11-1), 2076-&.

Nycz, J. (2010). Chemical weathering. Retrieved from http://teach.albion.edu/jjn10/chemical-weathering

Sposito, G. (1994). *Chemical equilibria and kinetics in soils* Oxford University Press on Demand.

Szecsody, J. E., Truex, M. J., Qafoku, N. P., Wellman, D. M., Resch, T., & Zhong, L. (2013). Influence of acidic and alkaline waste solution properties on uranium migration in subsurface sediments. *Journal of Contaminant Hydrology*, *151*, 155-175. doi:10.1016/j.jconhyd.2013.05.009

Ammonia Gas Treated Batch Experiments without Pure Minerals

In January, FIU started a new experiment with the objective of determining the lowest Si/Al concentration ratio at which uranium removal is accomplished through generation of U-bearing precipitates after ammonia gas injections. For this purpose, the first step consisting of preparing the U-bearing precipitate samples was completed. The following Tables 2-1 and 2-2 provide information on the type and amount of salts used to prepare stock solutions that were further used to achieve the targeted concentrations in the samples.

Table 2-1. Amount of Salts to Prepare 50mL of Stock Solutions and Targeted Concentrations in Samples

Stock Solution	Salt Used	Molecular Weight of Salt (g/mol)	Stock Solution Concentration (mM)	Amount to Prepare 50 mL (g)	Targeted Concentrations in Samples (mM)		
Bicarbonate	$KHCO_3$	100.114	400	2.002	3	50	
Metasilicate	$Na_2SiO_3 \cdot 9H_2O$	284.196	422.24	5.998	15	25	
Aluminum	$Al(NO_3)_3 \cdot 9H_2O$	375.129	50	0.938	5		
Calcium	$CaCl_2.H_2O$	147.01	1250	9.188	0	5	10
Uranium Nitrate	$UO_2(NO_3)_2\ 6H_2O$	238.03	1000				

Table 2-2. Number of Samples and Targeted Concentrations in Each Sample

Sample ID	Si/Al (mM)	HCO_3 (mM)	Ca (mM)	U (ppm)
1	3	3	0	2
2	3	3	5	2
3	3	3	10	2
4	3	50	0	2
5	3	50	5	2
6	3	50	10	2
7	5	3	0	2
8	5	3	5	2
9	5	3	10	2
10	5	50	0	2
11	5	50	5	2
12	5	50	10	2

In addition to the original twelve U-bearing precipitate samples, duplicated and triplicated samples were prepared to sum up to a total of 36 U-bearing precipitate samples. Table 2-3 below contains information on the amounts of stock solution and DI water necessary to prepare 5 mL of each sample.

Table 2-3. Amounts of Stock Solutions to Prepare 5mL of Sample

3 mM Si/Al – 3mM and 50mM HCO_3 - 0, 5, 10 mM Ca - 2ppm U						
Amount of Stock Solution and DIW (uL) to Prepare 50 mL of Mixed Sample				**5mL Mixed Sample Including Ca and U**		
	$Na_2SiO_3 \cdot 9H_2O$ (50mM)	**1,776**	**uL**	**$UO_2(NO_3)_2$ $6H_2O$**	100	ppm
	Al(NO3)3·9H2O (5mM)	**5,000**	**uL**	**$CaCl_2.H_2O$**	1250	mM
# Sample	**Sample**	***$KHCO_3$ (µL)**	**DIW(mL)**	****Ca (µL)**	**U(µL)**	**Mixed Sample (µL)**
1	3mM $KHCO_3$, no Calcium	375	42.849	0	100	4,900
2	3mM $KHCO_3$, 5mM Calcium	375	42.849	20	100	4,880
3	3mM $KHCO_3$, 10mM Calcium	375	42.849	40	100	4,860
1D	3mM $KHCO_3$, no Calcium	375	42.849	0	100	4,900
2D	3mM $KHCO_3$, 5mM Calcium	375	42.849	20	100	4,880
3D	3mM $KHCO_3$, 10mM Calcium	375	42.849	40	100	4,860
1T	3mM $KHCO_3$, no Calcium	375	42.849	0	100	4,900
2T	3mM $KHCO_3$, 5mM Calcium	375	42.849	20	100	4,880
3T	3mM $KHCO_3$, 10mM Calcium	375	42.849	40	100	4,860
4	50mM $KHCO_3$, no Calcium	6,250	36.974	0	100	4,900
5	50mM $KHCO_3$, 5mM Calcium	6,250	36.974	20	100	4,880
6	50mM $KHCO_3$, 10mM Calcium	6,250	36.974	40	100	4,860
4D	50mM $KHCO_3$, no Calcium	6,250	36.974	0	100	4,900
5D	50mM $KHCO_3$, 5mM Calcium	6,250	36.974	20	100	4,880
6D	50mM $KHCO_3$, 10mM Calcium	6,250	36.974	40	100	4,860
4T	50mM $KHCO_3$, no Calcium	6,250	36.974	0	100	4,900
5T	50mM $KHCO_3$, 5mM Calcium	6,250	36.974	20	100	4,880
6T	50mM $KHCO_3$, 10mM Calcium	6,250	36.974	40	100	4,860

* Varied from 3mM to 50mM

** Varied from 0, 5 and 10 mM

Samples were mixed and left for two days before centrifugation to separate the supernatant solution and precipitated solids. Uranium analyses are pending upon repair of the KPA instrument. Uranium analysis of the supernatant solutions collected in the month of December after sequential extractions experiments were not processed due to low sensitivity of the KPA instrument that requires replacement of the nitrogen laser.

FIU continued data analysis after EPMA and elemental mapping of precipitate samples cold-mounted in epoxy and polished by collaborators at PNNL. Analyses were completed using the Florida Center of Analytical Electron Microscopy's JEOL 8900R Superprobe equipped with 5 two-crystal WDS Spectrometers and a Single EDS-UTW detector. The settings were as follows: Accelerating Voltage: 20.0 kV; Spot Size: 5-10 µm; Dwell Time: 20 ms; Accumulations: 1-5 scans.

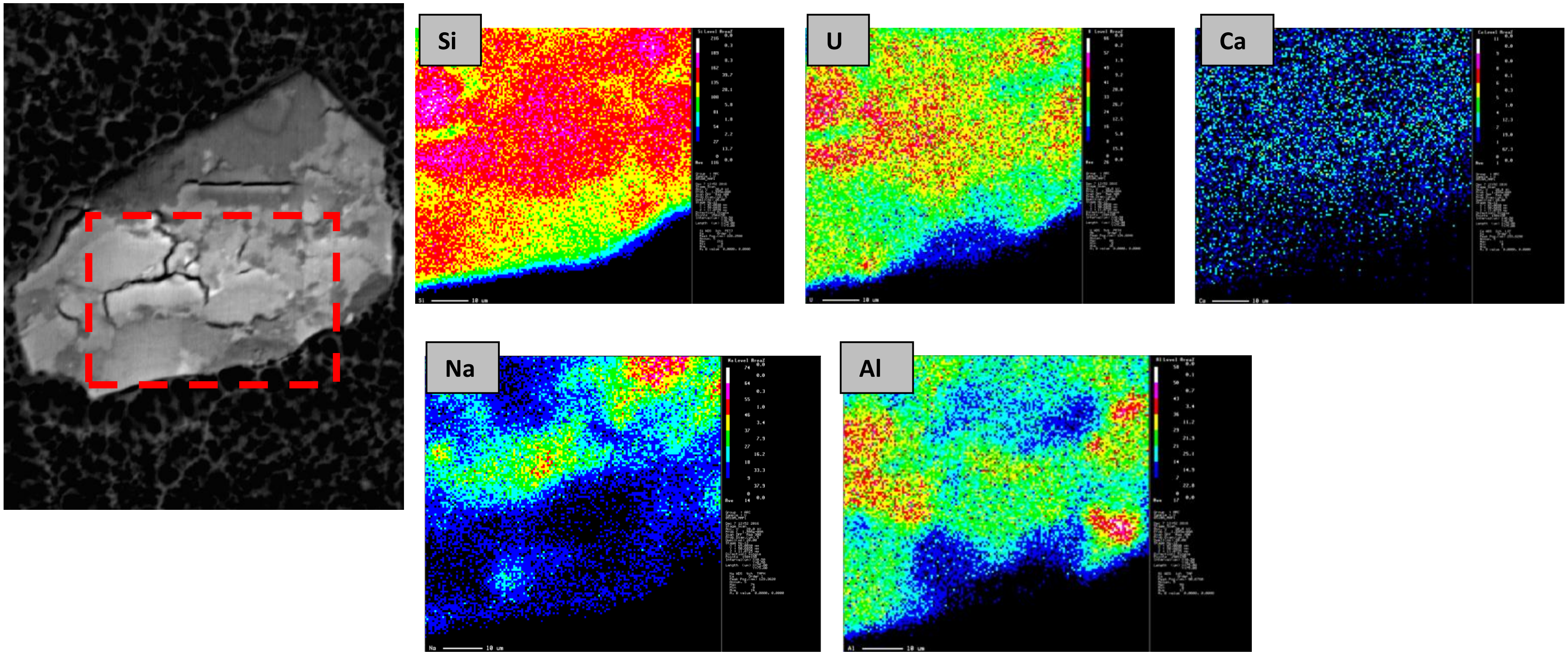

Figure 2-13. EPMA micrograph and corresponding elemental maps. This sample included 500 ppm U(VI), 100 mM Si, 5 mM Al, 5 mM HCO$_3$ and 10 mMCa.

In the exhibited sample (Figure 2-13), the elemental distribution maps present the abundance of silica across the entire sample surface. The map for uranium shows that it is present at a quantity and distribution that aligns well with that of silica. The relationship between these distribution maps could signify the presence of a uranyl-silicate form. This is consistent with interpretations of sequential extraction analysis and predictive speciation modeling results. Aluminum is aligned well with areas higher in Si content. Though its distribution is similar to that of the more significant contributors, the peak areas of aluminum concentration do not appear to align with distinctive peaks or valleys in the other targeted elements. Unlike other elements, sodium has a meager presence throughout the bulk of the analyzed area with some pockets of high concentration.

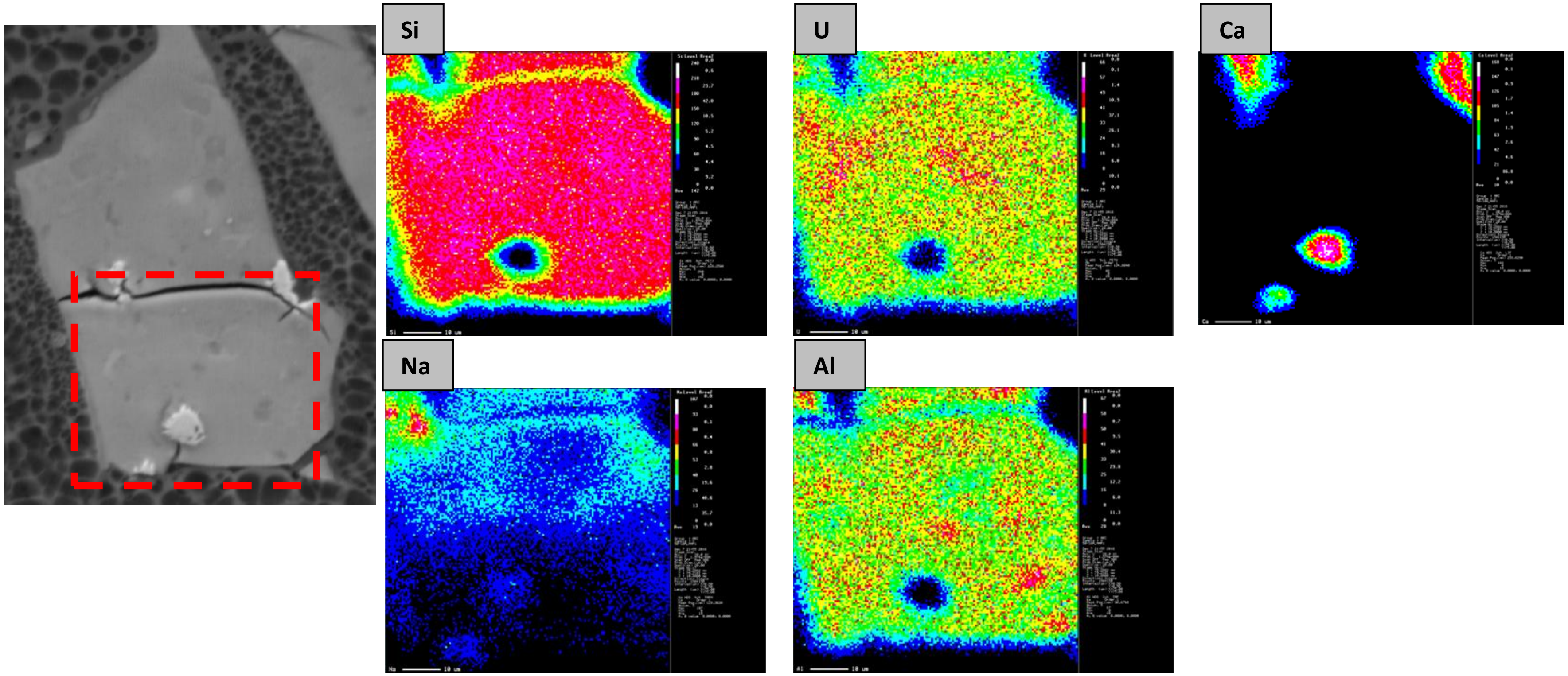

Figure 2-14. EPMA micrograph and corresponding elemental maps. This sample included 500 ppm U(VI), 100 mM Si, 5 mM Al, 50 mM HCO_3 and 10 mM Ca.

In the sample prepared with 50mM HCO_3, the elemental distribution maps also present the abundance of silica across the entire sample surface (Figure 2-14). The uranium map aligns well with silica. The formation of calcium carbonate solids is shown on the Ca map and its distribution is consistent with maps of other elements. Similar to the previous sample, aluminum is aligned well with areas higher in Si content.

In the month of February, FIU started the second part of a new experiment with the objective of determining the lowest Si/Al concentration ratio to which uranium removal is accomplished after ammonia gas injections to U-bearing precipitate samples. This time, the composition of pore water has been changed; instead of using Ca, Mg was used as a major cation component. For this purpose, the first step consisting of preparing the U-bearing samples was completed. The following Tables (2-4 and 2-5) provide information on the type and amount of salts used to prepare stock solutions that were further used to achieve the target concentrations in the samples.

Table 2-4. Amount of Salts to Prepare 50 mL of Stock Solutions and Target Concentrations in Samples

Stock Solution	Salt Used	Molecular Weight of Salt (g/mol)	Stock Solution Concentration (mM)	Amount to Prepare 50 mL (g)	Target Concentrations in Samples (mM)		
Bicarbonate	$KHCO_3$	100.114	400	2.002	3	50	
Metasilicate	$Na_2SiO_3\cdot 9H_2O$	284.196	422.24	5.998	15	25	
Aluminum	$Al(NO_3)_3\cdot 9H_2O$	375.129	50	0.938	5		
Magnesium	$H_{12}O_6MgCl_2$	203.3	1250	12.706	0	5	10
Uranium Nitrate	$UO_2(NO_3)_2\ 6H_2O$	238.03	1000				

Table 2-5. Number of Samples and Target Concentrations in Each Sample

Sample No.	Si/Al (mM)	HCO_3 (mM)	Mg (mM)	U (ppm)
1	3	3	5	2
2	3	3	10	2
3	3	50	5	2
4	3	50	10	2
5	5	3	5	2
6	5	3	10	2
7	5	50	5	2
8	5	50	10	2

In addition to the original eight U-bearing precipitate samples, duplicate and triplicate samples were prepared to sum up to a total of 36 U-bearing precipitate samples. Tables 2-6 and 2-7 present the amount of stock solution and DI water necessary to prepare 5 mL of each sample.

Table 2-6. Amount of Stock Solution to Prepare 5 mL of Precipitate Samples

3 mM Si/Al - 3 and 50 mM HCO3 -5,10 mM Mg – 2 ppm U						
Amount of Stock Solution and DIW (uL) to prepare 50 mL of mixed sample				5 mL Mixed Sample including Ca and U		
	$Na_2SiO_3 \cdot 9H_2O$ (50 mM)	1,776	uL	$UO_2(NO_3)_2$ $6H_2O$	100	ppm
	$Al(NO_3)_3 \cdot 9H_2O$ (5 mM)	5,000	uL	$H_{12}O_6MgCl_2$	1250	mM
Sample ID	Sample	*$KHCO_3$ (µL)	DIW(mL)	**Ca (µL)	U(µL)	Mixed Sample (µL)
13	3 mM $KHCO_3$, 5 mM Mg	375	42.849	20	100	4,880
14	3 mM $KHCO_3$, 10 mM Mg	375	42.849	40	100	4,860
13D	3 mM $KHCO_3$, 5 mM Mg	375	42.849	20	100	4,880
14D	3 mM $KHCO_3$, 10 mM Mg	375	42.849	40	100	4,860
13T	3 mM $KHCO_3$, 5 mM Mg	375	42.849	20	100	4,880
14T	3 mM $KHCO_3$, 10 mM Mg	375	42.849	40	100	4,860
15	50 mM $KHCO_3$, 5 mM Mg	6,250	36.974	20	100	4,880
16	50 mM $KHCO_3$, 10 mM Mg	6,250	36.974	40	100	4,860
15D	50 mM $KHCO_3$, 5 mM Mg	6,250	36.974	20	100	4,880
16D	50 mM $KHCO_3$, 10 mM Mg	6,250	36.974	40	100	4,860
15T	50 mM $KHCO_3$, 5 mM Mg	6,250	36.974	20	100	4,880
16T	50 mM $KHCO_3$, 10 mM Mg	6,250	36.974	40	100	4,860

Table 2-7. Amount of Stock Solution to Prepare 5 mL of Precipitate Samples

5 mM Si/Al - 3 and 50 mM HCO_3 - 5, 10 mM Mg – 2 ppm U						
Amount of Stock Solution and DIW (uL) to prepare 50 mL of mixed sample				5 mL Mixed Sample including Ca and U		
	$Na_2SiO_3 \cdot 9H_2O$ (50 mM)	2,960	uL	$UO_2(NO_3)_2$ $6H_2O$	100	ppm
	$Al(NO_3)_3 \cdot 9H_2O$ (5 mM)	5,000	uL	$CaCl_2.H_2O$	1250	mM
Sample ID	**Sample**	***$KHCO_3$ (µL)**	**DIW(mL)**	****Ca (µL)**	**U(µL)**	**Mixed Sample (µL)**
17	3 mM $KHCO_3$, 5 mM Mg	375	41.665	20	100	4,880
18	3 mM $KHCO_3$, 10 mM Mg	375	41.665	40	100	4,860
17D	3 mM $KHCO_3$, 5 mM Mg	375	41.665	20	100	4,880
18D	3 mM $KHCO_3$, 10 mM Mg	375	41.665	40	100	4,860
17D	3 mM $KHCO_3$, 5 mM Mg	375	41.665	20	100	4,880
18D	3 mM $KHCO_3$, 10 mM Mg	375	41.665	40	100	4,860
19	50 mM $KHCO_3$, 5 mM Mg	6,250	35.790	20	100	4,880
20	50 mM $KHCO_3$, 10 mM Mg	6,250	35.790	40	100	4,860
19D	50 mM $KHCO_3$, 5 mM Mg	6,250	35.790	20	100	4,880
20D	50 mM $KHCO_3$, 10 mM Mg	6,250	35.790	40	100	4,860
19T	50 mM $KHCO_3$, 5 mM Mg	6,250	35.790	20	100	4,880
20T	50 mM $KHCO_3$, 10 mM Mg	6,250	35.790	40	100	4,860

After preparing the samples, they will be centrifuged and supernatant solutions will be separated and collected in different vials in order to be analyzed for U concentration through KPA. It is important to note that this set of samples along with the one prepared in the month of January have been delayed for analysis given that the KPA instrument needs repair.

In the month of March, FIU started a new column experiment with objective of evaluating the relative extractability from artificially prepared U-bearing precipitates. This experiment will follow similar procedure as Smith and Szecsody's (2011) experiment. The method to evaluate the extractability is termed "continuous leach" and uses a small volume (~1 cm^3) precipitate-filled cell and saturated flow. Preliminarily, the following two extractants, which should access highly liable and hard-to-extract U phases, will be used for this method:

1. Synthetic Groundwater
2. Acetic Acid at pH 2.3

The process consists of injecting the extractant solutions into a small plastic column at a constant flow rate estimated to be 1 mL/day, and collecting discrete effluent samples over time. During the month of March, the preparation of the artificial U-bearing precipitates was accomplished. The protocol to prepare the samples was similar to the previous experiments. Table 2-8 provides information on the type and amount of salt used to prepare the stock solutions that were further used to achieve the target concentrations in the samples, as presented in Table 2-9.

Table 2-8. Salt to Prepare 50 mL of Stock Solution and Target Concentrations in Each Sample

Stock Solution	Salt Used	Molecular Weight of Salt (g/mol)	Stock Solution Concentration (mM)	Amount to prepare 50 mL (g)	Target Concentration in Samples (mM)	
Bicarbonate	$KHCO_3$	100.114	400	2.002	3	50
Metasilicate	$Na_2SiO_3·9H_2O$	284.196	422.24	5.998	50	
Aluminum	$Al(NO_3)_3·9H_2O$	375.129	50	0.938	5	
Calcium	$CaCl_2.H_2O$	147.01	1250	9.188	10	
Uranium Nitrate	$UO_2(NO_3)_2$ $6H_2O$	238.03	1000			

Table 2-9. Number of Samples and Target Concentrations in Each Sample

Amount of Stock Solution and DIW (uL) to prepare 50 mL of mixed sample					
$Na_2SiO_3·9H_2O$ (50mM)		5,921	uL	$UO_2(NO_3)_2$ $6H_2O$	1000 ppm
Al(NO3)3·9H2O (5mM)		5,000	uL	$CaCl_2.H_2O$	1250 mM
Sample Number	**Sample**	***$KHCO_3$ (µL)**	**DIW(mL)**	****Ca (µL)**	**U(µL)**
1	3 mM $KHCO_3$, 10 mM Calcium	375	38.204	400	100
2	50 mM $KHCO_3$, 10 mM Calcium	6,250	32.329	400	100

It is important to note that four (4) mixed sample centrifuge tubes for each sample composition were prepared to be able to obtain approximately 1 gram of dried solid precipitate. So, a total of eight (8) mixed sample centrifuge tubes were prepared. The needed volume was estimated and calculated based on past experimental experience and is as follows:

Needed Solution Volume Calculations		
Previous Volume prepared	10	mL
Previous Obtained Precipitate Weight	0.0452	g
Current Desired Precipitate Weight	1	g
Current Volume Needed	**221.24**	**mL**

By preparing approximately 200 mL of mixed solution, it is expected to yield 0.95-1 g of dried solid precipitate to fill the column in the future. The precipitates have been prepared and are currently set to dry in the oven. Additionally, the pump that will be used to control the flowrate of the extractant is currently being calibrated to obtain the desired flowrate of 1 mL/day. Since this flowrate is significantly low and to ensure accurate calibration, daily flowrate samples are being measured to obtain the daily averages over weeks.

Subtask 1.2. Investigation on Microbial-Meta-Autunite Interactions – Effect of Bicarbonate and Calcium Ions

In the month of January, the sterile media solutions prepared in December were moved to the anaerobic glove box with the 20-mL sacrificial vials. Vials that contained 19mg of autunite were then labeled with numbers (20 vials for each concentration with two controls) and color coded according to what concentration of $KHCO_3$ they received. 10-mL sterile media solutions were then distributed accordingly. A sampling schedule was then made for the following weeks. As sampling was about to start, FIU noticed turbidity in some of the vials and subsequently checked these samples under a light microscope. It was found that the vials with the turbidity were contaminated with bacteria other than the experimental bacteria, Shewanella MRI, which was not yet added to the vials. The contaminated vials were discarded appropriately and FIU has since restarted experimental preparation procedures including the synthesis of autunite and the media solutions, and vial preparations. Media solutions were made using 5.2-g of sodium-free Hepes buffer diluted in 1.0 L of DI water. The pH was then adjusted with 1.0-M sodium hydroxide to about 7.3, and 4.48-mL of 24-mmol/L sodium lactate was added to the solution. After being filter sterilized, one bottle was labeled as “No-bicarbonate”. Potassium bicarbonate was added to two of the remaining bottles in amounts that made the concentrations of 3 mM and 10 mM of $KHCO_3$ (Table 2-10). 20-mL sacrificial glass scintillation vials were cleaned and prepared for the biotic and abiotic control samples.

Table 2-10. Sterile Media Solutions Composition

Sterile Media Solutions Composition		
0 mM HCO_3	**3 mM HCO_3**	**10 mM HCO_3**
- 0.02-M Hepes buffer • 5.2-g Hepes • 4.48-mL 24 mmol/L sodium lactate	- 0.02-M Hepes buffer • 5.2-g Hepes • 4.48-mL 24 mmol/L sodium lactate - 0.09912-g KCO_3	- 0.02-M Hepes buffer • 5.2-g Hepes • 4.48-mL 24 mmol/L sodium lactate - 0.3304-g KCO_3

In the month of February, preparations to begin the microbial sub-task were continued. Sodium autunite was synthesized and allowed to dry. After drying, vials that contained 19-mg of autunite were then labeled with numbers (20 vials for each 0 mM, 3 mM and 10 mM bicarbonate concentration with two controls) and color coded according to what concentration of $KHCO_3$ they received. 10-mL sterile media solutions that contain sodium lactate were then distributed accordingly. A sampling schedule was then created for the following weeks. When the solution was added, two random samples (10-uL) were taken from the sacrificial vials and spread on agar plates to ensure no contamination was present. No growth was observed on these plates; so, the intended sampling schedule continued as planned. Three control samples were taken before the experimental bacteria, Shewanella MRI, was amended to the solutions in the concentration log6 cell/mL in each vial. The solution for control sampling was taken using a 1-mL syringe to extract 0.5-mL and filtered with a 2.0-uL filter to remove any particles or protein present. The solutions were filtered into a 1.5-mL brown glass sampler vial. This was done for each designated concentration control. A backup control was also made in case any contamination occurred. Before the experimental bacteria were amended, it was diluted 10 times with DI water. At this concentration, 49-uL of bacteria solution was added to each sacrificial vial kept in the anaerobic glove box besides the designated controls to target a cell concentration of log 6 cell/mL in each vial.

In the month of March, FIU initiated procedures for sampling of the inoculated vials after control sampling was completed. The culture of microorganism used for the inoculation of the experimental samples, *Shewanella* MRI, was prepared and diluted before being inoculated into sacrificial vials. A fresh culture of *Shewanella*, grown in 15-mL tubes, were placed in the incubator at 30ºC while being shaken at 100 rpm. The culture was then centrifuged and the media was removed and replaced with DI water. The average cell count was multiplied by the dilution and volume factor in order to calculate the final concentration of cells per mL. The number of cells/mL in the stock suspension was used to estimate a desired volume of a bacterial suspension needed for the inoculation of each bottle. About 49 µL of bacteria was distributed to each experimental vial. FIU initiated sampling of the inoculated vials kept in the anaerobic glove box. Sampling was done by using a 1-mL syringe to extract 0.5-mL of solution which was filtered through a 2.0-µm filter to remove any autunite particles or cells present. The solutions were filtered into a 1.5-mL brown glass sample vial. This was done for each concentration. The sacrificial vials were then placed under a biosafety cabinet and 10-uL (no dilution) of each concentration was plated on LB media. Bacteria were allowed to grow overnight and then counting was performed for each.

Subtask 1.3. Investigation of Electrical Geophysical Response to Microbial Activity in the Saturated and Unsaturated Environments

FIU continued to perform the column experiments related to the spectral induced polarization (SIP) signatures of microbial activity. Flow to the columns is powered by a peristaltic pump with a target flow rate of 50 mL/d for each column. In January, FIU converted columns 1 and 2 (former control and bicarbonate) into microbial columns by injecting microbes, while simultaneously initiating the pumping of glucose solution. There are two separate solutions which have been sparged with nitrogen in order to remove any dissolved gases which may form bubbles within the column; solution 1 is synthetic groundwater with glucose, while solution 2 is synthetic groundwater with glucose and bicarbonate. Each bottle of solution is connected to a bag full of nitrogen that prevents the solutions from equilibrating with carbon dioxide.

Since geochemical changes within the column due to microbial growth seem to be fast, this second experiment should not last more than two months and should produce results quickly. The analyses will include phase and resistivity (geophysical results), as well as fluid conductivity, pH, ORP, Fe^{2+}, and total Fe via ferrozine analysis.

The experiment involving columns 1 and 2 proceeded more smoothly than work previously performed due to accumulated experience running the columns.

A progress report was submitted in January summarizing previous work. Sample results from this report for column 4 which depict gradual changes are included in Figure 2-15, Figure 2-16 and Figure 2-17 below.

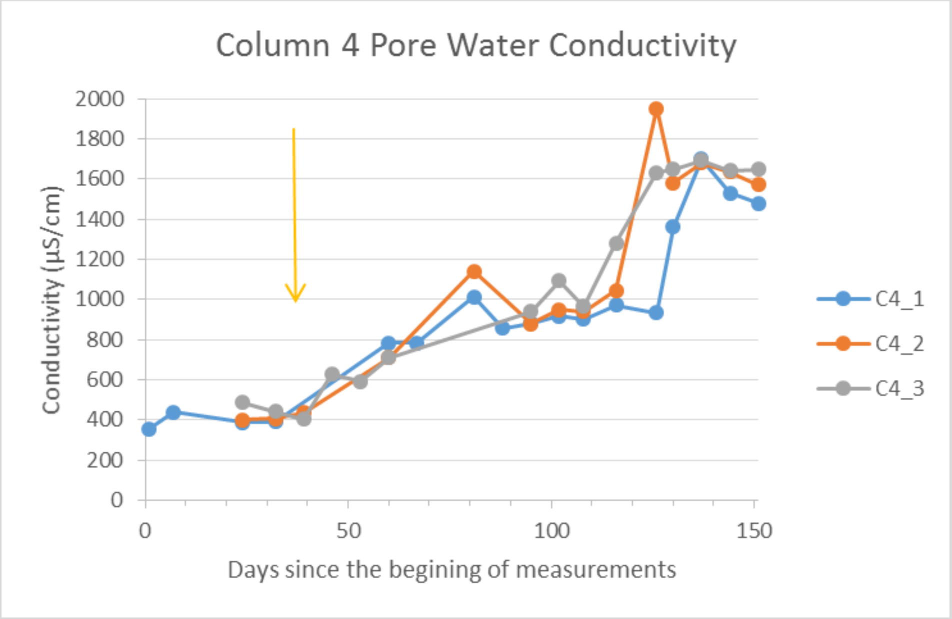

Figure 2-15. Column 4 pore water conductivity.

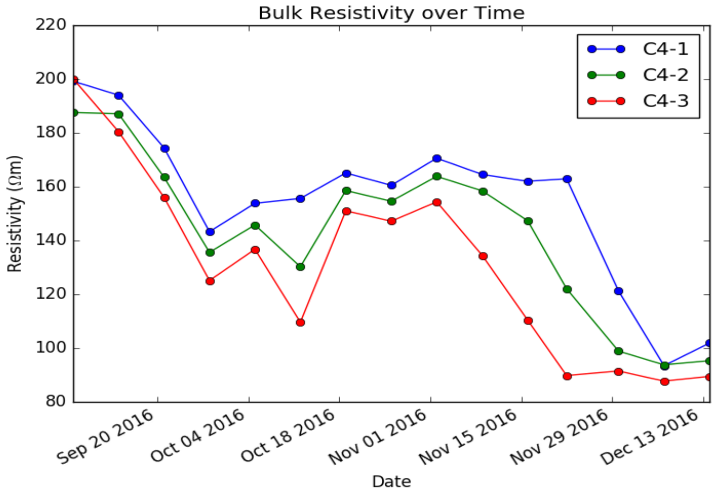

Figure 2-16. Column 4 bulk resistivity.

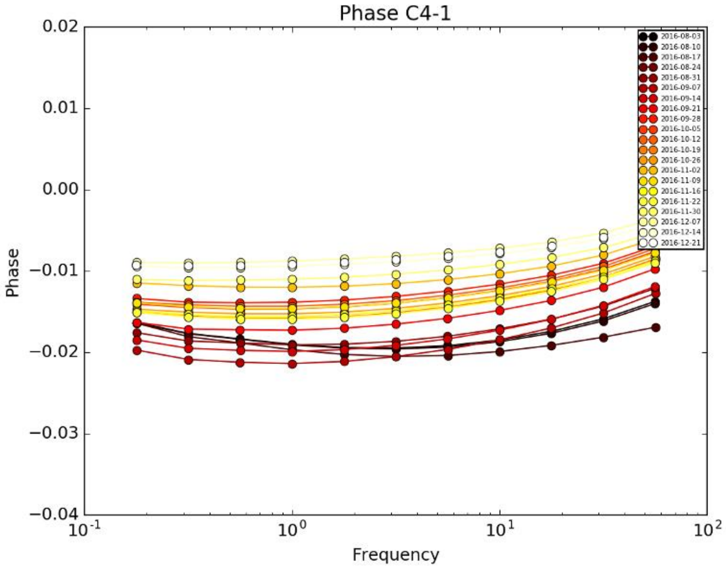

Figure 2-17. Column 4 Port 1 phase.

FIU has completed sample collection related to the spectral induced polarization (SIP) signatures of microbial activity. In January, FIU converted columns 1 and 2 (former control and bicarbonate-amended) into columns inoculated with microbial consortia enriched from Hanford soil, while simultaneously initiating the pumping of a glucose solution. For this experiment, two separate solutions were prepared and sparged with nitrogen in order to remove any dissolved gases that may form bubbles within the column. Solution 1 mimics the synthetic groundwater amended with glucose, while solution 2 was the same synthetic groundwater but amended with glucose and bicarbonate. Each bottle of solution was connected to a bag filled with nitrogen gas to prevent the solutions from equilibrating with the air.

Since geochemical changes within the column due to microbial growth occurred quickly, sample collection for this second experiment was completed in less than two months. Analysis of the pore water is currently underway and will include conductivity, pH, ORP, Fe^{2+}, and total Fe via ferrozine analysis. Future analysis will include Ca, P, Si, and Al via ICP-OES as well as U via the KPA instrument.

Geophysical data for column 2 is displayed in Figures 2-18 and 2-19.

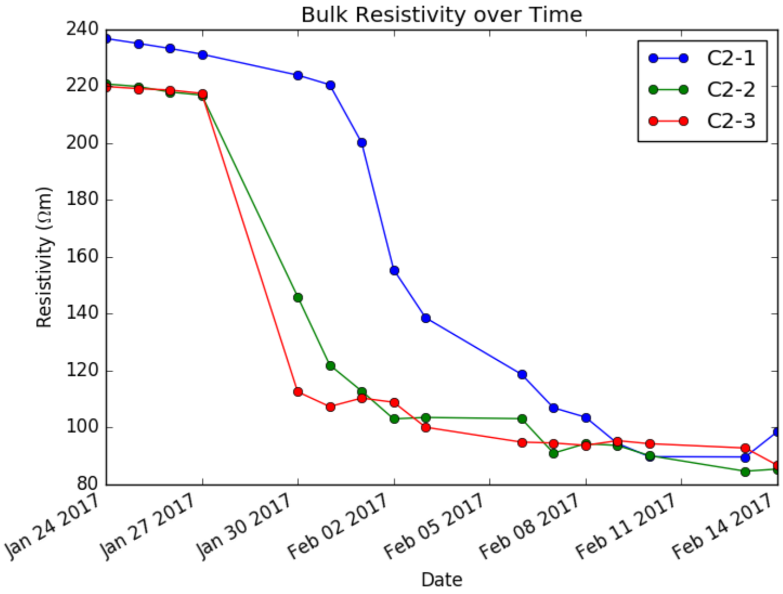

Figure 2-18. Column 2 bulk resistivity.

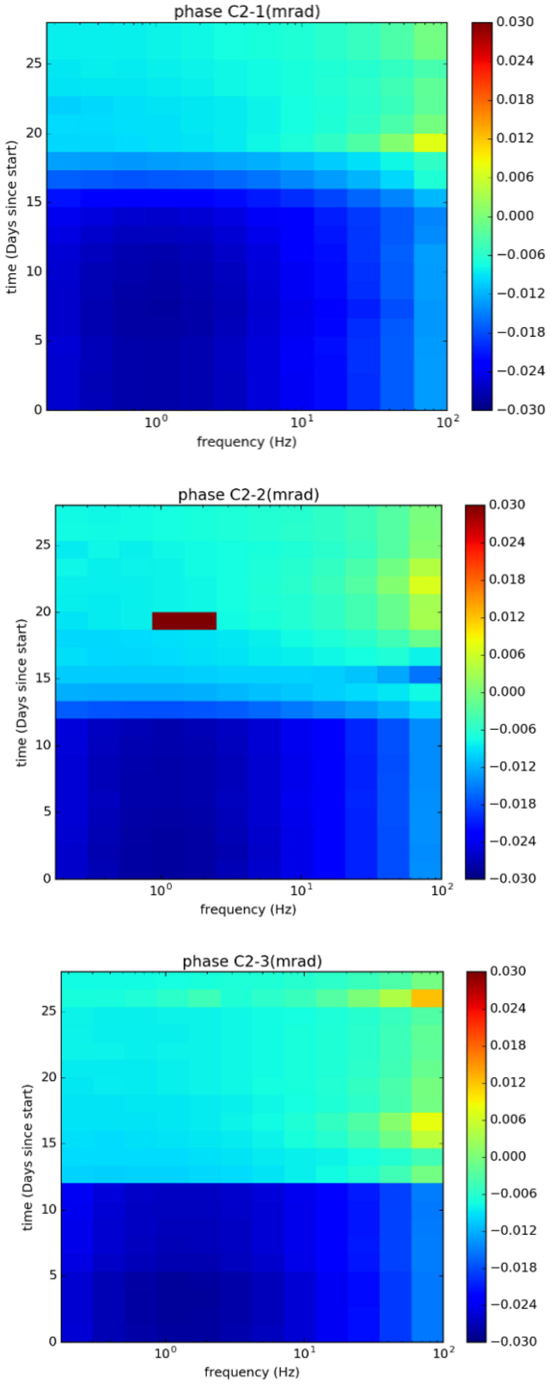

Figure 2-19. Column 2 phase for ports 1-3.

Future analysis will focus on other dissolved species using KPA to measure uranium and ICP-OES for calcium, phosphorus and total iron.

Results for Fe $^{2+}$ and total Fe analysis for column 2 is displayed in Figures 2-20 and 2-21.

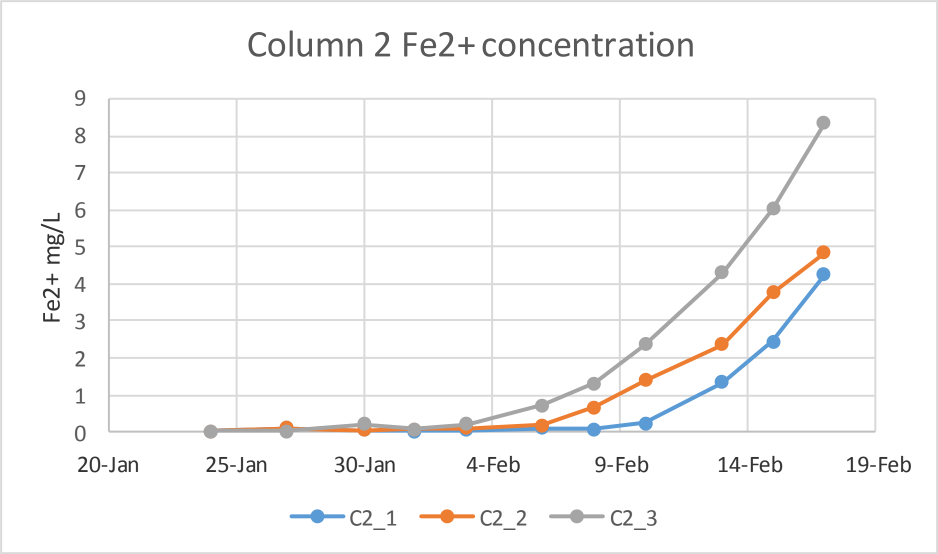

Figure 20. Fe^{2+} for Column 2.

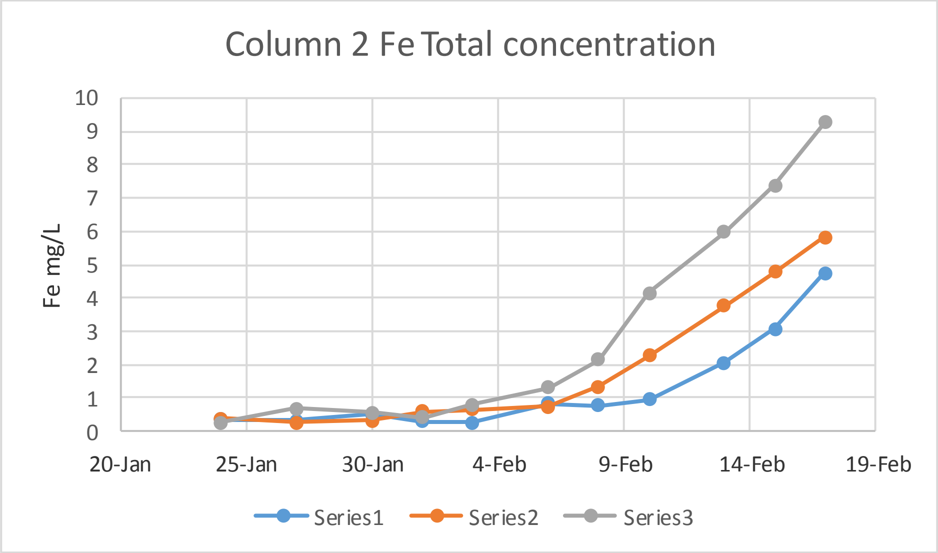

Figure 2-21. Column 2 phase for ports 1-3.

Subtask 1.4. Contaminant Fate and Transport under Reducing Conditions

FIU's prior experiments (sieving and specific surface area determination via BET method) assisted in categorizing Hanford soil into two major fractions: bulk (300 µm<d< 2mm) or fine (d< 300 µm) soil.

A literature review was conducted for mineralogical analysis in January 2017. The mineralogy and geochemical composition of the 200 Area at Hanford was studied in order to better understand the soil-contaminant(s) interactions. Xie et al. [1] researched the geochemical composition and mineralogy of the 200 Area and the results are compiled in Table 2-11. A total of 55 samples from the Hanford (HF) 200 Area and Ringold Formation were analyzed by means of electron microprobe (EM). The major minerals at HF 200 Area are quartz at approximately

38% by weight (wt), plagioclase ~22% wt, microcline ~15% wt, amphiboles ~5.5% wt, pyroxenes ~5% wt, and magnetite ~4.5% wt. The samples collected from the Ringold Formation originate at depths of 200-500 ft, whereas the samples from the HF 200 Area originate at depths of 25-100 ft.

Szecsody et al. [2] collected sediments from Hanford, Ringold, and Cool Creek with the ultimate goal being to determine the influence of acidic and alkaline waste solutions on uranium migration through the sediments. The mineralogical analysis was performed by means of X-Ray Diffraction (XRD) and the results are presented in Table 2-12. The samples were collected from depths 18-38 ft and are bulkily categorized into mineralogical fractions (mean diameter < 2mm) and clays (mean diameter < 2μm).

Table 2-11. Hanford 200 Area and Ringold Formation Mineralogy [1]

Mineral	Formula	Hanford Fm (% wt)	Ringold Fm (% wt)	Both Fm (% wt)
Quartz	SiO_2	38.4 ± 12.8	37.03 ± 12.4	37.7 ± 12.4
Microcline	$KAlSi_3O_8$	15.3 ± 4.4	18.7 ± 8.0	17.0 ± 6.7
Plagioclase	$NaAlSi_3O_8$-$CaAl_2Si_2O_8$	22.2 ± 7.2	15.5 ± 6.8	18.7 ± 7.7
Pyroxenes	$(Ca,Mg,Fe)Si_2O_6$	5.01 ± 7.83	1.14 ± 2.52	3.03 ± 5.99
Calcite	$CaCO_3$	1.91 ± 1.71	0.68 ± 0.92	4.97 ± 7.19
Magnetite	Fe_3O_4	4.46 ± 4.12	5.68 ± 4.63	5.09 ± 4.37
Amphiboles	$Ca_2(Mg, Fe, Al)_5\ (Al, Si)_8O_{22}(OH)_2$	5.46 ± 5.67	5.64 ± 6.40	5.55 ± 5.97
Apatite	$Ca_{10}(PO_4)_6(OH)_2$	0.52 ± 0.92	0.67 ± 1.16	0.60 ± 1.04
Mica*	$(K, Na,Ca)(Al, Mg, Fe)_{2\text{-}3}(Si,Al)_4O_{10}(O, F, OH)_2$	2.46 ± 3.74	1.71 ± 5.15	2.07 ± 4.47
Ilmenite	$FeTiO_3$	1.28 ± 1.51	3.67 ± 3.00	2.51 ± 2.66
Epidote	$\{Ca_2\}\{Al_2Fe^{3+}\}[O\vert OH\vert SiO_4\vert Si_2O_7]$	1.78 ± 3.75	1.52 ± 2.14	1.65 ± 2.98

* muscovite, biotite, phlogopite, lepidolite, clintonite, illite, phengite

Table 2-12. Hanford 200 Area, Cold Creek, and Ringold Borehole Mineralogy [2]

			Mineralogy (< 2mm)						Clays (<2μm)			
Formation	Borehole	Depth (m)	Quartz	Plagioclase	K-feldspar	Amphiboles	Clays	Calcite	Illite	Smectite	Chlorite	Kaolinite
Hanford	C4105, TX-106	18.6	34	39	15	2	8	1	47	26	20	7
Cold Creek	C4105, TX-106	28	11	18		7	10	55	50	35	10	5
Ringold	C4105, TX-106	38	27	43	12	4	11	4	40	40	13	7

* All meruments are repoted in percent by weight

Both studies concluded that quartz and plagioclase were the major minerals present in the sediments with mean diameter < 2mm. In spite of the soil sampling differences (depth and location), percentage levels of quartz and plagioclase were quite similar in both studies. Nevertheless, clays are a very important factor in the fate and transport of contaminants and their interactions with the soil due to their large surface area and chemical composition. Illite, smectite and chlorite were determined to be the major clays based on the study by Szecsody et al.

Determination of the mineralogy in the samples being used by FIU is a critical component of the experimental process. To this end, task lead, Dr. Vasileios Anagnostopoulos, and DOE Fellow, Mr. Alejandro Hernandez, went through X-ray Powder Diffractometer (XRD) training in January 2017 at FIU's Advanced Materials Engineering Research Institute (AMERI) Facility, where an XRD is located. The goal is to characterize the two major fractions identified by FIU, bulk (300 μm<d< 2mm) or fine (d< 300 μm) by means of XRD and consequently, also perform elemental analysis by means of SEM-EDS. These two techniques will help identify qualitatively and quantitatively the mineralogy of the Hanford soil that is being analyzed at FIU's facilities. Table 2-13 shows the primary reflecting angle for the different clays and minerals that are expected to be percent in the Hanford Soil [3]. These references will help guide the XRD analysis.

Table 2-13. XRD Reference for Minerals/Clay Primary Reflecting Angles [3]

Minerals and Clays	Primary Reflection ˚2θ
Quartz	26.6˚
Plagioclase	27.92˚
Microcline	21.1˚
Clinochlore	12.4˚
Amphibole	10.5˚
Calcite	29.45˚
Mica	8.8˚
Smectite	6.3˚

During month of February, mineralogical studies of the Hanford soil were performed. As discussed in previous reports, two fractions were identified for the Hanford soil available at the FIU facilities: bulk fraction (300 µm<d< 2mm) and fine fraction (d< 300 µm). These two different fractions were analyzed by means of XRD in an effort to identify qualitatively the mineralogy of the soil, since the mineralogical content of the soil can affect contaminant mobility.

Samples were prepared by crushing about 3 g of both bulk and fine fractions, to create a fine powder-like solid for the XRD analysis. The samples were crushed using a mortar and pestle in order to increase homogeneity. Figure 2-22 depicts an example of the morphology of the bulk soil fraction before and after grain size reduction. It was imperative for the morphology be as homogenous as possible, since the X-rays, in the case of a coarse sediment, may diffract several times on valleys and peaks formed by the sample's grains and this can lead to an increase in noise and weaker signals.

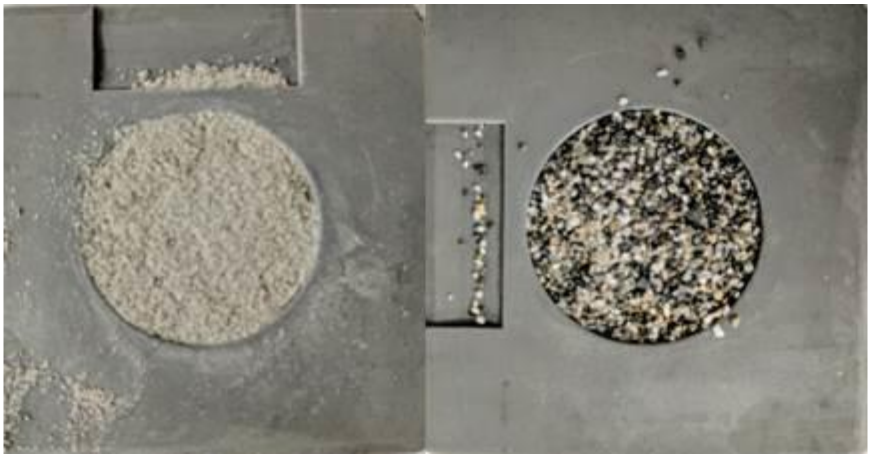

Figure 2-22. Bulk soil fraction crushed (right) and not-crushed (left).

The samples were analyzed at the Advanced Materials Engineering Institute (AMERI) facility, which is located at the FIU Engineering Campus. The XRD instrument is a Siemens D5000 diffractometer (Figure 2-23).

Figure 2-23. Siemens D5000 Diffractometer located at Advanced Materials Engineering Institute (AMERI) at the FIU Engineering campus.

Figures 2-24 and 2-25 illustrate the preliminary qualitative data obtained from the XRD analysis of the bulk and fine fractions. The samples were run from 2 to 40 2-theta and peak analysis was conducted by *MATCH!* software. As expected, the preliminary results of the bulk fraction show the presence of quartz, microcline, calcite, and magnetite. The fine fraction show the presence of quartz and magnetite; it is important to note that the legends in Figures 2-24 and 2-25 give a percentage that is associated with peak matches, not the percentage of mineral in the soil. In both figures, quartz seems to have the highest peak match when compared to some of the other possible matches. Based on the preliminary results by XRD, the primary reflection peaks for quartz (26.6^o), microcline (21.1^o) and calcite (29.45^o) were identified in accordance with previous PNNL publications [3].

To improve the reliability of the results, as well as increase the percent of peak matches for some of the other smaller percentage candidates, the samples will be reanalyzed by means of XRD in a range of 3 to 80 2-theta, in order to increase the possibility of peak matches after 40 2-theta. The analysis of the samples in a wider range of 2-theta angles took place recently and the spectra are currently being processed. A comparison effort will take place between the spectra below (Figures 2-24 and 2-25) and the new XRD spectra.

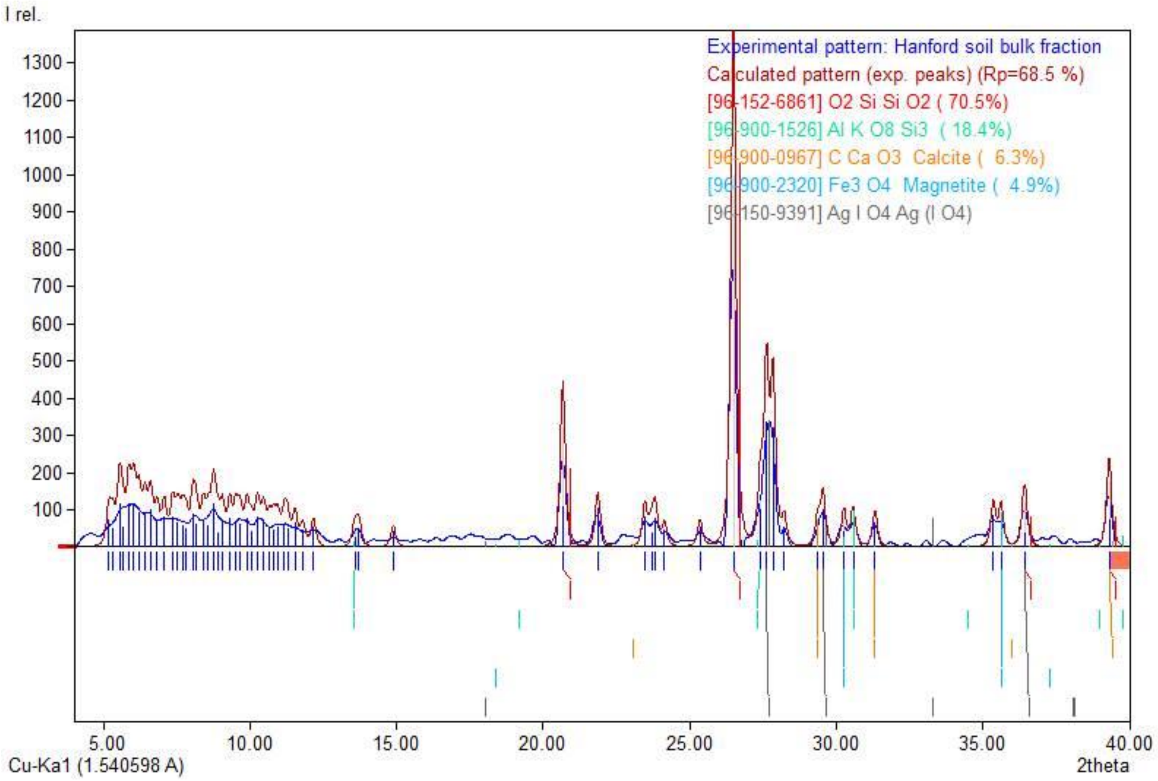

Figure 2-24. XRD analysis diagram of the bulk fraction.

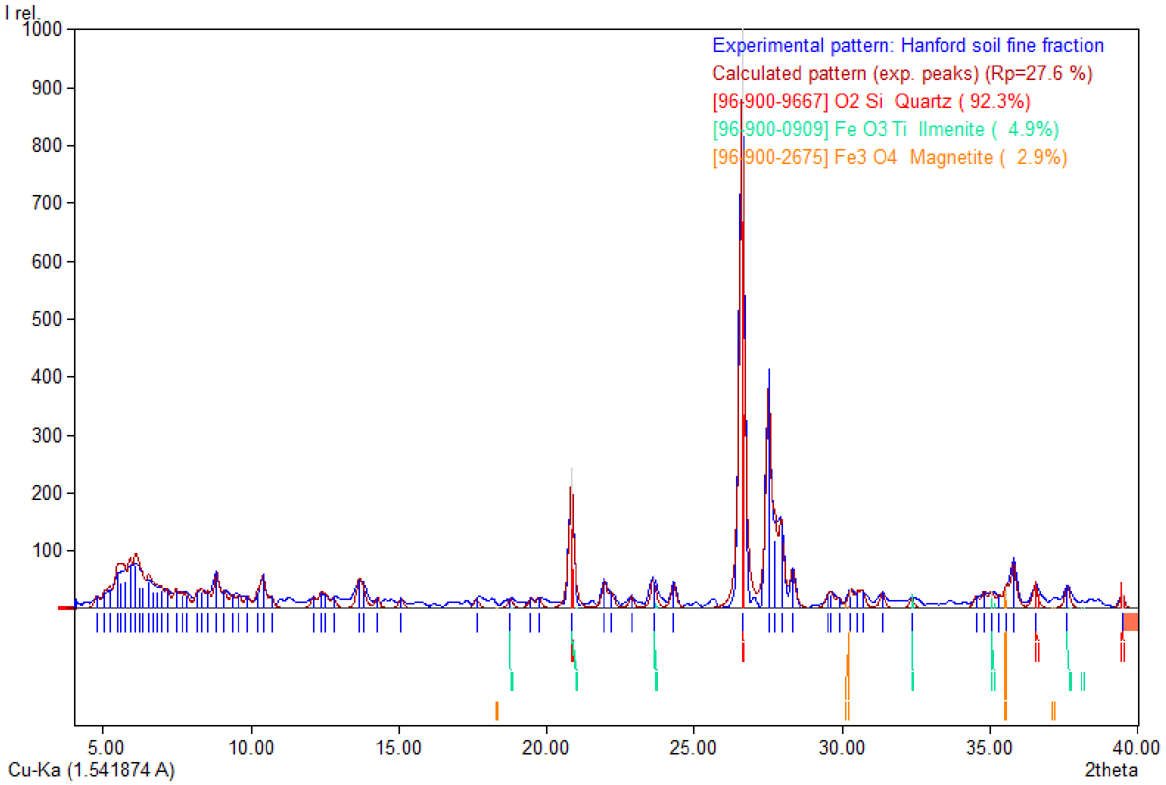

Figure 2-25. XRD analysis diagram of the fine fraction.

Samples were prepared by crushing approximately 3 g of bulk and fine fractions to create a fine powder-like solid that was placed in the sample holder of the XRD instrument (Siemens Diffraction D5000). The samples were crushed using a mortar and pestle to increase homogeneity. Figures 2-26 and 2-27 illustrate the spectrum analysis obtained from XRD for the bulk and fine fractions, respectively. The samples were run from 2 to 80 2theta and peak analysis was conducted using *MATCH!* software.

The results of the bulk fraction showed the presence of quartz, kaolinite, calcite, and pyroxenes. The fine fraction exhibited a wider variety of minerals such as quartz, microcline, plagioclase, magnetite, and at a lesser percentage ilmenite, calcite, and pyroxenes.

Table 2-14 summarizes the composition of the different soil fractions and provides the percentage of each mineral present in the soil. In both figures, quartz seems to have the highest percentage when compared to matches of other possible minerals, but that percentage decreases in the fine fraction. It is important to point out an increase in the presence of magnetite (Fe(II,III) oxide) in the fine fraction compared to the bulk fraction, as ferrous iron may play a significant role in the reduction of Tc-99 and, hence, its environmental mobility.

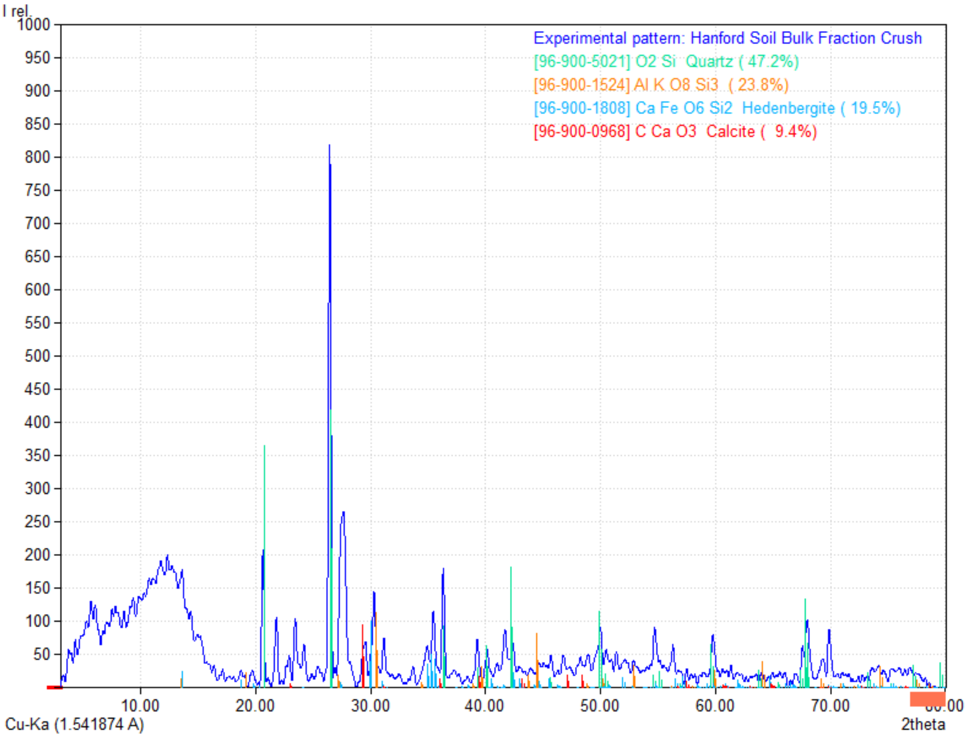

Figure 2-26. XRD analysis diagram of the bulk fraction.

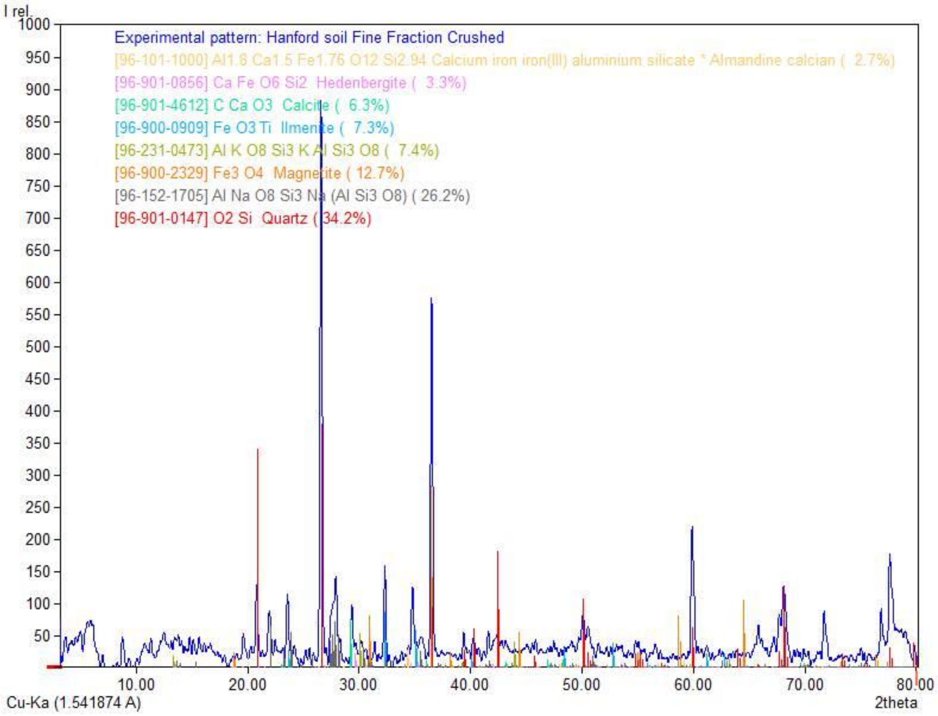

Figure 2-27. XRD analysis diagram of the fine fraction.

Table 2-14. Summary of XRD Results

Bulk Fraction (300 µm<d< 2mm)

	Quartz	Microcline[1]	Pyroxenes[2]	Calcite
Amount (%)	47.2	23.8	19.5	9.4

Fine Fraction (d< 300 µm)

	Quartz	Microcline[1]	Magnetite	Plagioclase[3]	Ilmenite	Calcite	Pyroxenes[2]
Amount (%)	34.2	26.2	12.7	7.4	7.3	6.3	3.3

[1] *In the form of* $KAlSi_3O_8$ [2] *In the form of* $(Ca,Fe)Si_2O_6$ [3] *In the form of* $NaAlSi_3O_8$

Furthermore, FIU completed the trial and error experiments for the separation of Tc(IV) and Tc(VII) in the aqueous phase. Separation of Tc(VII) from Tc(IV) in solution took place through a solvent extraction technique: tetraphenylphosphonium chloride (TPPC) in chloroform extracts pertechnetate, Tc(VII), in the organic phase, leaving reduced Tc(IV) in the aqueous phase.

In order to optimize this process, an experiment was conducted using different aliquots from a Tc stock solution that were isolated and mixed with TPPC (as discussed in the February monthly report), to achieve the following TPPC/Tc molar ratios: 0.25:1, 26:1, 41:1, 68:1. Two solutions were created for each molar ratio, one being a reference (not-manipulated) made from the stock Tc solution, and the other solution underwent the separation protocol. The separation process consisted of the addition of TPPC and chloroform; the solutions were subsequently vortexed and centrifuged, which resulted in phase separation. An aliquot from each phase was placed in a 15-ml of Ultima Gold Liquid Scintillation Cocktail (LSC). A pure Ultima Gold LSC solution was used as the background solution (Tc-free). The solutions were placed in the liquid scintillation analyzer (Perkin Elmer, Tri-carb 2910 TR) for three cycles, one minute counting time per sample. The results are summarized in Table 15.

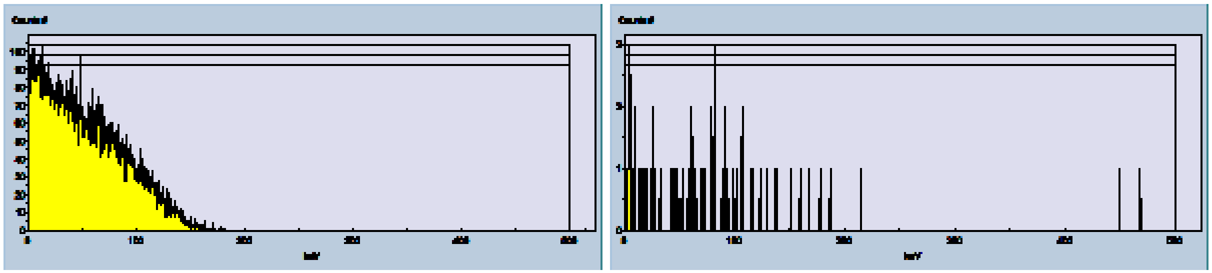

Figure 2-28. β-spectrum of Tc-99 for reference (left) and aqueous phase (right), which was identical to the background spectrum.

In the experiment conducted on the workbench (under oxidizing conditions), two distinct phases were observed: a bottom-organic phase, where Tc(VII) is quantitatively expected to be present; and a top-aqueous phase, where Tc in its reduced oxidation state is expected to be present. Since the experiment was conducted on the bench (under oxidizing conditions), the entire initial quantity of Tc introduced is expected to be present in the bottom-organic phase. Following the LSC analysis, the cpm of the background was subtracted by the cpm of each sample and the values were then compared with the standard solution in order to determine what percentage of each oxidation state was present in the solution.

The results showed that in TPPC/Tc molar ratios of less than 40:1, Tc recovery is not optimal; TPPC needs to be in excess in the solution, at least 40-fold. In molar ratios 40:1 and higher, a quantitative Tc recovery was achieved (Table 2-15).

Table 2-15. Optimizing the Molar Ratio of TPPC to Tc, for the Separation of Tc(VII) from Tc(IV)

Ratio (TPPC/Tc)	Average Tc (VII) Recovery (%)
0.25:1	48.3 ± 0.21
26:1	82.4 ± 0.49
41:1	94.5 ± 0.41
68:1	95.6 ± 0.45

Under future experimental conditions, the TPPC/Tc molar ration is expected to be ~100:1, assuring a successful separation between the two oxidative states.

References

[1] Xie, Y., Murray, C., Last, G., R. Mackley. 2003. Mineralogical and bulk-rock geochemical signatures of Ringold and Hanford formation sediments, PNNL-14202, Pacific Northwest National Laboratory, Richland, Washington.

[2] Szecsody, J. E., Truex, M. J., Qafoku, N. P., Wellman, D. M., Resch, T., & Zhong, L. (2013). Influence of acidic and alkaline waste solution properties on uranium migration in subsurface sediments. *Journal of Contaminant Hydrology*, 151, 155-175.

[3] Serne, RJ, BN Bjornstad, DG Horton, DC Lanigan, CW Lindenmeier, MJ Lindberg, RE Clayton, VL LeGore, RD Orr, IV Kutnyakov, SR Baum, KN Geiszler, MM Valenta, TS Vickerman and H. T. Schaef. 2004b. Characterization of Vadose Zone Sediments Below the T Tank Farm: Boreholes C4104, C4105, 299-W10-196 and RCRA Borehole 299-W11-39. PNNL-14849, Pacific Northwest National Laboratory, Richland, Washington.

Task 2: Remediation Research and Technical Support for Savannah River Site

Task 2 Overview

The acidic nature of the historic waste solutions received by the F/H Area seepage basins caused the mobilization of metals and radionuclides, resulting in contaminated groundwater plumes. FIU is performing basic research for the identification of alternative alkaline solutions that can amend the pH and not exhibit significant limitations, including a base solution of dissolved silica and the application of humic substances. Another line of research is focusing on the evaluation of microcosms mimicking the enhanced anaerobic reductive precipitation (EARP) remediation method previously tested at SRS F/H Area.

Task 2 Quarterly Progress

Subtask 2.1. Investigation on the Properties of Acid-Contaminated Sediment and its Effect on Contaminant Mobility

FIU analyzed samples collected in previous months by means of inductively coupled plasma optical emission spectrometry (ICP-OES). The concentrations of Fe, Al and Si in the supernatant, as a result of soil contact with nitric acid (pH 2.5), are presented below as a function of time. Batch experiments contained SRS F/H area soil of mean particle diameter 0.18<d<2 mm and HNO_3, pH 2.5.

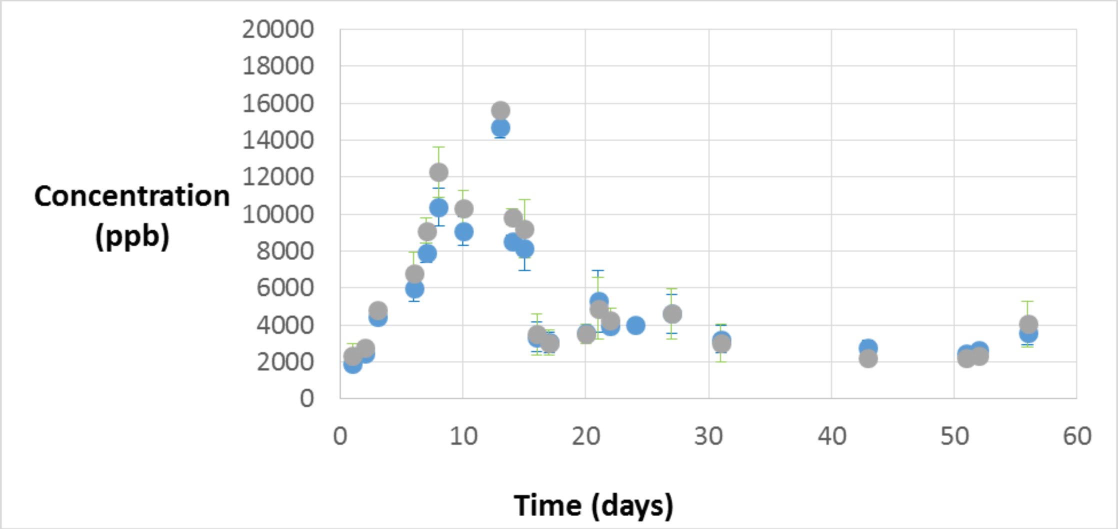

Figure 2-29. Concentrations of Al (blue dots) and Si (gray dots) as a function of time in the soil leachates, as a result of soil-nitric acid contact.

The experimental points are derived from triplicate batch experiments and the error bars represent the standard deviation. Figure 2-29 reveals an identical pattern for Al and Si release in the supernatant as a function of time: a gradual increase in concentration is observed from the first day up to the eighth day, followed by a sharp decrease and a plateau beyond day 16. For the time period 1-8 days, the concentrations of Al and Si are practically the same, taking into consideration the two elements' very close atomic mass. Furthermore, the average rate of release was calculated for the two elements for this time period and was found to be $3.5\cdot10^{-11} \pm 0.9\cdot10^{-11}$ mol/ml·min and $3.8\cdot10^{-11} \pm 1\cdot10^{-11}$ mol/ml·min for Al and Si respectively. All experiments were performed at room temperature (20^{o} C). Quartz dissolution rate at pH 2.5 and 70^{o} C is reported to be $6.4\cdot10^{-14.3}$ mol/ml·min [1] and is expected to be magnitudes of order lower at room temperature. Hence, the preliminary results indicate that Al and Si release is taking place due to kaolinite dissolution and quartz dissolution had very little effect, if any. Furthermore, there seems to be no preferential leaching of the one element over the other. On the contrary, there seems to be a stoichiometric release of Al and Si in the supernatant, since these two elements are found in equimolar composition in kaolinite's structure, $Al_2Si_2O_5(OH)_4$. In literature, it has been reported that kaolinite dissolves congruently at 25^{o} C for pH values lower than 4 and higher than 11, but incongruently in the in-between range [2,3]. Day 13 is believed to be an outlier.

Iron follows a very similar pattern of release in the aqueous phase (Figure 2-30), nevertheless the maximum amount of iron released (Day 8) is significantly lower than that of Al and Si: 6.6 ppm of Fe, as opposed to 12.2 ppm of Si and 10.4 ppm of Al. The average rate of Fe release was calculated to be $7.2 \cdot10^{-12} \pm 2 \cdot10^{-12}$ mol/ml·min, significantly lower than the corresponding rates of Al and Si release. This result could be expected since the concentration of Fe in the SRS soil (in the form of goethite) is smaller than that of Al and Si (in the form of kaolinite).

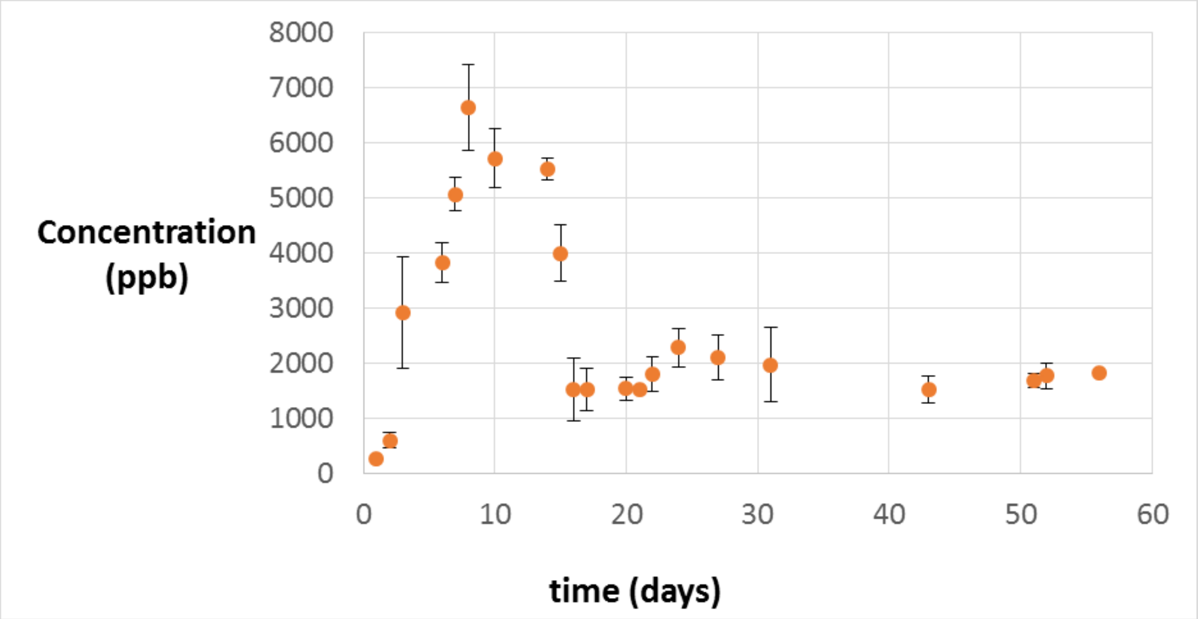

Figure 2-30. Concentration of Fe as a function of time in the soil leachates as a result of soil-nitric acid contact

The gradual decrease in concentrations of the elements being studied and the creation of a plateau can be explained by speciation calculations. With the aid of Visual Minteq, a list of aqueous species and saturated solids was created under the conditions studied and is presented in

Table 2-16. Concentrations of Al, Fe and Si in the calculations were derived from Day 8 experimental points ("peaks") with the atmospheric CO_2 included as well.

Table 2-16. Major Aqueous and Saturated Species at pH 2.5

Aqueous Species	Saturated Solids
Al^{3+}	Goethite - FeO(OH)
H_4SiO_4	Hematite – Fe_2O_3
Fe^{3+}	Lepidocrocite – γ-FeO(OH)
$Fe(OH)^{2+}$	Quartz – SiO_2

The software predicts the formation of several Fe- and Si-bearing solids that are in equilibrium with the Fe and Si aqueous species (plateau). Nevertheless, under the conditions studied there were no aluminosilicates or other Al-bearing solids predicted; a fact that would explain the decrease in Al concentration. An explanation of this phenomenon could be the co-precipitation of Al during the formation of iron- and silicon-bearing solids.

Based on the preliminary kinetic results, batch experiments were performed with the aqueous phase replenished every 7 days, and the concentrations of Fe, Al and Si were monitored. The purpose of this experiment (ongoing) is to obtain soil that has come in contact with nitric acid solution at pH 2.5 for different time intervals. This would help to identify changes in the soil physico-chemical properties due to this interaction affecting contaminant sorption. The results are presented in Figures 2-31 through 2-34.

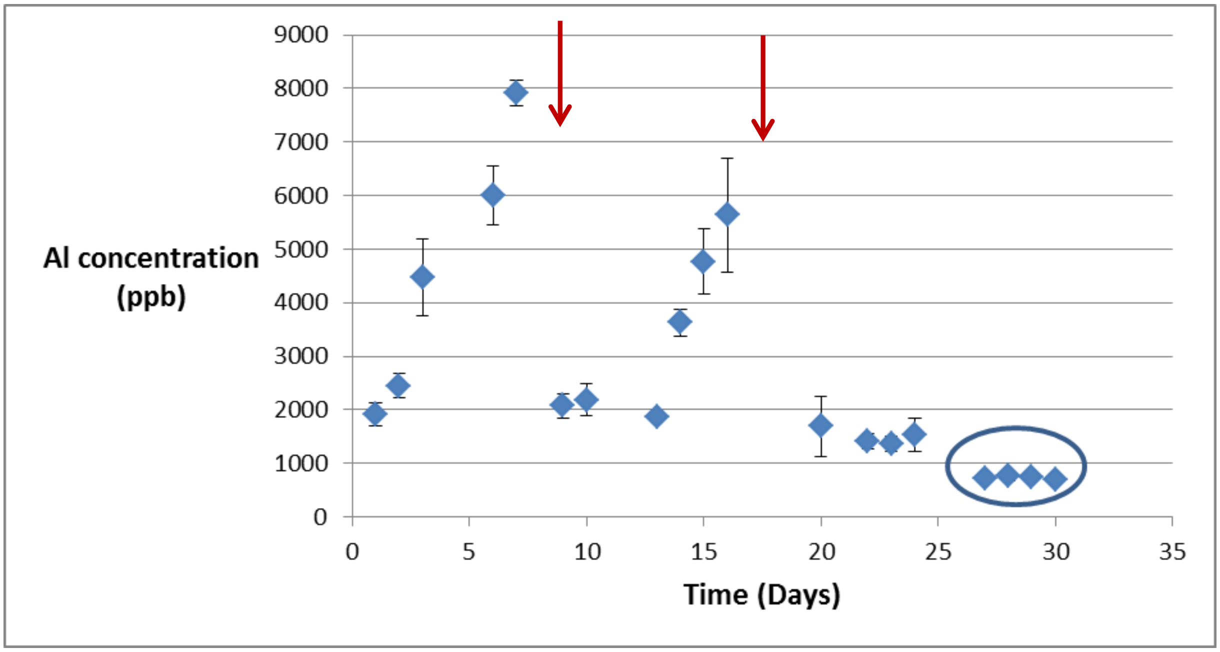

Figure 2-31. Concentration of Al (ppb) in the supernatant solution as a function of time. Error bars represent the standard deviation of triplicate samples. Red arrows are pointing to the time interval where the supernatant was replenished.

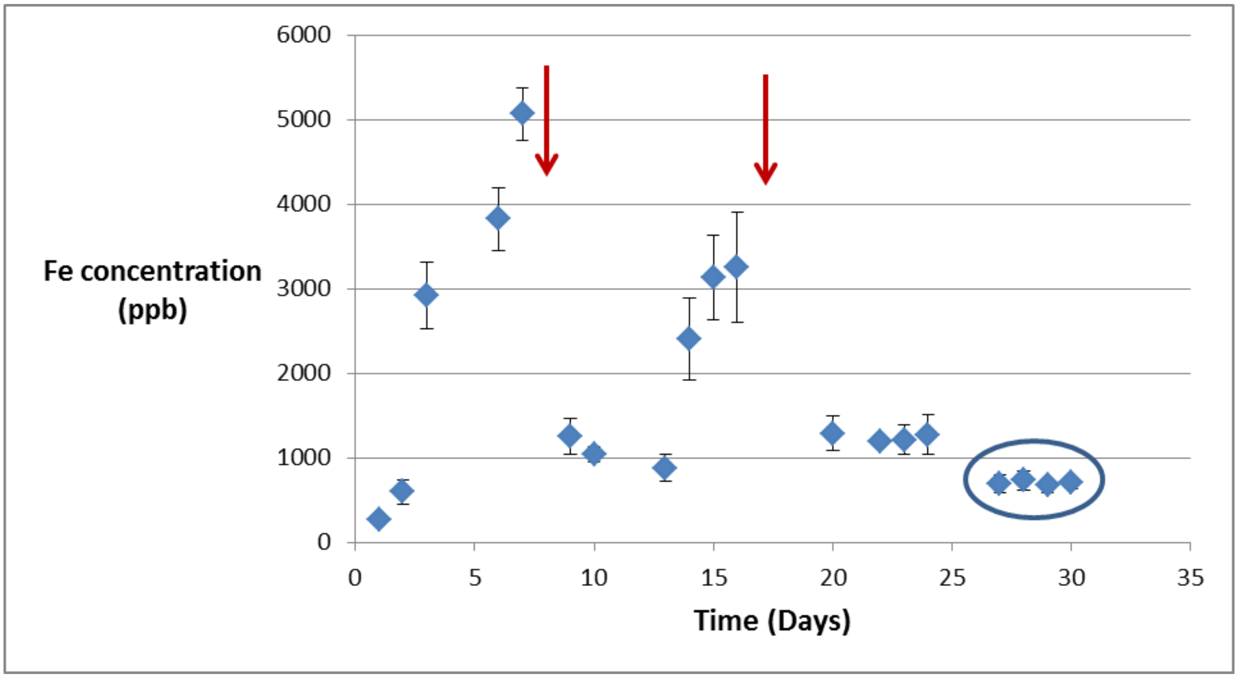

Figure 2-32. Concentration of Fe (ppb) in the supernatant solution as a function of time. Error bars represent the standard deviation of triplicate samples. Red arrows are pointing to the time interval where the supernatant was replenished.

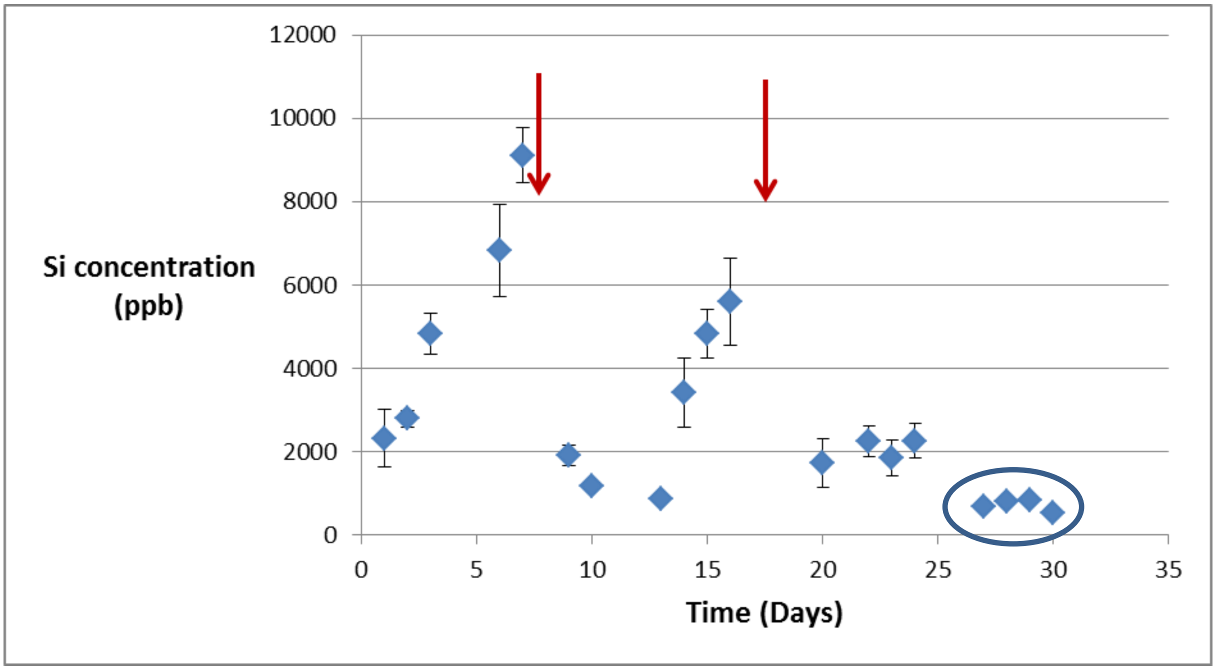

Figure 2-33. Concentration of Si (ppb) in the supernatant solution as a function of time. Error bars represent the standard deviation of triplicate samples. Red arrows are pointing to the time interval where the supernatant was replenished.

The elemental concentration gradually increases for all elements during the first 7 days and once the supernatant is replenished, the concentration drops to the initial levels. A lag period is observed for all three elements after each replenishment; the concentration of the elements remains stable for the first 3-4 days and then gradually increases. Furthermore, the maximum amount of each element released into the supernatant is significantly smaller than the corresponding amount during the first cycle. For example, the maximum concentration of Al during the first cycle was found to be 8 ppm, while for the second cycle it was 5.6 ppm; for Fe, it was 5 ppm during the first cycle versus 3.5 ppm during the second; and for Si, it was 9 ppm during the first cycle versus 5.6 ppm during the second. This pattern may be explained by the assumption that acid first "washes out" all fine particles present in the soil, which are more readily available due to their higher specific surface, and during the second and third cycle, larger particles are being more slowly dissolved. Finally, there seems to be no preferential dissolution of Al and Fe so far, since the concentrations are almost the same (Figure 2-34).

The circled experimental data in Figures 2-31 & 2-33 represent Al, Fe and Si concentrations determined in a period where ICP-OES was experiencing some technical issues. Hence, the samples of this period (Days 27-30) will be re-analyzed and re-processed, since they do not follow the established pattern.

In Table 2-17, the rates of Al, Fe and Si released in the aqueous phase for the different experimental cycles are presented. The rates of Al and Si released in both cycles are practically the same whereas the release rate of Fe is lower in all cycles. In all cases, the release rate in the second cycle was lower than the one from the first cycle for the same element.

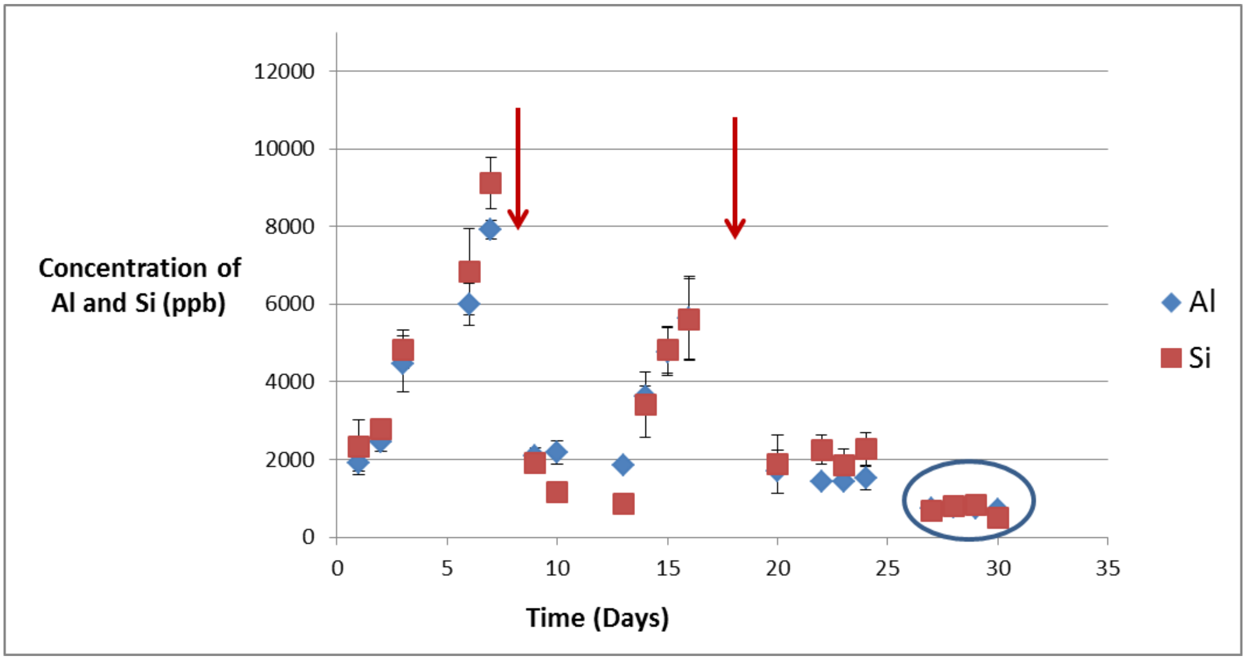

Figure 2-34. Concentration of Al and Si (ppb) in the supernatant solution as a function of time. Error bars represent the standard deviation of triplicate samples. Red arrows are pointing to the time interval where the supernatant was replenished.

Table 2-17. Average rates of release of Al, Fe and Si in the aqueous phase for two experimental cycles: days 1-7 and days 13-16, followed by relative standard deviation

	Rate of release (mol ml^{-1} min^{-1})		
	Al	**Fe**	**Si**
Cycle 1 (Days 1-7)	$3.5\cdot10^{-11} \pm 0.8\cdot10^{-11}$	$7.2\cdot10^{-12} \pm 2\cdot10^{-12}$	$3.8\cdot10^{-11} \pm 1\cdot10^{-11}$
Cycle 2(Days 13-16)	$6.9\cdot10^{-12} \pm 2\cdot10^{-12}$	$2.0\cdot10^{-12} \pm 0.7\cdot10^{-12}$	$6.0\cdot10^{-12} \pm 2\cdot10^{-12}$

During March, FIU continued to perform experiments for soil acidification and has identified the different profiles of acidified soil through dissolution batch experiments where the aqueous phase (HNO_3, pH 2.5) was replenished periodically.

The concentrations (mM) of Al, Fe and Si in the aqueous phase were determined by means of ICP-OES and the results are presented as a function of time in Figures 2-35 and 2-36. The concentrations of Al and Si are combined in one figure since they can be traced back to kaolinite, whereas Fe is found in the aqueous phase due to soil's goethite dissolution.

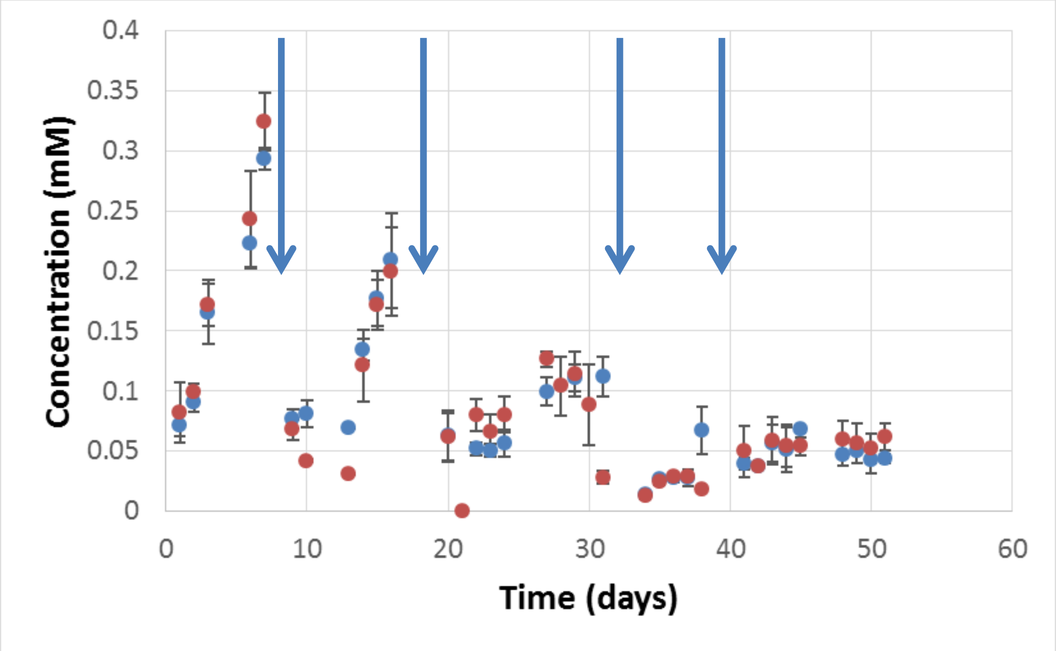

Figure 2-35. Al (blue dots) and Si (red dots) concentrations (mM) in the aqueous phase due to kaolinite and goethite dissolution, as a function of time. Error bars represent relative standard deviations from triplicate samples. Arrows point to the timeline where aqueous phase was replenished.

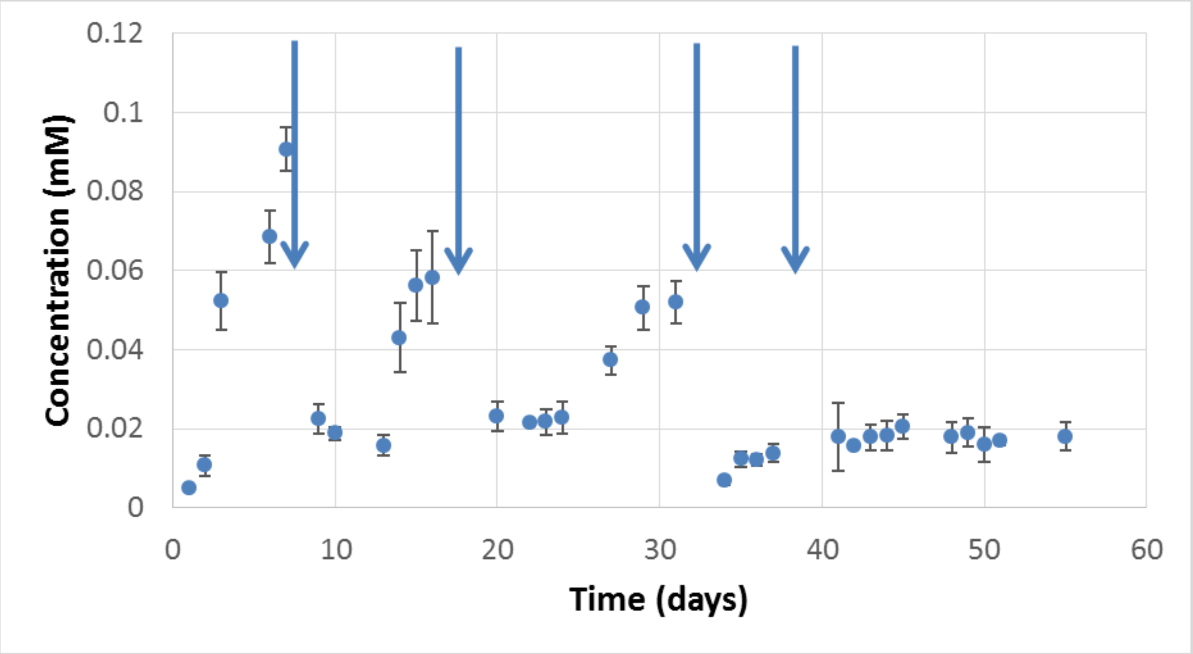

Figure 2-36. Fe concentrations in the aqueous phase due to goethite dissolution, as a function of time. Error bars represent relative standard deviations from triplicate samples. Arrows point to the timeline where aqueous phase was replenished.

The triplicate samples were removed from the platform shaker after 1, 3 and 5 cycle. The aqueous phase was discarded and the samples were dried in the oven at 150°C for 48h. The samples followed the same pattern observed in the preliminary experiments, where the aqueous phase was not replenished and, hence, the concentrations of Al, Fe and Si in the aqueous phase reached saturation levels. Secondary mineral precipitation was predicted by speciation software (Visual Minteq+), namely chalcedony and hematite, that were not original components in the soil (as reported in the January monthly), which may affect the soil's specific surface area and pore distribution.

Future experiments include the determination of the specific surface area and pore distribution of each profile and will attempt to correlate the changes in these physico-chemical characteristics with each profile's sorptive capacity. Nevertheless, the soil's alteration can be witnessed even with the bare eye, as the following photographs of each profile demonstrate.

Figure 2-37. Soil collected including secondary precipitates.

Figure 2-38. Soil after 1 cycle (7 days) contact with HNO_3.

Figure 2-39. Soil after 3 cycles (30 days) contact with HNO_3.

Figure 2-40. Soil after 5 cycles (50 days) contact with HNO_3.

DOE Fellow, Ms. Awmna Rana, presented the experimental findings of this task at the 2017 FIU Conference for Undergraduate Research.

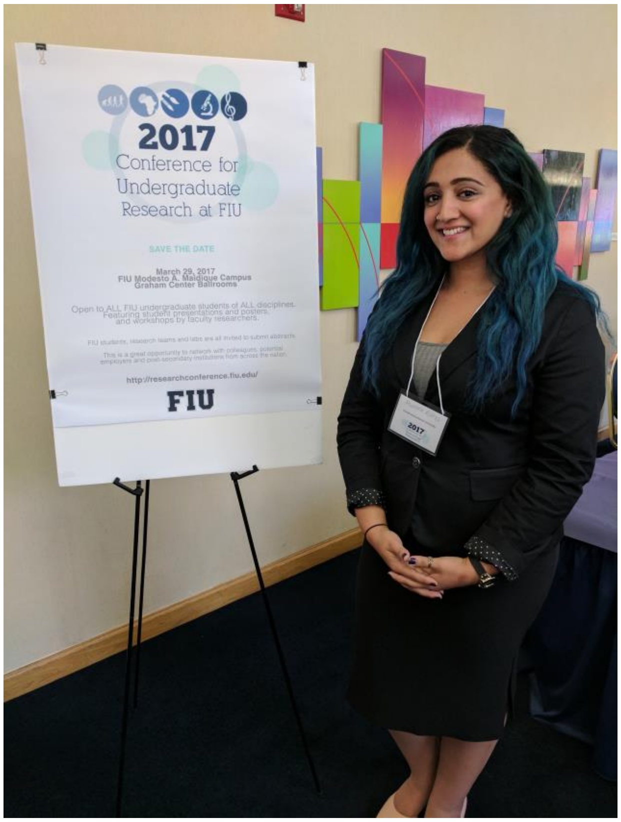

Figure 2-41. DOE Fellow Awmna Rana at the 2017 FIU Conference for Undergraduate Research.

References

a. Knauss K.G., Wolery T.J. (1987). The dissolution kinetic of quartz as a function of pH and time at 70^{o}C. *Cosmochimica et Geochimica Acta* 52, 43-53.
b. Carroll S.A., Walther J.V. (1990). Kaolinite dissolution at 25^{o,} 60^{o} and 80^{o} C. *American journal of Science* 290, 797-810.
c. Huertas J.H., Chou L., Wollast R. (1999) Mechanism of kaolinite dissolution at room temperature and pressure. Part II:kinetic study. *Cosmochimica et Geochimica Acta* 63, 3261-3275.

Subtask 2.2: The Synergistic Effect of Humic Acid and Colloidal Silica on the Removal of Uranium (VI)

FIU completed experiments with the pH 4 and 5 batch of samples containing 30 ppm humic acid, 3.5 mM of silica, 400 mg of sediment and 25 ppm uranium. The pH of the samples was adjusted with a stock solution of 0.01M HCl and 0.05M NaOH to pH 4 - 5 and samples were placed on a platform shaker. Uranium was added prior to the pH adjustment and precautions were taken to add less DIW so that the addition of acid/base will result in a total volume of approximately 20 mL. The pH of the samples was measured periodically and readjusted to pH 4-5 if a change was observed. Tables 2-18 through 2-21 show the overall and daily pH changes for the pH 4 and 5 sample batches. This experiment was completed and collected samples are being stored for uranium analysis using a KPA.

Table 2-18. Overall Sample Matrix of pH 4 Batch Samples

pH 4 Adjusted Set		Constituents							
		SiO_2	Humic Acid (HA)	Sediments	Uranium, U (VI)	Volume of acid/ base	DIW, H_2O	pH	
		ml	ml	mg	ml	ml	ml	Initial	Final
Batch No. 2	2.1	2.10	6.00	0	0.50	4.10	7.00	1.96	4.07
	2.2					3.71	7.00	1.98	4.08
	2.3					4.83	7.00	1.91	4.10
Batch No. 3	3.1	0	6.00	0	0.50	3.63	7.00	1.80	4.14
	3.2					3.65	7.00	1.82	4.10
	3.3					3.61	7.00	1.84	4.08
Batch No. 5	5.1	2.10	6.00	400.00	0.50	4.04	7.00	1.90	4.05
	5.2					3.37	7.00	1.88	4.08
	5.3					3.23	7.00	1.89	4.04
Batch No. 6	6.1	0	6.00	400.00	0.50	6.54	7.00	1.54	4.09
	6.2					6.50	7.00	1.51	4.07
	6.3					6.52	7.00	1.53	4.05

Table 2-19. Daily Change in pH of Samples

Sample #		pH 4						
		Day 1	Day 2	Day 3	Day 4	Day 5	Day 6	Day 7
Batch No. 2	2.1	1.96	3.63	4.07	4.00	3.91	4.00	4.07
	2.2	1.98	3.81	4.06	3.94	3.92	4.02	4.08
	2.3	1.91	2.74	4.13	4.00	3.95	4.07	4.10
Batch No. 3	3.1	1.80	4.02	4.06	4.02	3.90	4.03	4.14
	3.2	1.82	3.98	4.00	4.03	3.83	4.10	4.10
	3.3	1.84	4.05	4.05	4.07	3.89	4.10	4.08
Batch No. 5	5.1	1.90	4.26	3.96	4.04	4.10	4.08	4.16
	5.2	1.88	4.23	3.95	4.03	4.09	4.03	4.08
	5.3	1.89	4.06	3.88	4.02	4.11	4.02	4.04
Batch No. 6	6.1	1.54	4.03	3.88	4.02	4.11	4.05	4.09
	6.2	1.51	4.03	3.87	4.03	4.09	4.07	4.07
	6.3	1.53	4.01	3.84	4.02	4.12	4.12	4.05

Table 2-20. Overall Sample Matrix of pH 5 Batch Samples

pH 5 Adjusted Set		Constituents							
		SiO_2	Humic Acid (HA)	Sediment	Uranium, U (VI)	Volume of Acid/ Base	DIW, H_2O	pH	
		mL	mL	mg	mL	mL	mL	Initial	Final
Batch No. 2	2.1	2.10	6.00	0.00	0.50	7.97	3.50	2.00	5.02
	2.2					3.58	7.00	1.97	4.95
	2.3					3.34	7.00	1.93	4.92
Batch No. 3	3.1	0.00	6.00	0.00	0.50	3.56	9.00	1.70	4.96
	3.2					3.48	9.00	1.75	4.93
	3.3					3.28	9.00	1.75	4.92
Batch No. 5	5.1	2.10	6.00	400.00	0.50	3.28	7.00	1.85	5.01
	5.2					5.44	5.00	1.98	4.98
	5.3					3.37	7.00	1.95	4.93
Batch No. 6	6.1	0.00	6.00	400.00	0.50	4.64	7.00	1.79	5.05
	6.2					3.32	9.00	1.79	4.90
	6.3					3.38	9.00	1.76	4.99

Table 21-21. Daily Change in pH of Samples

Sample #		pH 5						
		Day 1	Day 2	Day 3	Day 4	Day 5	Day 6	Day 7
Batch No. 2	2.1	2.00	5.06	5.15	5.10	5.03	5.08	5.02
	2.2	1.97	5.12	5.06	5.13	5.07	5.08	4.95
	2.3	1.93	4.92	5.24	5.09	5.04	5.04	4.92
Batch No. 3	3.1	1.70	4.70	5.10	5.13	5.04	5.02	4.96
	3.2	1.75	4.81	5.15	5.07	5.12	5.01	4.93
	3.3	1.75	4.66	5.14	5.08	5.11	5.03	4.92
Batch No. 5	5.1	1.85	4.82	5.01	4.87	5.18	5.02	5.01
	5.2	1.98	4.64	4.95	4.90	4.99	5.01	4.98
	5.3	1.95	4.96	4.98	4.87	5.16	4.97	4.93
Batch No. 6	6.1	1.79	4.79	4.97	4.94	5.02	4.88	5.05
	6.2	1.79	4.93	4.89	5.07	5.17	4.93	4.90
	6.3	1.76	5.17	5.06	5.09	5.06	5.02	4.99

Samples of the pH 3 through pH 5 batches were centrifuged at 2700 rpm for 30 minutes to allow the separation of the solids from the solution. After being centrifuged, the filtered samples were diluted using 1% HNO_3 by a dilution factor of 10, filtered using a 0.45 µm syringe filter, and 4 mL were placed in each vial for uranium measurement via KPA. Similarly, unfiltered samples were diluted using 1% HNO_3 by a dilution factor of 10 and 4 mL samples were prepared for analysis. FIU installed a new laser plasma cartridge in the KPA instrument to improve the intensity and performed sensitivity testing to assess the performance. FIU also began preparation of pH 6 through pH 8 batch samples. The triplicate samples were prepared using the same known amount of constituents, including: 30 ppm humic acid, 3.5 mM silica, and 400 mg sediment. During the month of April, 25 ppm uranium will be added to the samples prior to pH adjustment with a stock solution of 0.01M HCl and 0.05M NaOH to the appropriate pH conditions and the samples will be placed on a platform shaker.

DOE Fellow Alexis smoot attended Waste Management Symposia held in Phoenix, AZ between March 6th through 10th, and the Conference of Undergraduate Research at FIU on March 29th and presented poster titled “The synergetic effect of humic acid and silica on the removal of uranium (VI)” based on the results obtained from previous studies related to this task (Figure 2-42).

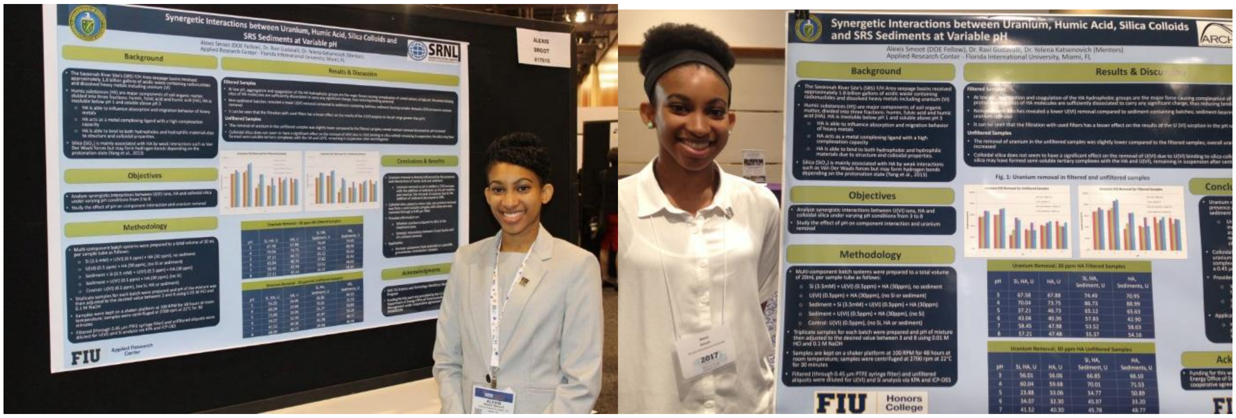

Figure 2-42. DOE Fellow Alexis Smoot at the Waste Management Symposia (left) and at the Conference of Undergraduate Research at FIU (right).

Subtask 2.3: Humic Acid Batch Sorption and Column Experiments with SRS Soil

During the month of January, the potentiometric titration experiments were performed using Huma-K product, refined humic acid, and modified humic acid in order to compare Huma-K with other humic materials. The potentiometric titration consisted of placing 500 mg of the material (HumaK, refined humic acid, and modified humic acid) dissolved in $NaNO_3$ in a closed beaker. The solution was stirred constantly and nitrogen was introduced in order to get rid of CO_2 and to create an inert atmosphere. Once the pH of the solution containing the material was stable, NaOH was added to raise the pH to 11 and to deprotonate the functional groups present in the material. Once the pH was stabilized again, the titration was initiated by adding small quantities of HNO_3. After each addition of HNO_3, the pH and the volume were recorded. The titration was ceased at approximately pH 3. In order to get just the $[H^+]$ consumed by the material, it was necessary to subtract the titration curve of the electrolyte ($NaNO_3$) from the material dissolved in the electrolyte. This was done by using OriginPro8 software.

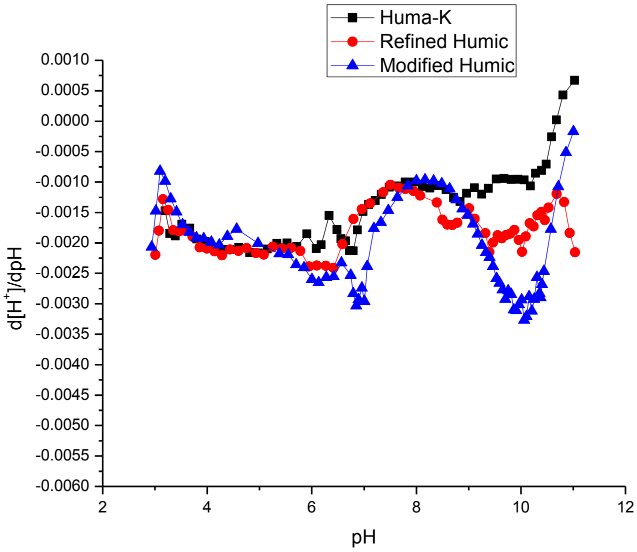

Figure 2-43. Differential potentiometric titration curves for Huma-K, refined humic acid and modified humic acid.

In the differential potentiometric titration curves, the protonation gradient, $\frac{d[H^+]}{dpH}$, is used to determine the hydrogen consumption by the surface of the material as the pH is changed. The reverse peaks correspond to the pK values of the functional groups present in the material that have acid/base properties that can be ionized. The differential potentiometric titration curve of each of the three materials revealed a broad peak between pH values 4 and 6, a fact that can be attributed to the presence of carboxyl groups arranged in different configurations, which have similar p*K* values (Figure 2-43). The peaks found at pH values between 8.5 and 11 can be attributed to the presence of phenol and amino groups. By comparing the three materials, it was noted that there was almost an identical consumption of H^+ in the acidic region (pH 4-6). This means that the three materials contain similar amounts of carboxyl groups. However, in the more basic pH (pH 8.5-11), there was a difference between the three materials. Modified humic acid showed a higher H^+ probably because it contains more functional groups, such as phenol and amino groups, than refined humic acid and Huma-K.

Humic Acid Batch Sorption Experiments

During the month of February, Fourier Transform Infrared analysis (FTIR) of Huma-K, modified humic acid, and refined humic acid was performed with the purpose of identifying the main functional groups present in the three samples. Before the analysis, the samples were mixed with KBr (10 mg of sample with 150 mg KBr) to reduce the blackness of the sample and also to get a better spectrum. Then the samples were oven dried at 80°C for 48 hours to remove moisture. Once dried, the samples were stored in a desiccator until analysis. Background was collected before analysis of each sample. Unfortunately, the pressure clamp of the FTIR was broken; so, it was not able to properly apply pressure to ensure good contact between the sample and the ATR crystal. This may have affected FTIR results. Spectra of the three samples are shown in Figure 2-44. It is suspected that peaks in the region 2700-1800 are not representative of the samples since they have never been observed in our previous analysis. These peaks may have arisen due to improper compaction of the samples at the ATR crystal. For example, the FTIR spectrum of Huma-K that was taken a year ago did not have peaks in this region, and the pressure clamp was working fine at that time. It is believed that since the pressure clamp was broken, this affected the FTIR results.

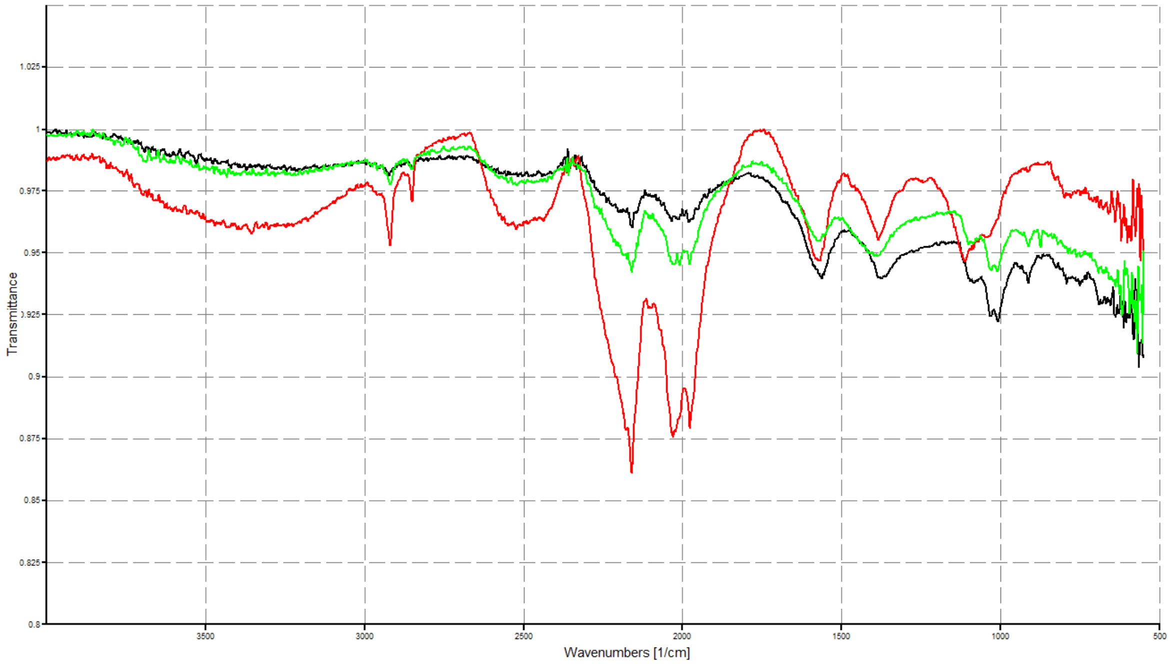

Figure 2-44. FTIR spectra of: Huma-K (black), refined humic acid (green), and modified humic acid (red).

During March, experiments to study the effect of pH on modified humic acid sorption onto SRS sediment (Figure 2-45) were performed. The purpose of these experiments was to compare sorption of Huma-K with other materials such as modified humic acid. For the experiment, a modified humic acid stock solution of 1000 mg/L was prepared by dissolving 1000 mg of modified humic in 1 L of deionized water. Batch sorption experiments were conducted by bringing 1 g of SRS soil in contact with 20 mL of modified humic acid solution at 25°C. The samples were homogenized by using a Thermolyne Maxi Mix Plus Vortex Mixer for 30 seconds. The vials were rotated on a platform shaker (100 rpm) to ensure homogeneous suspension contact throughout the sorption period. All samples were centrifuged for 30 minutes at 2700 rpm, and the residual modified humic acid in the supernatant was measured spectrophotometrically at 254 nm (Thermo Scientific Genesys 10S). The effect of pH on modified humic acid sorption onto SRS soil was studied at a pH range from 4 to 8 for five days with an initial modified humic acid concentration of 50 mg/L. The pH was adjusted with 0.1 M HCl or 0.1 M NaOH.

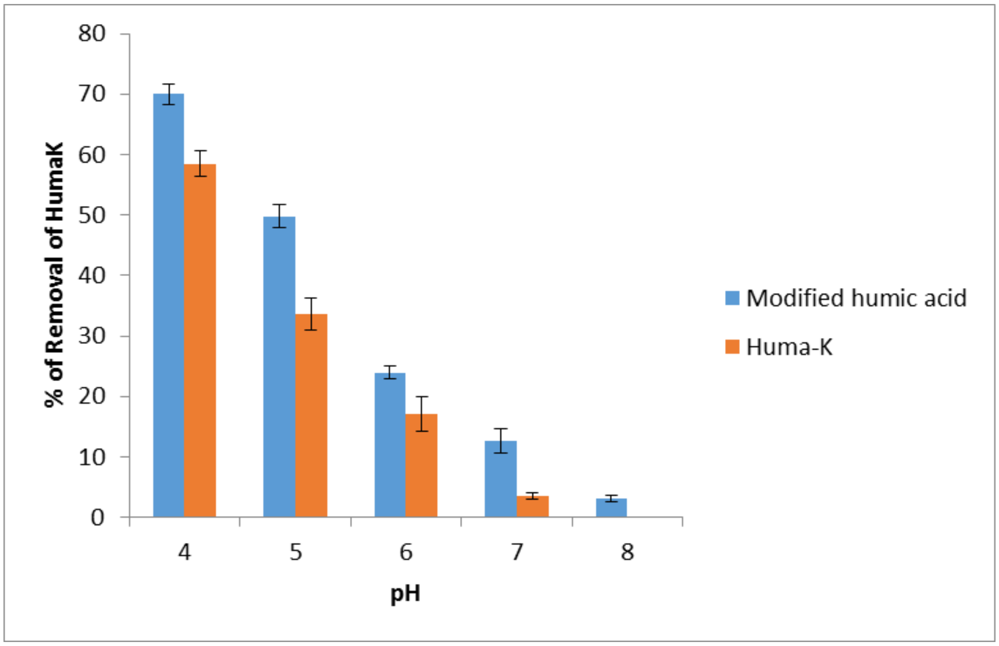

Figure 2-45. The effect of pH on modified humic acid sorption onto SRS sediment.

The results showed that modified humic acid had a higher sorption compared to Huma-K in the pH range studied. This is expected since the results of the potentiometric titrations showed a higher content of functional groups for modified humic acid compared to Huma-K. It is important to note that both materials (Huma-K and modified humic acid) followed the same trend. As the pH increased, the sorption of both materials gradually decreased. A possible explanation is that as the pH increased, the sediments and humic molecules became more negatively charged. The sorption may decrease due to the electrostatic repulsion between the humic molecules and sediments.

FIU is preparing to analyze the samples from the sorption kinetic experiment of uranium onto SRS sediments with and without a Huma-K coating at pH 4. In addition, an experiment will be performed to study the effect of pH on the precipitation of modified humic acid.

Humic Acid Column Experiments

During the reporting period, FIU concentrated on column tracer tests using rhenium as a tracer. Rhenium tracer test was performed by injecting 2.475 mL of 1000 ppm rhenium solution (2.475 mg) into a column containing SRS soil that was previously saturated with D.I. water. Thirty samples were collected at 3 minute intervals. Samples collected during the tracer test were analyzed using the ICP-OES. The effluent samples collected towards the end of the experiments showed higher concentrations of rhenium indicating an inconclusive tracer test. To achieve conclusive tracer data, there is a need to either reduce the mass of the tracer and/or increase the sampling time Therefore, a second rhenium tracer test with reduced concentration of rhenium and an increased collection time was conducted. 1.9174 mL of 500 ppm rhenium dilution solution (0.9587 mg) was then injected into the column containing D.I.-saturated SRS soil. Forty samples were collected for a total of 216 minutes at 5 and 7 minute intervals (Table 2-22). Samples were analyzed via ICP-OES for rhenium concentrations; Figure 2-46 shows the breakthrough curve of the rhenium tracer test, the concentration of rhenium towards the end of the experiment is greater than 200 ppb, indicating that more time is needed to flush out the rest of the rhenium from the column. From the data collected, a total of 0.805 mg of rhenium was recovered from the column, with a recovery of 81.5% with an effective flow rate of 1.849 mL/min.

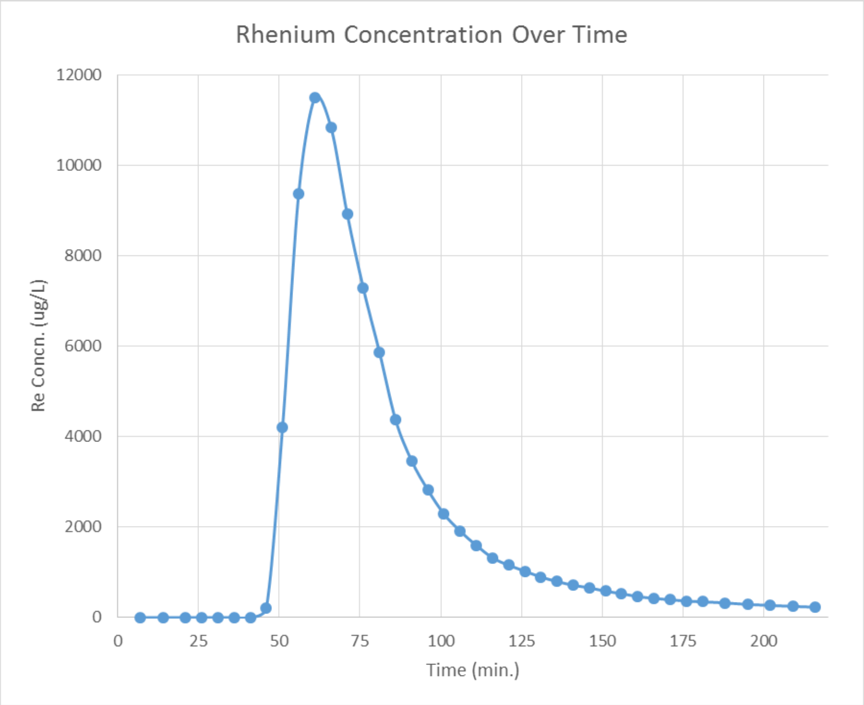

Figure 2-46. Concentration of rhenium against change in time during the tracer test performed with 500 ppm of rhenium.

Table 2-22. Tracer Test: Rhenium (Re) 500 ppm

Sample ID	Wt. test tube (g)	Time (min)	Total Time (min)	Wt. test tube + soln. (g)	Reported Re Conc. (ug/L)	Re Conc. (ug/L) Corrected	Total Vol (L)	Re Mass (ug)
Re_tracer1	5.326	7	7	16.851	2.407	2.407	0.012	0.028
Re_tracer2	5.426	7	14	18.135	1.587	1.587	0.013	0.020
Re_tracer3	5.382	7	21	18.279	2.207	2.207	0.013	0.028
Re_tracer4	5.425	5	26	14.747	1.17	1.17	0.009	0.011
Re_tracer5	5.406	5	31	14.796	1.86	1.86	0.009	0.017
Re_tracer6	5.384	5	36	14.806	1.748	1.748	0.009	0.016
Re_tracer7	5.307	5	41	14.764	1.817	1.817	0.009	0.017
Re_tracer8	5.385	5	46	14.845	217.2	217.2	0.009	2.055
Re_tracer9	5.455	5	51	14.856	2098	4196	0.009	39.447
Re_tracer10	5.444	5	56	14.789	1874	9370	0.009	87.563
Re_tracer11	5.320	5	61	14.668	2298	11490	0.009	107.409

Sample ID	Wt. test tube (g)	Time (min)	Total Time (min)	Wt. test tube + soln. (g)	Reported Re Conc. (ug/L)	Re Conc. (ug/L) Corrected	Total Vol (L)	Re Mass (ug)
Re_tracer12	5.338	5	66	14.658	2168	10840	0.009	101.029
Re_tracer13	5.352	5	71	14.654	1786	8930	0.009	83.067
Re_tracer14	5.404	5	76	14.735	1457	7285	0.009	67.976
Re_tracer15	5.390	5	81	14.733	1174	5870	0.009	54.843
Re_tracer16	5.396	5	86	14.779	1249	4371.5	0.009	41.018
Re_tracer17	5.383	5	91	14.757	989.6	3463.6	0.009	32.468
Re_tracer18	5.382	5	96	14.758	806	2821	0.009	26.450
Re_tracer19	5.311	5	101	14.716	653.8	2288.3	0.009	21.521
Re_tracer20	5.404	5	106	14.771	546	1911	0.009	17.900
Re_tracer21	5.387	5	111	14.727	456.4	1597.4	0.009	14.920
Re_tracer22	5.309	5	116	14.575	377.9	1322.65	0.009	12.256
Re_tracer23	5.433	5	121	14.68	330.9	1158.15	0.009	10.709
Re_tracer24	5.310	5	126	14.529	293.7	1027.95	0.009	9.477
Re_tracer25	5.320	5	131	14.542	256	896	0.009	8.263
Re_tracer26	5.441	5	136	14.694	399.3	798.6	0.009	7.389
Re_tracer27	5.398	5	141	14.685	356.5	713	0.009	6.622
Re_tracer28	5.452	5	146	14.754	329.7	659.4	0.009	6.134
Re_tracer29	5.433	5	151	14.729	291.8	583.6	0.009	5.425
Re_tracer30	5.381	5	156	14.678	264.3	528.6	0.009	4.914
Re_tracer31	5.429	5	161	14.681	464.7	464.7	0.009	4.299
Re_tracer32	5.399	5	166	14.602	424.9	424.9	0.009	3.910
Re_tracer33	5.388	5	171	14.576	393.8	393.8	0.009	3.618
Re_tracer34	5.395	5	176	14.571	365.7	365.7	0.009	3.356
Re_tracer35	5.320	5	181	14.511	348.3	348.3	0.009	3.201
Re_tracer36	5.396	7	188	18.309	324.5	324.5	0.013	4.190
Re_tracer37	5.388	7	195	18.381	291.1	291.1	0.013	3.782
Re_tracer38	5.321	7	202	18.235	269.3	269.3	0.013	3.478
Re_tracer39	5.394	7	209	18.225	247.3	247.3	0.013	3.173
Re_tracer40	5.304	7	216	18.003	230.2	230.2	0.013	2.923

Another tracer test was then performed to confirm that all of the injected rhenium is recovered from the column. A rhenium tracer test was performed by injecting 1.97 mL of 250 ppm rhenium solution (0.4925 mg) into a column containing SRS sediment that was previously saturated with DI water. Forty samples were collected over a total of 214 minutes at 4 and 7 minute intervals (Table 2-23).

Table 2-23. Tracer Test: Rhenium (Re) 250 ppm

Sample ID	Weight empty test tube (g)	Time (min)	Total Time (min)	Weight test tube + solution (g)	Solution Volume (L)	Total volume (L)
1	5.3251	7	7	19.0551	0.01373	0.01373
2	5.3153	7	14	19.0741	0.013759	0.027489
3	5.4315	7	21	19.2059	0.013774	0.041263
4	5.4032	4	25	13.2836	0.00788	0.049144
5	5.3086	4	29	13.2041	0.007896	0.057039
6	5.4072	4	33	13.2866	0.007879	0.064919
7	5.2942	4	37	13.1904	0.007896	0.072815
8	5.456	4	41	13.3449	0.007889	0.080704
9	5.3825	4	45	13.2571	0.007875	0.088578
10	5.3961	4	49	13.2714	0.007875	0.096454
11	5.3967	4	53	13.2744	0.007878	0.104331
12	5.4533	4	57	13.3268	0.007874	0.112205
13	5.3102	4	61	13.1713	0.007861	0.120066
14	5.3933	4	65	13.2646	0.007871	0.127937
15	5.3932	4	69	13.2737	0.007881	0.135818
16	5.32	4	73	13.196	0.007876	0.143694
17	5.401	4	77	13.2794	0.007878	0.151572
18	5.424	4	81	13.2865	0.007863	0.159435
19	5.4028	4	85	13.2705	0.007868	0.167302
20	5.3074	4	89	12.9889	0.007682	0.174984
21	5.324	4	93	13.1434	0.007819	0.182803
22	5.4342	4	97	13.3443	0.00791	0.190713
23	5.3128	4	101	13.2007	0.007888	0.198601
24	5.3913	4	105	13.2656	0.007874	0.206475
25	5.4514	4	109	13.3119	0.007861	0.214336
26	5.4255	7	116	19.1576	0.013732	0.228068
27	5.3939	7	123	19.1655	0.013772	0.24184
28	5.4004	7	130	19.1619	0.013762	0.255601
29	5.3856	7	137	19.1077	0.013722	0.269323
30	5.3881	7	144	19.0941	0.013706	0.283029
31	5.3917	7	151	19.1002	0.013709	0.296738
32	5.3854	7	158	19.0757	0.01369	0.310428
33	5.4266	7	165	19.1153	0.013689	0.324117
34	5.327	7	172	19.0462	0.013719	0.337836
35	5.3887	7	179	19.0935	0.013705	0.351541
36	5.3945	7	186	19.0939	0.013699	0.36524

Sample ID	Weight empty test tube (g)	Time (min)	Total Time (min)	Weight test tube + solution (g)	Solution Volume (L)	Total volume (L)
37	5.3908	7	193	19.0748	0.013684	0.378924
38	5.3168	7	200	18.9993	0.013683	0.392607
39	5.3989	7	207	19.0797	0.013681	0.406287
40	5.399	7	214	19.0861	0.013687	0.419975

Samples were prepared by making appropriate dilutions and then analyzed for rhenium using ICP-OES. The data analysis concluded that 0.4485 mg of rhenium was recovered from the column at 91% recovery with an effective flow rate of 1.96 mL/min. The breakthrough curve from the tracer test is shown in Figure 2-47. To improve the recovery of rhenium, the sample collection duration will be increased as the samples collected towards the end of the experiment showed detectable concentrations of rhenium.

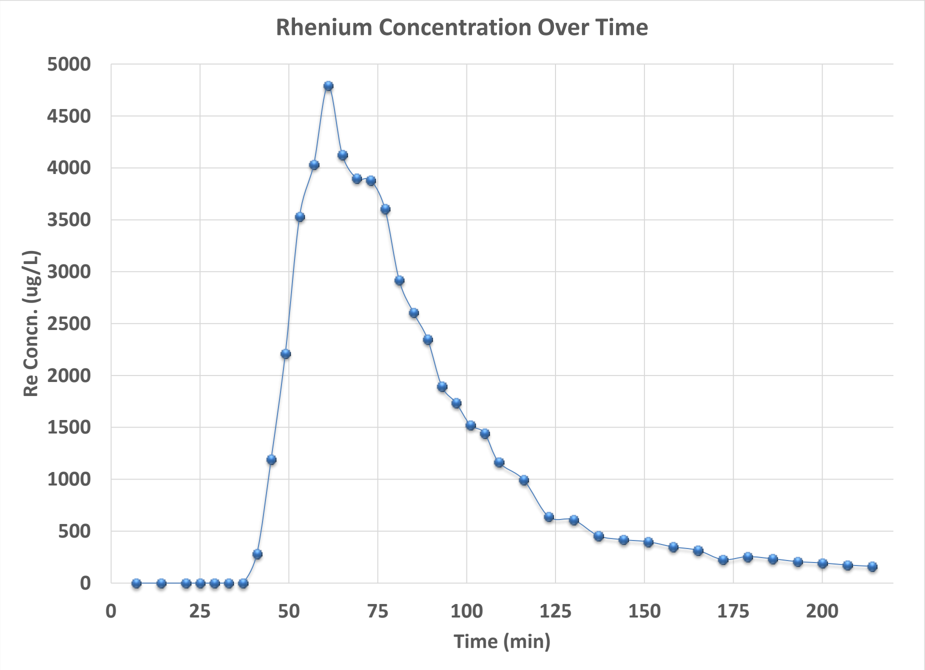

Figure 2-47. Rhenium breakthrough curve obtained for 250 ppm of rhenium tracer test.

DOE Fellow Ripley Raubenolt attended Waste Management Symposia held in Phoenix, AZ from March 6-10, and the Conference of Undergraduate Research at FIU on March 29. She presented a poster titled “Investigating the effect of sorbed humic acid on the mobility of uranium” based on the results obtained from previous studies related to this task (Figure 2-48).

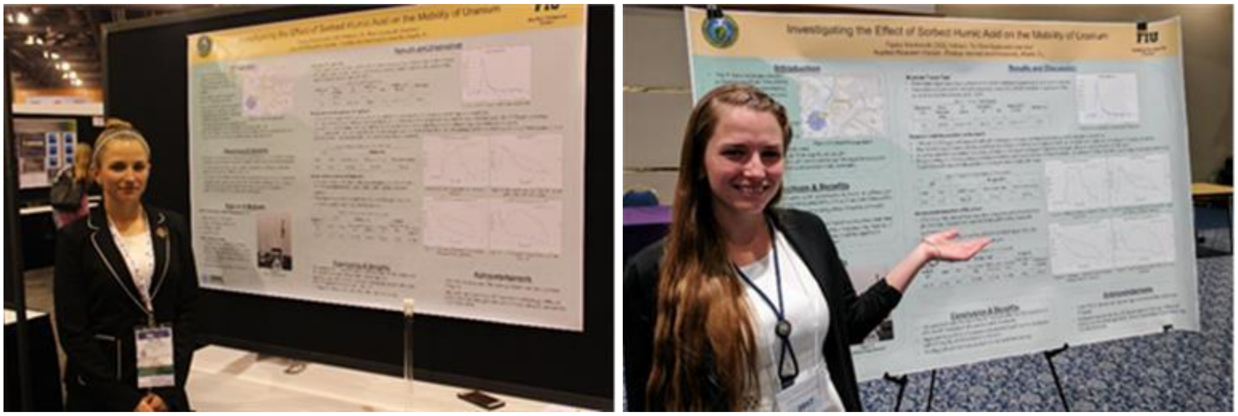

Figure 2-48. DOE Fellow Ripley Raubenolt at Waste Management Symposia (left) and at the Conference of Undergraduate Research at FIU (right).

Task 3: Surface Water Modeling of Tims Branch

Task 3 Overview

This task will perform modeling of surface water, and solute/sediment transport specifically for mercury and tin in Tims Branch at the Savannah River Site (SRS). This site has been impacted by 60 years of anthropogenic events associated with discharges from process and laboratory facilities. Tims Branch provides a unique opportunity to study complex systems science in a full-scale ecosystem that has experienced controlled step changes in boundary conditions. The task effort includes developing and testing a full ecosystem model for a relatively well defined system in which all of the local mercury inputs were effectively eliminated via two remediation actions (2000 and 2007). Further, discharge of inorganic tin (as small micro-particles and nanoparticles) was initiated in 2007 as a step function with high quality records on the quantity and timing of the release. The principal objectives are to apply geographical information systems and stream/ecosystem modeling tools to the Tims Branch system to examine the response of the system to historical discharges and environmental management remediation actions.

Task 3 Quarterly Progress

Subtask 3.1. Modeling of Surface Water and Sediment Transport in the Tims Branch Ecosystem

This quarter efforts on this subtask were focused on two major objectives: 1) model calibration and subsequent modification of both MIKE SHE and MIKE 11 models, and 2) continuing student mentorship and training to support the hydrological modeling efforts.

FIU completed milestone 2016-P2-M8 on March 1, 2017, which involved calibration of the MIKE SHE and MIKE 11 models. A memo for the milestone was submitted on March 1, 2017 to all DOE EM-HQ and SRS/SRNL/SREL points of contact. Currently, several modifications are being made based on the preliminary model results and sensitivity analyses that were carried out.

MIKE SHE Model Calibration and Sensitivity Analysis

FIU began the calibration process for the MIKE SHE overland flow model by performing simulations to identify the calibration parameters and the relative effect of the hydrological modules on the simulation results, making adjustments to the input parameters as necessary based on the results. Model calibration was conducted by focusing on one specific hydrological parameter (e.g., roughness coefficient, vegetation) at a time to understand the model's response to changes of each individual parameter. Sensitivity analyses were simultaneously performed to understand the behavior of each model when certain parameters were varied.

Overland flow:

Figure 2-49 shows screenshots of the results of overland flow simulations in MIKE SHE showing water depth with rainfall, evapotranspiration and unsaturated zone modules included. Because of the low impact of groundwater flow on the overland flow during the summer, no subsurface module was included. This particular simulation is used as a baseline to monitor the model's behavior during the calibration process.

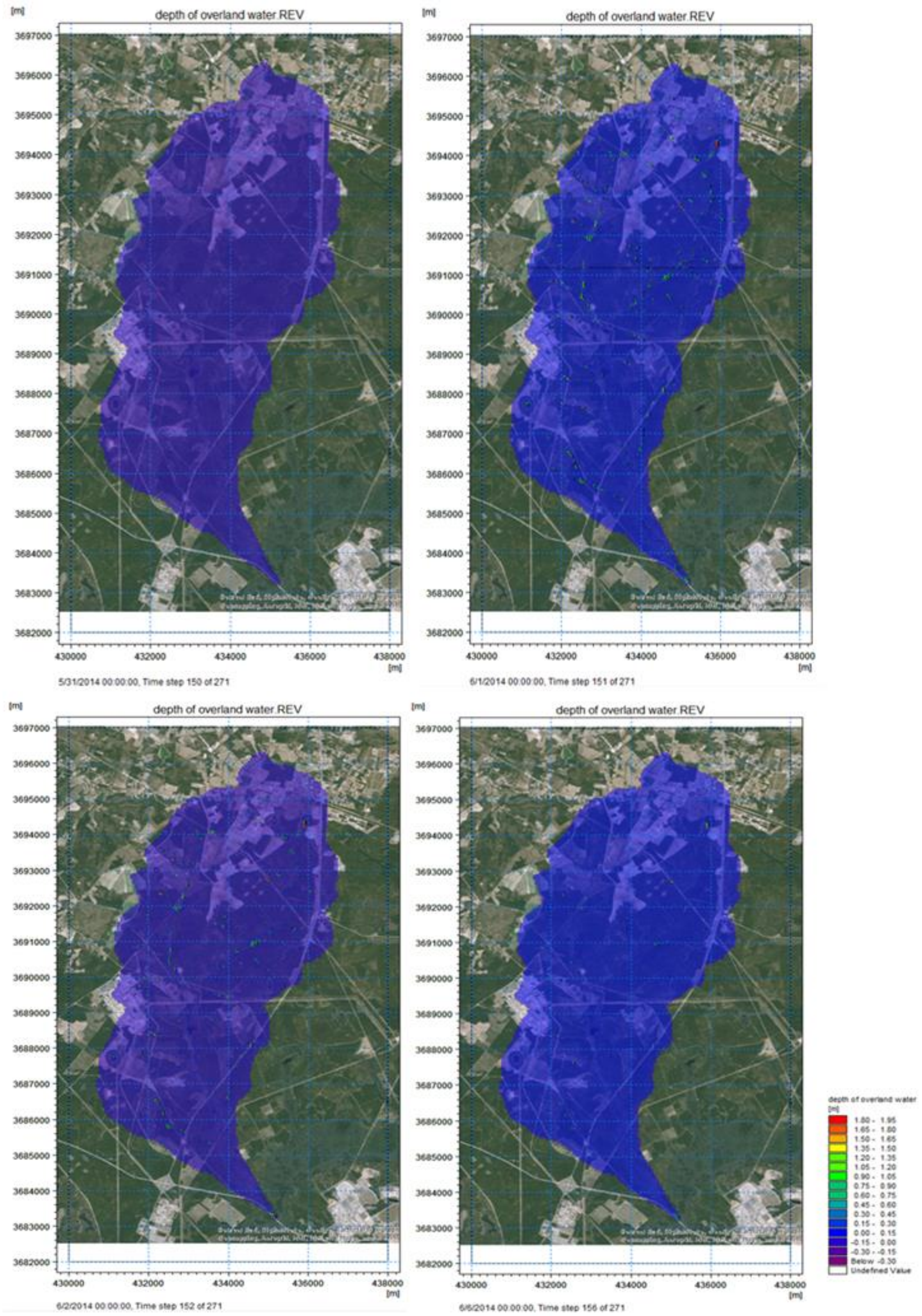

Figure 2-49. Overland flow simulation (evapotranspiration and unsaturated zone included) for 2-day rainfall event on June 1, 2014. An increase in depth of overland flow was observed as the rainfall progressed.

For the purpose of comparison, another simulation was performed with only the precipitation module included. Figure 2-50 illustrates the simulation results for the same period as in Figure 2-49. The increase in water depth downstream in Tims Branch indicates that evapotranspiration and unsaturated flow play an important role in overland flow depth in the Tims Branch watershed and cannot be ignored. As such, these modules are set to calibrate the model in the complete model set-up.

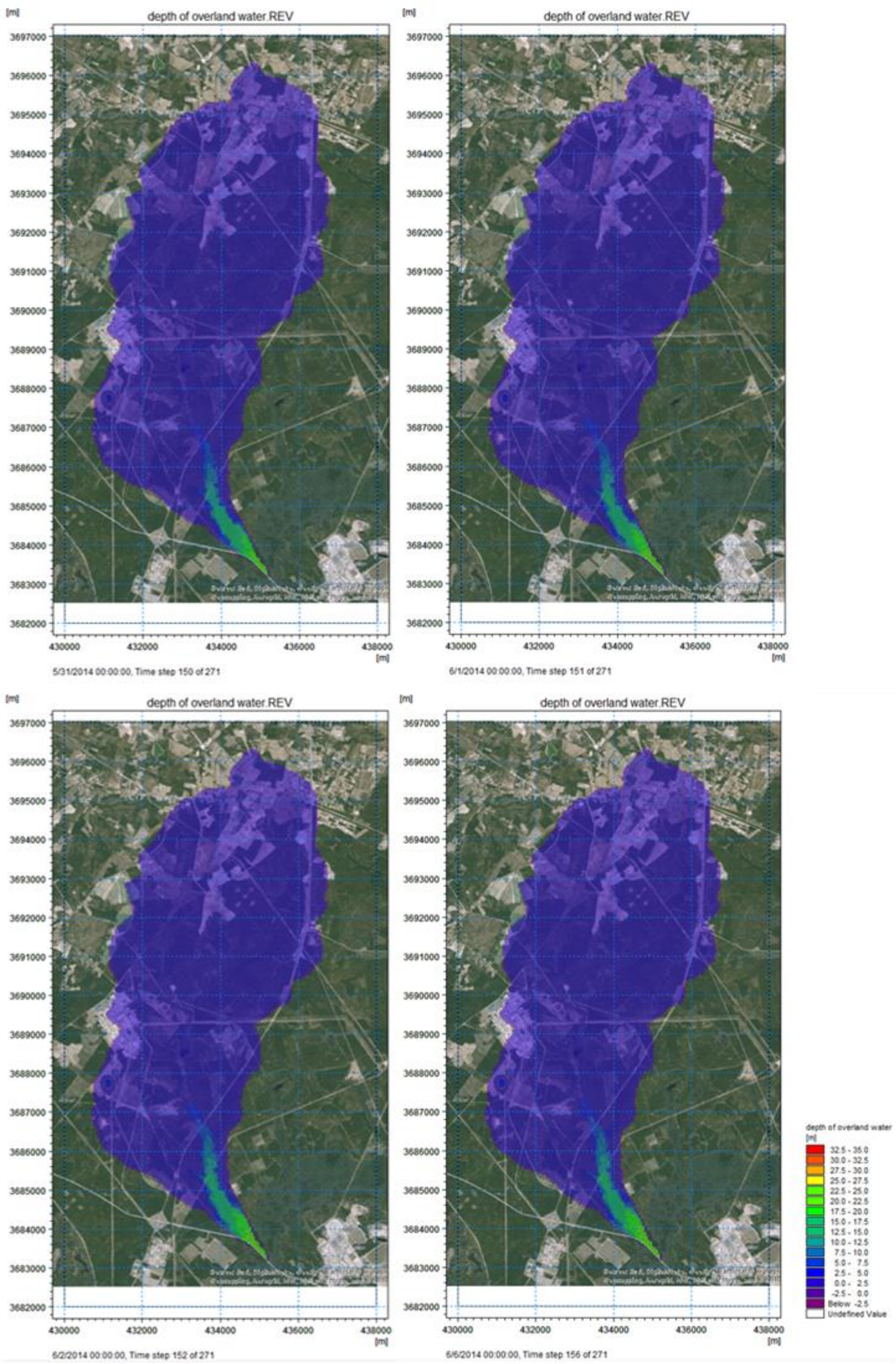

Figure 2-50. Overland flow simulation (precipitation only) for 2-day rainfall event on June 1, 2014. An increase in depth of overland flow was observed as the rainfall progressed.

The MIKE SHE overland flow simulations were conducted for a period of 9 months from 1/1/2014 to 9/30/2014. Two peak rainfall events were selected as the points for visual comparison. The rain events occurred on 2/14/2014 and 6/1/2014 (Figure 2-51). The Saturated Zone (SZ) module was excluded from these series of simulations.

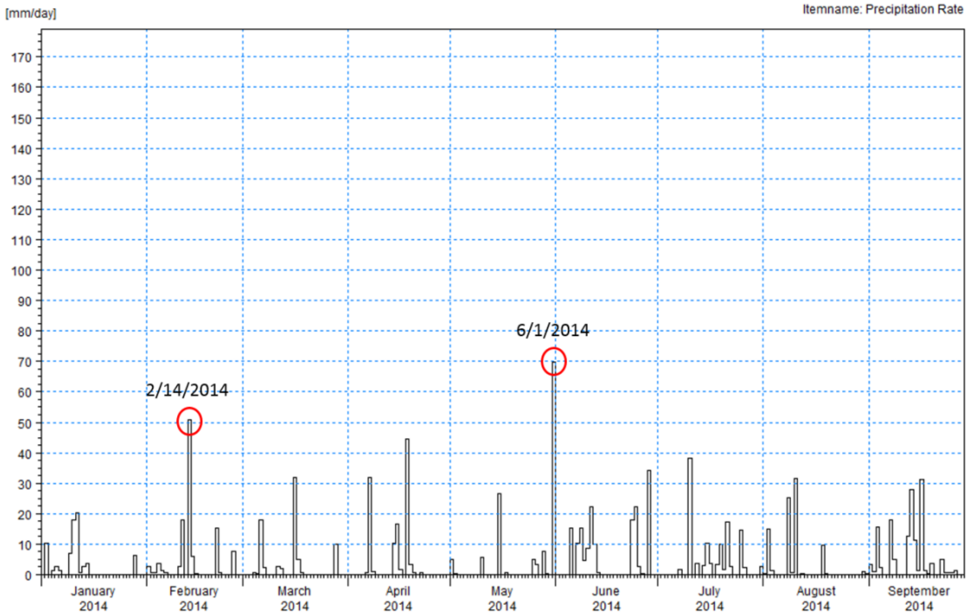

Figure 2-51. Rainfall events in 2014, SRS, SC. The two peak rainfall events in February and June are marked as red circles.

Detention Storage (DS):

The first sensitivity analysis was performed by changing the initial Detention Storage (DS) value in the MIKE SHE overland flow model. The initial value of DS was set to 2.5 mm (based on data derived from a comprehensive literature review, Ref. *Aadland, R. K., et al. 1995. Hydrogeologic framework of west-central South Carolina, State of South Carolina, Department of Natural Resources*). This value was adjusted by ± 5% (2.625 mm, 2.375 mm), ± 10% (2.75 mm, 2.25 mm), and ± 20% (3.0 mm, 2.0 mm). A total of 6 overland flow simulations were implemented. Results indicate that the overland flow model appears to be sensitive to changes in DS. It also shows that the sensitivity of the model to changes in DS increases as the amount of rainfall at one single event increases. A lower rainfall volume was recorded for the month February compared with the month of June which had a higher rainfall volume. Figures 2-52 and 2-53 show the results of simulations with an increase in DS value for both rainfall events taking place on 1/14/2014 and 6/1/2014, respectively. For the rainfall event on 1/14/2014 which had lower rainfall intensity, the change in the overland flow volume appears negligible; however, an increase in the depth of overland flow was observed for the higher rainfall event on 6/1/2014 when the DS value was increased. Therefore, the value of DS seems to be an important factor in calibration of the overland flow model.

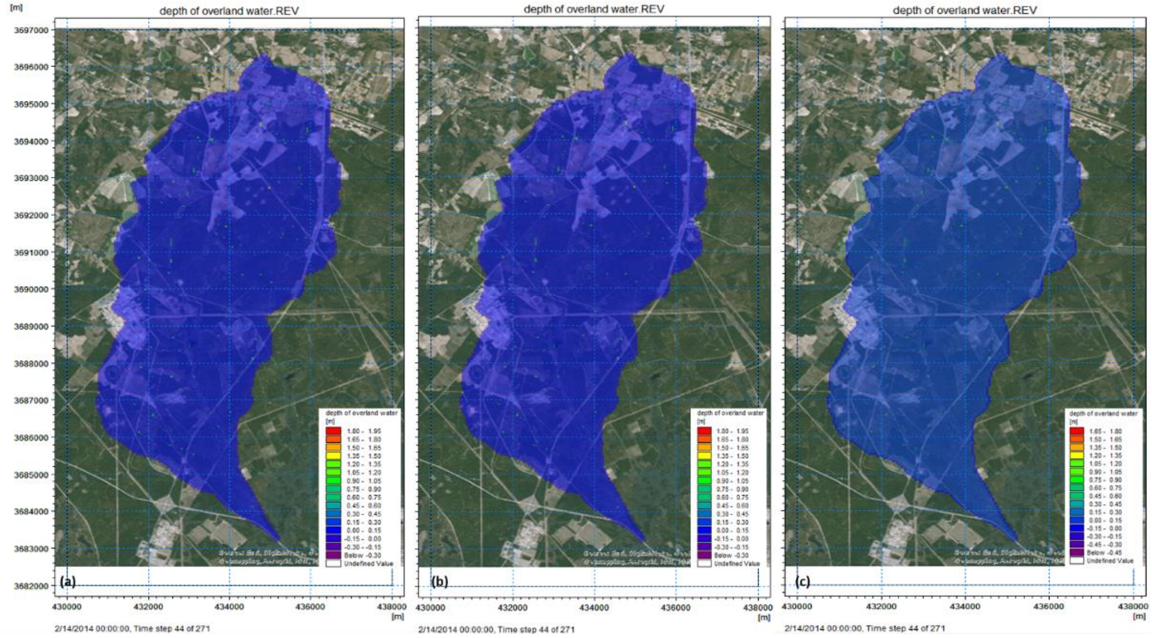

Figure 2-52. MIKE SHE simulation of overland flow depth for a rainfall event on 1/14/2014, with an increase in detention storage by (a) 5%, (b) 10%, and (c) 20%.

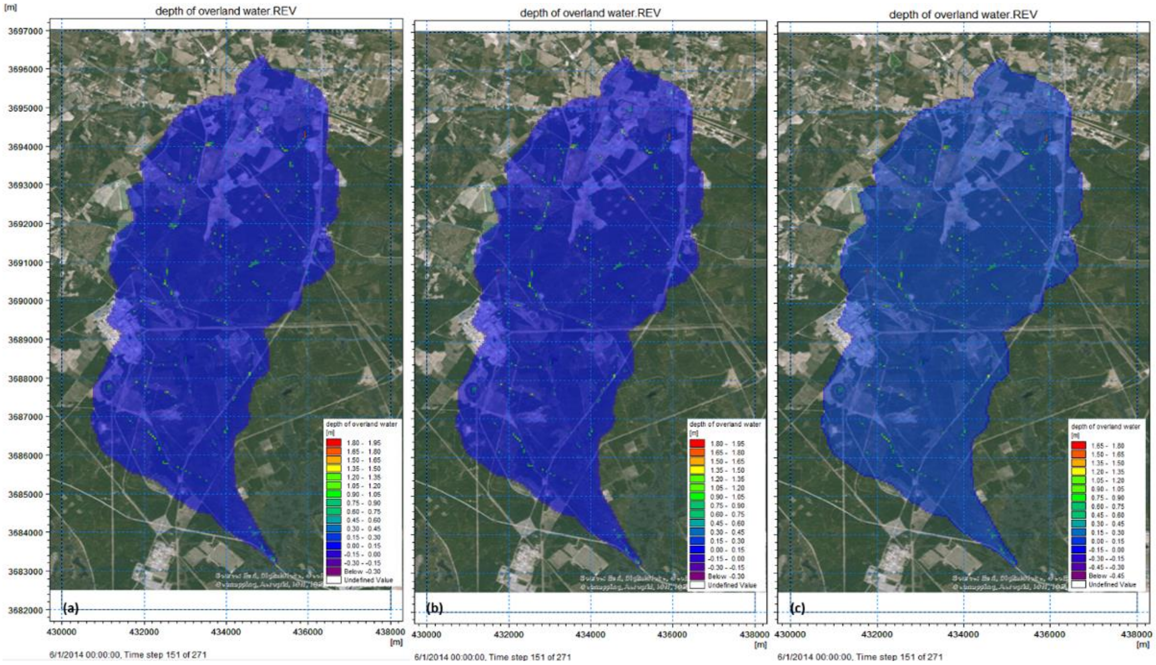

Figure 2-53. MIKE SHE simulation of overland flow depth for a rainfall event on 6/1/2014, with an increase in detention storage by (a) 5%, (b) 10%, and (c) 20%.

Figures 2-54 & 2-55 illustrate the results of simulations for both rainfall events with decreasing the amount of DS by 5%, 10%, and 20%. It appears that a decrease in DS value may cause a noticeable change in the overland flow depth for both rainfall events. This also indicates that the model is sensitive to changes in detention storage. Therefore, it is important to find a time series of DS that is temporally and spatially distributed rather than using a uniform value that is constant over time.

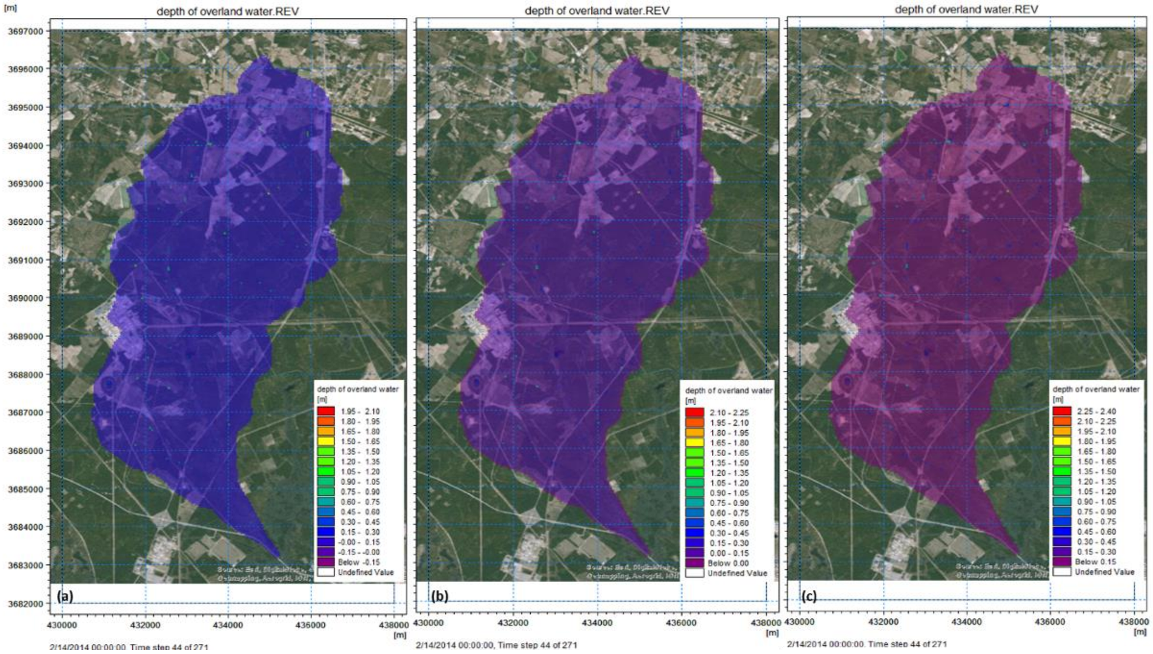

Figure 2-54. MIKE SHE simulation of overland flow depth for a rainfall event on 2/14/2014, with a decrease in detention storage by (a) 5%, (b) 10%, and (c) 20%.

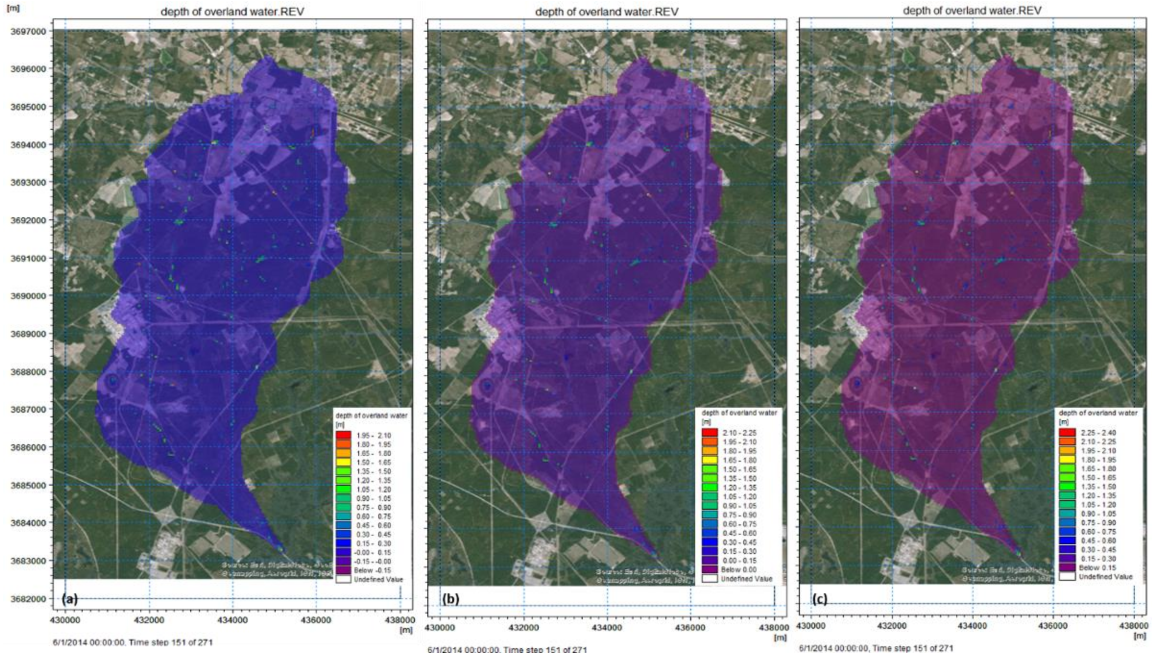

Figure 2-55. MIKE SHE simulation of overland flow depth for a rainfall event on 6/1/2014, with a decrease in detention storage by (a) 5%, (b) 10%, and (c) 20%. The images indicate that a decrease in DS decreases the overland flow depth.

Reference Evapotranspiration (RET):

Sensitivity analyses were also performed by changing the initial Reference Evapotranspiration (RET) value in the MIKE SHE overland flow model. The initial value of RET was set to 2.22 mm/d (based on data derived from a comprehensive literature review, Ref. *Aadland, R. K., et al. 1995. Hydrogeologic framework of west-central South Carolina, State of South Carolina, Department of Natural Resources*). This value was adjusted by ± 5% (2.625 mm/d, 2.109 mm/d), ± 10% (2.75 mm/d, 1.998 mm/d), and ± 20% (2.664 mm/d, 1.778 mm/d). A total of 6 overland flow simulations were implemented. Figures 2-56 and 2-57 show the results of the overland flow depth simulations when changing RET. The results indicate that the overland flow model appears not to be sensitive to the changes in RET. Increasing the amount of RET does not show any effect that is visible on the images of the simulated depth of water. Further investigation is in progress to better understand the effect of RET on depth of water in the overland flow simulation.

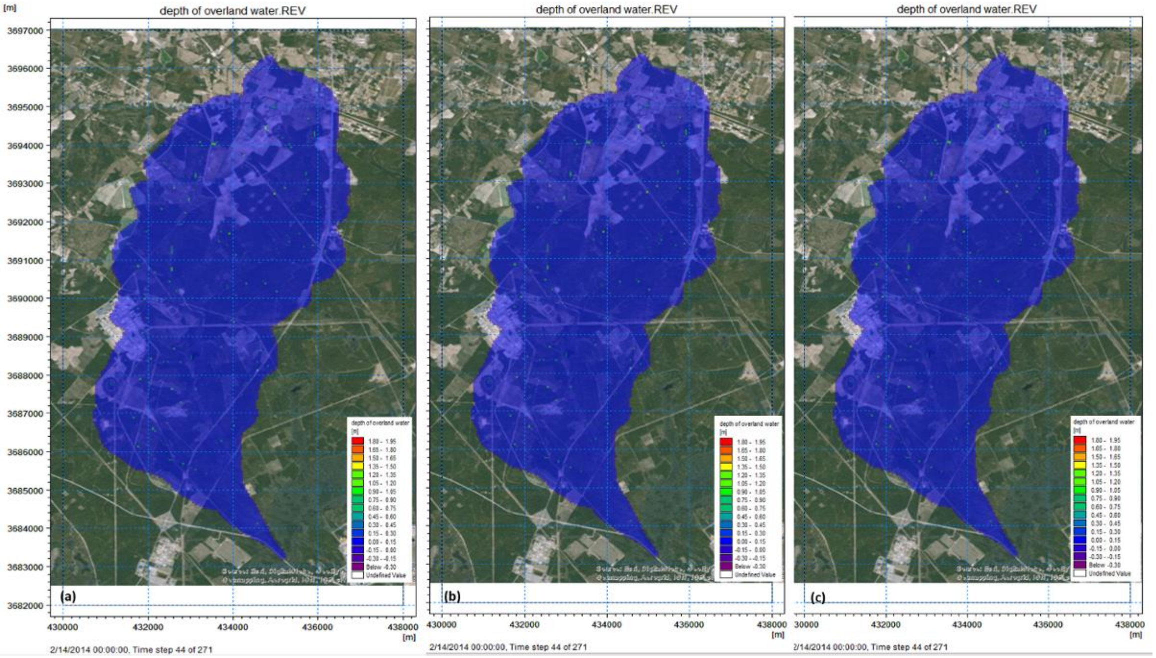

Figure 2-56. MIKE SHE simulation of overland flow depth for a rainfall event on 2/14/2014, with an increase in reference evapotranspiration by (a) 5%, (b) 10%, and (c) 20%. From the images, increasing the RET does not visually appear to have an effect on the overland flow depth.

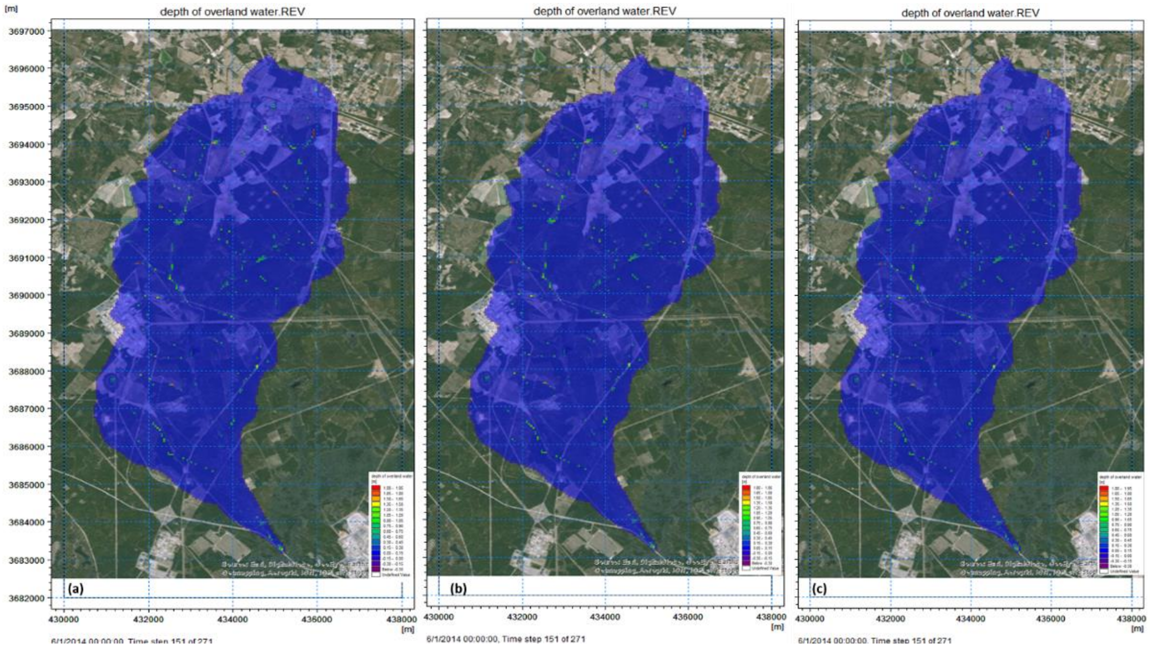

Figure 2-57. MIKE SHE simulation of overland flow depth for a rainfall event on 6/1/2014, with increase an in reference evapotranspiration by (a) 5%, (b) 10%, and (c) 20%. From the images, increasing the RET does not visually appear to have an effect on the overland flow depth.

As the results indicate, the uniformly distributed RET value of 2.22 mm/d seems to adequately represent the amount of RET in the SRS vicinity.

Vegetation:

The current version of the MIKE SHE overland flow model includes a vegetation file that consists of average Leaf Area Index (LAI) and average Root Depth (RD) values for each vegetation class. In this version, LAI and RD values are assumed to be constant during the year. In reality, LAI and RD change over the span of a year as vegetation growth is at maximum during the summer with highest leaf and root production, and at minimum during winter with lowest leaf and root growth.

To improve the model performance, a MIKE SHE vegetation file (*.etv) was generated that includes seasonal changes in both LAI and RD. LAI and RD increase as vegetation grows faster during spring and summer (the peak) while the growth slows down during fall. In winter, no growth is assumed and thus no increase in LAI and RD. The MIKE SHE configuration for seasonal changes in LAI and RD for evergreen vegetation is shown as an example in the following figure.

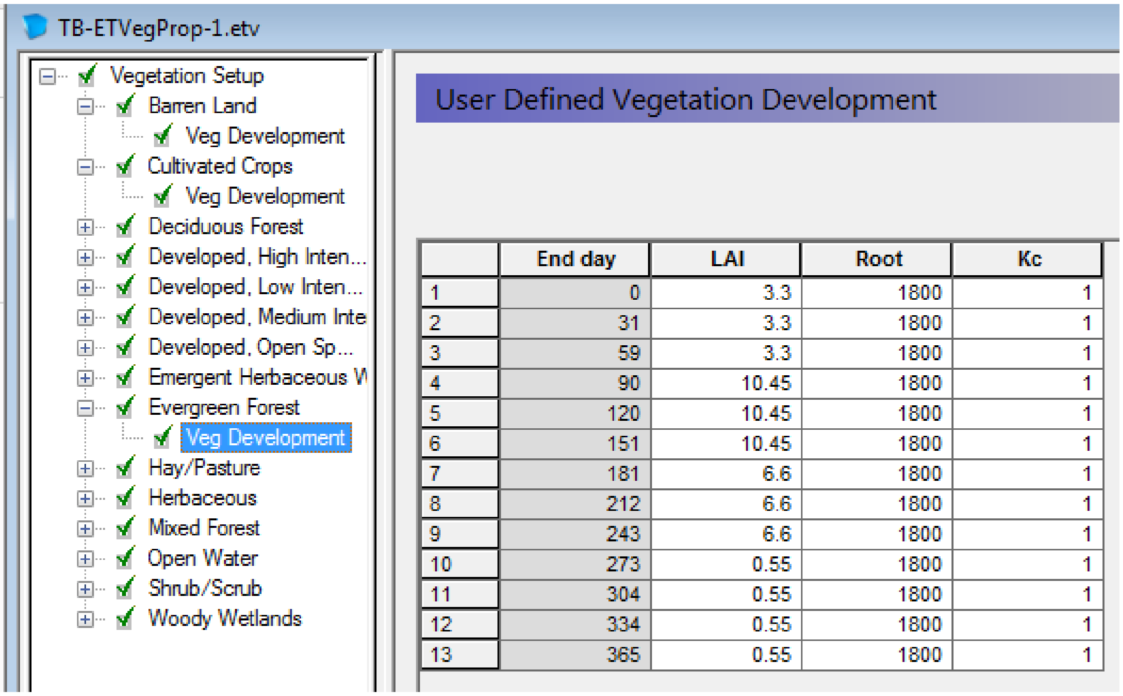

	End day	LAI	Root	Kc
1	0	3.3	1800	1
2	31	3.3	1800	1
3	59	3.3	1800	1
4	90	10.45	1800	1
5	120	10.45	1800	1
6	151	10.45	1800	1
7	181	6.6	1800	1
8	212	6.6	1800	1
9	243	6.6	1800	1
10	273	0.55	1800	1
11	304	0.55	1800	1
12	334	0.55	1800	1
13	365	0.55	1800	1

Figure 2-58. Screenshot of the MIKE SHE vegetation configuration file showing LAI and RD values for evergreen forest.

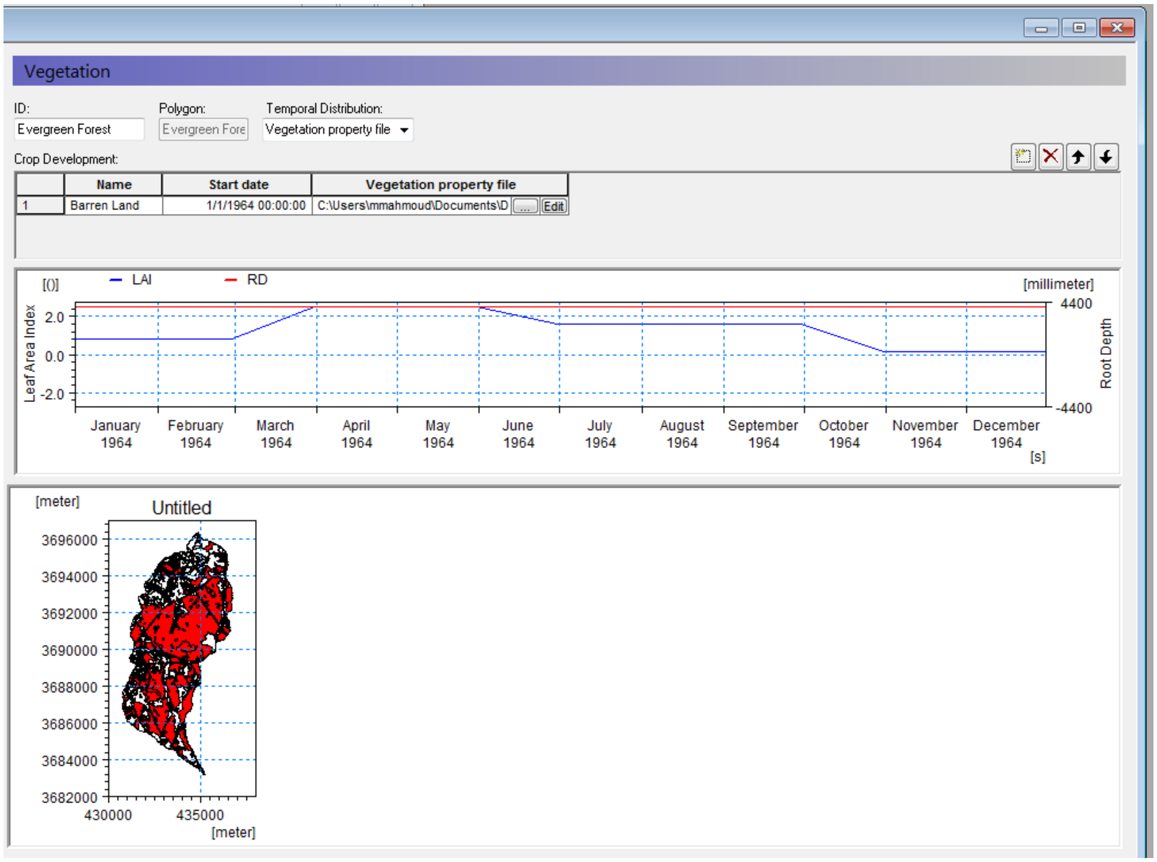

ID: Evergreen Forest

Polygon: Evergreen Fore

Temporal Distribution: Vegetation property file

Crop Development:

	Name	Start date	Vegetation property file
1	Barren Land	1/1/1964 00:00:00	C:\Users\mmahmoud\Documents\D

Figure 2-59. Screenshot of the MIKE SHE vegetation configuration file showing the annual variation of LAI and RD values for evergreen forest for the year 1964.

MIKE 11 Model Calibration and Sensitivity Analysis

During calibration, the MIKE 11 simulations exhibited some numerical errors resulting in an inconclusive calibration and sensitivity analysis. The model is currently under review. Further investigation is necessary to identify the source of these errors and to make substantial improvements to the model performance. Multiple simulations are being conducted to assess the numerical stability of the model and to complete the sensitivity analysis and calibration.

Student Mentorship and Training

During the month of January, training sessions on both GIS and the MIKE models were also provided to the DOE Fellow students to better equip them with the tools necessary to support this research. Specific attention was given to conducting literature reviews related to this research topic, highlighting available data resources including journal papers and reports, as well as digital online databases available on U.S. federal and state agency websites.

Subtask 3.2. Application of GIS Technologies for Hydrological Modeling Support

The use of GIS tools remains a continuous integrated component of the hydrological model development. FIU utilized a combination of ArcGIS and MIKE tools to refine the existing model grid currently being used in MIKE SHE to a smaller grid element size (from 3m to 1 m resolution) in order to capture more detail of the surface topography and man-made structures such as the roads, culvert and weir. Currently, a 1-m resolution DEM for the study domain is unavailable. Refinement of the grid mesh size will improve model accuracy in the event in situ data is unavailable.

The 3-m DEM which was provided by SRNS/SRNL that was derived from LIDAR data was imported into ArcMap after being projected to the appropriate UTM coordinate system (NAD_1983_UTM_Zone_17N). The Image Analysis toolbar was then activated and used to clip the DEM to the hydrological model study domain by overlaying a polygon shapefile of the Tims Branch watershed. The Image Analysis Tool provides an option to adjust the cell size when clipping the raster file (DEM). The grid cell size was adjusted to 1-m x 1-m and the process executed in ArcMap. The output raster was then converted to a MIKE SHE model-compatible format using a combination of ArcGIS and MIKE tools.

Work also continued on the delineation of the stream network and cross sections for the Tims Branch stream using a combination of ArcGIS and MIKE 11 tools. The more recently inducted DOE Fellows were trained on the use of ArcGIS tools to delineate a sub-catchment of the A-014/A-011 outfall tributaries, and to begin generating cross sections for the main Tims Branch stream. The students were instructed on the use of ArcHydro to delineate the stream networks and catchments from a South Carolina DEM. The use of GIS tools remains a continuous integrated component of the hydrological model development. The delineated shapefiles will be used in both the MIKE SHE and MIKE 11 models being developed for the A-014 outfall tributary as well as the main Tims Branch stream

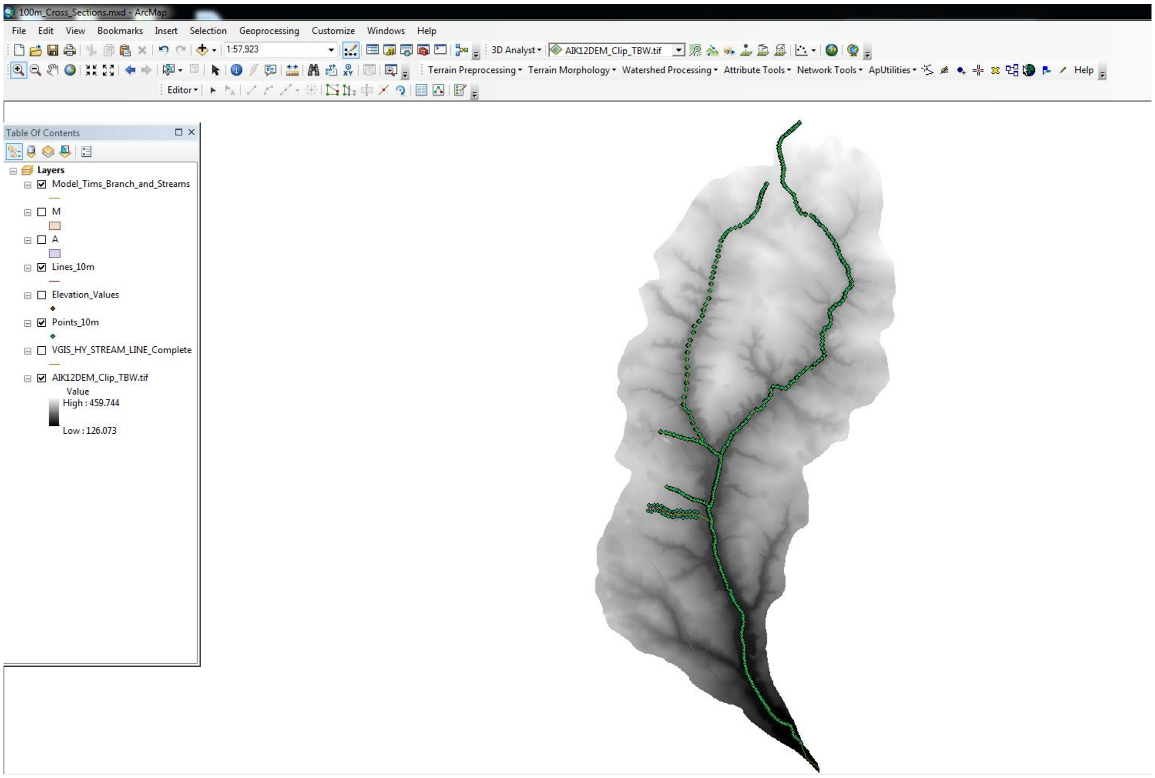

Figure 2-60. Delineated cross-sections of the main Tims Branch stream generated in ArcMap.

In addition, DOE Fellow Juan Morales completed his poster and presented at the WM17 Symposium in March for his research titled “Modeling the relationship between land use and surface water quality of Tims Branch, Savannah River Site, Aiken, SC.” This poster explores a watershed-based approach using a combination of statistical and geospatial (GIS) analyses of land cover change between 2001 and 2011 which will be coupled with hydrological modeling results to better understand the hydrologic effects of land cover change in Tims Branch watershed and establish an association between land cover change and water quality. The study, which is in its preliminary stages, is currently inconclusive; however, further data analysis and comparison with historical data pre- and post-remediation coupled with hydrological modeling results will help to establish if there is any significant relationship between the land cover change and in-stream water quality in Tims Branch. This study assumes that future land development can result in resuspension of sediment and potentially cause fluctuations in sediment-bound contaminant levels. The model being developed will help to predict future hydrological conditions in times of global environmental change, such as land use change, climate change, changes in total mass discharge loads (TMDLs), point source discharge or permit discharge conditions.

Subtask 3.3. Biota, Biofilm, Water and Sediment Sampling in Tims Branch

Proposed plans for follow-up sampling and data collection at SRS, as outlined in the project technical plan submitted to DOE, still requires further discussion. The timing and scope will be based on budget availability of both FIU and SRNL personnel. Refinement of the grid mesh size to improve model accuracy (as described above) by capturing more detail of the surface topography and man-made structures is a strategy also being pursued in the event in situ data is unavailable. Incorporation of the sampling and analysis as part of a student summer 2017 internship is also being considered. FIU has held discussions with SRNL and SREL personnel regarding implementation of monitoring stations in Tims Branch to collect timeseries water quality and flow data at strategic points along the stream, however this is entirely subject to available funding through the cooperative agreement.

The field sampling and data collection conducted by FIU ARC researchers and DOE Fellows in August 2016 was featured in an article entitled "DOE Fellows Help Develop Model to Assess SRS Watershed Contamination" in the DOE-EM Update Newsletter, Vol. 9, Issue 3, Feb. 14, 2017.

During the month of March, DOE Fellows supporting this task participated in the student poster competition at the Waste Management Symposium 2017. Mohammed Albassam, who is a graduate student pursuing a master's degree in engineering management, presented his poster entitled "In-Situ Water Quality Sampling and Flow Measurements to Support Hydrological Model Development for Tims Branch Watershed, Savannah River Site, SC." The poster was based on the field sampling and data collection conducted by FIU researchers and DOE Fellows in August 2016.

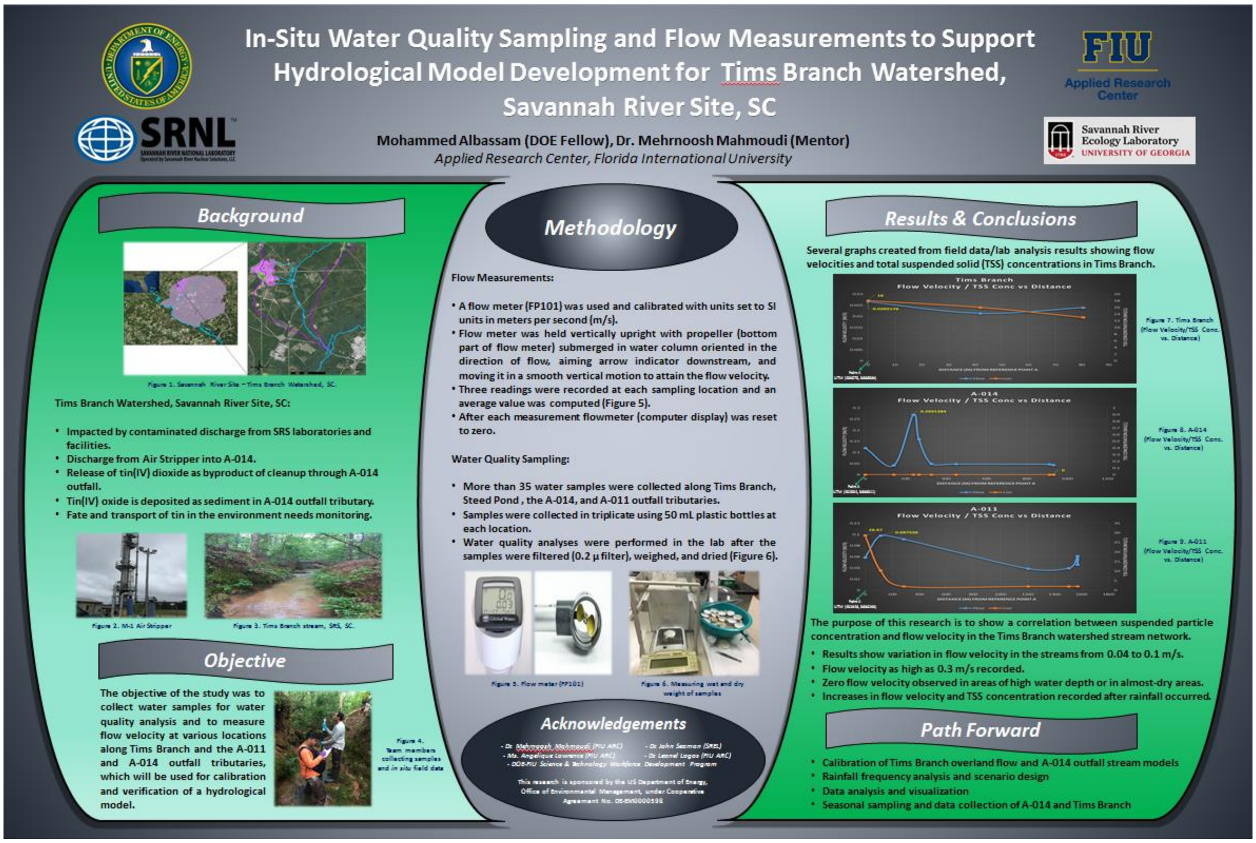

In-Situ Water Quality Sampling and Flow Measurements to Support Hydrological Model Development for Tims Branch Watershed, Savannah River Site, SC

Mohammed Albassam (DOE Fellow), Dr. Mehrnoosh Mahmoudi (Mentor)
Applied Research Center, Florida International University

Background

Figure 1. Savannah River Site – Tims Branch Watershed, SC.

Tims Branch Watershed, Savannah River Site, SC:

- Impacted by contaminated discharge from SRS laboratories and facilities.
- Discharge from Air Stripper into A-014.
- Release of tin(IV) dioxide as byproduct of cleanup through A-014 outfall.
- Tin(IV) oxide is deposited as sediment in A-014 outfall tributary.
- Fate and transport of tin in the environment needs monitoring.

Figure 2. M-1 Air Stripper

Figure 3. Tims Branch stream, SRS, SC.

Objective

The objective of the study was to collect water samples for water quality analysis and to measure flow velocity at various locations along Tims Branch and the A-011 and A-014 outfall tributaries, which will be used for calibration and verification of a hydrological model.

Figure 4. Team members collecting samples and *in situ* field data

Methodology

Flow Measurements:

- A flow meter (FP101) was used and calibrated with units set to SI units in meters per second (m/s).
- Flow meter was held vertically upright with propeller (bottom part of flow meter) submerged in water column oriented in the direction of flow, aiming arrow indicator downstream, and moving it in a smooth vertical motion to attain the flow velocity.
- Three readings were recorded at each sampling location and an average value was computed (Figure 5).
- After each measurement flowmeter (computer display) was reset to zero.

Water Quality Sampling:

- More than 35 water samples were collected along Tims Branch, Steed Pond , the A-014, and A-011 outfall tributaries.
- Samples were collected in triplicate using 50 mL plastic bottles at each location.
- Water quality analyses were performed in the lab after the samples were filtered (0.2 μ filter), weighed, and dried (Figure 6).

Figure 5. Flow meter (FP101)

Figure 6. Measuring wet and dry weight of samples

Acknowledgements

- Dr. Mehrnoosh Mahmoudi (FIU ARC)
- Ms. Angelique Lawrence (FIU ARC)
- DOE-FIU Science & Technology Workforce Development Program
- Dr. John Seaman (SREL)
- Dr. Leonel Lagos (FIU ARC)

This research is sponsored by the US Department of Energy, Office of Environmental Management, under Cooperative Agreement No. DE-EM0000598

Results & Conclusions

Several graphs created from field data/lab analysis results showing flow velocities and total suspended solid (TSS) concentrations in Tims Branch.

Figure 7. Tims Branch (Flow Velocity/TSS Conc. vs. Distance)

Figure 8. A-014 (Flow Velocity/TSS Conc. vs. Distance)

Figure 9. A-011 (Flow Velocity/TSS Conc. vs. Distance)

The purpose of this research is to show a correlation between suspended particle concentration and flow velocity in the Tims Branch watershed stream network.

- Results show variation in flow velocity in the streams from 0.04 to 0.1 m/s.
- Flow velocity as high as 0.3 m/s recorded.
- Zero flow velocity observed in areas of high water depth or in almost-dry areas.
- Increases in flow velocity and TSS concentration recorded after rainfall occurred.

Path Forward

- Calibration of Tims Branch overland flow and A-014 outfall stream models
- Rainfall frequency analysis and scenario design
- Data analysis and visualization
- Seasonal sampling and data collection of A-014 and Tims Branch

Figure 2-61. DOE Fellow poster presented at WM17 based on field research that supports development of a hydrological model of the Tims Branch watershed.

Task 5 Quarterly Progress

During the months of January through March, collection of data from the 0.1 and 5 M IS columns was continued and 3.0 M batch kinetics sampling was completed. In addition, batch experiments were set up for 0.5 M ionic strength. These samples are currently awaiting analysis at LANL-CEMRC. Preliminary results for modeling speciation of neodymium with respect to ionic strength are presented below alongside current experimental data.

DOE Fellow Frances Zengotita presented a poster for the student competition at the Waste Management Conference in Phoenix, AZ on March 6 and prepared a poster for the Life Sciences South Florida STEM poster competition in West Palm Beach, FL on April 1. Postdoctoral associate Hilary Emerson also gave an oral and poster presentation at the ABC Salt V Workshop in Ruidoso, NM on March 27.

Visual Minteq Modeling

Below are preliminary results for speciation of americium with respect to ionic strength for our batch and column systems. Data is presented for Am because all necessary parameters are not included for Nd. Furthermore, the model is assumed to be a closed system at pH 8.5 with 3.0 mM $NaHCO_3$ added in experimental systems to reach equilibrium with the atmosphere and 30 ppb Am. Davies corrections are used although they are generally not applicable above 0.7 mol/kg. Future modeling will investigate the use of Pitzer activity corrections.

The aqueous speciation with respect to ionic strength is shown in Figure 2-62 in terms of concentration. This figure shows that the $AmCl^{2+}$ species increases significantly. However, there are also small increases in the hydrolysis species and a decrease in the carbonate species that are not clearly depicted on the log scale. Figure 2-63 shows the fraction of Am species for comparison. It depicts clearly the increase in hydrolysis and decrease in carbonates. Table 2-24 below shows that the solubility decreases with increasing ionic strength based on saturation indices for $Am(OH)_3$ and $Am_2(CO_3)_3$.

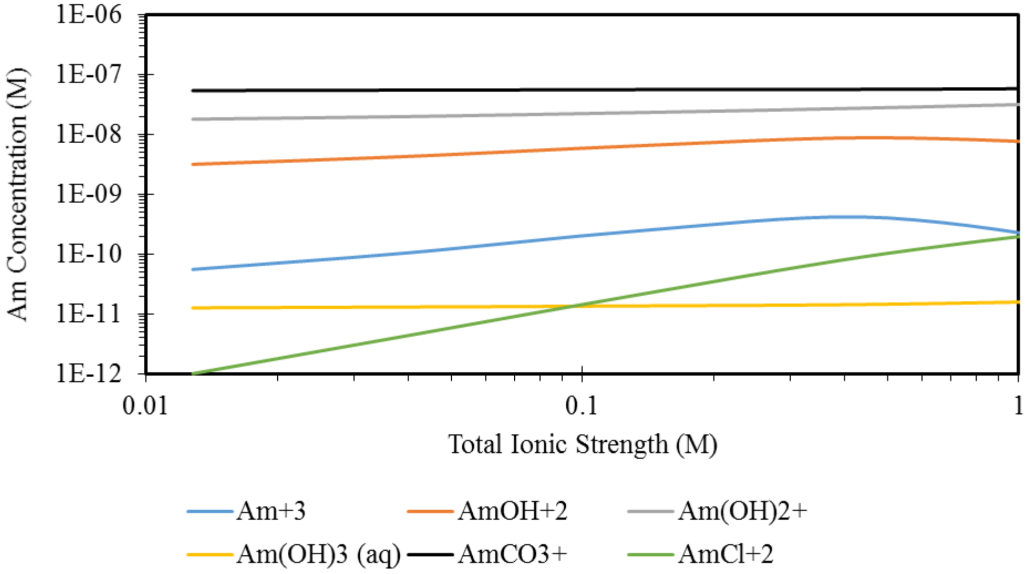

Figure 2-62. Concentration of Am species with respect to ionic strength in 3 mM $NaHCO_3$, with ionic strength varied using NaCl and Davis ionic strength corrections.

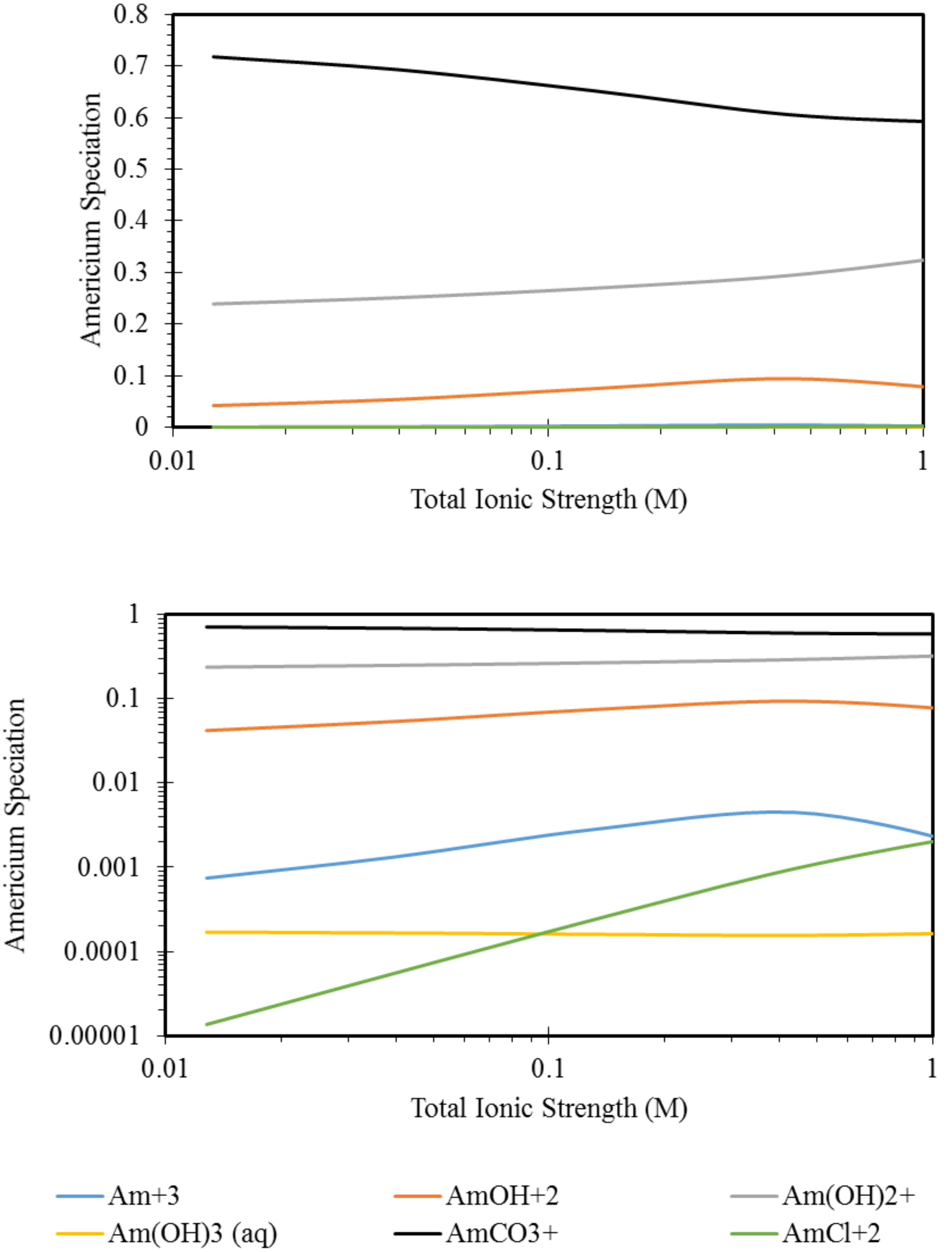

Figure 2-63. Am speciation as a fraction of total Am with respect to ionic strength in 3 mM $NaHCO_3$, with ionic strength varied with NaCl and Davis ionic strength corrections, Top – y-axis on a regular scale, Bottom – y-axis on a log scale for comparison.

Table 2-24. Saturation Indices for Major Am Solid Phases with Respect to Ionic Strength in 3 mM $NaHCO_3$, with Ionic Strength Varied with NaCl and Davis Ionic Strength Corrections

Ionic Strength M	$Am(OH)_3$ (am) Saturation Index	$Am_2(CO_3)_3(s)$ Saturation Index
0.0128	-2.093	-1.756
0.03948	-2.077	-1.833
0.13218	-2.049	-1.949
0.43438	-1.995	-2.05
1.20958	-1.865	-1.98
1.56474	-1.799	-1.915
1.69569	-1.774	-1.889
1.97646	-1.719	-1.834
2.24899	-1.664	-1.78
2.60673	-1.591	-1.711

Mini Column Experimental Results

The 0.1 and 5.0 M IS columns have now reached greater than 20% breakthrough after nearly 20,000 pore volumes (Figure 2-64). This represents approximately 5.5 L of 20 ppb Nd stock solution input to the one gram dolomite column over 154 days. During the injection period, the 0.1 and 5.0 M columns have similar breakthrough curves. These results are different from the trend shown below in Table 2-25 for the batch experiments, likely due to the lack of equilibration of both the dolomite mineral phase with the aqueous solution and sorption of Nd to the dolomite phase. If the centroid of the breakthrough curve had been reached, the equation below would predict a K_d of approximately 2000 mL/g for the current injection time.

$$R = 1 + \frac{\rho_b}{n_e} K_d$$

In this equation, R = retardation factor or the ratio of the contaminant breakthrough to a conservative tracer breakthrough, ρ_b = bulk density of dolomite (assumed 2.87 g/mL), n_e = porosity (0.277, as measured for this mini column). The K_d (mL/g) is an equilibrium partitioning coefficient for the contaminant of concern between the solid and aqueous phase based on the equation below.

$$K_d = \frac{C_{solid}}{C_{aqueous}}$$

Where C_{solid} = concentration of Nd in the solid phase in µg/g and $C_{aqueous}$ = the equilibrium concentration of Nd in the aqueous phase in µg/mL. Based on the retardation factor equation, the K_d can be estimated based on the effluent breakthrough. However, the K_d can also be estimated from the equilibrium measurements from the batch experiments based on the K_d equation.

The equilibrium K_d measured for the 5 g/L dolomite and 20 ppb Nd batch experiments was 6380 ± 3060 mL/g. Although the error is large on these measurements due to the significant dilution required for measurement on ICP-MS and the low concentrations of Nd, the column breakthrough and batch data confirms that our K_d values are greater than 2000 mL/g. Once the mini columns are saturated and 100% breakthrough occurs, a more accurate estimate for Nd partitioning will be possible.

Figure 2-64 compares the initial results for the 0.1 M column with the 5.0 M column breakthrough. During the initial injection period, the 0.1 and 5.0 M columns appear similar. However, breakthrough is expected to occur in the 0.1 M column prior to the 5.0 M column because the equilibrium K_d values measured in batch experiments are significantly lower (724 ± 105 versus 6380 ± 3060, respectively).

Comparison of Batch and Column Experiments

The equilibrium K_d values measured for removal of 20 ppb Nd in 5 g/L dolomite suspensions was 6380 ± 3060 mL/g at 5.0 M IS (Table 2-25). Although the error is large on these measurements, due to the significant dilution required for measurement on ICP-MS and the low concentrations of Nd, there is a clear trend showing an increase in K_d with respect to ionic strength in the batch experiments. The November and December monthly reports summarized some previous work investigating sorption of actinides and lanthanides at variable ionic strength. However, a more complete picture is described below.

Previous experiments have reported no effect of ionic strength [1, 2], a decrease in sorption with ionic strength [3], and an increase in sorption with ionic strength [3, 4]. Brady and team likely did not report an effect of ionic strength on sorption of Nd and Am to dolomite because of the low range of ionic strength (up to 0.5 M) in their experiments [1]. However, experiments by Schnurr et al. considered sorption of Eu above pH 8 to natural clay samples up to 4.37 m IS without observing an effect of ionic strength [2].

A decrease in sorption with respect to ionic strength may be observed if removal is due to ion exchange and the salts in suspension can compete with the actinide and lanthanide for ion exchange sites. However, the ionic radii of Na^+ versus Nd^{+3} and Am^{+3} in solution are quite different as discussed below, so competition for exchange sites is not expected. Furthermore, it is more likely that surface complexation processes are the dominant sorption reactions in this system. Surface complexation processes generally dominate at neutral to basic pH over ion exchange for trivalent actinides and lanthanides as observed for Eu on clays [5], and dolomite is not expected to have a significant cation exchange capacity based on its structure.

Mancinelli and team have shown that the hydration of Na^+ remains fairly constant (4.5 – 5.3) across the range of ionic strength in this study with a slight trend to decrease with increasing ionic strength (Table 2-27) [6]. Therefore, with a coordination number of 4 – 5, the ionic radii in aqueous solutions for Na^+ is 0.99 – 1.0 pm based on previous measurements [7]. The coordination number for trivalent actinides and lanthanides in water has been reported at 8 – 9, with a decreasing trend across each series. Although, recent EXAFS and modeling indicate that 9 may be the most likely coordination number for trivalent actinides and lanthanides across the series [8]. For a hydration of 8 – 9 water molecules, the ionic radii of Am^{3+} is 1.09 – 1.22 and for Nd^{3+} is 1.109 – 1.163 [7, 8].

An increase in removal of the contaminant with respect to ionic strength may be due to two different mechanisms: (1) the effects of increasing ionic strength on ion activity and speciation [4, 9] or (2) the effects of increasing ionic strength on mineral dissolution and contaminant removal through incorporation (Figure 2-65). Ams and team previously reported that the increase in ion activity led to an increase in hydrolysis and carbonate complexation constants for 2 and 4 M ionic strength [4]. This increase in hydrolysis species for Np(V) was hypothesized to lead to an increase in sorption to microbes based on the increased sorption affinity of these species. Similar conclusions were reached previously for phosphate sorption to calcite with surface complexation modeling [9].

However, in the dolomite system, FIU hypothesize that the second theory is the dominant process, leading to an increase in removal at greater ionic strength in the batch experiments based on the results and supported by previous work. In general, the carbonate minerals exhibit greater reactivity and dissolution than oxide and silicate minerals [10]. Moreover, the dissolution rate of minerals that produce charged ions [like dolomite, $CaMg(CO_3)_2$] increases with ionic strength as shown theoretically in Figure 2-65 and experimentally in Figure 2-66 [11, 12]. Based on this increased dissolution as the ionic strength increased, FIU expects greater surface precipitation and incorporation of Nd over time.

Coupled substitution of Na^+ and Am/Nd^{3+} with Ca^{2+} and Mg^{2+} in the dolomite mineral or secondary precipitates such as calcite is one process that may lead to incorporation of Nd. Previous analysis by Dawson on natural carbonatite samples containing dolomite and calcite from Phalaborwa, South Africa, observe some important trends in actinide and lanthanide partitioning in these minerals [13]: (1) significant concentrations of lanthanides and actinides are reported as shown in Table 2-27, (2) greater concentrations of actinides and lanthanides are observed in calcite as compared to doomite, and (3) Na concentrations are correlated with all rare earth element concentrations with 1.5 – 3.0 times more Na than required for coupled substitution.

Although the rate of dolomite dissolution is decreased at neutral to basic pH, it is still on the order of $5x10^{-12}$ mol/sec/cm^2 based on the review of carbonate mineral dissolution by Morse [10]. Because of the short (~20 minute) retention time of the solutions within the mini columns, there is not sufficient time for mineral dissolution and re-precipitation processes to remove Nd from the aqueous phase. Therefore, surface complexation is likely the dominant process in the mini column experiments and not ionic strength dependent for sorption of Nd to dolomite. Because of the increased reaction time of the aqueous phase with the dolomite mineral in the batch experiments, there is time for dissolution and re-precipitation processes to affect Nd removal from the aqueous phase.

Moreover, previous time-resolved laser fluorescence spectroscopy (TRLFS) measurements provide additional confirmation in a laboratory setting with observation of two surface species for Cm^{3+} interacted with calcite including: (1) a surface adsorbed species and (2) an incorporated species at pH 8.1 at 0.01 M IS (as $NaClO_4$) [14]. Further, sorption of Am on calcite was previously found to be largely irreversible, suggesting surface precipitation [15, 16]. Surface precipitation would result in incorporation within the solid phase as observed previously [14]. Therefore, it is likely that both sorption and incorporation (possibly as a coupled substitution) processes may be occurring in the FIU batch experiments.

Table 2-25. Summary of pH, pCH, and Kd Coefficients at 24 Hours for Variable Ionic Strength (3 mM $NaHCO_3$ + NaCl) Batch Experiments

	pH	pC_{H+}	K_d (mL/g)	K_d (m^2/g)
5.0 M	7.42±0.11	8.28±0.38	6380±3060	3750±1800
2.0 M	7.92±0.23	8.22±0.43	1180±450	695±262
1.0 M	8.29±0.08	8.41±0.38	819±225	482±132
0.1 M	8.64±0.08	8.59±0.38	724±105	426±62
0.01 M	8.67±0.11	8.60±0.39	503±129	296±76

Table 2-26. Number of H_2O Molecules Coordinated with Na^+ in Aqueous Solutions at Variable Ionic Strength [6]

Molar/Atom Ratio NaCl:H_2O	Concentration NaCl (mol/L)	NaO (CN)
1:83	0.66	5.3±0.8
1:40	1.34	5.1±0.9
1:17	3.00	4.6±1.4
1:10	4.83	4.5±1.4

Table 2-27. Na, Nd, Eu, Th and U Content in parts per million (ppm) in Natural Calcite and Dolomite Minerals from Phalaborwa, South Africa as Determined by Electron Probe [13]

Element	Calcite	Dolomite
Na	627	125
Nd	405	84
Eu	18.3	3.38
Th	0.02	-
U	-	0.01

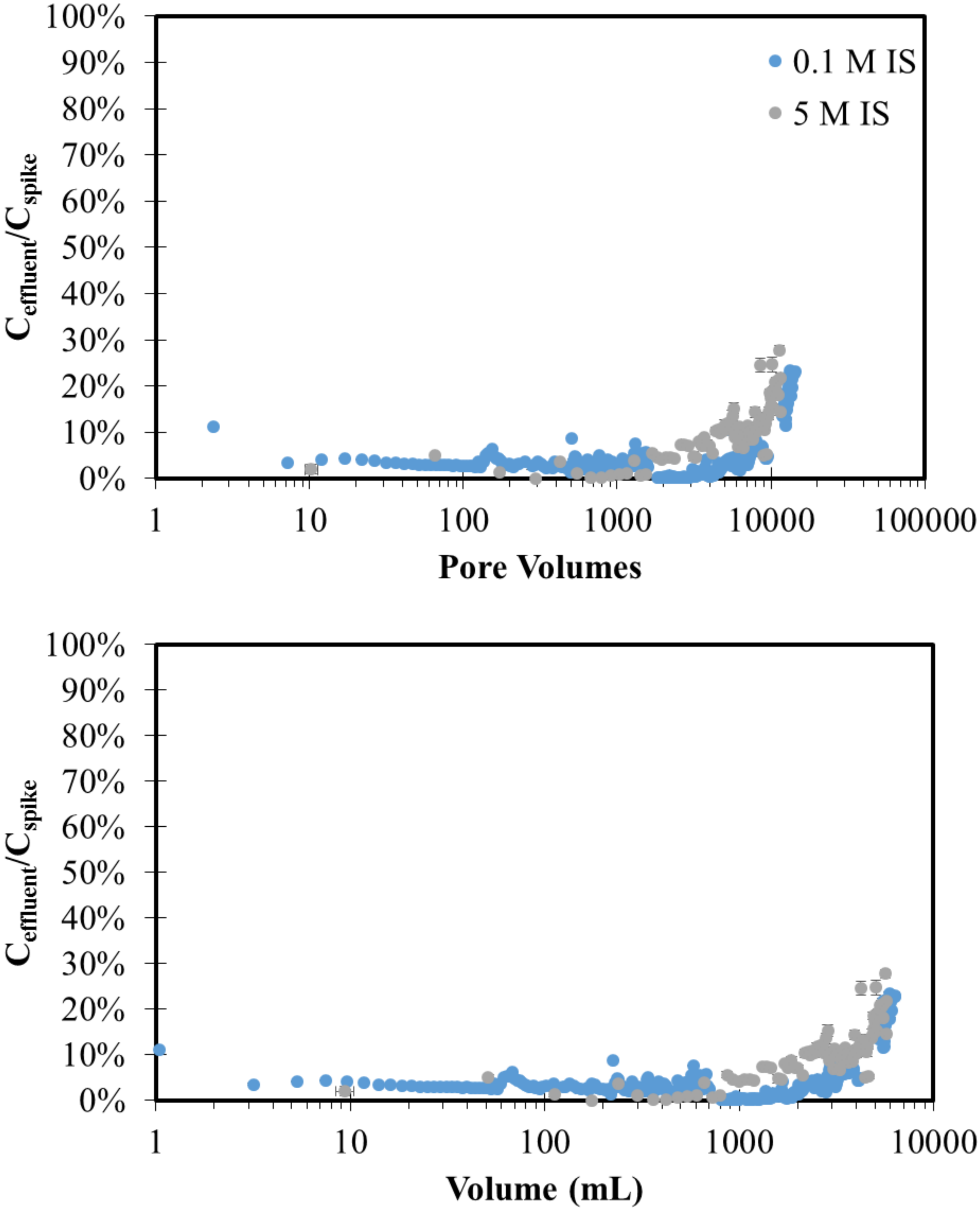

Figure 2-64. Comparison of breakthrough of Nd during continuous injection of 20 ppb Nd in 0.1 (blue) and 5.0 (gray) M IS (NaCl^{+3} mM NaHCO$_3$) at 1.5 mL/hr flow rate with respect to pore volume (top) and volume in mL (bottom), Note: error bars are based on triplicate measurements by ICP-MS.

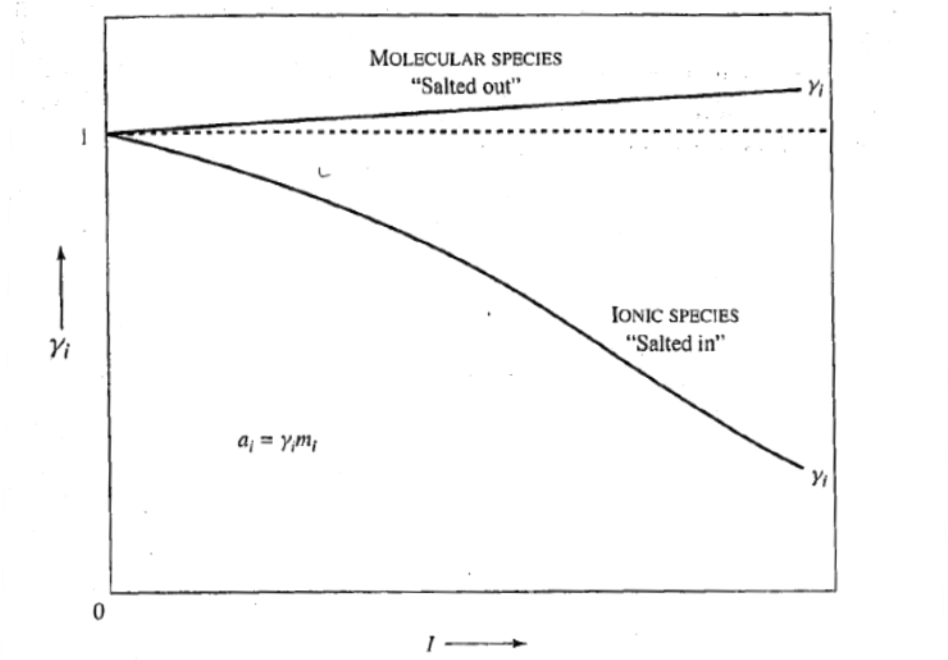

Figure 2-65. Plot representing the theoretical "salting in" γ < 1 and "salting out" γ > 1 behavior of ionic and molecular species, respectively [11].

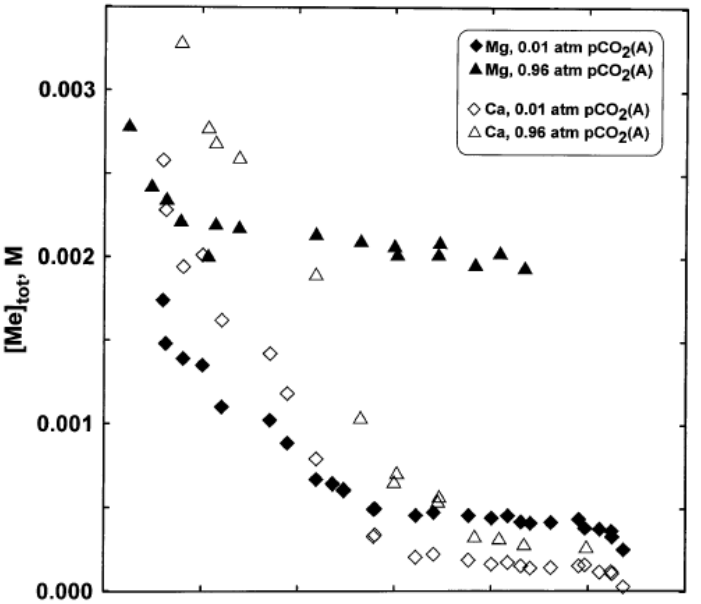

Figure 2-66. pH dependence of total Ca and Mg concentrations in stirred reactor suspension at variable ionic strength and atmospheric CO_2 as determined previously [12].

References:

1. Brady, P.V., H.W. Papenguth, and J.W. Kelly, *Metal sorption to dolomite surfaces.* Applied Geochemistry, 1999. **14**(5): p. 569-579.
2. Schnurr, A., et al., *Sorption of Cm (III) and Eu (III) onto clay minerals under saline conditions: Batch adsorption, laser-fluorescence spectroscopy and modeling.* Geochimica et Cosmochimica Acta, 2015. **151**: p. 192-202.
3. Powell, B., *Quantification of Cation Sorption to Engineered Barrier Materials Under Extreme Conditions*, in *Nuclear Energy University Programs Fuel Cycle Research and Development* 2016, Clemson University.
4. Ams, D.A., et al., *The effect of high ionic strength on neptunium (V) adsorption to a halophilic bacterium.* Geochimica et Cosmochimica Acta, 2013. **110**: p. 45-57.
5. Bradbury, M. and B. Baeyens, *Sorption of Eu on Na-and Ca-montmorillonites: experimental investigations and modelling with cation exchange and surface complexation.* Geochimica et Cosmochimica Acta, 2002. **66**(13): p. 2325-2334.
6. Mancinelli, R., et al., *Hydration of sodium, potassium, and chloride ions in solution and the concept of structure maker/breaker.* The Journal of Physical Chemistry B, 2007. **111**(48): p. 13570-13577.
7. Shannon, R.t., *Revised effective ionic radii and systematic studies of interatomic distances in halides and chalcogenides.* Acta crystallographica section A: crystal physics, diffraction, theoretical and general crystallography, 1976. **32**(5): p. 751-767.
8. D'Angelo, P., et al., *Hydration properties and ionic radii of actinide (III) ions in aqueous solution.* Inorganic chemistry, 2013. **52**(18): p. 10318-10324.
9. Sø, H.U., et al., *Sorption of phosphate onto calcite; results from batch experiments and surface complexation modeling.* Geochimica et Cosmochimica Acta, 2011. **75**(10): p. 2911-2923.
10. Morse, J.W. and R.S. Arvidson, *The dissolution kinetics of major sedimentary carbonate minerals.* Earth-Science Reviews, 2002. **58**(1): p. 51-84.
11. Langmuir, D., *Aqueous Environmental Geochemistry*, ed. R. McConnin, et al. 1997, Upper Saddle River, New Jersey: Prentice Hall. 600.
12. Pokrovsky, O.S., J. Schott, and F. Thomas, *Dolomite surface speciation and reactivity in aquatic systems.* Geochimica et Cosmochimica Acta, 1999. **63**(19): p. 3133-3143.
13. Dawson, J. and R. Hinton, *Trace-element content and partitioning in calcite, dolomite and apatite in carbonatite, Phalaborwa, South Africa.* Mineralogical Magazine, 2003. **67**(5): p. 921-930.
14. Fernandes, M.M., et al., *Incorporation of trivalent actinides into calcite: A time resolved laser fluorescence spectroscopy (TRLFS) study.* Geochimica et Cosmochimica Acta, 2008. **72**(2): p. 464-474.
15. Shanbhag, P. and J.W. Morse, *Americium interaction with calcite and aragonite surfaces in seawater.* Geochimica et Cosmochimica Acta, 1982. **46**(2): p. 241-246.
16. Higgo, J.J. and L.V. Rees, *Adsorption of actinides by marine sediments: effect of the sediment/seawater ratio on the measured distribution ratio.* Environmental science & technology, 1986. **20**(5): p. 483-490.

Milestones and Deliverables

The milestones and deliverables for Project 2 for FIU Performance Year 7 are shown on the following table. The technical report deliverable associated with subtask 1.3 on the results of columns monitoring using geochemical and SIP analyses, was submitted on January 30, 2017. The first part of milestone 2016-P2-M5 (subtask 1.4), to complete training on the LSC analytical technique, was completed with a 4-hour training webinar conducted on November 7, 2016. The second part of the milestone, to complete trial-and-error experiments for separations and determination of Tc(IV) and Tc(VII), was completed on April 4, 2017. A technical progress report on "Investigation of the Properties of Acid-Contaminated Sediment and its Effect on Contaminant Mobility" was submitted to DOE-HQ and site contacts on February 13, 2017 for subtask 2.1. Milestone 2016-P2-M8 which involved completion of the calibration processes of the MIKE SHE and MIKE 11 models was completed on March 1, 2017. Milestone 2016-P2-M9, to complete batch experiments on the biodissolution of Na-autunite (subtask 1.2) has been reforecast due to an experimental delay from the first set of samples developing contamination. FIU has repeated the experiment with fresh preparations and estimates the milestone will be completed by May 15, 2017. The deliverable for a technical report on the synergy between colloidal Si and HA on the removal of U(VI) (subtask 2.2) has been reforecast due to the KPA instrument having very low sensitivity. This task is heavily dependent on this instrument for uranium analysis. Once repairs to the KPA instrument are complete, FIU will reforecast the date for this deliverable, proceed with analyzing the samples collected to date under this subtask, and complete the technical report. FIU also reforecast milestone 2016-P2-M6 for subtask 2.3 due to the same issues with the requisite KPA instrument. This milestone will complete the batch experiments for uranium removal by Huma-K on SRS sediments. FIU is reforecasting the completion of the milestone by August 18, 2017. FIU has received the replacement nitrogen laser for the KPA instrument and repairs are in progress. All project delays have been communicated to the project task points-of-contact during regular project teleconferences and agreement has been reached on the planned path forward.

FIU Performance Year 7 Milestones and Deliverables for Project 2

Task	Milestone/ Deliverable	Description	Due Date	Status	OSTI
Project	2016-P2-M1	Submit three draft papers to Waste Management 2017 Symposium	11/4/16	Complete	
Task 1: Hanford Site	2016-P2-M2	Submit abstract to ACS Spring Conference (Subtask 1.1)	11/30/16	Complete	
	2016-P2-M5	Complete training on LSC analytical technique and trial-and-error experiments for separations and determination of Tc(IV) and Tc(VII) (Subtask 1.4)	1/27/17	Reforecast. Date TBD	
	2016-P2-M9	Complete batch experiments on the biodissolution of Na-autunite (Subtask 1.2)	3/20/17	Reforecast to 5/15/17	
	Deliverable	Technical report on the results of columns monitoring using	1/30/17	Complete	

		geochemical and SIP analyses (Subtask 1.3)			
Task 2: SRS	2016-P2-M4	Complete the creation of acid-impacted soil samples through conditioning of SRS F/H Area soil with acidified water in columns (Subtask 2.1)	12/15/16	Reforecast to 5/8/17	
	Deliverable	Technical report on the Investigation on the Properties of Acid-Contaminated Sediment and its Effect on Contaminant Mobility (Subtask 2.1)	2/13/17	Complete	
	2016-P2-M6	Continue batch experiments of uranium removal by Huma-K sorbed on SRS sediments (Subtask 2.3)	2/15/17	Reforecast to 8/18/17	
	2016-P2-M7	Complete a set of column experiments using modified humic acid (Subtask 2.3)	2/28/17	Reforecast Date TBD	
	Deliverable	Technical report on the synergy between colloidal Si and HA on the removal of U(VI) (Subtask 2.2)	3/31/17	Reforecast Date TBD	
	Deliverable	Technical report on the Investigation of the Removal of Uranium by Huma-K Sorbed on SRS Sediments via Batch Experiments (Subtask 2.3)	4/3/17	Reforecast to 8/18/17	
Task 3: Tims Branch	2016-P2-M3	Complete development of MIKE 11 stream flow model for A-014 outfall (Subtask 3.1)	12/8/16	Complete	
	2016-P2-M8	Complete calibration of MIKE SHE and MIKE 11 models (Subtask 3.1)	3/1/17	Complete	
	2016-P2-M10	Complete coupling of MIKE SHE and MIKE 11 models (Subtask 3.1)	5/5/17	Reforecast Date TBD	
	Deliverable	Technical report on the surface water modeling of Tims Branch (Task 3)	6/15/17	Reforecast to 8/17/17	
Task 5: WIPP	Deliverable	Technical report on the effect of ionic strength on the sorption of neodymium to dolomite (Task 5)	5/12/17	On Target	

Work Plan for Next Quarter

Task 1: Remediation Research and Technical Support for the Hanford Site

Subtask 1.1 – Remediation Research with Ammonia Gas for Uranium

- Conduct final batch experiments with ammonia gas injection into mineral suspensions.
- Finalize experimental data in the presence of minerals including statistical comparison of results for each treatment.
- Develop publication for Di Pietro's summer 2016 internship investigating mineral dissolution kinetics with basic treatment.
- Develop publication comparing treatment of batch samples with NaOH, NH_4OH and NH_3 gas on mineral dissolution/precipitation and uranium removal.
- Complete KPA analysis of collected samples.
- Initiate flow-through dissolution experiments using mini columns filled with uranium-bearing precipitates.
- Initiate experiments at low Si/Al ratios and variable HCO_3^-/Fe to determine the minimum concentration of Si in the system that causes coagulation reactions with U after ammonia gas applications.

Subtask 1.2. Investigation on Microbial-Meta-Autunite Interactions - Effect of Bicarbonate and Calcium Ions

- Complete sample analysis for uranium and phosphorus.
- Prepare samples and conduct microscopy analysis via SEM/EDS.
- Initiate biodissolution experiments with bacterial consortia.

Subtask 1.3. Investigation of Electrical Geophysical Response to Microbial Activity in the Saturated and Unsaturated Environments

- Complete analysis of porewater using ICP-OES to measure concentrations of Fe, Al, Ca, P, and Mg for samples collected during the fall of 2016.
- Complete KPA analysis for dissolved uranium for the samples from the fall of 2016 and spring of 2017 samples.
- Plot data and compare to geophysical results.

Subtask 1.4: Contaminant Fate and Transport under Reducing Conditions

- Optimize reducing conditions in the anaerobic glovebox.
- Experiment with the use of different reducing agents and record pH, Eh and monitor Tc behavior.
- Prepare Tc samples with and without carbonates under reducing conditions. Initiate Tc monitoring.

Task 2: Remediation Research and Technical Support for Savannah River Site

Subtask 2.1. FIU's Support for Groundwater Remediation at SRS F/H –Area

- Conduct sorption experiments of U(VI) on acidified soil at different pH values .
- Finalize specific surface area measurements of acidified soil.
- Initiate SEM-EDS analysis of the acidified soil.

Subtask 2.2 – The Synergistic Effect of Humic Acid and Colloidal Silica on the Removal of Uranium (VI)

- Prepare batch samples for pH 6-8 containing 25 ppm of uranium similar to previous batch samples.
- Analyze batch samples for pH 3-5 via KPA for uranium and via ICP for silica and iron and process the data and calculate uranium removal.

Subtask 2.3. Humic Acid Batch Sorption and Column Experiments with SRS Soil

- Conduct kinetic experiments of uranium sorption on SRS sediment amended with Huma-K at pH 4 and 7.
- Conduct batch experiments of uranium sorption (different concentrations) on SRS sediment with and without amended Huma-K.
- Submit Huma-K manuscript to a journal for publication.
- Conduct column experiments to evaluate the influence of sorbed modified humic acid on uranium mobility.
- Perform a column experiment to estimate uranium removal due to sorption onto the soil; this experiment will act as a control column test.

Task 3: Surface Water Modeling of Tims Branch

Subtask.3.1. Modeling of surface water and sediment transport in the Tims Branch ecosystem
FIU is reforecasting one milestone due in May and one deliverable due in June for this task:

- Milestone 2016-P2-M10, Complete coupling of MIKE SHE and MIKE 11 models (Subtask 3.1) – reforecast from 5/5/2017 – TBD
- Deliverable - Technical report on the surface water modeling of Tims Branch (Task 3) – reforecast from 6/15/2017 to 8/17/2017.

Subtask 3.2. Application of GIS technologies for hydrological modeling support

- Continue the use of GIS tools for the hydrological model development. Over the next few months, GIS will be used for cross section delineation and for preparing maps and charts of the study area that depict model results.

Subtask 3.3. Biota, biofilm, water and sediment sampling in Tims Branch

- Work in coordination with SREL and SRNL scientists to develop a scope for DOE Fellow, Ron Hariprashad, to complete a 10-week summer 2017 internship which incorporates some of the sampling and data collection required for this task.
- Plan a second follow-up field trip to the one conducted in August 2016 for Dr. Mahmoudi to train DOE Fellow Ron Hariprashad and also assist in collecting water samples and water quality data as well as measure cross section profiles along the main Tims Branch stream. Ron will then be guided and mentored primarily by Dr. John Seaman from SREL in collaboration with Dr. Brian Looney from SRNL in not only field sampling and data collection but also laboratory analysis of water (and possibly biofilm) samples collected in the field.

Task 5: Remediation Research and Technical Support for WIPP

- Finalize column breakthrough experiments and 0.5 M ionic strength batch kinetics samples.
- Characterize solid phase of 0.1 and 5.0 M batch and column experiments to observe sorption and incorporation processes in the absence and presence of flow, respectively.
- Conduct mini column experiments investigating transport of Nd complexed with EDTA and other relevant ligands (as part of Zengotita’s summer internship).
- Write and submit a publication finalizing the sorption and incorporation of Nd at variable ionic strength.

Project 3
Waste and D&D Engineering & Technology Development

Project Manager: Dr. Leonel E. Lagos

Project Description

This project focuses on delivering solutions under the decontamination and decommissioning (D&D) and waste areas in support of DOE EM. This work is also relevant to D&D activities being carried out at other DOE sites such as Oak Ridge, Savannah River, Hanford, Idaho and Portsmouth. The following tasks are included in FIU Performance Year 7:

Task No	Task
Task 1: Waste Information Management System (WIMS)	
Subtask 1.1	Maintain WIMS – database management, application maintenance, and performance tuning
Subtask 1. 2	Incorporate new data files with existing sites into WIMS
Task 2: D&D Support to DOE EM for Technology Innovation, Development, Evaluation and Deployment	
Subtask 2.1	D&D Technology Demonstration & Development and Technical Support to SRS's 235-F Facility Decommissioning
Subtask 2.2	Technology Demonstration and Evaluation
Subtask 2.3	Support to DOE EM-4.11 and the D&D Community
Task 3: D&D Knowledge Management Information Tool	
Subtask 3.1	Web and Mobile Application for D&D Decision Model
Subtask 3.2	Mobile Applications/Platforms for DOE Sites
Subtask 3.3	Development & Integration of International KM-IT Pilot for UK Collaboration
Subtask 3.4	Outreach and Training (D&D Community Support)
Subtask 3.5	Data Mining and Content Management
Subtask 3.6	D&D KM-IT Administration and Support

Task 1: Waste Information Management System (WIMS)

Task 1 Overview

This task provides direct support to DOE EM for the management, development, and maintenance of a Waste Information Management System (WIMS). WIMS was developed to receive and organize the DOE waste forecast data from across the DOE complex and to automatically generate waste forecast data tables, disposition maps, GIS maps, transportation details, and other custom reports. WIMS is successfully deployed and can be accessed from the web address http://www.emwims.org. The waste forecast information is updated at least annually. WIMS has been designed to be extremely flexible for future additions and is being enhanced on a regular basis.

Task 1 Quarterly Progress

The Waste Information Management System (WIMS) was developed to receive and organize the DOE waste forecast data from across the DOE complex and to automatically generate waste forecast data tables, disposition maps, GIS maps, transportation details, and other custom reports. WIMS is successfully deployed and can be accessed from the web address http://www.emwims.org. During this reporting period, FIU performed database management, application maintenance, and performance tuning to the online WIMS in order to ensure a consistent high level of database and website performance.

FIU prepared and made a professional technical presentation on *"*Waste Information Management System with 2016-17 Waste Streams*"* during session 72: Decisionmaking Tools and Frameworks that Enhance Communication for ER Cleanup Programs, at the Waste Management Symposium on March 7, 2017, to communicate to the D&D community new updates to the system during the last year.

FIU received a new set of waste stream forecast and transportation forecast data from DOE on March 18, 2017. The revised waste forecast data was received as formatted data files and, to incorporate these new files, FIU is building a data interface to allow the files to be received by the WIMS application and import it into SQL Server. SQL server is the database server where the actual WIMS data is maintained. FIU will complete the data import and deploy onto the test server for DOE testing and review. Once FIU has incorporated feedback from the data review, the new data will be deployed on the public server. The 2017 waste data will replace the existing previous waste data and will become fully viewable and operational in WIMS.

Task 2: D&D Support to DOE EM for Technology Innovation, Development, Evaluation and Deployment

Task 2 Overview

This task provides direct support to DOE EM for D&D technology innovation, development, evaluation and deployment. For FIU Performance Year 7, FIU will assist DOE EM-4.11 in meeting the D&D needs and technical challenges around the DOE complex. FIU will expand the research in technology demonstration and evaluation by developing a phased approach for the demonstration, evaluation, and deployment of D&D technologies. One area of focus will be working with the Savannah River Site to identify and demonstrate innovative technologies in support of the SRS 235-F project. FIU will further support the EM's International Program and the EM-4.11 D&D program by participating in D&D workshops, conferences, and serving as subject matter experts.

Task 2 Quarterly Progress

Subtask 2.1.1: Adaptation of Intumescent Coatings

The objective of this research task is to improve the operational performance of fixatives to mitigate the release of radioisotopes during fire and/or extreme heat conditions. FIU has performed a series of tests to subject test coupons of intumescent coatings (IC) to increasing temperatures using a muffle furnace along with adhesion and impact testing of these test coupons on various types of substrates, both before and after exposure to extreme heat conditions.

FIU used the ASTM D3359 standard protocol during the adhesion testing in order to quantify the ability of two selected intumescent coatings (FX and FD) to adhere to stainless steel substrates under various conditions. The results will serve as the basis for future testing efforts designed to determine the impacts of fixatives/intumescent coatings on the airborne release fraction (ARF) and respirable fraction (RF) coefficients in the source term formula used to calculate a facility's safety basis.

Subtask 2.1.2: Application of Intumescent Coatings to other DOE EM Problem Sets

Discussions with DOE site and DOE EM HQ personnel have highlighted the potential of intumescent coatings to have much broader applications at other sites. FIU will be engaging other DOE sites to share the results of the intumescent coatings research and its applications at SRS 235-F and to identify specific applications of intumescent coating technology to satisfy other problem sets and challenge areas related to fire / extreme heat conditions.

Subtask 2.1.3: Robotic Technologies for D&D Applications

As part of this subtask during FIU Performance Year 6, FIU performed research to identify robotic technology systems applicable to the challenges and needs of the SRS 235-F Facility. Research utilized the Robotic Database in D&D KM-IT to search and identify potential robotic technologies and compiled a spreadsheet of all of the available robotic technologies in the database. FIU is leveraging the research already completed to begin identifying cross-cutting applications of robotic technologies being developed at FIU in the high-level waste research area that could potentially be used in support of D&D activities.

Task 2.2: Technology Demonstration and Evaluation

The primary objective of this task is to standardize and implement proven processes to refine and better synchronize DOE-EM technology needs, requirements, testing, evaluation, and acquisition by implementing a three-phased technology test and evaluation model. The development of uniformly accepted testing protocols and performance metrics is an essential component for testing and evaluating D&D technologies.

Subtask 2.2.1: Uniform Testing Protocols and Performance Metrics for D&D

The development of uniformly accepted testing protocols and performance metrics is an essential component for testing and evaluating D&D technologies. During FIU Performance Year 6, an FIU representative obtained official membership on ASTM International's E10 Committee on Nuclear Technologies and Applications and was selected to lead the ASTM International E10.03 Subcommittee. In this position, FIU oversaw the development of two new draft standard specifications for removable/strippable coatings and permanent coatings/fixatives.

Joseph Sinicrope chaired the ASTM International E10.03 Subcommittee on Radiological Protection for Decontamination and Decommissioning for Nuclear Facilities and Components, on January 29 to February 1, 2017 (Figure 3-1), during which the Subcommittee completed drafting two (2) standard specifications related to permanent and removable/strippable coatings and fixatives.

The Subcommittee submitted the two (2) draft standard specifications which were released for a formal Subcommittee ballot on February 23, 2017. The voting period for the E10.03 Subcommittee concluded on March 23, 2017. The 71% return rate surpassed the requirement to have at least 60% of the Subcommittee membership return a ballot. Both standards were unanimously approved by the Subcommittee members, with only minor editorial comments suggested for the revision. Based on feedback received from the ASTM Staff Manager, both standards are ready for a full E10 Committee vote, which is the final step in the approval process. It is anticipated that the standards will be released for a ballot during the next cycle in early June.

The *"Standard Specification for Permanent Coatings Used to Mitigate Spread of Radioactive Contamination"* is intended to provide an international basis for identification of non-removable permanent coatings and fixatives as a long term measure used to immobilize radioactive contamination, minimize worker exposure, and to protect uncontaminated areas against the spread of radioactive contamination. The *"Standard Specification for Strippable & Removable Coatings to Mitigate Spread of Radioactive Contamination"* is intended to provide an international basis for identification of strippable/removable materials used to immobilize radioactive contamination, minimize worker exposure, and facilitate subsequent decontamination or to protect uncontaminated areas against the spread of radioactive contamination. Both of these standard specifications were modified based on comments from the various sites to better align the requirements with the source term formula, particularly in the technical areas related to measuring a fixative's impact on the airborne release fraction (ARF) and respirable fraction (RF) before and after being subjected to thermal and seismic stressors.

Figure 3-1. Photo shows Joseph Sinicrope (FIU ARC) and Dr. Connor Nicholson (SRNL) at the ASTM International Conference.

Subtask 2.2.2: Technology Demonstration under Nonradioactive Conditions at FIU

Leveraging the research being performed on intumescent coatings as part of subtask 2.1.1 and including close coordination with DOE EM, SRNL, and SRS, FIU will conduct a cold demonstration / test and evaluation of applying intumescent coatings in a full-scale SRS 235-F hot cell mock-up at the FIU Hot Cell Test Bed during FIU Performance Year 7.
The draft test plan, titled *"Adapting Intumescent Coatings as Fire Resilient Fixatives ISO SRS 235-F D&D Activities Phase II: Construction of SRS 235-F Hot Cell Test Bed and Application Demonstration"* was completed on January 6, 2017, per the milestones outlined in the PTP for Year 7, and forwarded to SRNL for review/comment. The final document received concurrence and was signed by all stakeholders at FIU and SRNL on February 6, 2017.

The test objectives outlined in the document were developed through extensive coordination with SRS 235-F site personnel (i.e., project managers, safety and fire representatives, etc.) and Savannah River National Laboratory (SRNL) research scientists. They are specifically designed to advance the testing, evaluation, and possible deployment of intumescent coating (IC) technologies as fire resilient fixatives to mitigate the potential release of radioisotopes during postulated fire scenarios highlighted in the Basis for Interim Operations (BIO) and contingency planning documents in support of D&D activities at SRS 235-F, with a particular emphasis on the 235-F PuFF Facility Cells 6-9.

This test plan addresses Phase II of the overall research effort, with the first main objective centered on constructing a to-scale SRS 235-F Hot Cell Test Bed on-site at ARC that mirrors the operating environment encountered in an adjoining corner and middle hot cell configuration at the SRS 235-F facility (Figure 3-2). The second main objective involves an evaluation of the mechanics and processes associated with applying the selected intumescent coatings in the hot cell configurations using: 1) the approved tools as identified in the 235-F Risk Reduction Tooling List, Rev 0, dated January 26, 2015; and 2) alternative application methods, such as airless sprayers, recommended by the IC manufacturer.

FIU made significant progress on the construction of the SRS 235-F Hot Cell Test Bed to support the test plan. The construction is nearing completion, including framing out the desired dimensions of the corner and middle hot cell and hanging 1/16" stainless steel. As shown in Figures 3-1 and 3-2, a pass-through port with dimensions 16" x 16" has been included.

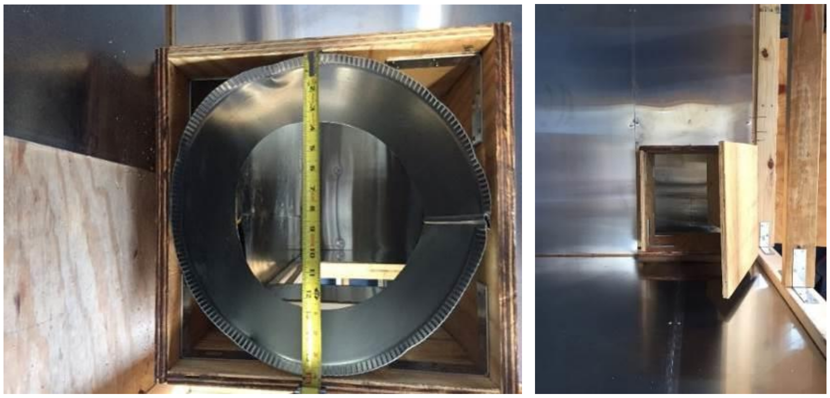

Figure 3-1. Pass-through port between the corner and middle hot cells (left) with doors opening towards the glove ports (right).

Figure 3-2. View of dividing wall and pass-through port from corner hot cell.

Subtask 2.2.3 Support to SRNL and SRS 235-F for Onsite Demonstration

FIU is coordinating with SRNL and SRS 235-F to support a possible onsite intumescent coating demonstration on a contaminated apparatus (i.e., hot demonstration). The objective of this subtask is to select and validate operational performance of fire resilient fixative coating material(s) for residual surface contamination after gross decontamination is completed.

Task 3: D&D Knowledge Management Information Tool (KM-IT)

Task 3 Overview

The D&D Knowledge Management Information Tool (KM-IT) is a web-based system developed to maintain and preserve the D&D knowledge base. The system was developed by Florida International University's Applied Research Center (FIU-ARC) with the support of the D&D community, including DOE-EM (EM-4.11 & EM-5.12), the former ALARA centers at Hanford and Savannah River, and with the active collaboration and support of the DOE's Energy Facility Contractors Group (EFCOG). The D&D KM-IT is a D&D community driven system tailored to serve the technical issues faced by the D&D workforce across the DOE Complex. D&D KM-IT can be accessed from web address http://www.dndkm.org.

Task 3 Quarterly Progress

FIU provided DOE with a raw web analytic report targeting Mobile usage and DOE HQ activity. This report was sent to DOE on January 12, 2017. The report included the following information:

1. D&D KM-IT device access - Overall device category of how the users access D&D KM-IT
2. Mobile Devices - A drill down into mobile devices (types/brand)
3. Mobile Devices Operating System (iOS, Android, Windows, etc.)
4. Network Traffic from U.S. Department of Energy

On January 26, 2017, FIU provided DOE with a KM-IT presentation for DOE HQ to target upcoming workshops to educate the D&D community about the features and capabilities of D&D KM-IT. Some of the presentation topics include D&D KM-IT scope and objectives, knowledge management and its importance to EM, international and corporate interest. A summary of the D&D KM-IT modules was included along with statistical data about the number of registered users, subject matter specialists (SMS), vendors, technologies and more.

FIU also provided DOE with an updated chart that shows the growth in number of registered users and SMS through December 2016. The graph highlights major conferences where a significant increase in users and SMS has been recorded. See Figure 3-3 below.

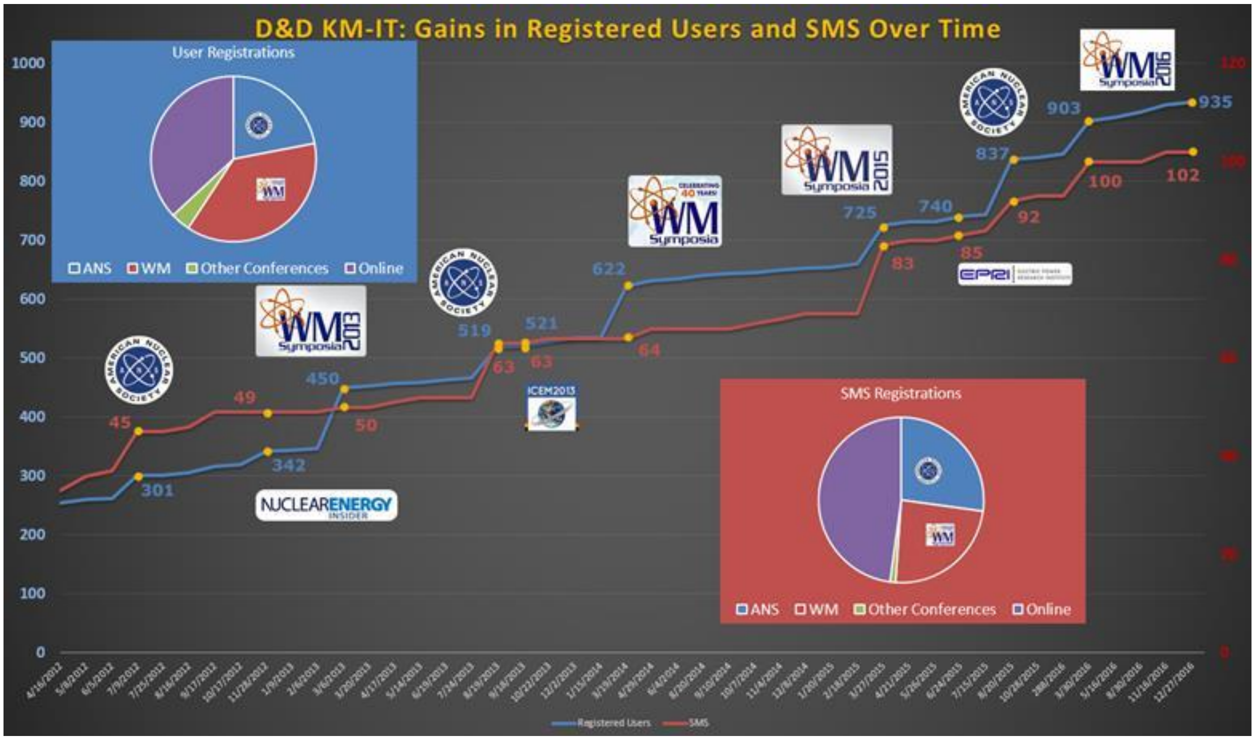

Figure 3-3. D&D KM-IT Users and SMS registration over time.

The *"Strategic Approach for the Long-Term Sustainability of Knowledge"* report, also known as, the D&D KM-IT Strategic Plan, was sent to DOE on January 26, 2017, highlighting the updates on the system and recommended actions to improve user engagement with the D&D KM-IT website.

FIU completed revisions to the infographic on Knowledge Management based on comments received from DOE and sent the updated infographic to DOE on February 2, 2017 (Figure 3-2). The updates to the infographic included:

- Replaced the Wikipedia definition at the top with: Knowledge management is the strategies and practices used to identify, preserve, and share information.
- Under WHAT: Changed “WHAT is KM” to “WHAT is knowledge” since knowledge management was already defined.
- Updated the description of book box to: Knowledge includes the integration of life-experiences into an understanding of the information. Consider the difference between reading how to refinish a wooden table with the experience of running your hand over the smooth silky surface of a well-sanded surface.
- Changed text in right box of WHAT: Learning and knowledge only increase when used and shared by curious people who acknowledge its value.
- Increased the book under WHAT to accommodate additional text.
- Added a more visible separation for the "Example of a Knowledge Management Application”.
- Updated the stats for Documents, Technologies, Vendors and SMS.
- Scaled the stat graphic a bit more.
- Added a simple footer with a revision date.

Knowledge Management

Knowledge management is the strategies and practices used to identify, preserve, and share information

WHAT

WHAT is knowledge?
Knowledge includes the integration of life-experiences into an understanding of the information. Consider the difference between reading how to refinish a wooden table with the experience of running your hand over the smooth silky surface of a well-sanded surface.

Learning and knowledge only increase when used and shared by curious people who acknowledge its value.

WHY

To provide a smooth transition for new workforce

To minimize loss of organization memory due to retirement

To identify critical areas so organization "knows what it knows and why"

To build a toolkit of methods and resources that can be used to maximize company goals

Do you agree that KM systems are too difficult to implement and maintain?

Disagree	53%
Strongly Disagree	19%
Agree	19%
Strongly Agree	8%

W/O Knowledge Management

If we only knew what we know

We continue to reinvent the wheel

And let knowledge walk out of the door

HOW

- Facilitate organizational learning
- Leverage internal expertise
- Increase communication
- Crowd-source difficult problems
- Manage intellectual property

Example of a Knowledge Management Application

dndkm.org

D&D KM-IT

Deactivation and Decommissioning Knowledge Management Information Tool

Most Popular Document Category
Innovative Technology Summary Reports (ITSRs)

Modules

Hotline
Technology
Web Crawler
Mobile System
Lessons Learned
Vendors
Best Practices
Training
Picture Video Library
Document Library
Specialist Directory
Collaborations Tools

Figure 3-2. Knowledge Management infographic sent to DOE on 2/1/2017.

FIU made a professional technical presentation on *"Application of Robotic Technologies to D&D"* during session 132: Robotics and Remote Systems-Nuclear Environments: International Applied D&D Operations at the Waste Management Symposium on March 9, 2017. This presentation included information on the robotics database within D&D KKM-IT.

D&D KM-IT has been showcased over the last couple of years at different conferences. Most recently, it was demonstrated at Waste Management 2017 Symposium in Phoenix, AZ at the FIU booth in the conference exhibition hall. FIU staff used the opportunity to demonstrate the system to industry users, who were engaged and interested in the product. As a result, there was an increase of 43 registered users during WM17. To date, conferences have proven to be the most effective marketing tool for D&D KM-IT.

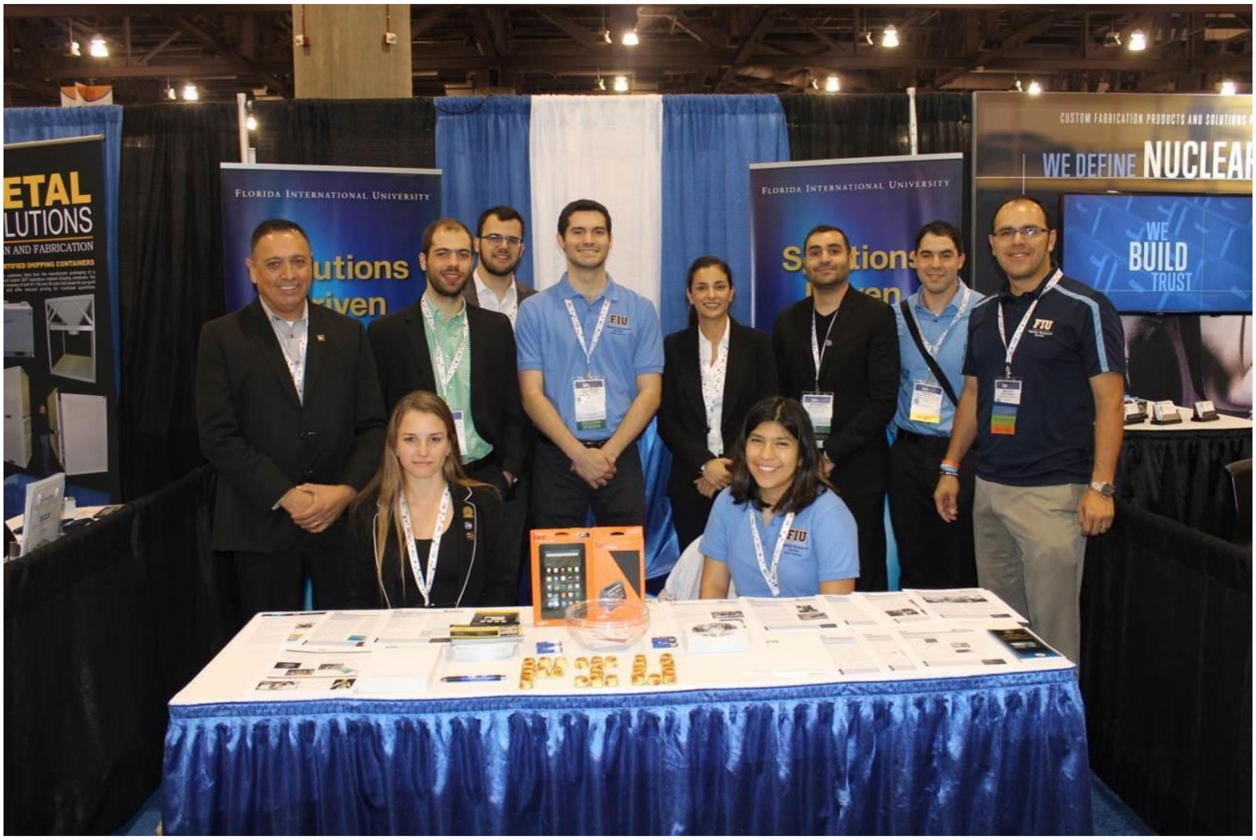

Figure 3-3. DOE Fellows and ARC staff at FIU booth during WM17 Exhibit Hall.

DOE Fellows are supporting D&D KM-IT by reviewing the information in the vendor and technology modules and researching new vendors and technologies for adding to the system. As of April 11, 2017 the system included a total of 953 vendors and 1,329 technologies (including 521 robotic technologies). In addition, there were 982 registered users and 102 subject matter specialists. Figure 3-4 shows a couple of the technologies recently added to the system.

Figure 3-4. Technologies recently added to D&D KM-IT: 510 Packbot (Endeavor Robotics) on left and Spotmini (Boston Dynamics) on right.

During March, FIU completed the development of a Google Web Analytic report for D&D KM-IT for the fourth quarter of 2016 (October to December). This report includes information from Google Analytics (GA) and Google Web Master Tools (GWT) and a narrative to explain the results. Highlights from this report include:

- The fourth quarter outperformed the third quarter for the first time since the analytics have been tracked. The metrics with double digit improvements over the previous quarter included Pageviews, Avg. Session Duration, and Pages per Session. Sessions and Users also had significant increases.
- During 2016 Q4, the D&D KM-IT website served 285 unique documents.
- There was a total of 5,677 total combined visits (GA + GWT).
- Combined sessions improved by 18.9% over the same quarter last year.
- Safari took the third spot for the most used browser, passing Firefox for the first time.
- Six out of the top ten documents were Innovative Technology Summary Reports (ITSRs).
- The term “Mobile System” is back on top with the most impressions.
- The top 3 performing modules this quarter were Technology, Vendors and Global Search.
- The Technology module continues to capture the interest of the visitors with over 42% of the visits going to this module.
- There was an increase in direct and referral traffic and a decrease in search traffic.
- A significant increase in visitors from the state of Texas was noted, following the New Mexico surge during the last period.

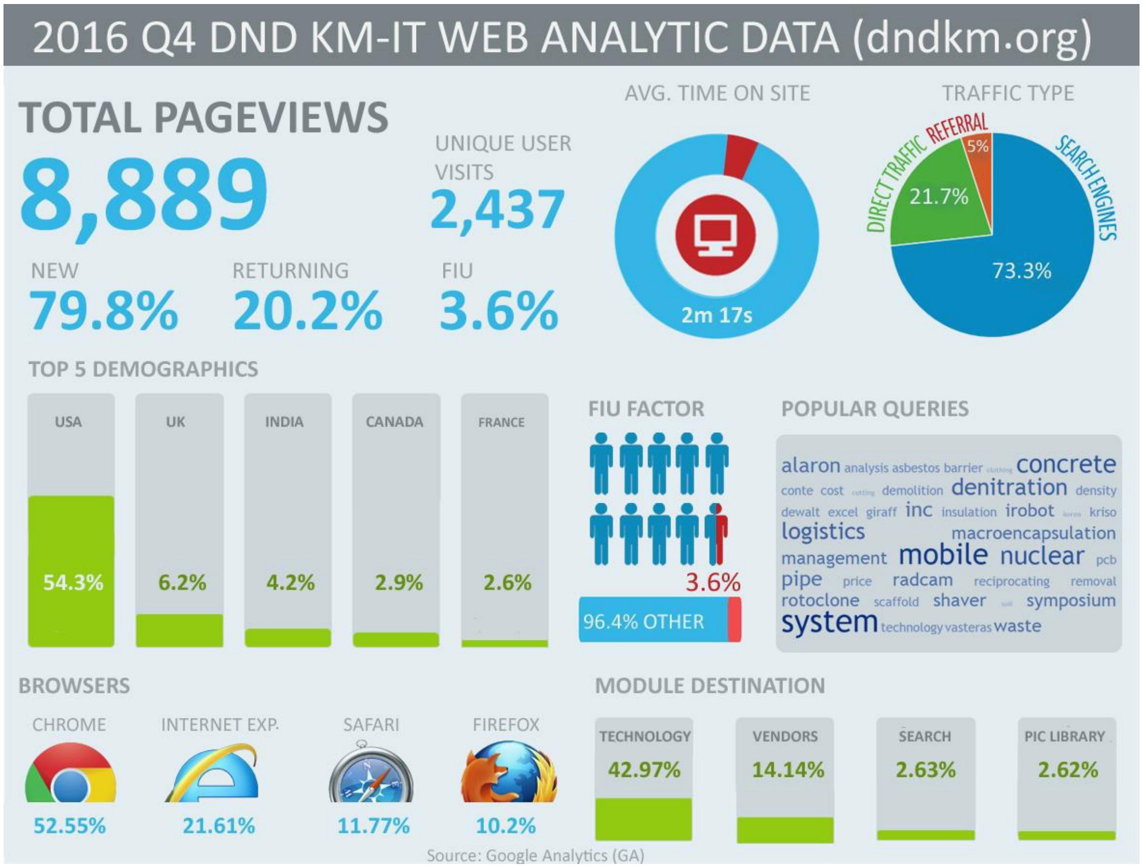

Source: Google Analytics (GA)

Figure 3-5. Infographic for 2016 Q4 Based on Web Analytic Data

FIU also completed the development of a metrics progress for outreach and training activities for D&D KM-IT. This document provides a performance year 7 mid-year report of the progress being made towards accomplishing the outreach and training goals and objectives set forth in the document titled, “Metric Definition for D&D KM-IT Outreach and Training,” which was developed during performance year 5 and expanded on the outreach and training activities for D&D KM-IT as described in the annual PTP by defining specific metrics and capturing the tools and techniques that will be applied to track and report the results. Outreach and training is a critical element towards the long-term sustainability of knowledge and essential for the long-term strategic vision of D&D KM-IT: it will continue to grow and mature into a self-sustaining system through the active participation of the D&D community it was designed to serve.

Milestones and Deliverables

The milestones and deliverables for Project 3 for FIU Performance Year 7 are shown on the following table. The deliverable associated with subtask 2.2.2, draft test plan for the technology demo/test & evaluation at FIU was completed. The draft test plan, titled *“Adapting Intumescent Coatings as Fire Resilient Fixatives ISO SRS 235-F D&D Activities Phase II: Construction of SRS 235-F Hot Cell Test Bed and Application Demonstration”* was submitted on January 6, 2017 to SRNL for review/comments, and the final document received concurrence and was signed by all stakeholders at FIU and SRNL on February 6, 2017. Milestone 2016-P3-M2.1 was completed with the participation in the January ASTM E10 Committee Meeting to coordinate the development of standardized testing protocols and performance metrics for D&D technologies (subtask 2.2.1). The preliminary metrics progress report on outreach and training activities for D&D KM-IT was completed in March and sent to DOE on April 4 and the latest infographic on Knowledge Management was revised and sent to DOE on February 1. A D&D KM-IT workshop was provided to the D&D community via demonstrations at the FIU conference booth at Waste Management 2017 from March 5-9, which completed a project deliverable. The four Wikipedia integration edits/articles, for milestone 2016-M3-M3.2 is in progress and has been reforecast for completion by June 30, 2017. Milestone 2016-P3-M2.2 is being reforecast to June 16. The test plan associated with this milestone includes constructing a to-scale SRS 235-F Hot Cell Test Bed on site at ARC that mirrors the operating environment encountered in an adjoining corner and middle hot cell configuration at the SRS 235-F facility. The second main objective involves an evaluation on the mechanics and processes associated with applying the selected intumescent coatings in the hot cell. The first part of this test plan is currently being executed as allowed by the incremental funding received and construction of the hot cell test bed is expected to be completed by May 12. The second part of the text plan is expected to be executed in late May to early June. FIU has communicated closely with the project contacts at Savannah River on the progress and scheduling of this task. They are in agreement with the new dates and will be visiting FIU to review the completed construction of the hot cell test bed and preparations for the execution of the testing and evaluation, tentatively planned for May 18.

FIU Performance Year 7 Milestones and Deliverables for Project 3

Task	Milestone/ Deliverable	Description	Due Date	Status	OSTI
Task 1: WIMS	2016-P3-M1.1	Import 2017 data set for waste forecast and transportation data	Within 60 days after receipt of data from DOE	On Target	
	2016-P3-M1.2	Draft paper submitted to WM17 conference	11/04/16	Complete	
Task 2: D&D	Deliverable	Draft Test Plan for IC Demo / Test & Evaluation at FIU (subtask 2.2.2)	1/6/17	Complete	OSTI
	2016-P3-M2.1	Participate in ASTM E10 committee meeting to coordinate developing standardized testing protocols and performance metrics for D&D technologies (subtask 2.2.1)	2/28/17	Complete	
	2016-P3-M2.2	Complete demonstration / test and evaluation of IC on FIU hot cell test bed (subtask 2.2.2)	4/28/17 Reforecasted to 6/16/17	Reforecast	
	Deliverable	Decision brief to DOE EM on recommended D&D technologies to test for FIU Performance Year 8 using the 3-phased model	4/28/17**	On Target	
	Deliverable	Draft summary report of robotic technologies for D&D (subtask 2.1.3)	5/31/17	On Target	OSTI
	Deliverable	Draft progress report on the adaptation of IC to enhance fire resiliency (subtask 2.1.1)	6/30/17	On Target	OSTI
	2016-P3-M2.3	Participate in ASTM E10 committee meeting to coordinate developing standardized testing protocols and performance metrics for D&D technologies (subtask 2.2.1)	7/31/17	On Target	
	Deliverable	Draft progress report on the identification of IC applications to other DOE EM problem sets	7/31/17	On Target	OSTI

		(subtask 2.1.2)			
	Deliverable	Draft technical reports for demonstrated technologies	30-days after evaluation/ demo	On Target	OSTI
	Deliverable	Draft Tech Fact Sheet for technology evaluations/ demonstrations	30-days after evaluation/ demo	On Target	
Task 3: D&D KM-IT	2016-P3-M3.1	Waste Management Symposium Draft Paper	11/4/16	Complete	
	Deliverable	D&D KM-IT Workshop to DOE EM staff at HQ	2/28/17** Reforecast TBD	Reforecast	
	Deliverable	Preliminary Metrics Progress Report on Outreach and Training Activities	3/10/17	Complete	
	Deliverable	Unclassified summary report on the status and findings of the KM-IT audits	3/24/17 Reforecast TBD	Reforecast	
	2016-P3-M3.2	Four Wikipedia integration edits/articles	3/31/17 Reforecast to 6/30/17	Reforecast	
	Deliverable	First D&D KM-IT Workshop to D&D community /DOE Site	3/31/17	Complete	
	Deliverable	First infographic to DOE for review	3/31/17	Complete	
	2016-P3-M3.3	Deploy pilot video onto YouTube platform	4/28/17	On Target	
	2016-P3-M3.4	Deployment of pilot native mobile application for D&D Fixatives Module	5/31/17	On Target	
	Deliverable	Second infographic to DOE for review	7/31/17	On Target	
	Deliverable	Metrics Progress Report on Outreach and Training Activities	8/18/17	On Target	
	Deliverable	Unclassified summary report on the status and findings of the KM-IT audits	8/25/17	On Target	
	Deliverable	Second D&D KM-IT Workshop to D&D community / DOE Site	8/25/17	On Target	
	Deliverable	D&D KM-IT Web Analysis Report	Quarterly	On Target	
	Deliverable	Draft Tech Fact Sheet for new modules or capabilities of D&D KM-IT	30-days after deployment of new module or capability	On Target	

**Completion of this deliverable depends on scheduling and availability of DOE EM staff

Work Plan for Next Quarter

Task 1: Waste Information Management System

- Perform database management, application maintenance, and performance tuning to WIMS.
- Complete integration of 2017 data set for waste forecast and transportation data from DOE into WIMS.

Task 2: D&D Support

- Complete construction of the SRS 235-F hot cell mock-up and execute the test plan for the cold demonstration / test & evaluation of intumescent coatings at FIU.
- Continue leading the working group in for ASTM International's E10 Committee on Nuclear Technologies and Applications and Subcommittee E10.03 - Radiological Protection for Decontamination and Decommissioning of Nuclear Facilities and Components to support the initiative of developing and promulgating uniform testing protocols and performance metrics for D&D technologies across the stakeholder community. Participate in the June 2017 conference.

Task 3: D&D Knowledge Management Information Tool

- Develop quarterly website analytics report and submit to DOE for review.
- Develop website analytics report for calendar year 2016 and submit to DOE for review.
- Perform outreach and training, community support, data mining and content management, and administration and support for the D&D KM-IT system, database, and network.
- Complete four new Wikipedia integration edits/articles in support of D&D topics.
- Perform outreach and training, community support, data mining and content management, and administration and support for the D&D KM-IT system, database, and network.

Project 4
DOE-FIU Science & Technology Workforce Development Initiative

Project Manager: Dr. Leonel E. Lagos

Project Description

The DOE-FIU Science and Technology Workforce Development Initiative has been designed to build upon the existing DOE/FIU relationship by creating a “pipeline” of minority engineers specifically trained and mentored to enter the Department of Energy workforce in technical areas of need. This innovative program was designed to help address DOE’s future workforce needs by partnering with academic, government and DOE contractor organizations to mentor future minority scientists and engineers in the research, development, and deployment of new technologies, addressing DOE’s environmental cleanup challenges.

Project Overview

The main objective of the program is to provide interested students with a unique opportunity to integrate course work, Department of Energy (DOE) field work, and applied research work at ARC into a well-structured academic program. Students completing this research program would complete the M.S. or Ph.D. degree and immediately be available for transitioning into the DOE EM’s workforce via federal programs such as the Pathways Program or by getting directly hired by DOE contractors, other federal agencies, and/or STEM private industry.

Project Quarterly Progress

FIU STEM (science, technology, engineering, and math) students are actively supporting the research efforts under the DOE-FIU Cooperative Agreement during FIU Performance Year 7. The following DOE Fellows are supporting the research under Projects 1-3:

Project 1: Gene Yllanes (undergraduate, electrical engineering), John Conley (undergraduate, mechanical engineering), Max Edrei (graduate, M.S., mechanical engineering), Sebastian Zanlongo (graduate, Ph.D., computer science), Clarice Davila (undergraduate, mechanical engineering) and Michael DiBono (undergraduate, mechanical engineering).

Project 2: Alejandro Garcia (graduate, M.S. geoscience), Alejandro Hernandez (undergraduate, chemistry), Alexis Smoot (undergraduate, environmental engineering), Awmna Kalsoom Rana (undergraduate, chemistry), Christine Wipfli (undergraduate, environmental engineering), Christopher Strand (undergraduate, civil & environmental engineering), Claudia Cardona (graduate, PH.D., environmental engineering), Hansell Gonzalez (graduate, Ph.D., chemistry), Sarah Bird (undergraduate, environmental engineering), Silvina Di Pietro (graduate, Ph.D., chemistry), Sarah Solomon (undergraduate, environmental engineering), Mohammed Albassam (undergraduate, environmental engineering), Frances Zengotita (undergraduate, chemistry and health), Juan Morales (graduate, M.S., public health), Ripley Raubenolt (undergraduate, environmental engineering), and Ron Hariprashad (undergraduate, environmental engineering).

Project 3: Jesse Viera (undergraduate, mechanical engineering), Alexander Piedra (undergraduate, mechanical engineering), Andres Cremisini (undergraduate, computer science), and Daniel Khawand (undergraduate, computer science).

Fellows continue their support to the DOE-FIU Cooperative Agreement by actively engaging in EM applied research and supporting ARC staff in the development and completion of the various tasks. The program director continues to work with DOE sites and HQ to fully engage DOE Fellows with research outside ARC where Fellows provide direct support to mentors at DOE sites, DOE-HQ, and DOE contractors. All Fellows also participated in a weekly meeting conducted by the program director, a conference line has been established to enable DOE Fellows conducting internship to join to weekly meeting and update program director on their internship. During each of these meetings, one DOE Fellow presents the work they performed during their summer internship and/or EM research work they are performing at ARC.

The DOE Fellows program director continued communications to coordinate with DOE-HQ, DOE sites, DOE national laboratories, and DOE contractors for placement of DOE Fellows for summer 2017 internships. Preliminary planned internships for spring/summer 2017 include:

Table 4-1. Summer 2017 Internships

Site	Mentor(s)	DOE Fellow(s)
DOE-HQ	Skip Chamberlain	Juan Morales and Mohammed Albassam
SRNL	Dan Kaplan	Sarah Solomon and Ripley Raubenolt
SRNL/SREL	Brian Looney/John Seaman	Ron Hariprashad
Sandia	Phil Heermann	Sebastian Zanlongo
Los Alamos	Doug Kautz	Michael Di Bono
PNNL	Duriem Calderin / Vicky Freeman / Jim Szecsody	Andres Cremisini
SRNL	Aaron Washington/ Connor Nicholson	Alex Piedra
WRPS/Richland	Ruben Mendoza	Clarice Davila
WIPP	Tim Dittrich	Francis Zengotita

DOE Fellow Christine Wipfli completed her internship work with the International Atomic Energy Agency (IAEA) in the Waste Technology Section, Division of Nuclear Fuel Cycle & Waste Technology after returning to FIU to take courses during the spring 2017 semester. Christine participated in this one-year internship from April 2016 through March 2017.

DOE Fellows completed preparation and participated in the Waste Management 2017 Symposia (WM17) in Phoenix, AZ, from March 5-9, 2017. The DOE Fellows completed technical posters, presentation materials, written biographies, and resumes for the WM conference to introduce themselves and their research.

A total of seventeen (17) DOE Fellows attended WM17 and presented technical posters during Session 33 (Student Posters: The Next Generation – Industry Leaders of Tomorrow) on Monday, March 6, 2017. The posters presented the DOE-EM research that they have performed at FIU's ARC and during their summer internships at DOE sites, HQ, and national research laboratories, in the research areas of high level waste/waste processing, soil and groundwater modeling and remediation, and deactivation and decommissioning. The DOE Fellow posters presented during the Student Poster Competition at WM17 are presented below.

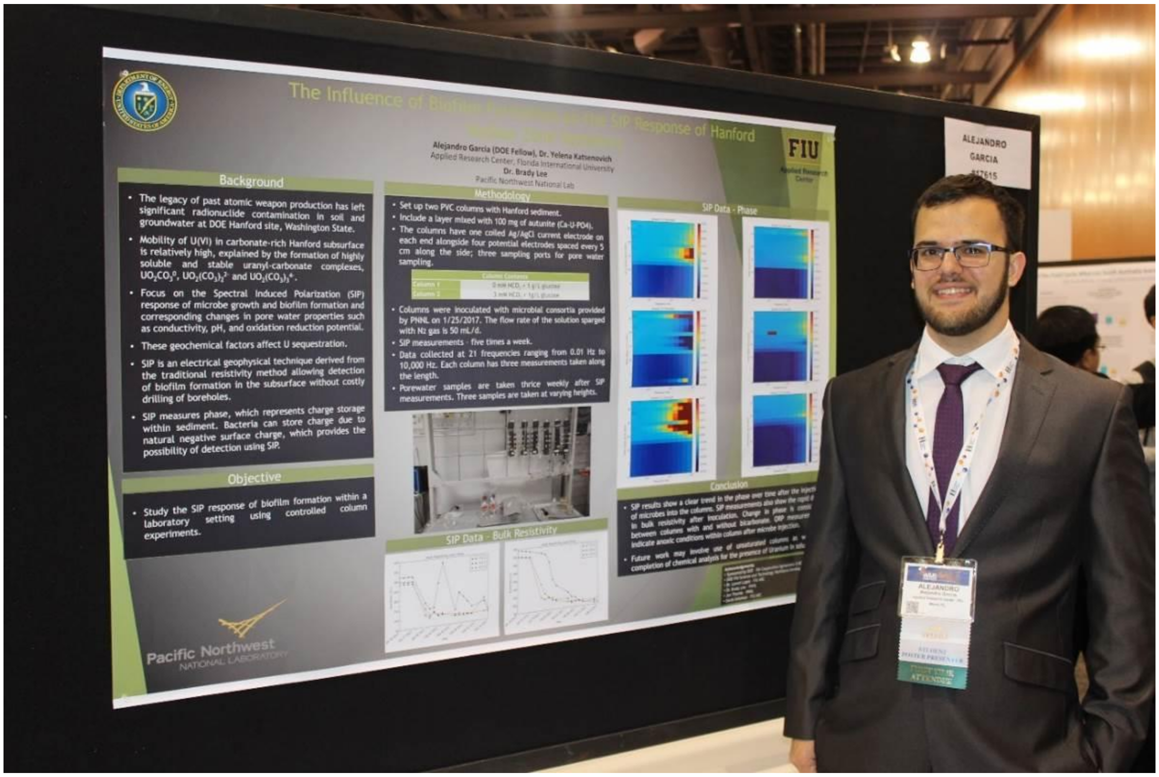

Figure 4-1. The Influence of Biofilm Formation on the SIP Response of Hanford Vadose Zone Sediment Alejandro Garcia

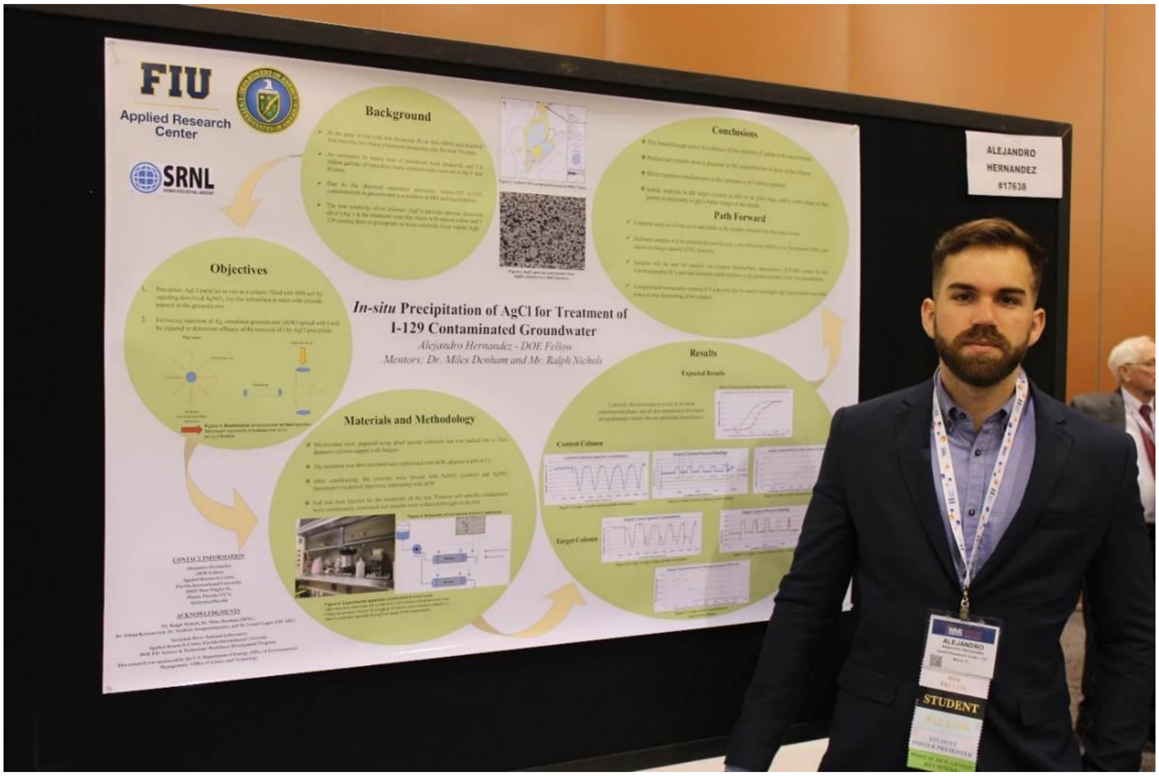

Figure 4-2. In Situ Precipitation of Silver Chloride for Treatment of I-129 Contaminated Groundwater Alejandro Hernandez

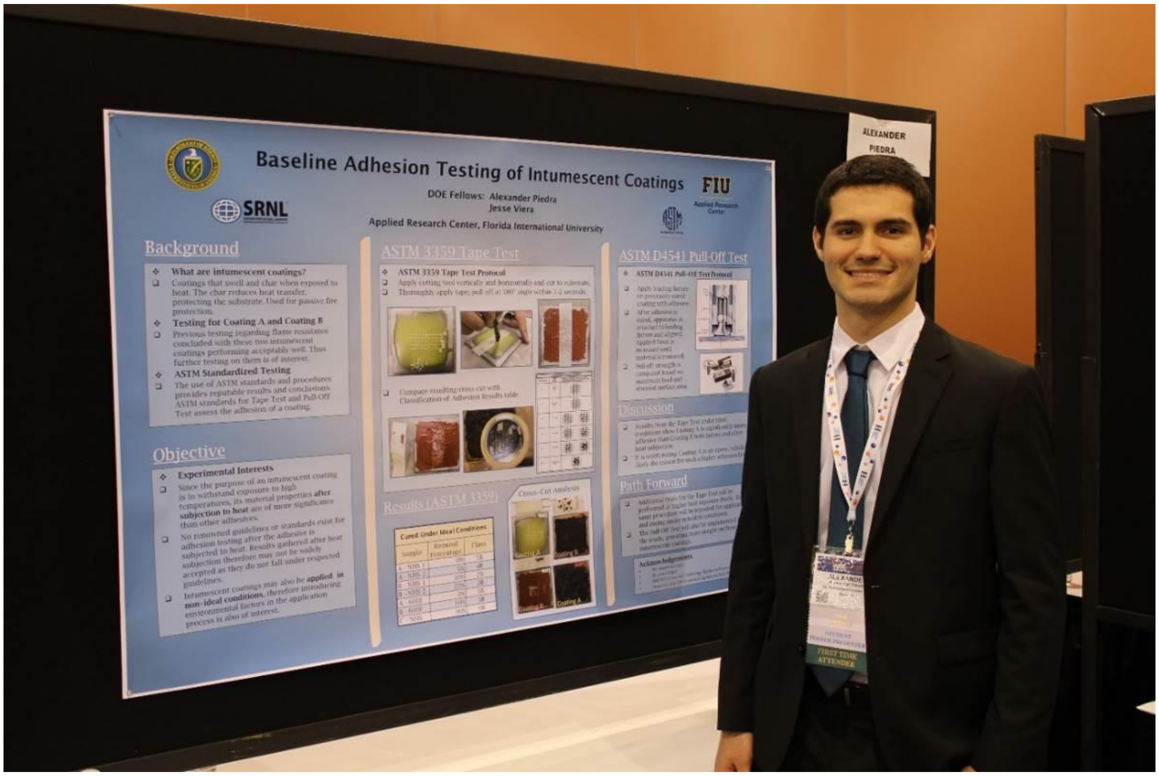

Figure 4-3. Baseline Adhesion Testing of Intumescent Coatings Alexander Piedra

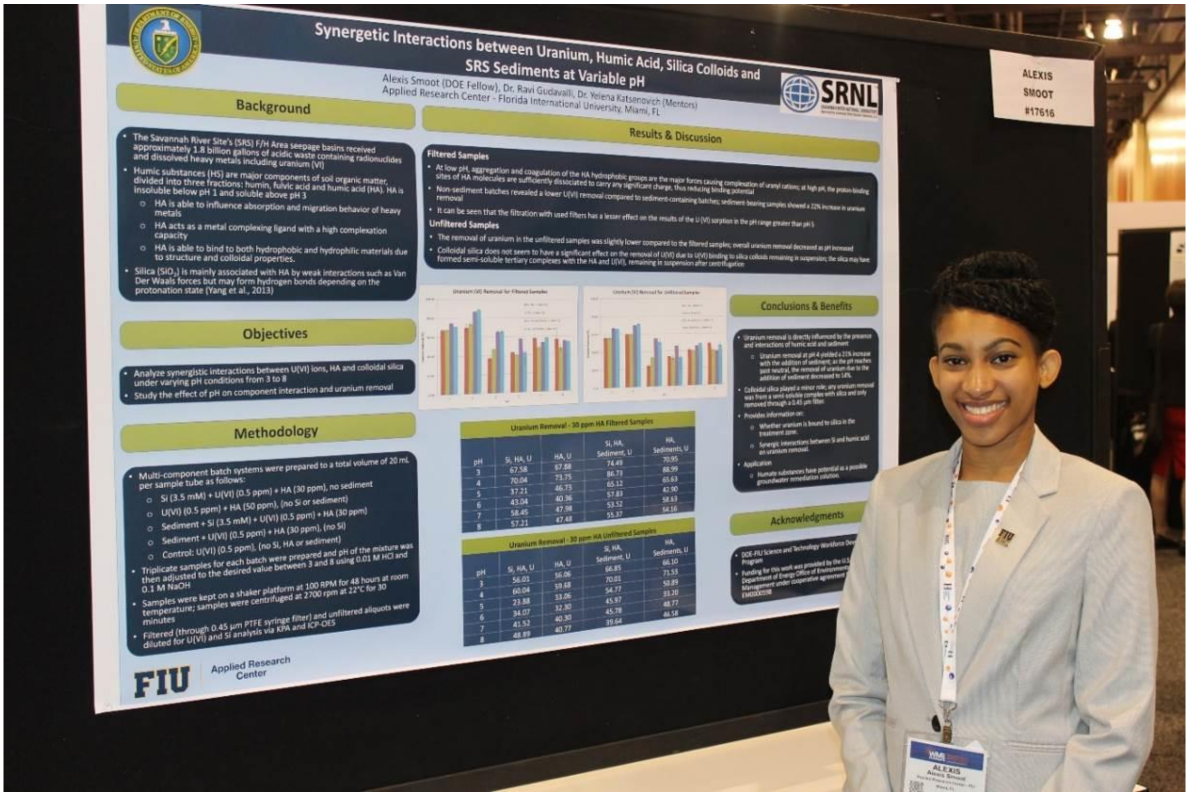

Figure 4-4. Synergetic Interactions between Uranium, Humic Acid, Silica Colloids & SRS Sediments at Variable pH - Alexis Smoot

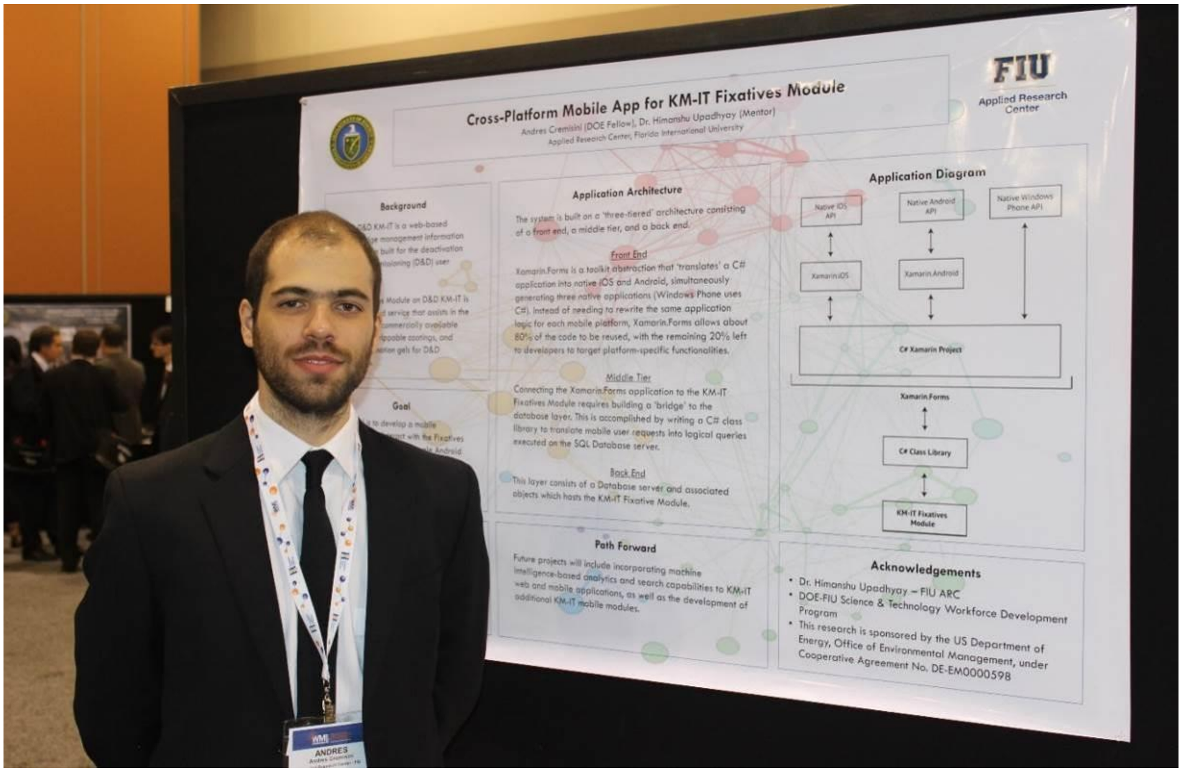

Figure 4-5. Cross-Platform Mobile App for KM-IT Fixatives Module
Andres Cremisini

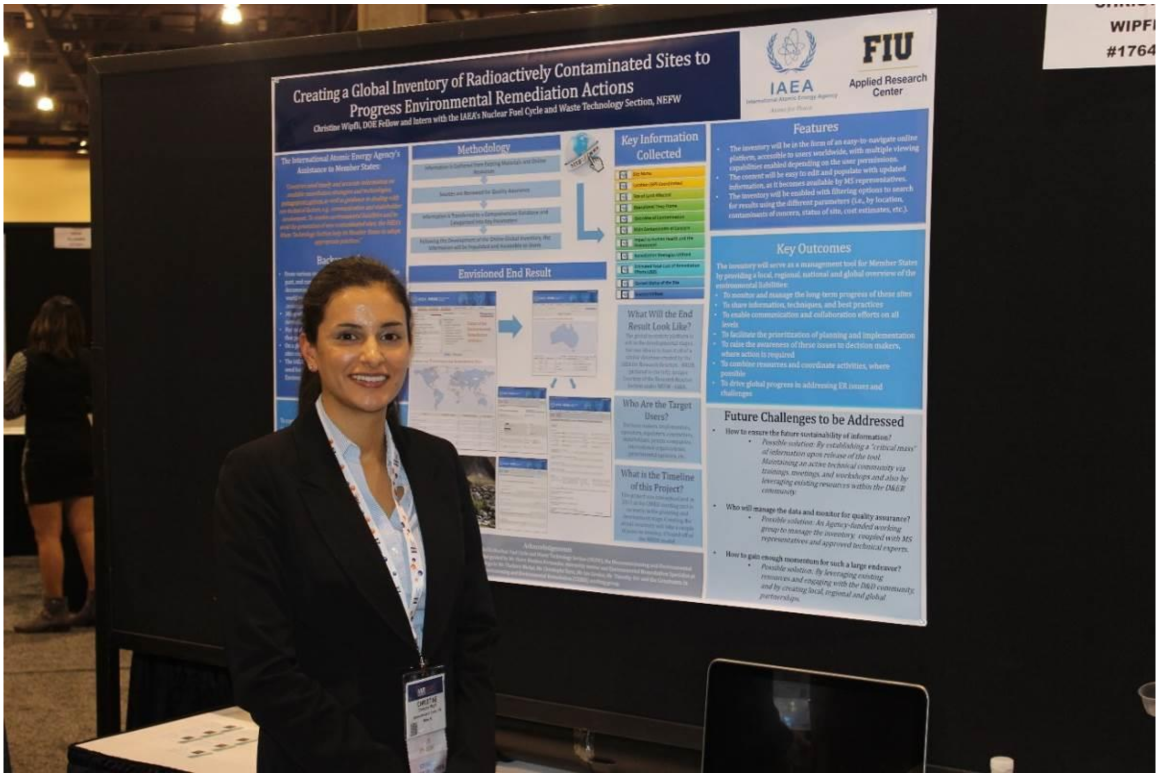

Figure 4-6. Creating a Global Inventory of Radioactively Contaminated Sites to Progress Environmental Remediation Actions - Christine Wipfli

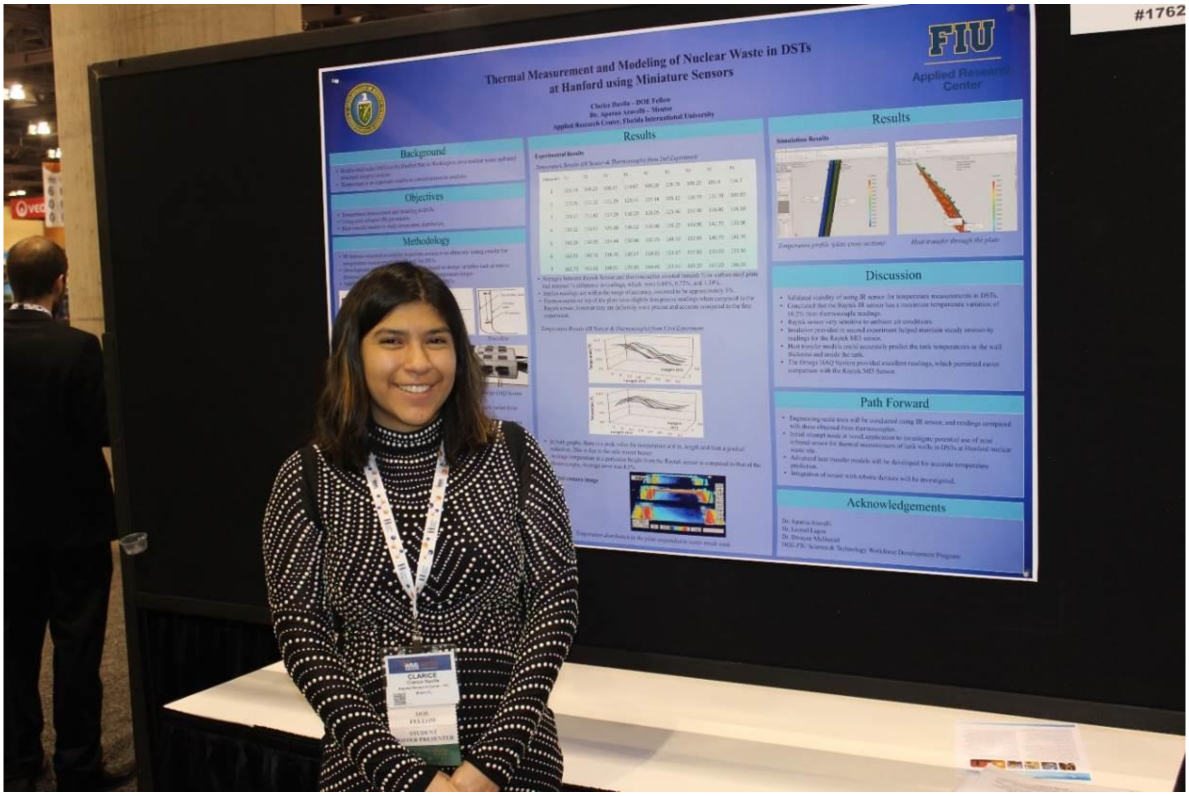

Figure 4-7. Thermal Measurement and Modeling of Nuclear Waste in DSTs at Hanford using Miniature Sensors Clarice Davila

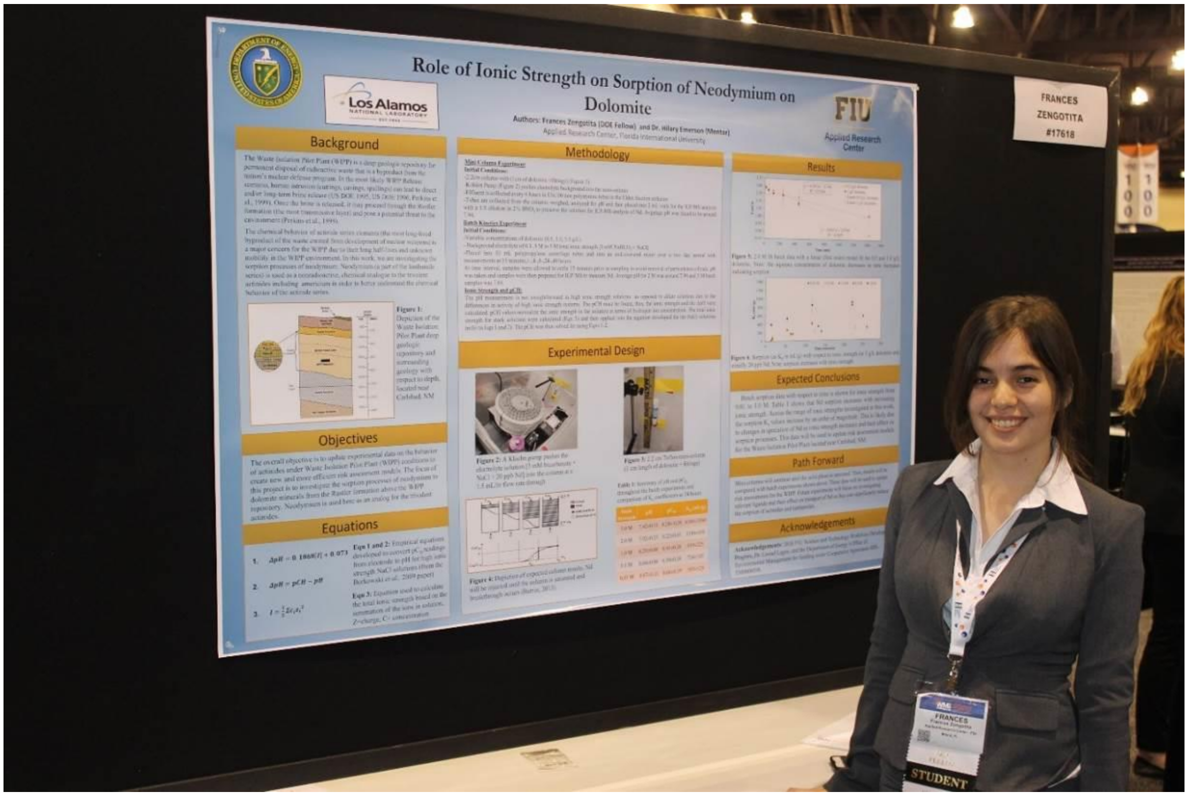

Figure 4-8. Role of Ionic Strength on Sorption of Neodymium on Dolomite
Frances Zengotita

Figure 4-9. A Multipurpose All-Terrain Robotic Platform: T-Rex
Gene Yllanes

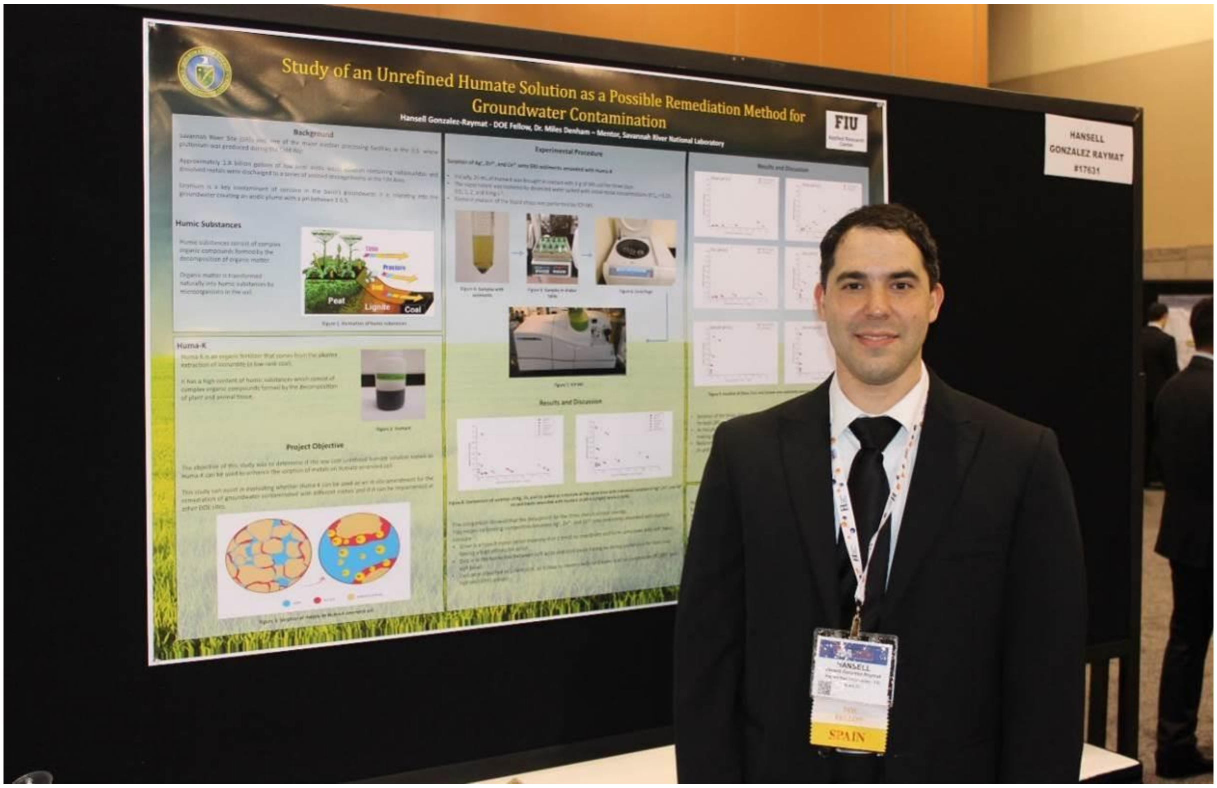

Figure 4-10. Study of an Unrefined Humate Solution as a Possible Remediation Method for Groundwater Contamination – Hansell Gonzalez Raymat

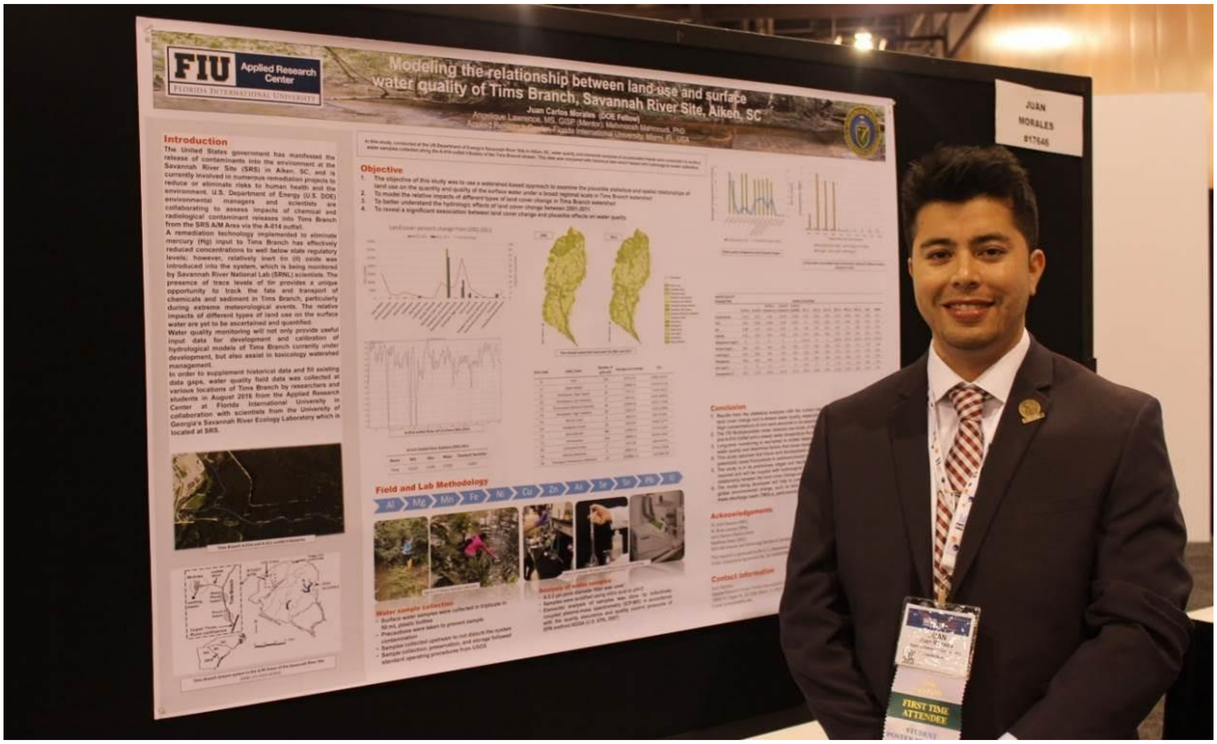

Figure 4-11. Modeling the Relationship between Land Use and Surface Water Quality of Tims Branch, Savannah River Site, Aiken, SC - Juan Morales

Figure 4-12. Miniature Motorized Inspection Tool for DOE Hanford Site Tank Bottoms Michael DiBono

Figure 4-13. In-Situ Water Quality Sampling and Flow Measurement to Support Hydrological Model Development for Tims Branch Watershed, Savannah River Site, SC - Mohammed Albassam

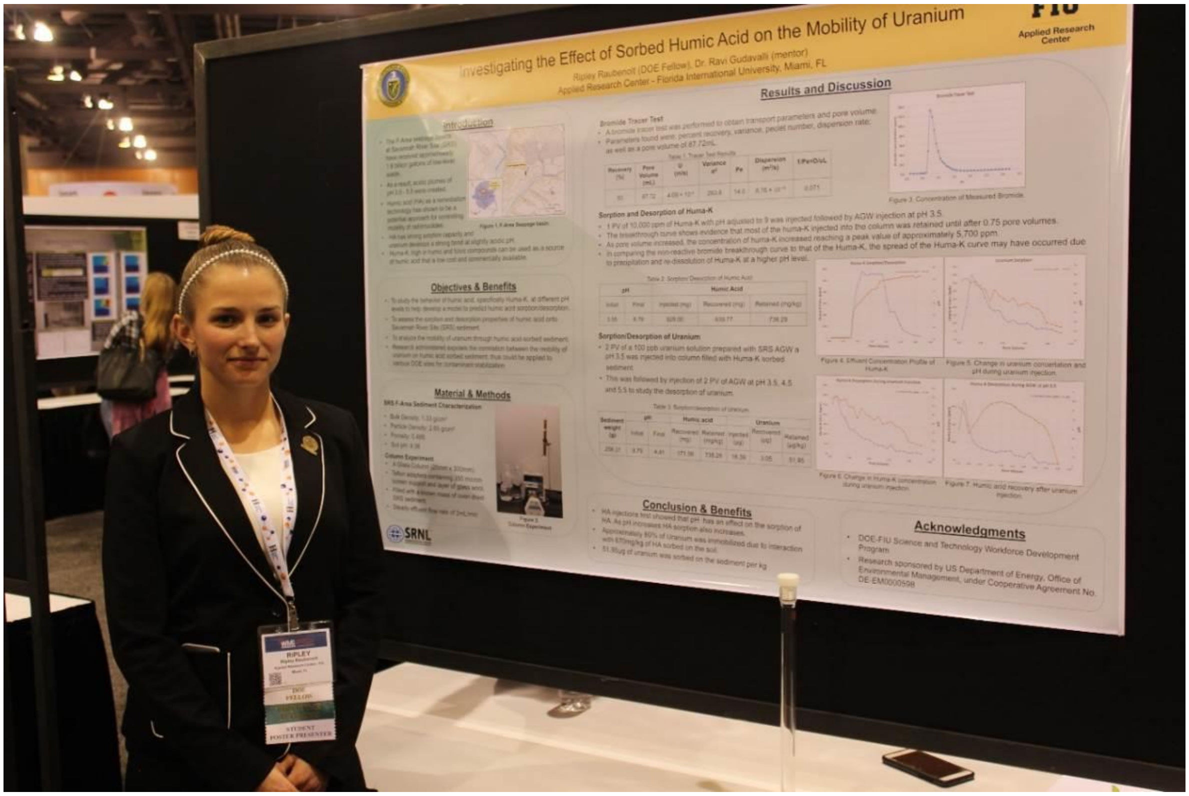

Figure 4-14. Investigating the Effect of Sorbed Humic Acid on the Mobility of Uranium
Ripley Raubenolt

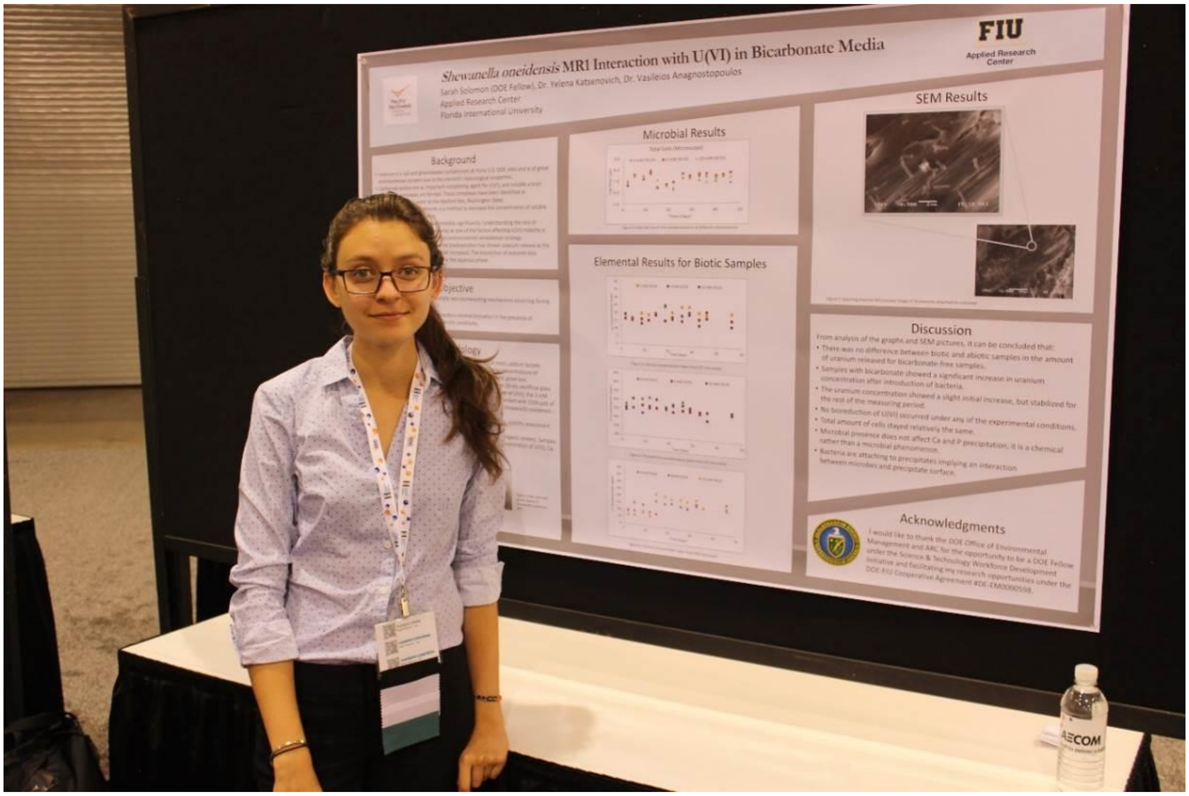

Figure 4-15. *Shewanella oneidensis* MR1 Interaction with U(VI) in Bicarbonate Media
Sarah Solomon

Figure 4-16. Low-Cost Robotic Platform for D&D Activities
Sebastian Zanlongo

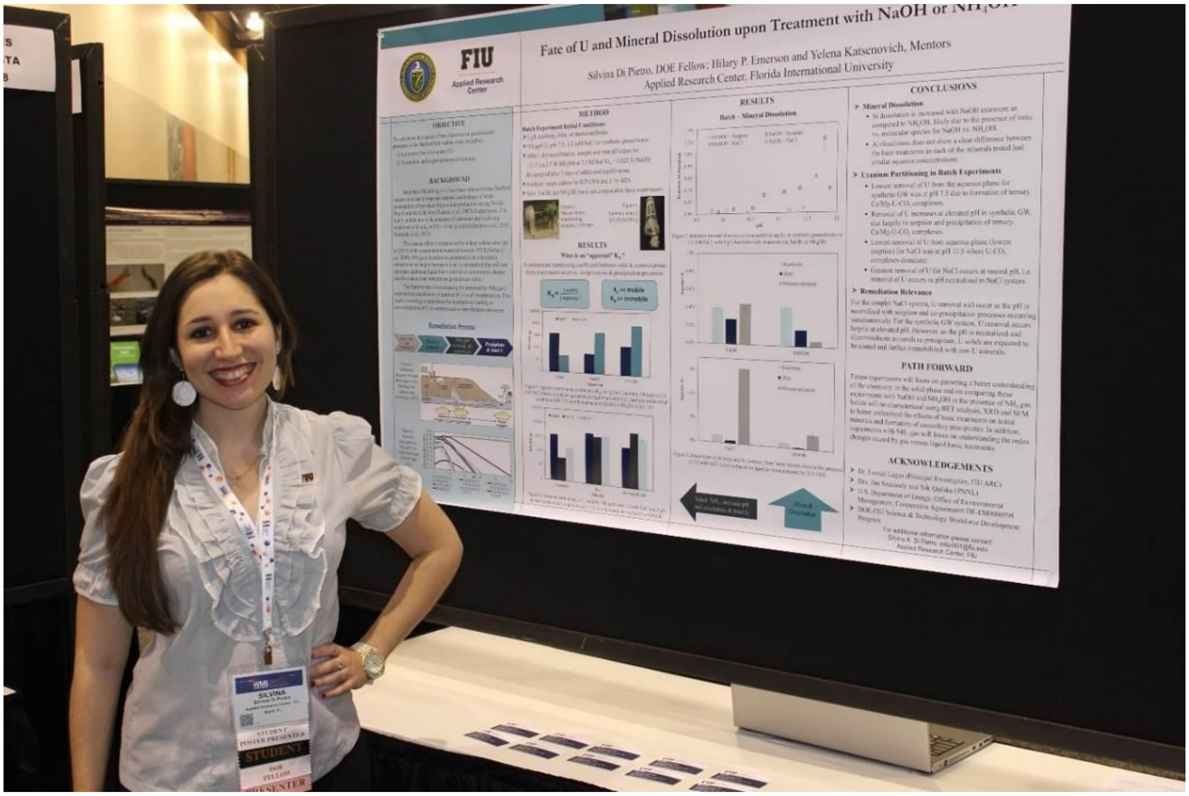

Figure 4-17. Fate of U and Mineral Dissolution upon Treatment with NaOH or NH_4OH
Silvina Di Pietro

In addition, two DOE Fellows gave professional oral presentations based on the applied research being conducted by ARC on behalf of DOE-EM in major areas of research, including:

- Ammonia Gas Treatment for Uranium Immobilization at US DOE Hanford Site. Silvina Di Pietro, Hilary Emerson, Yelena Katsenovich (FIU). **Presenter: Silvina Di Pietro (DOE Fellow)**
- Development and Testing of Robotic Inspection Tools for the High-Level Waste Double Shell Tanks at Hanford. Michael DiBono, Dwayne McDaniel, Yew Teck (William) Tan, Anthony Abrahao, Ryan Sheffield (FIU). **Presenter: Michael DiBono (DOE Fellow)**

Session 41 on Tuesday, March 7, hosted a panel discussion on Graduating Students and New Engineers: Wants and Needs - STEM Students: Industry Dialog & Exchange of Knowledge Session. **DOE Fellow Christine Wipfli** participated as the panel reporter and **DOE Fellow Michael DiBono** participated in the panel discussion. This panel focused on new hires and graduating engineers having open lines of communication with employers. Considering the projected shortfalls in the workforce, effective communication of wants-and-needs of both the employer and employee must exist.

In addition, Session 042, also on Tuesday, hosted a panel discussion on Young Professionals in Nuclear Science and Engineering: An International Perspective Session. **DOE Fellow Christine Wipfli** participated in this panel discussion. This panel focused on young professionals and covers views on radioactive waste management from young persons' perspectives from all around the world with an aim to encourage fresh thinking and provide an opportunity for an open and frank discussion on issues.

Figure 4-18. DOE Fellow Christine Wipfli during panel session at WM 17.

A 2017 Roy G. Post Foundation Scholarship at the Undergraduate Student Level was awarded to **DOE Fellow Alejandro Hernandez** during the WM2017 Conference Honors and Awards Luncheon on Tuesday, March 7, 2017.

Figure 4-19. Announcement of scholarship award to DOE Fellow Alejandro Hernandez at WM17.

The DOE Fellows joined staff from the Applied Research Center at Florida International University to host a booth in the exhibitor hall during the conference, interacting with conference attendees on how FIU-ARC provides support to the DOE EM in their mission of accelerated risk reduction and environmental legacy cleanup. DOE Fellows also participated as Student Assistants during the conference, assisting conference organizers and presenters during the technical sessions.

Figure 4-20. DOE Fellows and ARC staff at FIU booth during WM17 Exhibit Hall.

Figure 4-21. DOE Fellows at the FIU booth during WM17.

FIU hosted a visit from Ms. Vivian Cato from SRNL on January 23 and 24, 2017. Ms. Cato is the program manager for the U.S. Department of Energy Office of Environmental Management's Minority Serving Institutions Partnership Program (MSIPP). Ms. Cato had an opportunity to meet with our DOE Fellows as well as tour ARC's and Department of Chemistry's research facilities. In addition, Ms. Cato provided a comprehensive overview of the MSIPP program during a presentation attended by DOE Fellows, ARC researchers/staff and FIU Department of Chemistry faculty. Ms. Cato also had an opportunity to meet with NRC's Fellows and Scholars.

Figure 4-1. Ms. Vivian Cato with Dr. Lagos (ARC Director of Research) and FIU-DOE Fellow students/

DOE Fellows Alexis Smoot presented a poster titled "Sustainability Index" at an FIU Undergraduate Research Presentation for FIU's Foundation Board of Directors hosted by FIU's Honors College on Friday January 27, 2017. The poster Alexis presented was based on her summer internship research carried out at DOE HQ at the Germantown facility. The goal of her research project to develop a high level sustainability analysis comparing active and passive remediation technologies at Hanford 100 and 200 area sites and the Mound, Ohio site. The sustainability index attempts to quantify the relative sustainability of active and passive remediation strategies by examining a variety of metrics and perspectives from those involved in the decision-making process.

Figure 4-2. Student presenters at the FIU Honors College Board of Directors Research Event (Far Right: DOE Fellow Alexis Smoot)

In addition, Alexis Smoot submitted an abstract for the "Sustainability Index" to the 2017 National Conference of Undergraduate Research and was selected to present an academic research poster at the conference held in Memphis, TN. Selected from a pool of 4,000 submissions, the abstract demonstrated "a unique contribution" to the field of environmental engineering and remediation. Alexis will present the sustainability index poster in April.

DOE Fellow Silvina Di Pietro was invited to talk at the FIU's Panther Alumni Week (PAW) 1st year Honors College interdisciplinary course. She presented her undergraduate experience within FIU and the FIU's Honors College and advised students on leadership. She stressed the importance of participating in an internship before graduating and shared her internship experience at PNNL last summer as part of the DOE Fellows Program at FIU. She concluded her presentation by providing students with information about the DOE Fellows Program.

Figure 4-2. DOE Fellow Silvina Di Pietro guest lecture at Panther Alumni Week (PAW).

Figure 4-3. Silvina Di Pietro introducing FIU students to the DOE Fellows Program.

FIU hosted a visit from Dr. David Shuh on February 3, 2017 and the DOE Fellows participated in lab tours during his visit. Dr. Shuh gave a lecture titled “Soft X-ray Radiation Investigations of Materials Relevant to Actinide Science."

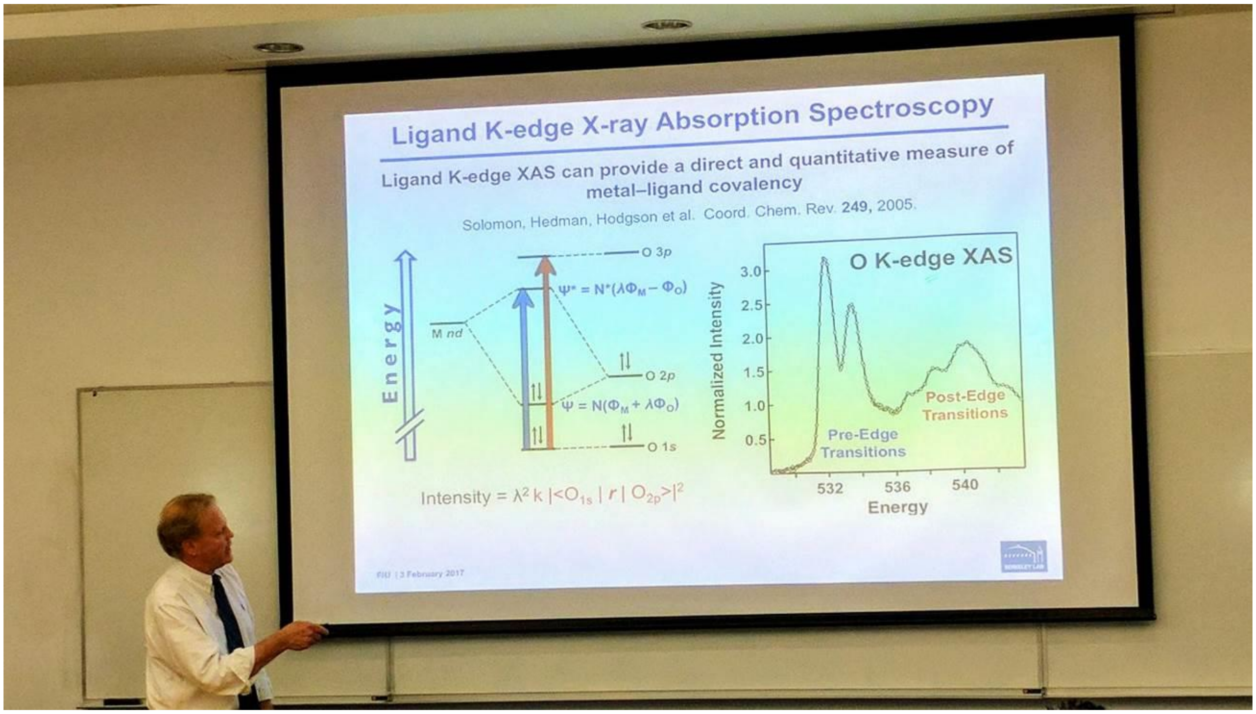

Ligand K-edge X-ray Absorption Spectroscopy

Ligand K-edge XAS can provide a direct and quantitative measure of metal–ligand covalency

Solomon, Hedman, Hodgson et al. Coord. Chem. Rev. 249, 2005.

Intensity = $\lambda^2 k\,|\langle O_{1s}\,|\,r\,|\,O_{2p}\rangle|^2$

FIU | 3 February 2017

Figure 4-4 Dr. David Shuh during his visit to FIU.

On February 7, 2017, Dr. Michael Poirier (SRNL) visited FIU’s Applied Research Center. Dr. Poirier met with our DOE Fellows and the Project 1 researchers/scientists and faculty. The main purpose of his visit was to identify areas of collaboration in the area of tank waste as well as understand FIU-ARC’s overall research and student program (DOE Fellows program). Dr. Poirier was also interested in potential summer internships for our DOE Fellows and recruitment of FIU graduates.

DOE Fellow, Hansell Gonzalez-Raymat received a master’s degree in chemistry for fulfilling the requirements as a part of his Ph.D. program. He is expected to graduate with his Ph.D. degree in the spring of 2018.

DOE Fellows Alexander Piedra, Gene Yllanes, Frances Zengotita and Ripley Raubenolt prepared abstracts based on their DOE-EM related research to present at 2017 Life Sciences South Florida STEM Undergraduate Research Conference to be held on April 1, 2017 at Palm Beach State College, FL.

DOE Fellow Juan Carlos Morales was awarded the Robert Stempel College of Public Health & Social Work Path Merit Award Scholarship for outstanding achievements during his program of study. The award provides supplemental funds to students who have an exemplary academic record, participate in student activities, and demonstrate notable achievements in helping the community. In efforts to complete his master’s degree, Morales has participated in numerous research projects and community activities which made him an eligible candidate for the award.

This scholarship has given him the opportunity to travel to several conferences. More importantly, he has gained experience which has aided in his research approach and communication skills.

DOE Fellow Juan Carlos Morales also recently attended the 2017 Society of Toxicology Expo (March 12-17, 2017) to present his technical research conducted for SRS. Before his abstract acceptance, Morales performed in-situ sampling and field data collection in Tims Branch at SRS. The data collected will subsequently be used for contaminant transport modeling and an environmental human exposure assessment. He was able to extrapolate his data and develop an abstract titled, "*Accumulated Metalloestrogens Analysis for Health Risk Assessment and Watershed Toxicology Management in Tims Branch, Savannah River Site, Aiken, S.C.,"* which was accepted for presentation at the Ecotoxicology ToxExpo poster session.

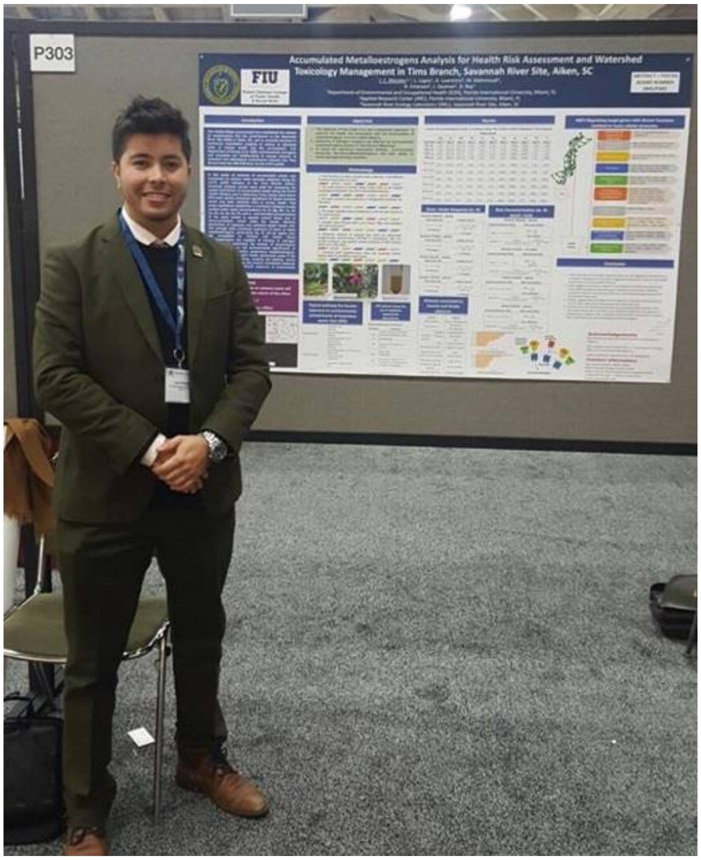

Figure 4-22. DOE Fellow Juan Morales presenting his research poster at the Society of Toxicology Expo.

Three DOE Fellows participated in the 2nd Annual FIU Undergraduate Research Conference on March 31, 2017. Fellow Ripley Raubenolt presented the effect of sorbed humic acid on the mobility of uranium, Awmna Rana presented the investigation of the properties of acid-contaminated sediments and its effect on contaminant mobility, and Alexis Smooth presented the synergetic interactions between uranium, humic acid, silica colloids and SRS sediments at variable pH.

Figure 4-23. DOE Fellows Ripley Raubenolt (top left), Alexis Smoot (bottom left) and Awmna Rana (Right) presenting their research posters at the FIU undergraduate research conference.

Two DOE Fellows, including Sarah Solomon and Ron Hariprashad, were in the team of FIU STEM students who were awarded 2nd Place in the 2016-2017 Environmental Engineering and Science Foundation (EESF)/Association of Environmental Engineering and Science Professors (AEESP) Student Video Competition for their video production entitled “Take Action on Climate Change.” This video is intended to motivate and teach young adults how they can impact climate change through their own day to day activities. The team will be traveling to Washington, DC to receive their award on April 13, 2017 at the 2017 Excellence in Environmental Engineering and Science Awards Luncheon and Conference. The video can be viewed on YouTube via the following link: *https://www.youtube.com/watch?v=dOyhrCQKobc*

DOE Fellows participated in lab tours during Dr. Howard Hall’s visit to FIU on March 17. Dr. Hall is the director of the Global Security program and Governor’s Chair for Global Nuclear Security. During his visit, Dr. Hall gave a talk titled “Radiochemistry Center of Excellence: Expanding the Horizons of Nuclear Forensics Analysis."

Also, DOE Fellows attended a lecture series featuring Drs. Altmaier and Kienzler from Karlsruhe Institute of Technology - Institute for Nuclear Waste Disposal (KIT-INE) during their visit to FIU on March 24. The titles for their talks were “Recent Advances on Aquatic Radionuclide Chemistry” and “Site Selection Process in Germany and Overview on Disposal Related R&D at KIT,” respectively.

Figure 4-24. Drs. Altmaier and Kienzler from Karlsruhe Institute of Technology - Institute for Nuclear Waste Disposal (KIT-INE) with ARC staff.

DOE Fellows attended the ARC Lecture Series held on March 31, featuring Dr. Lou Centofanti (CEO, Perma-Fix Environmental Services, Inc.). The title of his talk was "The Evolution of Chemical Waste Treatment in the Nuclear Industry - Simple Solutions for Complex Problems."

DOE Fellows spring recruitment efforts were initiated on March 29 and will run through April 14. Recruitment campaigns were conducted by placing recruitment tables at the College of Engineering and at the main FIU campus in the Physics & Chemistry building and Computer Science building. Large group of students showed interest in the program and a signup sheet was used to collect student information. Emails were sent to interested students with information on requirements and components of the program along with application procedure and application checklist. Deadline for FIU students to submit applications for DOE Fellowship will be April 14, 2017. Applications will be reviewed by ARC researches and staff and interviews will be conducted during the months of April and May 2017.

FIU continued working with DOE Fellows interested in federal jobs. FIU supports our Fellows with identifying federal entry-level career opportunities within DOE and other federal agencies on USA Jobs and forward those vacancy announcements to the DOE Fellows. FIU also continues to identify those DOE Fellows who are preparing to transition from academia to the workforce within the next year for conducting focused mentoring sessions with those Fellows on resume preparation and the USA Jobs application process.

During this month, the Fellows continued their research in the DOE EM applied research projects under the cooperative agreement and research topics identified as part of their summer internships at DOE sites, national labs, and/or DOE HQ. Each DOE Fellow is assigned to DOE EM research projects as well as ARC mentors. A list of the current Fellows, their classification, areas of study, ARC mentor, and assigned project task is provided below.

Table 4-2. Project Support by DOE Fellows

Name	Classification	Major	ARC Mentor	Project Support
Alejandro Garcia	Graduate - B.S.	Geoscience	Dr. Yelena Katsenovich	Influence of microbial activity on corresponding electrical geophysical response after ammonia injections in the vadose zone
Alejandro Hernandez	Undergrad - M.S.	Chemistry	Dr. Vasileios Anagnostopoulos	Contaminant Fate & Transport Under Reducing Conditions
Alexander Piedra	Undergrad - B.S.	Mechanical Eng.	Mr. Joseph Sinicrope	Database of Robotic Technologies for D&D
Alexis Smoot	Undergrad - B.S.	Envr. Eng.	Dr. Ravi Gudavalli	Synergistic Effects of Silica & Humic Acid on U(VI) Removal
Andres Cremisini	Undergrad - B.S.	Computer Science	Dr. Himanshu Upadhyay	D&D KM-IT
Awmna Kalsoom Rana	Undergrad - B.S.	Chemistry	Dr. Vasileios Anagnostopoulos	Investigation on the Properties of Acid-Contaminated Sediment and its Effect on Contaminant Mobility
Christine Wipfli	Undergrad - B.S.	Envr. Eng.	Dr. Vasileios Anagnostopoulos	Groundwater Remediation at SRS F/H Area
Christopher Strand	Undergrad - B.S.	Civil & Env. Eng.	Dr. Noosha Mahmoudi	Surface Water Modeling of Tims Branch
Clarice Davila	Undergrad - B.S	Mechanical Eng.	Dr. Aparna Aravalli	Investigation Using an Infrared Temperature Sensor to Determine the Inside Wall Temperature of DSTs
Claudia Cardona	Graduate - Ph.D.	Envr. Eng.	Dr. Yelena Katsenovich	Sequestering Uranium at the Hanford 200 Area Vadose Zone
Daniel Khawand	Undergrad - B.S.	Computer Science	Dr. Himanshu Upadhyay	D&D KM-IT
Frances Zengotita	Undergrad - B.S.	Chemistry & Health	Dr. Hilary Emerson	Absorption of Neodymium into the Dolomite Mineral
Gene Yllanes	Undergrad - B.S.	Electrical Eng.	Mr. Anthony Abrahao	Development of Inspection Tools for DST Primary Tanks
Hansell Gonzalez	Graduate - Ph.D.	Chemistry	Dr. Yelena Katsenovich	Sorption Properties of Humate Injected into the Subsurface System
Jesse Viera	Undergrad - B.S.	Mechanical Eng.	Mr. Joseph Sinicrope	Incombustible Fixatives
John Conley	Undergrad - B.S.	Mechanical Eng.	Mr. Anthony Abrahao	Development of Inspection Tools for DST Primary Tanks
Juan Morales	Graduate – M.S.	Public Health	Ms. Angelique Lawrence / Dr. Reinaldo Garcia	Development of Flow and Contaminant Transport Models for SRS

Name	Classification	Major	ARC Mentor	Project Support
Maximiliano Edrei	Graduate – M.S.	Mechanical Eng.	Dr. Dwayne McDaniel	Computational Fluid Dynamics Modeling of a Non-Newtonian Fluid Undergoing Sparging for Estimating PJM Mixing Times
Michael DiBono	Undergrad - B.S.	Mechanical Eng.	Mr. Anthony Abrahao	Development of Inspection Tools for DST Primary Tanks
Mohammed Albassam	Graduate – M.S.	Envr. Eng.	Dr. Noosha Mahmoudi	Environmental Remediation and Surface Water Modeling of Tims Branch Watershed at SRS
Ripley Raubenolt	Undergrad - B.S.	Envr. Eng.	Dr. Ravi Gudavalli	Modeling of the Migration and Distribution of Natural Organic Matter Injected into Subsurface Systems
Ron Hariprashad	Undergrad - B.S.	Envr. Eng.	Dr. Noosha Mahmoudi	Surface Water Modeling of Tims Branch
Ryan Sheffield	Undergrad - B.S.	Mechanical Engineering	Dr. Dwayne McDaniel	Development of Inspection Tools for DST Primary Tanks
Sarah Bird	Undergrad - B.S.	Envr. Eng.	Dr. Noosha Mahmoudi	Surface Water Modeling of Tims Branch
Sarah Solomon	Undergrad - B.S.	Envr. Eng.	Dr. Yelena Katsenovich	Investigation on Microbial-Meta-Autunite Interactions - Effect of Bicarbonate and Calcium Ions
Sebastian Zanlongo	Graduate - Ph.D.	Computer Science	Dr. Dwayne McDaniel	Cooperative Controls for Robotic Systems
Silvina Di Pietro	Graduate - Ph.D.	Chemistry	Dr. Hilary Emerson	Evaluation of Ammonia for Uranium Treatment

Milestones and Deliverables

The milestones and deliverables for Project 4 for FIU Performance Year 7 are shown on the following table. Milestone 2016-P4-M4, submission of student poster abstracts to Waste Management Symposium 2017, was completed by January 16, 2017 with the submission of 17 student abstracts.

FIU Performance Year 7 Milestones and Deliverables for Project 4

Milestone/ Deliverable	Description	Due Date	Status	OSTI
2016-P4-M1	Draft Summer Internships Reports	10/14/16	Complete	
Deliverable	Deliver Summer 2016 interns reports to DOE	10/31/16	Complete	OSTI
Deliverable	List of identified/recruited DOE Fellow (Class of 2016)	10/31/16	Complete	
2016-P4-M2	Selection of new DOE Fellows – Fall 2016	10/31/16	Complete	
2016-P4-M3	Conduct Induction Ceremony – Class of 2016	11/04/16	Complete	
2016-P4-M4	Submit student poster abstracts to WM17 Symposium	1/16/17	Complete	
Deliverable	Update Technical Fact Sheet	30 days after end of project	On Target	

Work Plan for Next Quarter

- Continue research by DOE Fellows in the four DOE-EM research projects under the cooperative agreement and research topics identified as part of their summer internships.
- Complete spring 2017 campaign to recruit DOE Fellows into the program.
- Complete coordination of internship placements for summer 2017 at DOE sites, national laboratories, DOE-HQ, and DOE contractors and make arrangements for travel and housing. DOE Fellows will begin summer internships in June 2017.